The role and regulation of TMEM16A in the vascular system

Kathryn Emma Acheson

The Queen's College

University of Oxford

Thesis submitted for the degree of Doctor of Philosophy

Cardiovascular Science

Trinity term

2019

The role and regulation of TMEM16A in the vascular system

Kathryn Emma Acheson

The Queen's College

Doctor of Philosophy

Trinity term 2019

Abstract

TMEM16A is a Ca^{2+}-activated Cl^- channel (CaCC) encoded by the *TMEM16A* gene, expressed in vascular smooth muscle cells (VSMCs). TMEM16A has a proposed role in depolarising the membrane potential (*Vm*) in response to activation of the Gq-protein coupled receptor (Gq-PCR) signalling cascade. Therefore, TMEM16A may constitute a key contractile mechanism in VSMCs. Recent elucidation of the TMEM16A channel structure has revealed that the pore region is partially exposed to the plasma membrane. It is therefore hypothesised that TMEM16A may be sensitive to the lipid composition of the plasma membrane. This thesis explores the lipid regulation of cloned TMEM16A channels, and the role of lipids in the control of native TMEM16A currents in VSMCs, and the importance of this in murine arterial (aortic) tone.

The main findings of this thesis are:

1, The TMEM16A pharmacological modulator 2-(4-chloro-2-methylphenoxy)-N-[(2-methoxyphenyl)methylideneamino]-acetamide (Ani9) is currently the most potent and efficacious modulator of TMEM16A available. This study demonstrated that Ani9 was selective for TMEM16A in VSMCs. Studies involving Ani9 and a heterozygous knock-out of TMEM16A were used to confirm that TMEM16A is functionally expressed in VSMCs, and that TMEM16A has a key role in vascular contraction.

2, Plasma membrane levels of the intracellular signalling lipid phosphatidylinositol 4,5-bisphosphate (PIP_2) are dynamically controlled during activation of Gq-PCR. Whether these changes affect TMEM16A was unknown. Here, it was found that PIP_2 increased TMEM16A channel activity. This effect was especially pronounced at physiologically relevant intracellular Ca^{2+} concentrations ($[Ca^{2+}]_i$) and membrane potentials (*Vm*). This revealed a novel pathway in the Gq-PCR signalling cascade.

3, The dietary polyunsaturated fatty acid (PUFA) docosahexaenoic acid (DHA) was found to inhibit cloned and native TMEM16A channels. Consistent with this observation, DHA reduced agonist-induced contraction of isolated aortic rings. This observation provided a mechanistic basis for the reported vasodilator properties of DHA.

To conclude, the research in this thesis has demonstrated that TMEM16A is highly sensitive to both intracellular lipids (PIP_2) and extracellular lipids (DHA). This could form the basis for future studies investigating the TMEM16A pore region, in order to explore whether the TMEM16A pore region could be exploited as a target for pharmacological intervention.

Word count: 50,192

Acknowledgements

I have no doubt that I would not be at this point without the unwavering support of my parents Anne and Michael, and my sister Isabel. They have not only given me limitless friendship and emotional support, but also great food and holidays to keep me going. I would also like to thank my grandfather, Morrin, for sharing his College with me.

My partner Joseph Lawrence has been a constant source of positivity, support, and fun. When I reflect, it is difficult to succinctly describe how much he has assisted and empowered me throughout this DPhil. Thank you for all the adventures that have made my DPhil a little less tough. I would also like to thank Joe's parents, Jane Elliott and Jon Lawrence, for their support, guidance, and excellent wine.

The friendship of the coffee group has been a highlight of my four years in the Department of Pharmacology. I would especially like to thank Ria Dinsdale and Lara Scofano from the Tammaro group, Abigail Wilson, Elisa Venturi, and Chris Lindsay from the Sitsapaesan group, and Razik Mu-u-Min from the Terrar and Lei groups.

Thank you to David Greaves, my course director, for his support over the last four years and to my BHF cohort Irina Lupu, Hamish Lemmey, and Matthew Kerr.

I would like to thank Paolo Tammaro for his supervision of my DPhil, encouragement, and mentoring over the last four years. I would also like to thank all current and past members of the group for their friendship and support. It has been an honour to be a member of the team.

Finally, I would like to thank the British Heart Foundation for their funding.

Contents

List of figures

List of tables

List of abbreviations

$[Ca^{2+}]_i$	Intracellular free Ca^{2+} concentration
$[ion]_e$	Extracellular ion concentration
$[ion]_i$	Intracellular ion concentration
A9C	Anthracene-9-carboxylic acid
ABC	ATP-binding cassette
ADP	Adenosine diphosphate
Ani9	2-(4-chloro-2-methylphenoxy)-N-[(2-methoxyphenyl)methylideneamino]-acetamide
ARRIVE	Animal Research: Reporting of *In Vivo* Experiments
ATP	Adenosine triphosphate
BK_{Ca}	Big conductance K^+ channel
bp	base pairs
Ca^{2+}-CaM	Ca^{2+}-bound CaM
CaCC	Ca^{2+}-activated chloride channel
cADPR	Cyclic ADP-ribose
CaM	Calmodulin
cAMP	Cyclic adenosine monophosphate
Ca_V	Voltage-gated Ca^{2+} channels
CFTR	Cystic fibrosis transmembrane receptor
cGMP	Cyclic guanosine monophosphate
CICR	Ca^{2+}-induced calcium release
CLCA	Ca^{2+}-dependent Cl^- channel
ClCs	Voltage-gated Cl^- channels
cryo-EM	Electron cryomicroscopy
DAG	Diacylglycerol
ddH_2O	Double-distilled H_2O
DHA	Docosahexaenoic acid
DHPs	Dihydropyridines
diC8-PIP_2	Dioctanoylglycerol phosphatidylinositol 4,5-bisphosphate
DIDS	4,4'-Diisothiocyano-2,2'-stilbenedisulfonic acid
DM	Dissociation medium
DMSO	Dimethyl sulfoxide
dNTP	Nucleoside triphosphate
DPBS	Dulbecco's Phosphate-Buffered Saline solution
DrVSP	*Danio rerio* voltage-sensitive phosphatase
dsDNA	Double stranded DNA
DTT	Dithiothreitol
E_{ion}	Reversal potential for a given ion
E_{rev}	Reversal potential
Eact	Naroylaminothiazole

EDH	Endothelium-dependent hyperpolarisation
EPA	Eicosapentaenoic acid
ESCC	Esophageal squamous cell carcinoma
EtBr	Ethidium bromide
Fact	Tetrazolylbenzamide
γ	Single channel conductance
G-PCR	G-protein coupled receptor
GRb1	Ginsenoside Rb1
HEK-293T	Human embryonic kidney 293T
HNSCC	Head and neck squamous cell carcinoma
ICC	Interstitial cells of Cajal
IK	Intermediate conductance
$\mathbf{I_{max}}$	Maximal current
IntCir	Internal circumference
$\mathbf{IP_3}$	Inositol-1,4,5-triphosphate
$\mathbf{IP_3R}$	Inositol-1,4,5-triphosphate-sensitive receptor
IPAH	Idiopathic pulmonary hypertension
$\mathbf{I_{ss}}$	Steady-state current
$\mathbf{K_{ATP}}$	ATP-dependent K^+ channel
$\mathbf{K_{ir}}$	Inwardly rectifying K^+ channel
LB	Lysogeny broth
MHC	Myosin heavy chain
MLC	Myosin light chain
MLCK	Myosin light-chain kinase
MONNA	N-((4-methoxy)-2-naphthyl)-5-nitroanthranilic acid
NA	Nicotinic acid
NAADP	Nicotinic acid adenine dinucleotide phosphate
NADP+	Nicotinamide adenine dinucleotide phosphate
NC3Rs	National Centre for the Replacement, Refinement, and Reduction of Animals in Research
NCX	Na^+/Ca^{2+}-exchanger
***Nectria haematococca* TMEM16**	nhTMEM16
NFA	Niflumic acid
NKCC1	$Na^+/K^+/2Cl^-$ cotransporter
NO	Nitric oxide
NSCCs	Non-selective cation channels
NTD	N-terminal domain
OD	Optical density
PASMC	Pulmonary arterial smooth muscle cells
PCR	Polymerase chain reaction
PE	L-phenylephrine hydrochloride
Pi	Inorganic phosphate

PI	Phosphoinositide
PI5K	PIP 5-kinase type I
PIP_2	Phosphatidylinositol-4,5-bisphosphate
PIPs	Phosphatidylinositol phosphates
PLC	Phospholipase C
P_o	Open probability
POPC	1-Palmitoyl-2-oleoylphophatidylcholine
POPE	1-palmitoyl-2-oleoyl-sn-glycero-3-phosphoethanolamine
POPS	Palmitoyl-oleoyl phosphatidylserine
PSS	Physiological salt solution
PUFAs	Polyunsaturated fatty acids
ROCCs	Receptor-operated cation channels
RyR	Ryanodine receptors
SERCA	Sarcoplasmic reticulum Ca^{2+} ATPase
SK	Small conductance
SM	Smooth muscle
SMCs	Smooth muscle cells
SOCCs	Store-operated cation channels
SR	Sarcoplasmic reticulum
SUR	Sulfonylurea receptor
SV40	Simian Virus 40
$\tau_{a0.5}$	Activation time constant
$\tau_{d0.5}$	Deactivation time constant
τ_r	Time constant of recovery
TAE	Tris-actetate EDTA
TMEM16A-het-KO	TMEM16A heterozygous knock-out
TPC	Two-pore channels
TRP	Transient receptor potential
Vm	Membrane potential
VSMCs	Vascular smooth muscle cells
VSP	Voltage-sensitive phosphatase

Chapter 1

Introduction

Chapter 1 – Introduction

This chapter outlines fundamental concepts in the physiology of the mammalian cardiovascular system, with emphasis on the role of ion channels in vascular smooth muscle cells (VSMCs). Specifically, the calcium-activated chloride channel (CaCC) encoded by the *TMEM16A* gene is hypothesised to have a pivotal role in vascular contractility. The molecular physiology of TMEM16A and its role in VSMCs will therefore be comprehensively reviewed in this chapter.

1.1. General aspects of cardiovascular physiology

The cardiovascular system evolved to provide a transport system for the blood, which carries crucial molecules such as oxygen from the external environment to all cells and tissues in the body. The blood is pumped into the pulmonary and the systemic circulatory systems by the activity of the heart (Herring and Paterson, 2018, Klabunde, 2012).

The volume of blood ejected by a ventricle in a singular contraction is referred to as the stroke volume, and primarily depends on two factors: the force generated by contraction of the ventricles (inotropy), and the pressure in both circulations that must be overcome by the action of the heart (afterload). The stroke volume is also regulated by the amount of blood entering the ventricles before the ventricular contraction (preload), and the associated Frank-Starling mechanism (Herring and Paterson, 2018, Klabunde, 2012). The Frank-Starling mechanism stipulates that the stroke volume increases as a result of an increased preload, ventricular stretch, and consequent increase in inotropy (Herring and Paterson, 2018, Klabunde, 2012). Myocardial inotropy

is also controlled by the autonomic nervous system and circulating endocrine inotropic substances such as adrenaline (Klabunde, 2012, Herring and Paterson, 2018).

The volume of blood ejected by each ventricle per minute is the cardiac output, and is equal to the stroke volume multiplied by heart rate. In humans, cardiac output is usually ~4-7 litres per minute, however this is constantly adapted to accommodate changes in demand from the body. For example, during exercise the cardiac output can increase up to six-fold (Herring and Paterson, 2018).

1.2. Vascular structure and function

Blood vessels characteristically have a cross-section involving three layers (or *tunicae*): the *tunica intima*, *tunica media*, and *tunica adventitia* (Klabunde, 2012, Herring and Paterson, 2018).

The *tunica intima* is the innermost layer of the blood vessel, and is composed of a single sheet of endothelial cells and the basal lamina, which is a mesh of extracellular matrix that provides mechanical stability, and separates the *tunica intima* from the *tunica media*. The *tunica intima* also has a role in secreting vasoactive chemicals, such as the antithrombotic vasodilator nitric oxide (NO) (Garland and Weston, 2011, Wellman et al., 1996, Palmer et al., 1987).

The *tunica media* provides the blood vessel contractile force, as it is mainly composed of VSMCs. VSMCs are arranged in an orderly system, supported by a matrix containing collagen, elastin, and glycoproteins. The *tunica media* varies in thickness depending on the type of blood vessel and its requirement for eliciting contractile force.

The *tunica adventitia* consists largely of collagen, which provides mechanical support to the blood vessel. It also contains fibroblasts and other progenitor cells (Hu et al., 2004,

Zengin et al., 2006), in addition to cells of the immune system (Galkina et al., 2006, Swedenborg et al., 2011, Tieu et al., 2009). The *tunica adventitia* is also the location of sympathetic nerve terminals, which provides transmitter release that regulates blood vessel tone and local blood flow (Klabunde, 2012, Herring and Paterson, 2018).

Arterial histology varies significantly as the distance from the heart increases. As the distance increases, vascular wall thickness and diameter tends to decrease. The largest artery is the aorta, which has a diameter of ~25 mm in humans and can tolerate blood pressures of up to ~120 mmHg (and higher in hypertension) (Herring and Paterson, 2018, Narayan et al., 2017, Borghi et al., 2017). The large wall thickness of the aorta (and of other large arteries) require a specific blood supply to the deeper parts of the artery wall. This is provided by the *vasa vasorum*, a network of small blood vessels and capillaries embedded within the blood vessel wall (Billaud et al., 2017, Heistad and Marcus, 1979).

Capillaries are the smallest blood vessels with a diameter of ~8 µm in humans. Capillaries are composed of a single layer of endothelial cells, which facilitates movement of substances between blood and the surrounding tissues. Veins have a reduced smooth muscle (SM) and elastin content. In contrast, large arteries such as the aorta have a high proportion of elastin that facilitates passive stretch and recoil, which is important for the accommodation the ejection of the stroke volume from the left ventricle. Overall, this process known as the Windkessel effect (Westerhof et al., 2009, Klabunde, 2012, Levy et al., 2007).

1.2.1. Vascular haemodynamics

Vascular haemodynamics is defined as the relationship between blood flow, pressure, and resistance within blood vessels (Herring and Paterson, 2018, Klabunde, 2012). The perfusion pressure of the cardiovascular system is the pressure gradient driving the blood flow, which equates to the arterial minus the venous blood pressure. Blood flow (F) through a blood vessel is described as the pressure gradient (ΔP) driving the blood flow, divided by the resistance (R) to blood flow.

$$F = \frac{\Delta P}{R} \quad [1.1]$$

Blood flow is regulated via changes in blood vessel resistance, which depends on three main variables: vessel length (L), blood viscosity (η), and vessel radius (r).

$$R \propto \frac{\eta.L}{r^4} \quad [1.2]$$

Resistance is therefore directly proportional to blood vessel length, and inversely proportional to the power 4 of the blood vessel radius. This relationship highlights that vessel radius is the dominant factor in defining blood flow within the cardiovascular system. However, in physiological conditions, blood vessel length is not dynamically regulated and therefore blood viscosity and vessel radius are the two main parameters that allow regulation of the resistance and blood flow (Herring and Paterson, 2018, Klabunde, 2012). Blood viscosity is another factor that opposes blood flow, as it is related to the friction generated within the fraction of red blood cells in the total volume

of blood (the haematocrit), and also between the haematocrit and the lining of the blood vessel. Blood vessel radius, which is the most important factor in determining resistance, is finely controlled by a variety of stimuli (Herring and Paterson, 2018, Klabunde, 2012).

Combining equations 1.1 and 1.2 gives Poiseuille's equation (equation 1.3). Poiseuille's equation describes how flow of a ligand is related to perfusion pressure, vessel radius, vessel length, and fluid viscosity.

$$F \propto \frac{\Delta P.r^4}{\eta.\mathrm{L}} \qquad [1.3]$$

Poiseuille's equation does not exactly describe blood flow, as it is based on the following three assumptions. *(i*) blood vessels are straight, inflexible pipes, *(ii)* blood viscosity is constant and independent of the blood flow, and *(iii)* blood is flowing under steady, non-turbulent conditions (laminar flow) (Herring and Paterson, 2018, Klabunde, 2012). In spite of these assumptions, Poiseuille's equation remains a useful concept in vascular physiology as it highlights the key factors determining blood flow. It should be noted that the Poiseuille's equation relates to a single blood vessel, however the vasculature is a complex network of blood vessels. Overall, the cardiovascular system is arranged as a circuit in series, with blood vessels branching into smaller parallel circuits. When resistances are arranged in parallel, the reciprocal of the total resistance is equal to the sum of the reciprocal resistances as:

$$\frac{1}{R_T} = \frac{1}{R_1} + \frac{1}{R_2} + \frac{1}{R_3} \qquad [1.4]$$

The total resistance of a network in a parallel arrangement is less than the resistance of the single lowest resistance in the system; therefore, the organisation of blood vessels in parallel reduces the overall resistance they produce on blood flow.

The sum of resistances arranged in series (R_T) is equal to the sum of the individual resistances (equation 1.5).

$$\mathrm{R_T} = R_A + R_a + R_c + R_v + R_V \qquad [1.5]$$

Where A = artery, a = arterioles, c = capillaries, v = venules, and V = veins.

The biophysical concepts described above have important physiological implications. For example, they illustrate the fact that the parallel arrangement of capillaries within an organ has evolved to ensure effective organ blood perfusion while limiting the overall resistance to blood flow and therefore demand on the heart. Furthermore, understanding the biophysics of haemodynamics demonstrates that diseases associated with narrowing of the blood vessel lumen (e.g. narrowing of arteriolar diameter in atherosclerosis) result in an increased R_A, and consequently of R_T, an event that produces additional demand on the heart.

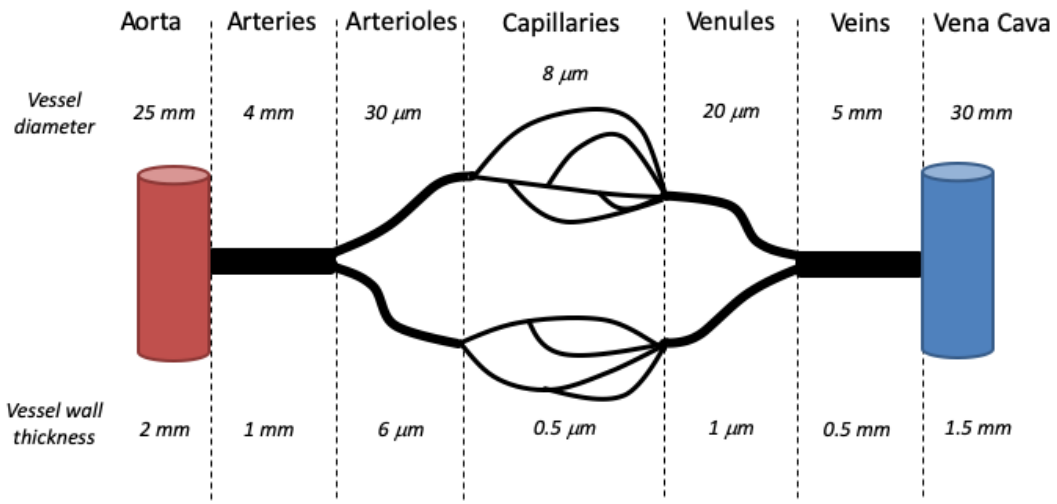

Figure 1.1. Organisation and size of blood vessels in the vascular system

1.3. Vascular smooth muscle cells

VSMCs have a spindle morphology, and are usually 5-10 µm in diameter and 50-300 µm in length. Numerous small invaginations (caveolae) in the cell membrane increase the membrane surface area of VSMCs (Dart, 2010, Popescu et al., 2006). Caveolae also result in the clustering of lipid domains and membrane proteins, such as ion channels, transporters, and receptors (Dart, 2010, Popescu et al., 2006). Membrane proteins in the caveolae may also be brought in close proximity to sites of release of Ca^{2+} from intracellular stores, an arrangement that favours coupling between intracellular Ca^{2+} handling and cell electrical activity (Dart, 2010, Hill-Eubanks et al., 2011). As in other muscle types, contraction of VSMCs requires interaction between the contractile proteins actin and myosin. However, these proteins are not organised into distinct bands as is typical in striated muscle (Herring and Paterson, 2018). In VSMCs individual

myosin filaments are surrounded by several actin filaments in a bundle-like structure (Webb, 2003, Herring and Paterson, 2018).

Actin filaments in VSMCs are composed of α-actinin, and are organised into dense bands on the inner cell membrane and dense bodies in the cytoplasm (Webb, 2003, Herring and Paterson, 2018). Intermediate filaments contain the proteins desmin and vimentin, which function as cytoskeletal elements linking the dense bodies and bands, facilitating the coordinated contraction of the cell (Webb, 2003, Herring and Paterson, 2018). In order to initiate VSMC contraction, cytosolic calmodulin (CaM) must bind free Ca^{2+}. The Ca^{2+}-bound CaM (Ca^{2+}-CaM) activates the enzyme myosin light-chain kinase (MLCK). MLCK phosphorylates myosin light chain (MLC) in an adenosine triphosphate (ATP)-dependent process (Webb, 2003, Herring and Paterson, 2018). MLC is non-covalently bound to myosin heavy chain (MHC), and regulates ATPase-mediated interactions between actin and the MHC head group. Under resting conditions, the MHC head group has a low affinity for actin filaments as it is bound to ATP. When MLC is phosphorylated, ATPase activity is increased, and adenosine diphosphate (ADP) and inorganic phosphate (Pi) are formed. Pi is donated to MLC and induces a conformational change that favours actin-myosin crossbridge formation, which causes contraction as the myosin head rotates to create tension, and the entities are pulled together (Fig. 1.2) (Marchand et al., 2012, Herring and Paterson, 2018).

The VSMC contractile regulatory proteins, caldesmon and calponin, are localised on actin filaments. Caldesmon inhibits the ATPase activity of the myosin until acted upon by Ca^{2+}-CaM. Calponin is an actin-associated protein that inhibits ATPase activity and crossbridge formation, which results in the inhibition of VSMC contraction (Webb, 2003, Herring and Paterson, 2018).

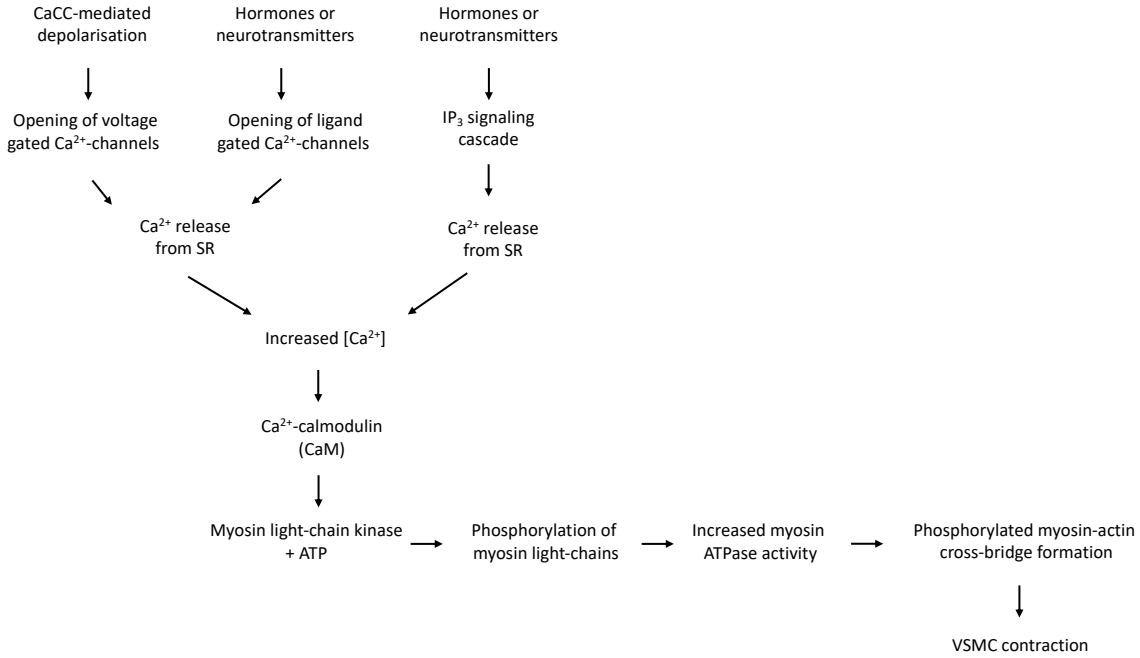

Figure 1.2. Schematic of VSMC contraction mechanism

1.4. Types of contractile and relaxation stimuli

Stimuli that modulate contractility of VSMCs can be divided into two categories: intrinsic and extrinsic. These mechanisms ultimately regulate intracellular free Ca^{2+} concentration ($[Ca^{2+}]_i$) in VSMCs, which is the pure determinant of VSMC tone.

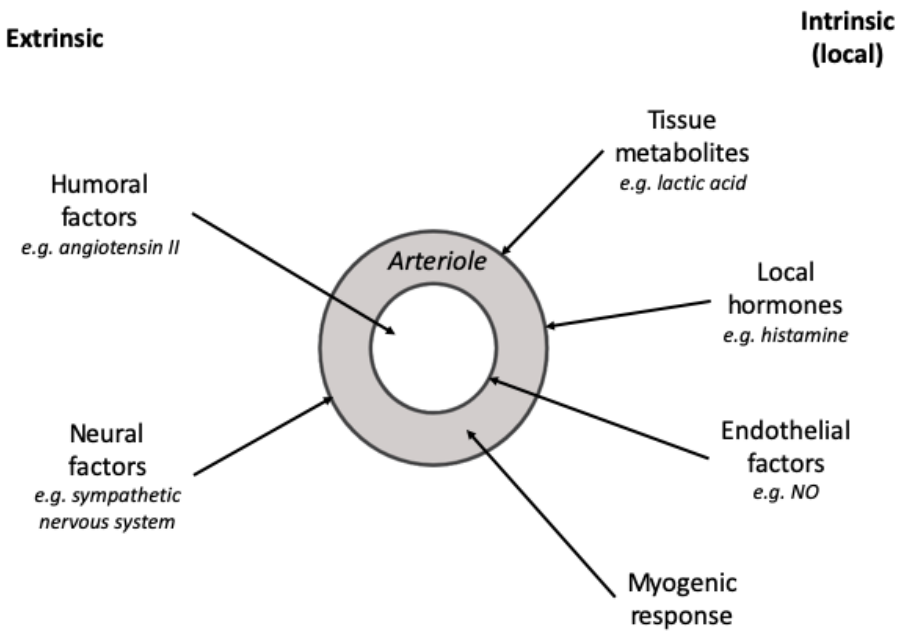

Figure 1.3. Intrinsic and extrinsic factors that regulate blood vessel tone

Changes in transmural pressure can modulate vascular tone via the Bayliss myogenic response, which causes arterial vessels to contract when blood pressure is acutely raised (Schubert et al., 2008, Herring and Paterson, 2018). A mechanism that can antagonise the Bayliss myogenic response is an increase in wall tension and endothelial shear stress, which stimulates the endothelium to produce increased levels of NO and endothelium-dependent hyperpolarisation (EDH), which assist in preventing excessive vasoconstriction. These processes combine to regulate blood vessel tone (Schubert et al., 2008, Herring and Paterson, 2018).

G-Protein coupled receptors

The majority of agonists acting on G-protein coupled receptors (G-PCR) modulate vascular tone by acting as vasoconstrictors or vasodilators (Althoff and Offermanns, 2015, Di Salvo and Nelson, 1998). There are three types of G-PCR: Gi-PCR, Gs-PCR, and

Gq-PCR. Each type triggers a different intracellular signalling cascade. Gi-PCRs, such as the α2-adrenergic receptor in SM, inhibit adenyl cyclase and cyclic adenosine monophosphate (cAMP) pathway, which in turn results in a decrease in K_{ATP} channel conductance and associated depolarisation and vasoconstriction (Lee and Debernardis, 1990, Kuo and Ehrlich, 2015, Althoff and Offermanns, 2015). Gs-PCRs have the opposite effect, increasing cAMP formation by stimulating adenylyl cyclase. Examples of Gs-PCRs expressed in VSMCs include the prostacyclin receptor, whose agonist prostacyclin is a potent vasodilator (Moncada and Vane, 1979, Kuo and Ehrlich, 2015, Althoff and Offermanns, 2015).

Gq-PCR activation in turn activates the enzyme phospholipase C (PLC), which cleaves the membrane bound phosphoinositide (PI) phosphatidylinositol-4,5-bisphosphate (PIP_2). This releases water-soluble inositol-1,4,5-triphosphate-sensitive (IP_3) into the cytosol, and leaves the lipophilic secondary messenger diacylglycerol (DAG) localised in the plasma membrane. IP_3 then activates the inositol-1,4,5-triphosphate-sensitive receptor (IP_3R), which releases Ca^{2+} from the sarcoplasmic reticulum (SR). This increase in $[Ca^{2+}]_i$ results in vasoconstriction (Fig. 1.4). Examples of Gq-PCRs include α1-adrenergic, AT_1, ET_A, V_1, and M_3. Their respective agonists are noradrenaline/adrenaline, angiotensin II, endothelin-1, vasopressin, and acetylcholine (Herring and Paterson, 2018, Klabunde, 2012).

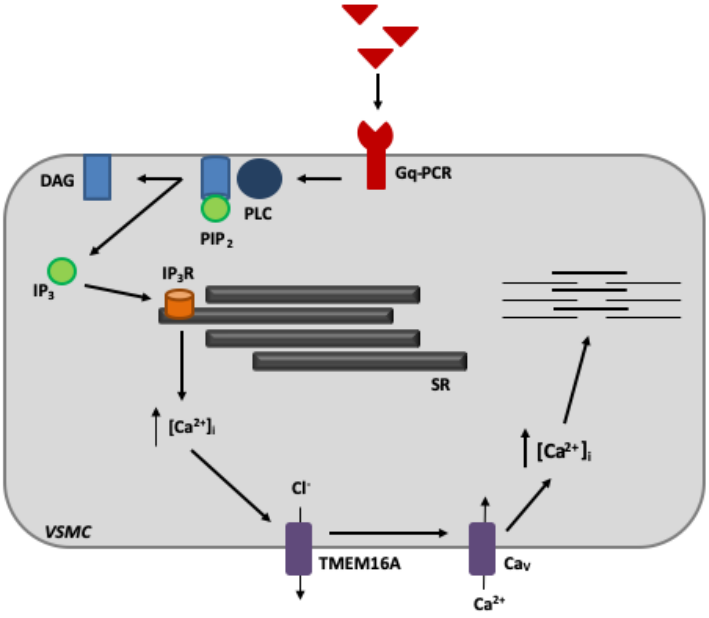

Figure 1.4. The Gq-PCR signalling cascade

1.5. Regulation of intracellular Ca^{2+}

Regulation of $[Ca^{2+}]_i$ is crucial in the regulation of SM tone, as an increase or decrease in $[Ca^{2+}]_i$ is the principal mechanism that initiates contraction or relaxation in SM. Under resting conditions VSMCs maintain a $[Ca^{2+}]_i$ at ~100 nM (Knot and Nelson, 1998, Herring and Paterson, 2018, Hill-Eubanks et al., 2011, House et al., 2008, Bolton, 1979, Marin, 1993, Orallo, 1996), however free extracellular free Ca^{2+} concentration ($[Ca^{2+}]_e$) is ~10,000 fold higher (~1.2 mM) (Missiaen et al., 1992, Himpens et al., 1992), which causes a significant concentration gradient that promotes Ca^{2+} entry.

There are three mechanisms of $[Ca^{2+}]_i$ control: Ca^{2+} entry via plasma membrane Ca^{2+}-permeable channels, Ca^{2+} release from intracellular stores, and Ca^{2+} transport mechanisms that ensure Ca^{2+} extrusion from the plasma membrane and Ca^{2+} reuptake into intracellular stores. The $[Ca^{2+}]_i$ increasing mechanisms can be grouped into

pharmacomechanical coupling and excitation-contraction coupling (Somlyo et al., 1999, Baron et al., 1984, Casteels et al., 1985, Ebashi, 1991). Pharmacomechanical and excitation-contraction coupling coexist in VSMCs. Pharmacomechanical coupling refers to Ca^{2+} release from intracellular stores or Ca^{2+} entry from the extracellular space through receptor-operated or store-operated Ca^{2+}-permeable channels, in response to neurotransmitters or endocrine signalling. Excitation-contraction coupling describes Ca^{2+} entry from the extracellular space into VSMCs via plasma membrane Ca^{2+}-permeable channels. The Ca^{2+} entry from plasma membrane channels is controlled and influenced by the *Vm*, which is determined by the complement of ion channels and transporters present on the plasma membrane.

1.5.1. Intracellular ion channels

The sarcoplasmic reticulum is the main intracellular Ca^{2+} store in VSMCs. Ca^{2+} is released from the SR as a consequence of Gq-PCR stimulation via the IP_3R (Berridge, 1993). Activation of Ca^{2+} permeable stores in intracellular compartments such as lysosomes is also an important mechanism (Fameli et al., 2017). Combined, Ca^{2+} release from the SR and lysosomes can increase cytosolic $[Ca^{2+}]_i$ by up to 100-fold (Brozovich et al., 2016).

Release of $[Ca^{2+}]_i$ via IP_3R and RyR

The IP_3Rs in the SR are conjugated to Ca^{2+} release channels (IP_3-Ca^{2+} release channels), and form a co-dependent structure. IP_3 is produced upon activation of the Gq-PCR signalling cascade. Ca^{2+} release is triggered by IP_3 in an all or nothing (stochastic) manner, leading to Ca^{2+} blips or puffs. A Ca^{2+} blip is the IP_3-dependent opening of a single IP_3Rs (Thul, 2014, Qi et al., 2014). A Ca^{2+} puff is a short Ca^{2+} release event arising

from a small cluster of IP_3R (Bootman and Berridge, 1996). The result of Ca^{2+} blips or puffs is the subsequent opening of nearby IP_3R and RyRs, which are named Ca^{2+} waves. Ca^{2+} waves can be propagated along the length of the VSMC and to neighbouring cells, resulting in their conduction (Foskett et al., 2007, Hill-Eubanks et al., 2011).

SR also contain RyRs, an additional Ca^{2+}-release channel. RyR channels release brief bursts of Ca^{2+}, called Ca^{2+} sparks (Nelson et al., 1995, Hill-Eubanks et al., 2011). Ca^{2+} sparks mediate Ca^{2+}-induced calcium release (CICR) is a process in which opening of RyR triggers opening of nearby RyR (Nelson et al., 1995, Hill-Eubanks et al., 2011). RyR are in close proximity to ion channels on the plasma-membrane, such as Ca^{2+}-activated Cl^- channels (CaCCs), which upon activation cause membrane depolarisation that results in the triggering of Ca^{2+} influx via voltage-gated Ca^{2+} channels (Ca_V) (Matchkov et al., 2012). RyR are also localised in close proximity to large conductance Ca^{2+}-activated K^+ channels (BK_{Ca}) (Ledoux et al., 2006). A single Ca^{2+}-spark can increase the open probability of ~30 neighbouring BK_{Ca} channels by 100-fold (Jaggar et al., 2000, Perez et al., 2001). The resulting outward hyperpolarising current causes vasodilation (Nelson et al., 1995).

The IP_3R and RyR have differing expression profiles in arteries and arterioles. IP_3R and RyR are both localised in arteries and participate in conducting Ca^{2+} waves, however arteriolar Ca^{2+} waves are completely mediated by IP_3R (Westcott et al., 2012, Brozovich et al., 2016). In both types of blood vessel, Ca^{2+} waves were depleted in the presence of a PLC inhibitor. In isolated vessels this resulted in vasodilation, which suggests the IP_3R contributes to Ca^{2+} waves as part of a positive feedback loop for myogenic tone (Westcott et al., 2012, Brozovich et al., 2016).

Regulation of $[Ca^{2+}]_i$ via two-pore channels

Nicotinic acid adenine dinucleotide phosphate (NAADP) is a potent regulator of cytosolic $[Ca^{2+}]_i$ (Clapper et al., 1987, Pitt et al., 2016). NAADP behaves as a potent second messenger that releases Ca^{2+} from the endolysosomal system, via activation of two-pore channels (TPC) (Calcraft et al., 2009). TPCs trigger release of Ca^{2+}, which is amplified by CICR from the SR (Patel and Kilpatrick, 2018, Brailoiu et al., 2010).

NAADP is synthesised via the bifunctional lymphocyte differentiation antigen, CD38 (Howard et al., 1993). CD38 and ADP-ribosyl cyclase can both synthesise cyclic ADP-ribose (cADPR). CD38 and the resulting cADPR can catalyse the exchange of the nicotinamide group of nicotinamide adenine dinucleotide phosphate (NADP+) with nicotine acid (NA), producing NAADP (Aarhus et al., 1995). In VSMCs, production of NAADP can be induced in by vasoconstrictors such as ET-1 (Zhang et al., 2006). NAADP-mediated Ca^{2+} release displays a bell-shaped concentration-response curve, whereby an optimum $[NAADP]_i$ results in maximal Ca^{2+} release and higher $[NAADP]_i$ results in a block of Ca^{2+} release (Cancela et al., 1999, Berg et al., 2000, Rosen et al., 2009).

In VSMCs, increasing $[NAADP]_i$ is associated with biphasic cytosolic $[Ca^{2+}]_i$ signalling: a slow initial increasing $[Ca^{2+}]_i$ transient, leading to a second large $[Ca^{2+}]_i$ transient (Kinnear et al., 2004, Kinnear et al., 2008). This effect was replicated in a transiently transfected HEK-293 cell system, further implicating TPC and NAADP in this response (Calcraft et al., 2009). As outlined in greater detail in section 1.7.2, a range of ion channels on the plasma membrane are responsible for Ca^{2+} entry from the extracellular space into the cytoplasm of VSMCs.

1.5.2. Ca^{2+} removal mechanisms – SERCA, PMCA, NCX

The sarcoplasmic reticulum Ca^{2+} ATPase (SERCA) pump transports cytosolic Ca^{2+} into the SR for storage. SERCA activity is triggered by an increase in $[Ca^{2+}]_i$, caused by Ca^{2+} entry into the cell or a reduction in Ca^{2+} efflux. In VSMCs, SERCA activity is also stimulated by calreticulin, a protein that binds free Ca^{2+} within the SR. This results in a lower free Ca^{2+} gradient for SERCA to pump against (Milner et al., 1991, Matthew et al., 2004).

The plasma membrane Ca^{2+} ATPase (PMCA) is a transport protein localised in the plasma membrane that pumps Ca^{2+} out of the cell (Schatzmann, 1966, Stafford et al., 2017). Genetic knock-out of PMCA1, an isoform of PMCA expressed in arteries (Little et al., 2017) results in hypertension (Kobayashi et al., 2012).

The Na^+/Ca^{2+}-exchanger (NCX) is a plasmalemmal antiporter that transports Ca^{2+} from the cytosol into the extracellular space. Under resting conditions, NCX uses the favourable electrochemical gradient for every three Na^+ entering the cell to provide energy to export one Ca^{2+}. NCX knock-out mice (Blaustein et al., 2009, Zhang et al., 2010) and pharmacological inhibition of NCX (Matsuda et al., 2001, Iwamoto et al., 2004) result in increased VSMC tone in a variety of artery types.

1.6. Overview of biophysics of cell excitability

The plasma membrane facilitates maintenance of different concentrations of ions across the lipid bilayer, resulting in cells storing potential energy in the form of electrochemical gradients (Alberts, 2008).

Plasma membranes have a structure composed of a thin layer (~5 nm) of lipid and protein molecules, held together via noncovalent interactions. Lipid and protein

molecules are constantly moving in the fluid plasma membrane, an arrangement originally defined as the “fluid mosaic model” (Singer and Nicolson, 1972). The lipid molecules are arranged in a continuous double layer, the phospholipid bilayer, which provides the flexible but impermeable barrier to water soluble molecules. Membrane proteins typically span the lipid bilayer and mediate nearly all of the other membrane functions, for example transport of substances in and out of the cell, and receptors that detect and transduce chemical signals (Alberts, 2008).

1.6.1. Electrical activity in membranes

The electrochemical gradient across the plasma membrane is maintained via co-transporters, exchangers, and ATP-dependent pumps, which move ions against their concentration gradient (table 1.1) (Herring and Paterson, 2018).

Table 1.1. Ionic concentrations in VSMCs

Ion	$[ion]_i$ (mM)	$[ion]_e$ (mM)	E_{ion} (mV)
K^+	165	5	-89
Na^+	9	137	69
Ca^{2+}	0.0001	1.2	124
Cl^-	54	134	-23
HCO_3^-	7.3	15.5	-19
H^+	8.7×10^{-8}	4×10^{-8}	-20

Data reproduced from (Herring and Paterson, 2018). $[ion]_i$: intracellular ionic concentration, $[ion]_e$: extracellular ionic concentration, E_{ion}: ionic equilibrium potential. Ionic concentrations assume VSMCs are in a relaxed state, with $[Ca^{2+}]$ indicating free, unbound ionic concentration.

Ions are inclined to diffuse down the electrochemical gradient until they reach a chemical and electrical equilibrium (Alberts, 2008, Hille, 2001). The Nernst equation predicts the point at which this is achieved for individual ion types:

$$E_X = \frac{RT}{ZF} \ln \frac{[X]_{out}}{[X]_{in}} \quad [1.6]$$

E_x is the equilibrium potential across the membrane for ion 'x'. At this *Vm*, the net movement of ion 'x' is zero. R is the universal gas constant, T is the temperature (K), $[X]_{out}$ and $[X]_{in}$ are the concentrations of ions outside and inside the cell, respectively. F is the Faraday constant, and z is the valency of the ion (Alberts, 2008, Hille, 2001).

Under physiological conditions, the plasma membrane of a cell is permeable to multiple types of ion. The resting *Vm* is therefore determined by the plasma membrane combined permeability of the membrane to different types of ion and their concentrations on either side if the plasma membrane (table 1.1). This relationship is described by the Goldman-Hodgkin-Katz equation:

$$V_m = \frac{RT}{F} \ln \left(\frac{p_K[K^+]_o + p_{Na}[Na^+]_o + p_{Cl}[Cl^-]_i}{p_K[K^+]_i + p_{Na}[Na^+]_i + p_{Cl}[Cl^-]_o} \right) \quad [1.7]$$

Where p_{ion} is the permeability for a given ion type. The *Vm* of a typical VSMC at rest is between -75 mV and -40 mV, which is close to the E_K value (~-80 mV) determined by the Nernst equation. This suggests that K^+ current is the main contributor to *Vm*, however other ionic currents must contribute to the *Vm* explaining the divergence in resting *Vm* from E_K (Nelson et al., 1990b, Hirst and Edwards, 1989).

1.6.2. *Vm* and regulation of arterial tone

The *Vm* of SM in the arterial wall is a key regulator of blood vessel tone. Under resting conditions, the relationship between the *Vm* and arterial tone is very steep. Fluctuations of a few mV is sufficient to result in a significant change in blood vessel diameter (Brayden and Nelson, 1992, Nelson et al., 1990a). The resting *Vm* of VSMCs (~-50 mV) resides in the range in which Ca^{2+}-influx via plasma membrane voltage gated Ca^{2+} channels (VGCCs) is highly voltage dependent (Nelson et al., 1990a). The steep relationship between *Vm* and blood vessel tone is likely to reflect the tight voltage dependency of the open probability of VGCCs around the resting *Vm*; a ~3 mV change in resting *Vm* can result in a ~2-fold increase in Ca^{2+}-influx (Nelson et al., 1990a).

1.7. Ion channels in the VSMC plasma membrane

There are four main types of ion channels in VSMCs: K^+, Ca^{2+}, Cl^-, and non-selective cation channels (Fig. 1.5). Voltage-gated Na^+ channels are also expressed in some vascular beds, however their role in control of arterial tone remains poorly understood (Tykocki et al., 2017, Jackson, 2000).

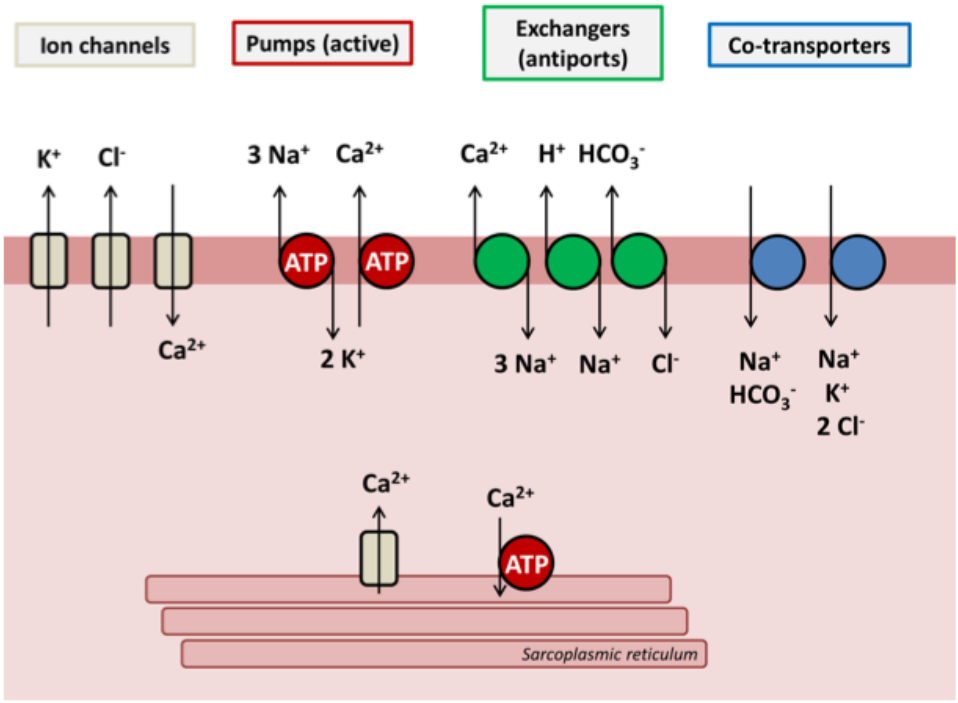

Figure 1.5. Ion channels and transporters expressed in VSMCs

1.7.1. K^+ channels in VSMCs

As outlined above, K^+ channels are a key determinant of resting *Vm* in VSMCs. Therefore K^+ channel closure will cause *Vm* depolarisation and blood vessel contraction, while opening of these channels will result in *Vm* hyperpolarisation and inactivation of Ca_V and CaCC channels (Jackson, 2017). There are various types of K^+ channels expressed in VSMCs, which are reviewed below.

Inwardly-rectifying K^+ channel (K_{ir})

K_{ir} channels are typically composed of four homomeric or heteromeric subunits, each composed of two transmembrane domains (Hibino et al., 2010, Park et al., 2008). K_{ir} channels are expressed in VSMCs of virtually all artery types, including: small arterioles (Edwards and Hirst, 1988), cerebral arteries (Edwards et al., 1998), and coronary

arteries (Smith et al., 2008), and are characterised by their K^+ current's inward rectification. This means conduction of inward K^+ current is more favourable at hyperpolarised *Vm* than at depolarised *Vm*. K_{ir} are usually active at resting *Vm*, and therefore contribute to the resting *Vm* of VSMCs (Park et al., 2008).

The inward rectification of K_{ir} channels is a result of their voltage-dependent asymmetric pore block by divalent ions, e.g. Mg^{2+}, in the cytoplasm (Guo et al., 2003). This ionic block only occurs at depolarised *Vm*, when the divalent ions are driven into the pore (Hille and Schwarz, 1978, Matsuda, 1991). Ba^{2+} is an inhibitor of K_{ir} channels, and caused constriction of isolated coronary and cerebral arteries (Park et al., 2007).

The K_{ir} channel open probability (P_o) increases in response to increased $[K^+]_o$ in the range of 5-25 mM, which means it acts as a K^+ sensor (Edwards et al., 1998). Activity in the presence of increased $[K^+]_o$ shifts the *Vm* towards E_K, which hyperpolarises the VSMCs and causes vessel relaxation (Knot et al., 1996). This occurs in coronary arteries during increased metabolic activity, and in cerebral arteries to module blood flow (Longden and Nelson, 2015, Knot et al., 1996). Blockage of vascular K_{ir} channels induces vasodilation in resistance vasculature (Dwivedi et al., 2005). Genetic deletion of $K_{ir}2.1$ and $K_{ir}2.2$ channels prevented $[K^+]_o$-mediated K_{ir} currents and prevented cerebral arterial vasodilation (Zaritsky et al., 2000).

ATP-dependent K^+ channel (K_{ATP})

K_{ATP} channels are inhibited by intracellular ATP (Kakei et al., 1985, Noma, 1983), and activated by Mg-ATP and Mg-ADP via interactions with the channels auxiliary subunit (Proks et al., 2010, Dunne and Petersen, 1986). This duel regulation allows K_{ATP} channels to respond to the metabolic state of the VSMCs (Nelson and Quayle, 1995).

K_{ATP} channels consist of a $K_{ir}6.1$ pore-forming α-subunit, in combination with four sulfonylurea receptor (SUR) auxiliary subunits, tethered to the α-subunit by their respective N-terminal domain (NTD) (Martin et al., 2017, Seino and Miki, 2003). The SUR subunit is part of a family of ATP-binding cassette (ABC) proteins crucial for the formation of a functional K_{ATP} channel. The composition of the SUR subunit isoforms is tissue-specific and determines the biophysical properties of the K_{ATP} channel (Foster and Coetzee, 2016). In VSMCs, K_{ATP} channels are composed of $K_{ir}6.1$ pore-forming α-subunits and SUR2B auxiliary subunits (Yoshida et al., 2004, Seino and Miki, 2003), and are expressed in arteries (Standen et al., 1989, Yoshida et al., 2003, Cui et al., 2002), arterioles (Spruce et al., 1987), and capillaries (Schnitzler et al., 2000). Cromakalim is a an activator of K_{ATP} channels, which causes vasodilation that can be reversed in the presence of the K_{ATP} specific blocker glibenclamide (Standen et al., 1989, Spruce et al., 1987). Vasoconstriction in the presence of glibenclamide suggests that K_{ATP} channels have a crucial role in the regulation of vascular tone (Samaha et al., 1992, Nelson et al., 1990a). Consistent with this finding, a loss of function mutation in SUR2B causes coronary vasospasm in humans (Smith et al., 2013).

Big conductance (BK) Ca^{2+}-activated K^+ channels (K_{Ca})

There are three types of K_{Ca}: Big conductance (BK_{Ca}), intermediate conductance (IK_{Ca}), and small conductance (SK_{Ca}) channels (Dong et al., 2016). BK_{Ca} channels are the type most robustly expressed in VSMCs (Neylon et al., 1999), and have a large conductance of 100-300 pS (Pantazis and Olcese, 2016). Similar to other K^+ channels in the vasculature, their main role in in VSMCs is regulating *Vm* and therefore blood vessel tone (Ledoux et al., 2006).

The BK_{Ca} channel is composed of eight subunits, four α-subunits that form the 11 transmembrane domain pore, and four auxiliary β-subunits (Knaus et al., 1994, Tanaka et al., 1997). The BK_{Ca} channel is sensitive to $[Ca^{2+}]_i$ and *Vm* (Cui et al., 1997, Magleby, 2003), and unlike the K_{ir} channels, BK_{Ca} channels are outwardly rectifying (Gonzalez-Perez and Lingle, 2019). In VSMCs, BK_{Ca} channels are localised near sites of Ca^{2+} release from the SR, which suggests they have a crucial role in coupling of $[Ca^{2+}]_i$ and vascular tone (Nelson et al., 1995, Lifshitz et al., 2011).

BK_{Ca} channels are blocked by paxilline, a tremorogenic fungal alkaloid, in a manner inversely dependent on BK_{Ca} channel P_o (Yu et al., 2016, Zhou and Lingle, 2014). The IC_{50} for paxilline was found to be ~10 nM when P_o was low, and 10 μM towards maximal Po (Zhou and Lingle, 2014). Taken together these findings suggests that BK_{Ca} channels are more potently blocked by paxilline in the closed state (Zhou and Lingle, 2014). Therefore, to dissect the role of BK_{Ca} channels in arteries, a concentration of paxilline ≥ 10 μM is required to ensure channel inhibition in a range of *Vm* and $[Ca^{2+}]_i$.

1.7.2. Ca^{2+} channels in VSMCs

Plasma membrane Ca^{2+}-permeable channels in VSMCs can be grouped into two main categories: *(i)* voltage-gated Ca^{2+} channels (VGCCs), and *(ii)* non-selective, non-voltage-gated cation channels (NSCCs).

Voltage-gated Ca^{2+} channels

L-type voltage gated Ca^{2+} (Ca_V) channels (VGCCs) provide the majority of the influx of Ca^{2+} influx required to trigger VSMC contraction (Catterall, 2011, Knot and Nelson, 1998). The “L” in L-type VGCCs is due to the long lasting inward currents mediated

during depolarisation by these channels (Zamponi et al., 2015). In VSMCs, L-type VGCCs initiate contraction by opening in response to a depolarised *Vm*, which facilitates an influx of Ca^{2+} and results in opening of SR localised Ca^{2+} channels (section 1.5) (Tsien, 1983, Bers, 2002). This facilitates a positive feedback loop that results in an overall increase in $[Ca^{2+}]_i$ and therefore VSMC contraction (Bannister and Beam, 2013, Catterall, 2011).

The Ca_v family of channels consists of 10 members with specialised functions; the CaV1.2 subfamily is mainly expressed in VSMCs (Catterall, 2011). L-type Ca_V channels are composed of five subunits forming a large complex. The $\alpha 1$ subunit forms the pore, and is connected by disulphide bonds to the glycoprotein $\alpha 2$ and δ subunits, and a transmembrane γ subunit. The β subunit is localised intracellularly (Takahashi et al., 1987). The $\alpha 1$ subunit is targeted by the 1,4-dihydropyridines (DHPs) class of Ca^{2+} channel blockers, which includes nifedipine (Catterall and Swanson, 2015, Hockerman et al., 1997). Nifedipine is used therapeutically to treat hypertension, and has also been used experimentally to dissect the role of Ca_V channels in various cell types.

1.7.3. Non-selective cation channels in VSMCs

In addition to via VGCCs, Ca^{2+} can enter VSMCs through non-selective cation channels (NSCCs), which are generally permeable to both monovalent and divalent cation channels. Two types of NSCCs are expressed in VSMCs: receptor-operated cation channels (ROCCs), and store-operated cation channels (SOCCs) (Large, 2002, McFadzean and Gibson, 2002, Leung et al., 2008).

SOCCs are plasma membrane ion channels activated by the depletion of Ca^{2+} from intracellular Ca^{2+} stores, and are therefore highly sensitive to $[Ca^{2+}]_i$. SOCCs are usually

a component in a biphasic Ca^{2+} signalling mechanism involving a combination of Ca^{2+} entry through Ca^{2+}-permeable channels on the plasma membrane, and Ca^{2+}-release from intracellular Ca^{2+} stores (Putney et al., 2017). SOCC channels were identified when thapsigargin was found to passively empty intracellular Ca^{2+} stores, independent of the IP_3 signalling cascade (Ali et al., 1985, Jackson et al., 1988), in addition to simultaneously activating plasma membrane Ca^{2+} channels (Takemura et al., 1989). The molecular identity of SOCCs have now been revealed; the Ca^{2+} release-activated Ca^{2+} modulator 1 (ORAI1) protein forms the pore of the channel, while the protein stromal interaction molecule 1 (STIM1) in the SR serves as the detector of Ca^{2+} levels (Ambudkar et al., 2017, Hogan, 2015).

ROCCs have been reported in a variety of vascular beds, and activated by a range of receptors (Wynne et al., 2009, Earley, 2006). Externally applied ATP acts on P2X receptors, and has been demonstrated to cause a rapid and transient membrane depolarisation of ear artery SM, caused by a NSCC with significant Ca^{2+} permeability (Benham and Tsien, 1987).

Another type of ROCCs are transient receptor potential (TRP) channels, a family of cation channels expressed in the vasculature with varying ionic specificity (Minke, 2010, Mulier et al., 2017). TRP channels were initially identified in *Drosophila*, and are thought to be responsible for ROCCs in VSMCs (Minke, 2010). TRP channels facilitate Ca^{2+} entry to the VSMC, and therefore have a role in excitation-contraction coupling and modulation of vascular tone (Earley and Brayden, 2015).

TRP channels are comprised of four subunits, each consisting of six transmembrane domains. The TRP pore is formed by a re-entrant loop between transmembrane domains five and six, with a short selectivity filter (Rosasco and Gordon, 2018). The N

and C termini are cytosolic, and interact to coordinate the four subunits (Liao et al., 2013, Cao et al., 2013, Rosasco and Gordon, 2018).

In humans, 28 isoforms of TRP channels have been identified, 11 of which are expressed in VSMCs (Earley and Brayden, 2015). TRP channels expressed in the vasculature are important in regulating vascular tone, and their dysfunction is implicated in cardiovascular disease. In experimental mouse models of hypertension, TRPC3 and TRPC6 channels have been associated with a chronic elevation in blood pressure (Mathar et al., 2010). In a hypertensive animal model TRPC3 was upregulated in arterial SMCs, which was accompanied by an increase in vascular contractility (Liu et al., 2009, Noorani et al., 2011).

1.7.4. Cl^- channels in VSMCs

Four types of Cl^- channels are expressed in VSMCs: voltage-gated Cl^- channels (ClCs), cystic fibrosis transmembrane receptor (CFTR), bestrophins, and CaCCs (Bulley and Jaggar, 2014, Duran et al., 2010). Cl^- channels are expressed in VSMCs across a variety of blood vessel types (White et al., 1995, Casteels et al., 1977, Smith and Jones, 1985, Van Renterghem and Lazdunski, 1993). Non-specific blockers of Cl^- current such as 4,4'-Diisothiocyano-2,2'-stilbenedisulfonic acid (DIDS) cause hyperpolarisation and blood vessel relaxation (Nelson et al., 1997). This data has been replicated by replacing extracellular Cl^- with methanesulfonate, which potentiated agonist-induced blood vessel contraction while K^+-mediated contractility was unaffected (Dai and Zhang, 2002, Dai and Zhang, 2001, Lamb and Barna, 1998).

ClCs are expressed in many tissue types, with ClC-3 expressed in the arterial SMCs (Hume et al., 2010, Bulley and Jaggar, 2014). ClC proteins are dimeric, with two identical

subunits composed of 18 α-helixes (Dutzler et al., 2002). ClC-3 proteins compensate for cell swelling in VSMCs, by stimulating compensatory mechanisms that re-establish cell volume (Eggermont et al., 2001, Guan et al., 2006). VSMC migration in pathologies such as atherosclerosis involves cell swelling and shrinkage. When ClC-3 was genetically deleted, migration of VSMCs was reduced, suggesting that ClC-3 and its role in Cl^- transport has a key role in vascular remodelling (Ganapathi et al., 2013).

CFTR is expressed in VSMCs (Robert et al., 2007, Robert et al., 2004), and is an ABC-binding cassette that also functions as a Cl^- channel (Liu et al., 2017). Activation of the cAMP pathway and pharmacological activators of CFTR relaxed isolated preconstricted aortic rings (Robert et al., 2004, Robert et al., 2005), however whether relaxation was due to cAMP or to CFTR activation remains to be established.

The bestrophin family contains four proteins, that are cyclic guanosine monophosphate (cGMP) dependent CaCCs that are independent of voltage regulation . A lower $[Ca^{2+}]_i$ is required to activate bestrophins than TMEM16x proteins (Piper and Large, 2004, Matchkov et al., 2005). The X-ray structure of bestrophin-1 has revealed that it exists as a pentamer, with each subunit composed of four α-helixes (Dickson et al., 2014).

Bestrophin-3 is expressed in rat aortic SMCs and mesenteric arteries (Piper and Large, 2004, Matchkov et al., 2013), expression of which was localised to areas of cGMP-dependent CaCC currents (Matchkov et al., 2009). Genetic deletion of bestrophin-3 reduced cGMP-dependent CaCC current but did not affect TMEM16x mediated CaCC current (Matchkov et al., 2009).

The TMEM16x family of CaCCs are the main focus of this DPhil project, therefore it will be reviewed in greater detail in section 1.8.

1.7.5. VSMC ion channels modulated by lipids

This section will focus on the lipids explored in this thesis, the intracellular signalling lipid PIP_2 and extracellular dietary polyunsaturated fatty acids (PUFAs) such as docosahexaenoic acid (DHA), and how they modulate VSMC ion channel activity.

Composition of the plasma membrane

Ion channel and transporters can be modulated by the lipids of the plasma membrane. Plasma membrane proteins and phospholipids are not uniformly distributed, and have been found to gather in more temporary and dynamic configurations (Alberts, 2008). Phospholipids and cholesterol form specialised plasma membrane domains known as lipid rafts (Kinoshita et al., 2017). Lipid rafts regulate signal transduction along the plasma membrane, mediating interactions between signalling proteins (Levental and Veatch, 2016, Simons and Toomre, 2000). Lipidomics suggests that lipid profiles vary between cell types (Klose et al., 2012), and are modulated by endogenous processes such as the cell cycle (Atilla-Gokcumen et al., 2014) and exogenous processes such as incorporation of dietary PUFAs (Abbott et al., 2012, Levental et al., 2016)

PIP_2 modulation of vascular ion channels

Phosphoinositides (PIs) are acidic phospholipids found in plasma membranes, whose main function is interacting with proteins to modulate their function (Falkenburger et al., 2010a). PIs typically represent less than 10% of phospholipids in mammalian cells, yet control many aspects of cellular life and death (Irvine, 2016, Balla, 2013). PIs can be rapidly cycled through phosphorylation and dephosphorylation at the 3', 4', and 5' positions of their inositol head groups to form phosphatidylinositol phosphates (PIPs,

Fig 1.6). PIPs modulate membrane protein activity, through targeting ion channels, pumps, and transporters. A variety of ion channels are modulated by PIP_2 such as K_v, K_{ir}, BK_{Ca}, Ca_V, TRP, and CaCC channels (Hille et al., 2015, Falkenburger et al., 2010a).

PIP_2 content in the plasma membrane is depleted by cleavage by PLC during Gq-PCR activation (discussed in more detail in section 1.4). PIP_2-sensitive ion channel activity therefore changes upon activation of the Gq-PCR. For example, the KCNQ K^+ current is supressed by the activation of M_1 muscarinic receptors (Falkenburger et al., 2010b, Suh and Hille, 2002, Zhang et al., 2003, Brown and Adams, 1980). As PIP_2 interacts with a number of ion channels, changes in PIP_2 levels can have a profound effect on the electrical activity of excitable and non-excitable cells, including VSMCs (Suh and Hille, 2008).

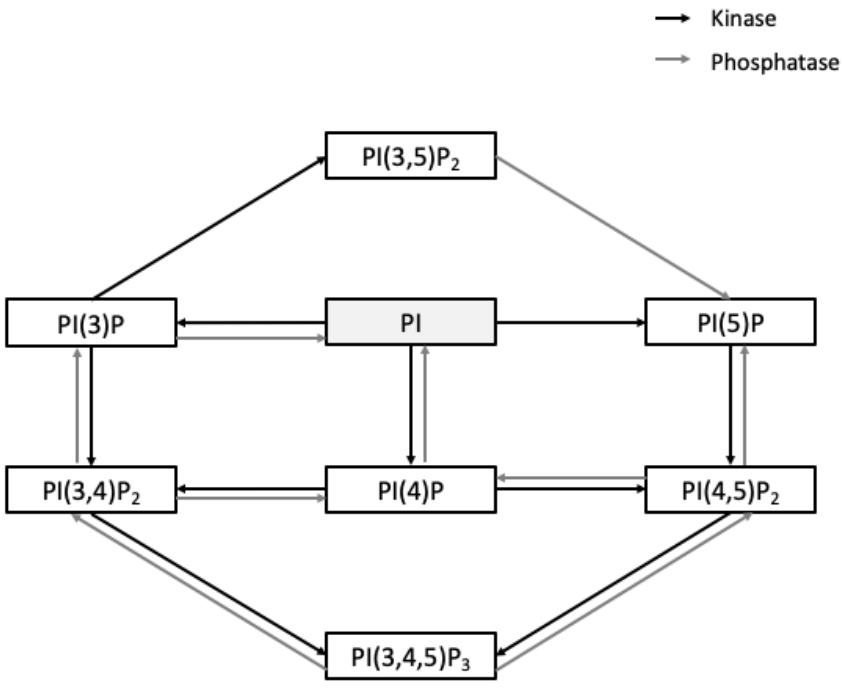

Figure 1.6. Synthesis and breakdown of phosphoinositides

Dietary fatty acid modulation of vascular ion channels

Omega-3 dietary PUFAs such as docosahexaenoic acid (DHA) and eicosapentaenoic acid (EPA) are typically found in oily fish, or are synthesised from the plant-derived PUFA α-linolenic acid (Peltomaa et al., 2017). Omega-3 refers to the position of the first carbon double bond, when counting from the carboxyl group. PUFAs are widely reported to have beneficial cardiovascular effects (Saravanan et al., 2010). Dietary supplementation of fish oils in humans results in a substantial increase in PUFAs in the blood plasma (Herold and Kinsella, 1986). Typical levels of PUFAs in the plasma is ~50 μM (De Caterina et al., 2000, Fraser et al., 2003, Siddiqui et al., 2008), although this can increase up to 400 μM (Siddiqui et al., 2008, Kuriki et al., 2002, Fraser et al., 2003, Bonaa et al., 1990). The ketogenic diet is used as a non-pharmacological treatment for epilepsy (Freeman et al., 1998, Cunnane et al., 2002), which significantly increases (to ~800 μM) the concentration of PUFAs in the plasma (Xu et al., 2008, Dahlin et al., 2007). Plasma concentrations are appropriate for the modulation of VSMC ion channels under physiological conditions (Elinder and Liin, 2017).

Dietary PUFAs can incorporate into the plasma membrane of cells including VSMCs. Experiments using dietary supplementation with PUFAs have demonstrated that membrane fatty acid composition is altered following chronic exposure (Levental et al., 2016, Abbott et al., 2012), as a result of favourable incorporation into the plasma membrane (Cao et al., 2006, Levental et al., 2016, Lands et al., 1990). In contrast to lipid raft domains, PUFAs do not pack tightly into organised pools (Wassall and Stillwell, 2008, Soni et al., 2008), and do not favour interactions with cholesterol (Pitman et al., 2004, Wassall and Stillwell, 2009). It has, however, been proposed that PUFAs regulate plasma membrane cholesterol-rich domains by disrupting their packing (Williams et al.,

2012). PUFAs can have a modulatory effect on plasma membrane proteins, which can be through direct interaction or via alterations to the lipid composition of the plasma membrane, which may affect membrane fluidity (Murphy, 1990).

Diets that are regularly high in oily fish, and therefore PUFAs, reduce the risk of sudden cardiac death (Siscovick et al., 2000, Burr et al., 1989). Overweight individuals who consumed salmon three times per week had a decreased diastolic blood pressure similar to that of omega-3 supplementation (Ramel et al., 2010), while dietary supplementation of DHA and EPA caused vasodilation and decreased diastolic blood pressure in dyslipidaemic and hypertensive patients (Bonaa et al., 1990, Nestel et al., 2002, Liu et al., 2011). Patients with hypercholesteremia had improved arterial flow following PUFA supplementation (Goodfellow et al., 2000).

One research group reports that DHA but not EPA has a vasodilatory effect in humans (Mori et al., 1999). Overweight male patients supplemented with 4 g per day DHA, EPA, or olive oil (placebo) exhibited a DHA mediated vasorelaxation (Mori et al., 2000). Forearm microcirculation blood-flow was less affected by vasoconstrictors such as norepinephrine following dietary supplementation with DHA (Mori et al., 2000). DHA alone was found to attenuate vasoconstriction, an endothelium-independent effect attributed to the DHA targeting the VSMCs (Mori et al., 2000). This study provides evidence that DHA and not EPA is responsible for the vasodilatory effect of PUFAs. It should be noted that dietary supplementation with PUFAs or high oily fish diet has no effect on human cholesterol levels (Harris, 1996).

VSMC ion channels such as K_v, BK_{Ca}, Ca_V, TRP, and CaCC channels are modulated by dietary PUFAs (Elinder and Liin, 2017, De Jesus-Perez et al., 2018, Boland and Drzewiecki, 2008), which provides a compelling link between PUFA ion channel

modulation and the vasodilatory properties of DHA. It is not fully understood which of these channel types are responsible for DHA-mediated vasorelaxation.

1.8. The Calcium-activated Chloride Channel encoded by the *TMEM16A* gene

CaCCs were first identified in in the 1980s in the Xenopus oocyte (Barish, 1983), where they play a pivotal role in the prevention of polyspermy (Kuruma and Hartzell, 1999, Miledi, 1982). After this initial discovery, CaCCs were identified in additional cell types, including SMCs (Large and Wang, 1996, Toland et al., 2000).

The molecular identity of CaCCs, had been elusive for several years. Candidates had been proposed including the Ca^{2+}-activated Cl^- channel (CLCA), which was identified when the gene was cloned from an expression library, and the purified protein behaved as a CaCC when incorporated in to artificial bilayers (Cunningham et al., 1995). However, some cell types that do not express CLCA do express native CaCCs (Papassotiriou et al., 2001), and there is no conclusive evidence that CLCA is a *bone fide* ion channel (Hartzell et al., 2009). Another proposed candidate was the *Drosophila* gene Tweety, that has homology to the human genes *hTTHY2* and *hTTYH3* (Suzuki, 2006, Suzuki and Mizuno, 2004). This protein appears to function as a Cl^- channel in heterologous expression systems, but has a much larger conductance than native CaCCs (Hussy, 1992, Fahmi et al., 1995). Bestrophins have also been proposed to constitute native CaCCs, and these proteins do form functional Cl^- channels (Barro-Soria et al., 2008). Mutations in the gene of human bestrophin-1 (hBest-1) results in defective Cl^- conduction (Hartzell et al., 2008) and their 3D structure has been recently determined (Miller et al., 2019).

However, the biophysical profile of bestrophin channels do not fully match that of native CaCCs in VSMCs.

Three independent research groups elucidated the molecular identity of TMEM16A as a CaCC in 2008 (Caputo et al., 2008, Schroeder et al., 2008, Yang et al., 2008). TMEM16A is expressed in numerous cell types, such as VSMCs, vascular endothelial cells, cardiomyocytes, interstitial cells of Cajal (ICC), as well as olfactory sensory, nociceptive, and somatosensory neurones (Ma et al., 2017, Oh and Jung, 2016, Wang et al., 2017, Ji et al., 2019). TMEM16A is a member of a 10 gene family.

1.8.1. TMEM16x family

The 10 member TMEM16x family are denoted by letters (with I missing, Fig 1.7). The TMEM16x proteins have different functional roles. TMEM16A and TMEM16B serve unambiguously as CaCCs, while TMEM16C, TMEM16D, TMEM16E, TMEM16F, TMEM16G, and TMEM16J function as Ca^{2+}-dependent phospholipid scramblases (Gyobu et al., 2016, Suzuki et al., 2013). TMEM16H, TMEM16J, and TMEM16K are poorly or not expressed on the plasma-membrane, and are proposed to have intracellular functions (Tian et al., 2012).

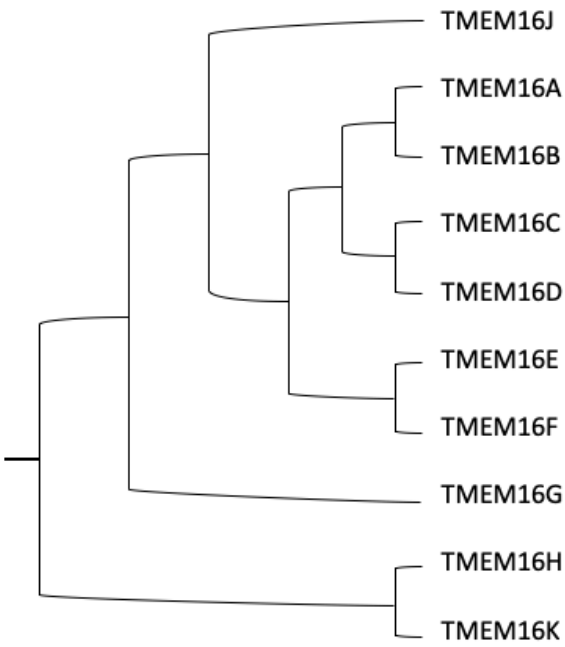

Figure 1.7. Human TMEM16x family phylogenetic tree

TMEM16F simultaneously behaves as a phospholipid scramblase and a non-specific anion channel (Suzuki et al., 2010, Brunner et al., 2014, Acheson, 2016). This protein has attracted significant interest from the research community involved in scramblases and channels, and are therefore studied in greater detail than other TMEM16x family members (Acheson, 2016).

Phospholipid scramblases are protein channels that lower the energy barrier for movement of lipids between the inner and outer leaflets of the plasma membrane, the composition of which effects fluidity and many cell signalling pathways (Suzuki et al., 2010, Malvezzi et al., 2013). The pore of TMEM16F is proposed to be hydrophilic, with phospholipid head groups being transported along the same conduction pathway as the ionic current (Whitlock and Hartzell, 2017). Mutations in TMEM16F cause Scott syndrome, a bleeding disorder resulting from dysfunctional phospholipid scrambling in

platelets (Yang et al., 2012, Suzuki et al., 2010). The truncating Scott syndrome mutation in TMEM16F is the only mutation in a TMEM16x protein to have been linked to a human disease so far.

TMEM16A gating mechanisms

The main gating factor of TMEM16A is intracellular Ca^{2+}. Voltage is also important as the effect of Ca^{2+} is more pronounced at positive *Vm* (Picollo et al., 2015, Pedemonte and Galietta, 2014, Hartzell et al., 2009). There a two hypotheses for this phenomenon: either Ca^{2+} binding occurs at a site within the membrane electric field and therefore is favoured at a depolarised *Vm*, or the channel possesses a voltage sensing domain that moves in response to changes in voltage (Picollo et al., 2015, Pedemonte and Galietta, 2014, Hartzell et al., 2009). However, inspection of the primary structure does not reveal any charged components analogous to the voltage sensor of voltage-gated channels (Contreras-Vite et al., 2016). Furthermore, the channel is not associated with gating currents like those observed in voltage-gated channels. This indicates that the first hypothesis is more plausible (Contreras-Vite et al., 2016).

Additional factors that affect TMEM16A gating are *(i)* the nature of the permeating ion (Sagheddu et al., 2010, Schroeder et al., 2008, Yang et al., 2008), which is not unprecedented in Cl^- channels (Jentsch and Pusch, 2018, Lisal and Maduke, 2009), *(ii)* extracellular protons which activate the channel (Cruz-Rangel et al., 2017), and *(iii)* as outlined below, lipids are also major regulators of the channel.

1.8.2. TMEM16A channel structure and function

The structure of TMEM16A was elusive until nearly ten years after the initial cloning of the TMEM16A gene. Previous to the determination of the structure, biochemical experiments demonstrated that TMEM16A exists as a homodimer with two independent pores (Sheridan et al., 2011, Fallah et al., 2011). This finding was confirmed in 2014 when the X-ray structure of the TMEM16A fungal homologue *Nectria haematococca* TMEM16 (nhTMEM16) was published (Brunner et al., 2014). NhTMEM16, like TMEM16F, functions as a phospholipid scramblase, and can therefore inform us about the structure of mammalian TMEM16x members, such as that TMEM16A and TMEM16F that share the same ion conduction pore (Lee et al., 2018, Jiang et al., 2017, Yu et al., 2015).

The structure of mouse TMEM16A has recently been elucidated using single-particle electron cryomicroscopy (cryo-EM), which can provide direct understanding of the structure/function relationship of human TMEM16A (Paulino et al., 2017, Dang et al., 2017). TMEM16A is a protein with ten α-helix transmembrane domains. All ten helices transverse the plasma membrane with various degrees of tilt (Paulino et al., 2017, Brunner et al., 2014). The N- and C-terminal domains are cytosolic and participate in an intra-subunit interaction. The TMEM16A subunits of the homodimer also interact via residues in the N-terminus α10 helix and the α3 helix at the cytoplasmic end (Paulino et al., 2017, Brunner et al., 2014). The ion conduction pore is formed by helices α4-α6, which surround a subunit cavity that houses the conserved Ca^{2+} binding site (Paulino et al., 2017, Brunner et al., 2014, Dang et al., 2017). Movement of the α6 helix is understood to facilitate channel opening and ion permeation, following binding of two Ca^{2+} (Paulino et al., 2017). Ca^{2+}-binding alters the electrostatic properties of the pore

region and causes a conformational change of the channel, directly coupling Ca^{2+}-binding and channel opening (Paulino et al., 2017). Figure 1.8 provides a diagrammatic representation of this structure.

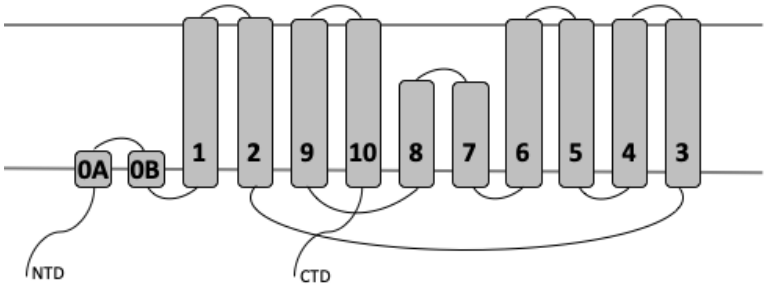

Figure 1.8. Structure of TMEM16A
Diagrammatic representation of TMEM16A, reproduced from (Ji et al., 2019).

Elucidating the TMEM16A Ca^{2+} binding site has been instrumental in beginning to understand how the channel operates at a molecular level. In 2014, using site-directed mutagenesis, it was demonstrated that the cytoplasmic α2-α3 loop structure is crucial for regulation of voltage and Ca^{2+}-sensitivity of TMEM16A (Xiao and Cui, 2014). Truncation of this site was found to be key in regulating channel activation and inactivation, and lead to a reduction in the Ca^{2+}-sensitivity (Strege et al., 2017, Peters et al., 2015). A mutagenesis study of α6-α8 resulted in the identification of five acidic amino acids as Ca^{2+}-binding residues: E654, E702, E705, E734, and D738 (Tien et al., 2014). The cryo-EM structure revealed that these residues form two well-defined Ca^{2+}-binding pockets (Dang et al., 2017).

1.8.3. Biophysical properties of cloned TMEM16A currents

Functional TMEM16A channels are outwardly rectifying Cl^- channels sensitive to voltage and $[Ca^{2+}]_i$ (Schroeder et al., 2008, Caputo et al., 2008). TMEM16A can be activated by <100 nM $[Ca^{2+}]_i$ (Adomaviciene et al., 2013, Ferrera et al., 2009). Human TMEM16A has been purified and reconstituted into proteoliposomes, which demonstrated that Ca^{2+} alone is sufficient to activate TMEM16A, independent of CaM (Terashima et al., 2013). TMEM16A is observed to have fast and slow gating mechanisms, regulated by extracellular Cl^- in combination with *Vm* (Cruz-Rangel et al., 2015). It has been observed that TMEM16A can be activated without $[Ca^{2+}]_i$ by strong membrane depolarisation of 200 mV (Cruz-Rangel et al., 2015, Contreras-Vite et al., 2016, Xiao et al., 2011). The combined Ca^{2+} and *Vm* TMEM16A gating is due to Ca^{2+} binding reducing the energy barrier required for channel opening at a given *Vm* (Zhang et al., 2014). The same study proposed that activated TMEM16A currents could be appropriately fitted with a double exponential; this indicates that at least two states are required for activation, each involving binding of a Ca^{2+} ion. A detailed Markov chain model with 12 states for TMEM16A has been developed to account for the complex regulation of TMEM16A by Ca^{2+}, voltage, and permeating ions (Contreras-Vite et al., 2016, Ji et al., 2019).

1.8.4. The TMEM16A channel pore

The determination of the TMEM16A structure has enabled the elucidation of the ion permeation pathway (Paulino et al., 2017, Dang et al., 2017). The open conformation of the TMEM16A pore appears to have a section in almost direct contact with the plasma membrane, and therefore it is partially lined with lipids (Paulino et al., 2017, Dang et al., 2017). It is therefore hypothesised that TMEM16A is sensitive to lipid modulation

due to the proximity of the pore region to the plasma membrane (Whitlock and Hartzell, 2017).

TMEM16A has an ionic permeability preference for ions larger than Cl^-, with an ionic permeability of $SCN^- > I^- > Br^- > Cl^- > F^-$ (Sagheddu et al., 2010, Schroeder et al., 2008, Yang et al., 2008, Adomaviciene et al., 2013). Both pores in the homodimer function as independent entities (Jeng et al., 2016, Lim et al., 2016). Chimeras exchanging pore regions between TMEM16A and TMEM16F have conferred scramblase activity to TMEM16A and prevented scramblase activity in TMEM16F (Jiang et al., 2017). Initially, the TMEM16F residues E313 and R432 in the extracellular region of the protein were identified as crucial for scramblase activity, alongside E352 and K353 in the cytoplasmic region (Bethel and Grabe, 2016). The studies outlined above suggest that ion and lipid transport in TMEM16x may involve similar structures. Additional studies revealed T333 in α4 and Y436 in α6 to be crucial for gating (Jiang et al., 2017), with mutations in T333 significantly reducing phospholipid scrambling (Jiang et al., 2017). The conductance of the TMEM16A channel is ~3 pS, which was determined by noise analysis as single channel data has not yet been reported (Ta et al., 2017, Adomaviciene et al., 2013).

1.8.5. The role of CaCCs in VSMC contraction

The existence of CaCCs in VSMCs had been proposed before the 2008 discovery of TMEM16A (Nelson et al., 1997, Matchkov et al., 2012, Hartzell et al., 2005, Large and Wang, 1996, Leblanc et al., 2005). TMEM16A is expressed in VSMCs, while expression of the CaCC TMEM16B is negligible (Manoury et al., 2010, Thomas-Gatewood et al., 2011, Davis et al., 2010).

Physiologically, TMEM16A is activated as a result of adrenergic, histaminergic, or cholinergic activation of the Gq-PCR signalling cascade (Byrne and Large, 1987, Janssen and Sims, 1993, Pacaud et al., 1989), which mediates an increase in $[Ca^{2+}]_i$ and activates TMEM16A. The proposition that TMEM16A opening facilitates an efflux of Cl^-, and leads to depolarisation of the VSMC plasma membrane was originally made by Large and Wang (1996), and was later reinforced by the work of others (Manoury et al., 2010). Depolarisation caused by TMEM16A leads to activation of L-type Ca_V channels, which facilitate Ca^{2+} influx, and results in VSMC contraction.

Consistent with this concept, the Gq-PCR α1-adrenergic receptor mediates contractility in VSMCs, and has recently been demonstrated to rely on Cl^- to provide the driving force for membrane depolarisation in isolated human blood vessels (obtained from surgical donors) (Mohanakumar et al., 2018). Cytosolic $[Cl^-]$ in VSMCs is maintained by plasma membrane localised transporters like the $Na^+/K^+/2Cl^-$ (NKCC1) cotransporter (Chipperfield and Harper, 2000). NKCC1 knockout mice have reduced vascular tone and reduced blood pressure, attributed to changes in E_{Cl} (Meyer et al., 2002).

Wire-myography in isolated murine blood vessels demonstrates that knock-down of TMEM16A reduces agonist-induced vascular contractility (Dam et al., 2014, Jensen et al., 2018). This effect can be replicated by inducing the myogenic response in blood vessels, where increases in intraluminal pressure induces Ca^{2+} sparks (detailed in section 1.6.3), which in turn activated TMEM16A and caused blood vessel contractility (Yip et al., 2018).

TMEM16A also has a role in the signal transduction of vasomotion, a process in which intermittent $[Ca^{2+}]_i$ release from intracellular stores causes oscillations in blood vessel tone (Peng et al., 2001). Vasomotion influences local blood flow and pressure, and can

become enhanced under conditions of low blood pressure and hypoperfusion to regulate tissue oxygenation (Intaglietta, 1991, Pradhan and Chakravarthy, 2011).

1.8.6. TMEM16A pharmacology

TMEM16A is an intriguing drug target for a variety of pathophysiological conditions, however its pharmacology is still at early stages of development (Huang et al., 2012). Pharmacological modulators of TMEM16A will be outlined here, with structures of modulators tested in this thesis presented in chapter 2.

Activators of TMEM16A from natural sources have been identified, such as ginsenoside Rb1 (GRb1) and resveratrol (RES) (Chai et al., 2017, Guo et al., 2017). Chemically synthesised activators of TMEM16A have also been identified. Naroylaminothiazole (Eact) has been reported to activate TMEM16A current in conditions of 0 $[Ca^{2+}]_i$ and tetrazolylbenzamide (Fact) potentiates TMEM16A current (Namkung et al., 2011c). Anthracene-9-carboxylic acid (A9C) has an activatory and inhibitory dual effect on TMEM16A, which suggests it has a role in channel gating (Ta et al., 2016).

Inhibitors of TMEM16A have been more comprehensively developed and studied, and can also be grouped into inhibitors from natural sources and chemically synthesised inhibitory molecules. Natural inhibitors of TMEM16A tend to be dietary, such as gallotannins, which are related to tannic acid and found in red wine and green tea (Namkung et al., 2010). Other examples include dietary PUFAs (De Jesus-Perez et al., 2018), 4-allyl-2-methoxyphenol (eugenol) found in clove oil (Yao et al., 2012), cholesterol (Sones et al., 2010), and flavonoid compounds such as luteolin, galangin, quercetin, and fisetin (Zhang et al., 2017). Chinese herbal medicine has also produced

some examples of TMEM16A inhibitors, such as shikonin (Jiang et al., 2016), and dehydroandrographolide (DP) (Sui et al., 2015).

Synthetic inhibitors of TMEM16A have been developed, with the most efficacious being 2-(4-chloro-2-methylphenoxy)-N-[(2-methoxyphenyl)methylideneamino]-acetamide (Ani9), which has reported selectivity for TMEM16A and is potent in the nM range (Seo et al., 2016). Other examples include 2-acylaminocycloalkylthiophene-3-carboxylic acid arylamides (AACTs) (Truong et al., 2017), N-((4-methoxy)-2-naphthyl)-5-nitroanthranilic acid (MONNA) (Oh et al., 2013), $CaCC_{inh}$-A01 (De La Fuente et al., 2008), and $T16A_{inh}$-A01 (Namkung et al., 2011a). Common Cl^- channel blockers also inhibit TMEM16A, such as niflumic acid (NFA), DIDS, and flufenamic acid (Liu et al., 2015b).

1.8.7. TMEM16A pathophysiology

TMEM16A is hypothesised to be a suitable drug target in the treatment of a variety of diseases, such as cancer, cystic fibrosis (CF), and hypertension (Ji et al., 2019, Huang et al., 2012).

TMEM16A is expressed in the airway epithelia (Namkung et al., 2011b), where it conducts Cl^- alongside CFTR (Benedetto et al., 2017, Lerias et al., 2018, Benedetto et al., 2019). TMEM16A is profoundly upregulated in CF and asthma (Huang et al., 2009, Kondo et al., 2017, Miner et al., 2017). CF is characterised by the dysfunction of the CFTR, a Cl^- channel that facilitates trans-epithelial Cl^- transport (Rafeeq and Murad, 2017). TMEM16A is hypothesised to be a suitable drug target, as increased TMEM16A-mediated Cl^- current would increase trans epithelial Cl^- secretion and may overcome the loss of CFTR channels in CF patients (Li et al., 2017, Pedemonte and Galietta, 2014).

TMEM16A is upregulated and overexpressed in a number of cancers, such as eosophageal cancer (Kashyap et al., 2009), pancreatic ductal adenocarcinoma (Sauter et al., 2014), colon cancer (Sui et al., 2014), head and neck squamous cell carcinoma (HNSCC) (Dixit et al., 2015), gastric cancer (GC) (Liu et al., 2015a), gastrointestinal (GI) stromal tumours (Espinosa et al., 2008), bladder cancer (Katoh and Katoh, 2003), and breast cancer (Britschgi et al., 2013).

Overexpression of TMEM16A promotes invasion, proliferation, and metastasis (Ayoub et al., 2010) and enhances cancer cell migration (Jacobsen et al., 2013), while inhibition of TMEM16A reduces tumour growth both *in vivo* and *ex vivo* (Duvvuri et al., 2012). TMEM16A knockdown decreases proliferation of a variety of cancer cell lines, for example PC-3 prostate cancer cells (Liu et al., 2012), in MDA-MB-415 breast cancer cells (Britschgi et al., 2013), and in esophageal squamous cell carcinoma (ESCC) KYSE30 and KYSE510 cells (Shi et al., 2013). Pharmacological and genetic silencing of overexpressed TMEM16A in human prostate carcinoma cells induces apoptosis (Song et al., 2018).

TMEM16A is expressed in intestinal epithelial cells (Namkung et al., 2011b), and has an important role in gastric mobility. TMEM16A is involved in generation of slow waves in the intestines, due to robust expression in the ICC (Sanders, 1996, Malysz et al., 2017). In TMEM16A knockout mice, intestinal slow waves fail to develop (Hwang et al., 2009). Upregulation of TMEM16A is implicated in irritable bowel syndrome (IBS) and colonic hypermobility (Lin and Yu, 2018).

TMEM16A is highly expressed in VSMCs (Davis et al., 2010, Oh and Jung, 2016, Thomas-Gatewood et al., 2011), and is thought that its dysfunction may contribute to cardiovascular diseases such as hypertension. Research carried out by the Tammaro group has demonstrated that TMEM16A is the characteristic slow-activating,

outwardly-rectifying CaCC current component of pulmonary VSMCs (Manoury et al., 2010). In addition to this, it has been demonstrated that disruption of TMEM16A in the vasculature reduces systemic blood pressure in a murine mouse model (Heinze et al., 2014).

TMEM16A is overexpressed in the VSMCs of a spontaneously hypertensive rat model (Wang et al., 2015), in basilar smooth muscle cells (Wang et al., 2012), and in cerebral artery SMCs (Wang et al., 2012). In humans, TMEM16A is markedly upregulated in pulmonary arterial smooth muscle cells (PASMC) during idiopathic pulmonary hypertension (IPAH) (Papp et al., 2019). Disease phenotype donor cells were isolated and cultured, and it was demonstrated that inhibition or knock-down of TMEM16A reduced cellular proliferation. Conversely, cells from healthy donors in which overexpression of TMEM16A was induced, produced an IPAH-like phenotype (Papp et al., 2019). Taken together, this data suggests that TMEM16A could be an interesting pharmacological target in the treatment of hypertension.

1.9. Hypothesis and aims

Following the recent elucidation of the TMEM16A structure, we are now aware that the TMEM16A pore region is in close proximity to the plasma membrane. I therefore hypothesise that TMEM16A is sensitive to the composition of the plasma membrane, and that TMEM16A can be modulated by both intracellular and extracellular lipids. As TMEM16A is expressed in VSMCs and provides a key mechanism of depolarisation, it is hypothesised that TMEM16A regulation by lipids represents an important pathway in the regulation of blood vessel tone.

The specific aims of this research project are:

- To study a range of known pharmacological modulators of TMEM16A, for use as tools to understand the contribution of TMEM16A to vascular contraction.
- To investigate the role of the intracellular signalling lipid PIP_2 on cloned TMEM16A channels.
- To examine the effect of the dietary lipid DHA on cloned and native TMEM16A channels, and understand how this interaction can affect blood vessel tone.

Chapter 2

Methodology

Chapter 2 - Methodology

2.1. Chemicals and reagents

All chemicals, enzymes for cell isolations, and standard salts for electrophysiological solutions were purchased from Sigma-Aldrich, UK, unless otherwise indicated. A list of the specialist reagents and DNA plasmids used in this thesis is presented in tables 2.1-2.3.

Compounds were usually dissolved in dimethyl sulfoxide (DMSO) (Sigma-Aldrich, UK), at an appropriate stock concentration, aliquoted, and stored at -20 °C. The final concentration of DMSO in electrophysiology solutions never exceeded 0.1%. The water-soluble PIP_2 analogue, dioctanoylglycerol PIP_2 (diC8-PIP_2), was dissolved in ddH_2O (double-distilled H_2O) (Qiagen, UK). DHA, EPA, DHA-methyl ester, and acetic acid were dissolved in 99.5% ethanol (Sigma-Aldrich, UK) and 0.05% ddH_2O, and were sonicated thrice for 5 seconds in experimental solutions before use. In chapter 4, diC8-PIP_2 is expressed in terms of both μg/ml and μM as both terms are used in the literature.

Table 2.1. Small-molecule modulators utilised in this thesis

Compound	Structure
A9C	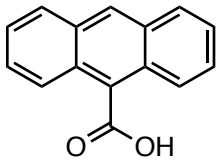
Ani9	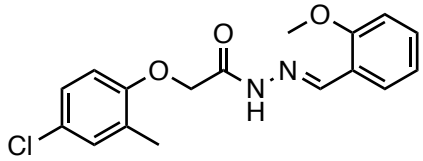

β-Cyclodextrin	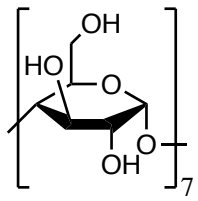
Bumetanide	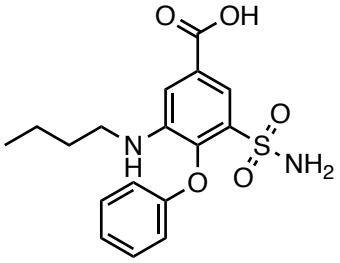
Clotrimazole	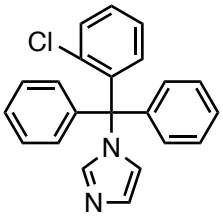
Eact	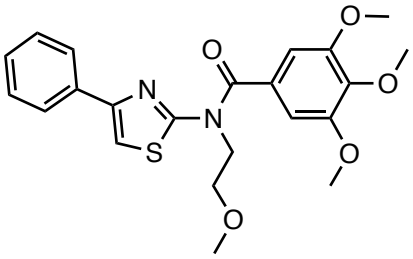
Glibenclamide	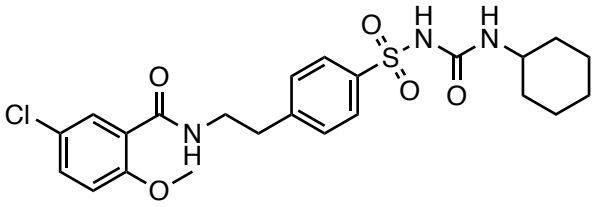
K-methanesulfonate	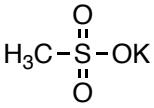
L-NAME	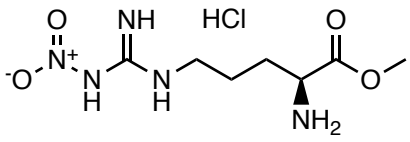
MONNA	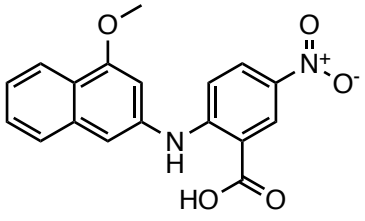

Nifedipine	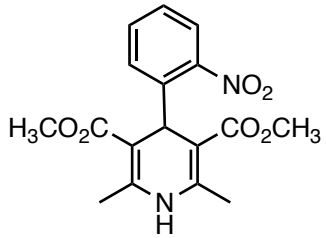
Paxilline	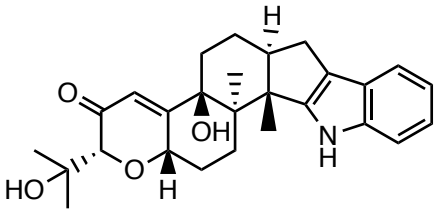
Phenylephrine	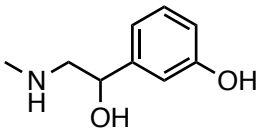

Table 2.2. Lipids utilised in this thesis

Compound	Structure
Acetic Acid	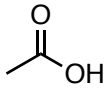
DHA	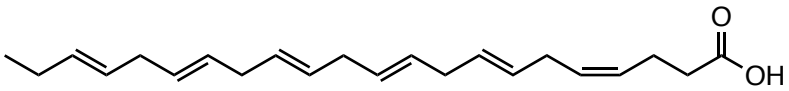
DHA-methyl ester	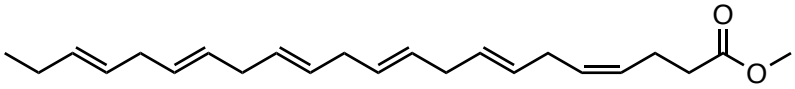
PIP_2	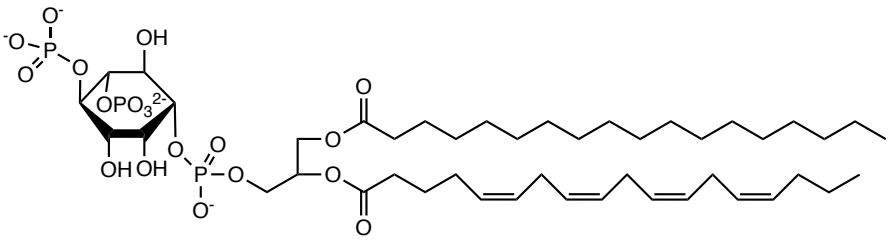
EPA	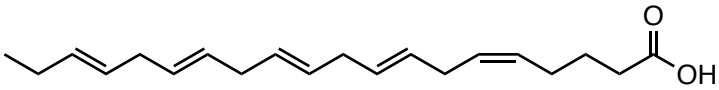

Table 2.3. DNA plasmids utilised for transfection in HEK-293T cells

DNA construct	Vector	Resistance	Gene accession number (Pubmed)	Provider
TMEM16A (isoform (ac))	PcDNA3.1	Ampicillin	NM_178642.5	OriGene, USA
TMEM16B (isoform (A))	PcDNA3.1	Ampicillin	NM_153589.2	OriGene, USA
DrVSP	pIRES-EGFP	Ampicillin	NM_001025458.1	Prof Y. Okamura, Osaka University
α1-adrenergic receptor	PcDNA3.1	Ampicillin	NM_000680	cDNA, USA
CD8	PcDNA3.1	Ampicillin	NM_001145873.1	OriGene, USA

2.2. Electrophysiological solutions

Standard solutions for recording CaCC currents

To record CaCC currents, a Cs^+ based intracellular solution was used, as detailed in table 2.4. This solution was referred to as "standard CaCC solutions". Replacement of K^+ with Cs^+ prevented endogenous K^+ currents in HEK-293T cells (Adomaviciene et al., 2013, Tammaro et al., 2005). Osmolarity was maintained at ~300 mOsm for the intracellular solution and ~330 mOsm for extracellular solutions, and adjusted as required with D-Mannitol.

Table 2.4. Standard CaCC intracellular solution.

Compound	Concentration (mM)
CsCl	130
EGTA/HEDTA	10
$MgCl_2$	1
HEPES	10
$CaCl_2$	See table 2.6
pH to 7.3 with NaOH	

Table 2.5. Standard CaCC extracellular solution.

Compound	Concentration (mM)
NaCl	150
$CaCl_2$	1
$MgCl_2$	1
Glucose	10
D-Manitol	10
HEPES	10
pH to 7.4 with NaOH	

Standard CaCC Solutions - Adjusting intracellular Ca^{2+} concentrations

EGTA or HEDTA were used to obtain different levels of free intracellular Ca^{2+} ($[Ca^{2+}]_i$) according to calculations using Patcher's Power tool software (Dr Mendez and Dr Wurriehausen, Max Planck Institute). These two different chelators were used due to their differing affinities for Ca^{2+} which make them suitable to obtain different degrees of free $[Ca^{2+}]_i$ (McGuigan and Stumpff, 2013). Specifically, for 0 and 0.3 μM free $[Ca^{2+}]_i$, EGTA was used as a chelator, and for all $[Ca^{2+}]_i$ above this equimolar HEDTA was used.

Concentrations of $CaCl_2$ required to produce a given $[Ca^{2+}]_i$ are detailed in Table 2.6.

Table 2.6. Adjusting $[Ca^{2+}]_i$ in standard CaCC intracellular solutions

Concentration $CaCl_2$ (mM)	Ca^{2+} chelator	$[Ca^{2+}]_i$ (μM)
-	EGTA	0
8	EGTA	0.3
2.1	HEDTA	0.6
3.1	HEDTA	1
4.8	HEDTA	2
7.8	HEDTA	12
9	HEDTA	78

Solutions for recording CaCC currents in PIP_2 recovery experiments

Experiments in chapter 4 required the inclusion of 1 mM MgATP to the standard CaCC intracellular solution to facilitate re-synthesis of endogenous PIP_2 by PIP 5-kinase type I γ (PI5K). This enabled PIP_2 to be re-synthesised following depletion of endogenous PIP_2 by *danio rerio* voltage-sensitive phosphatase (DrVSP). The resulting solution contained 0.3 μM free $[Ca^{2+}]_i$. These experiments were carried out with the standard CaCC extracellular solution.

Low EGTA CaCC intracellular solution

"Low EGTA CaCC intracellular solution" was used for experiments involving TMEM16A co-transfected with the α1-adrenergic receptor (chapters 4 and 5). Low EGTA solutions

were used to demonstrate the effects of Ca^{2+} release from intracellular Ca^{2+} stores on TMEM16A channels, as the EGTA concentration is low and therefore Ca^{2+} ions released from the SR are not rapidly buffered. This formulation results in a CaCC solution containing 0.21 μM free $[Ca^{2+}]_i$, summarised in table 2.7.

Table 2.7. Low EGTA CaCC intracellular solution

Compound	Concentration (mM)
CsCl	130
EGTA	1.5
$MgCl_2$	1
$CaCl_2$	1
HEPES	10
pH to 7.3 with NaOH	

Solutions for recording of cationic currents in VSMCs

Experiments designed to study cationic currents of VSMCs (chapters 3 and 5) required intracellular and extracellular solutions containing ionic components in concentrations typically found in VSMCs (tables 2.8 and 2.9). In the intact cell, the $[Ca^{2+}]_i$ was <10 nM to prevent activation of CaCC currents in VSMCs.

Table 2.8. Standard cationic extracellular solution

Compound	Concentration (mM)
NaCl	140
KCl	5.4
$MgCl_2$	1
$CaCl_2$	1.8
HEPES	10
D-glucose	10
pH 7.4 with NaOH	

Table 2.9. Standard cationic intracellular solution.

Compound	Concentration (mM)
NaCl	10
K-Aspartate	80
KCl	50
$MgCl_2$	1
EGTA	10
HEPES	10
$CaCl_2$	3
pH 7.4 with NaOH	

Solutions for recording Ca_V currents in VSMCs

To record Ca_V currents in VSMCs (chapters 3 and 5), K^+ was replaced with Cs^+ in the intracellular solution to inhibit endogenous K^+ channel activity. Extracellular Ca^{2+} was replaced with Ba^{2+}, to induce Ba^{2+} currents through Ca_V channels (tables 2.10 and 2.11). Ba^{2+} has a greater permeability through Ca_V channels, and reduces Ca^{2+}-dependent inactivation of these channels, which favours detection of Ca_V channel activity (Rorsman et al., 2018, Tammaro et al., 2001, Tammaro et al., 2005).

Table 2.10. Standard Ca_V extracellular solution.

Compound	Concentration (mM)
NaCl	104
CsCl	5.4
TEA-Cl	20
$BaCl_2$	5
$MgCl_2$	1
NaH_2PO_4	1
D-glucose	10
HEPES	5
pH 7.4 with NaOH	

Table 2.11. Standard Ca_V intracellular solution.

Compound	Concentration (mM)
CsCl	112
Na_2-ATP	3
HEPES	5
EGTA	10
$MgSO_4.7H_2O$	1
pH 7.4 with NaOH	

Solutions for cell isolation

Aortic SMCs were isolated and stored in dissociation medium (DM) (table 2.12), as described fully in section 2.6.

Table 2.12. Dissociation medium (DM).

Compound	Concentration (mM)
NaCl	110
KCl	5
HEPES	10
KH_2PO_4	0.5
NaH_2PO_4	0.5
Taurine	10
EDTA	10
D-glucose	10
$CaCl_2$	0.16
$MgCl_2$	2
Phenol red	0.03
pH to 7.3 with NaOH	

Solutions for myography experiments

Isolated aortic rings were dissected, stored, and studied using myography in physiological salt solution (PSS) (table 2.13). Experiments in chapter 5 involve myography under conditions of low $[Cl^-]_o$ PSS. In these experiments, [NaCl] was reduced in the PSS, and replaced with equimolar Na-methanesulfonate (table 2.14).

Table 2.13. Composition of standard PSS solution.

Compound	Concentration (mM)
NaCl	122
KCl	5
HEPES	10
KH_2PO_4	0.5
NaH_2PO_4	0.5
$MgCl_2$	1
$CaCl_2$	1.8
D-glucose	11
pH 7.4 with NaOH	

Table 2.14. Low Cl^- PSS solution.

Compound	Concentration (mM)
NaCl	22
KCl	5
HEPES	10
KH_2PO_4	0.5
NaH_2PO_4	0.5
$MgCl_2$	1
$CaCl_2$	1.8
Glucose	11
Na-methanesulfonate	100
pH 7.4 with NaOH	

2.3. Use of animals

All animal care and experiments were approved by the University of Oxford Ethics Committee and were in compliance with the UK Scientific Procedures (Animals) act, 1968. Male mice (C57BL6) were culled aged 8-10 weeks using a Schedule 1 method in accordance with UK Home Office guidelines.

2.3.1. Power calculations

Power calculations were carried out prior to experimentation for this project, to estimate the number of mice required for this study. The following factors were taken into consideration when carrying out power calculations (Festing, 2002, Festing and Altman, 2002, Festing, 2016): *(i)* the effect size of biological interest; *(ii)* the standard

deviation; *(iii)* the significance level; *(iv)* the desired power of the experiment; *(v)* selection of appropriate statistical test. The sections below provide details on how these factors were considered.

The magnitude of a biologically significant difference

For measurements of VSMC currents recorded in voltage-clamp mode during electrophysiological recording, a change of ~5% was considered significant. This is because the input resistance is high in VSMCs and therefore small changes in ion channel activity equate to significant changes in *Vm* (Nelson et al., 1990b).

During myography experiments, changes of ~5% were also considered significant, as these changes are sufficient to affect blood vessel diameter, which significantly impacts blood flow (as outlined in section 1.2.1).

Precision and variance measurements within each sample

The magnitude of standard deviation of each variable have been obtained from experiments previously carried out in the Tammaro research group, or from relevant published papers (Adomaviciene et al., 2013, Manoury et al., 2010, Rorsman et al., 2018).

The significance level of the test

Significance level was fixed at 5% (p=0.05). This is a threshold commonly used in biomedical research (Festing, 2016).

Desired statistical power

The power of the binary hypothesis test is set at 80%, a value commonly used in biomedical research. This value reflects the probability of the test correctly rejecting the null hypothesis (Festing, 2016).

Statistical tests

Statistical comparison of the variables measured involved a paired or unpaired Student's t-test, or an ANOVA as detailed in section 2.10.

Sample size

The program G-Power (Faul et al., 2007) was used to perform the calculation for the number of animals required for each experiment in the proposal. Achieving all aims in the project will require a series of electrophysiological experiments involving isolated VSMCs, as well as on intact aortic vessels using the myography setup. The total number of mice used for this research was calculated as follows:

Aim 1 – Studies involving freshly isolated VSMCs

VSMCs experiments will require n≥5 animals, with analysis of n≥7 cells per condition. During patch-clamp electrophysiology, only cells that maintain high seal resistance for the entire duration of the experiment (assessed at the beginning and the end of each experiment) could be used for data analysis. Based previous experience with experiments of this type in the Tammaro group, we anticipated that a maximum of five cells could be successfully recorded per day. Eight pharmacological agents were used for this set of experiments. These modulators were used in various combinations to

study CaCC, cationic, and Ca_v currents (table 2.1 and table 2.2). Cells obtained for TMEM16A heterozygous KO model were studied using the same methodology.

Therefore the number of mice required for these sets of experiments was estimated as: 8 (cells) x 11 (conditions (pharmacological agents and electrophysiological solutions)) / 5 (cells patch-clamped per preparation) = 18 mice

Aim 2 – Studies involving isolated aortic rings in the myography setup

Myography experiments will require n≥5 animals, with analysis of n≥7 aortic rings per condition. The myography setup has two chambers, so two experiments were conducted in parallel. Due to the length of the experiments, four aortic rings could be studied per mouse on a given day. However, occasionally fewer aortic rings were obtained due to variability during dissection. Eight pharmacological agents were used for this set of experiments. These modulators were used in various combinations to study aortic contraction, which was also studied in low $[PSS]_e$ (table 2.1 and table 2.2). Aortic rings obtained from the TMEM16A heterozygous KO model were studied using the same methodology.

Therefore: 7 (aortic rings) x 13 (experimental conditions) / 4 (aortic rings per preparation) = 23 mice

Overall power calculation

Studies involving freshly isolated cardiomyocytes were not included in these power calculations as they were kindly donated by Razik Mu-u-Min the Terrar/Lei groups.

Total:

Odd-sized litters and bias to a particular genotype or gender are common. Therefore, 5% extra mice are required to allow for such variations.

Minimal number of mice required for these studies:

41 mice (Aim1 + Aim2 + Aim 3) + 5% = 44 mice

2.4. Mice with deletion of one allele of the TMEM16A gene

2.4.1. Generation of heterozygous TMEM16A-KO mice

TMEM16A knock-out mice were obtained through a collaboration with Professor Jason Rock (University of California, San Francisco, USA) and Professor Brian Harfe (Duke University, North Carolina, USA). The generation of these transgenic mice is described in detail in (Rock et al., 2008). Briefly, exon 12 of TMEM16A gene was removed resulting in deletion of 53 amino acids in the TM2 domain and the extracellular link between TM1 and TM2 domains. This deletion also induced frameshift mutation 3' of the deletion that led to out-of-frame errors and premature termination codon 40 amino acids downstream of the deletion. The C-termini was then located in the extracellular domain as a result of the deletion, which prevented translation of the conserved DUF590 domain. The null allele was introduced into murine embryonic stem cells via homologous recombination. Cells expressing the construct were selected using neomycin as the vector encompassed a neomycin resistance cassette.

The heterozygous TMEM16A-KO (knock-out) strain was established on a C57Bl6 background. Homozygous TMEM16A-KO died in utero or soon after birth (Rock et al., 2008), therefore it was not possible to obtain a homozygous KO for functional studies. The heterozygous TMEM16A-KO mice displayed normal life span and reduced

expression of TMEM16A channels in various tissues (Dixon et al., 2012, Faria et al., 2014, Huang et al., 2009, Ousingsawat et al., 2009). This includes studies carried out within the Tammaro group by Hannah Garnet (unpublished data). Wild-type and heterozygous TMEM16A-KO mice were used at age 8-10 weeks, as previous analysis has shown no sex difference. Heterozygous TMEM16A-KO mice were used in this project as a model of loss of TMEM16A function in arteries.

2.4.2. DNA extraction for genotyping

Genotyping of wild-type and transgenic mice was performed using DNA obtained from ear punches taken soon after birth. Ear punches were incubated overnight at 55°C in 500 µl cell lysis solution (Qiagen, UK) supplemented with 0.01% proteinase K (Invitrogen, UK). Samples were then vortexed. Phenol:chloroform (500 µl) was added to promote the partitioning of lipids and cellular debris into the organic phase, leaving the isolated DNA in the aqueous phase (Schiebelhut et al., 2017). Samples were then vortexed, and centrifuged at 3,500 G for 5 minutes. The upper aqueous layer containing genomic DNA was transferred to a new Eppendorf tube and 500 µl ice-cold isopropanol added to precipitate the DNA from the solution. Samples were vortexed and centrifuged at 3,500 G for a further 20 minutes. The supernatant was removed and the DNA pellet washed in 500 µl 70% ethanol during a 5-minute centrifugation at 3,500 G. All centrifugation steps were performed at 4 °C and samples were processed on ice. The ethanol supernatant was discarded and the DNA pellet dried for 10 minutes at 37 °C. DNA was eluted in 100 µl in RNAse-free H_2O at 55 °C for 60 minutes. The DNA concentration was assessed using a Nanodrop 2000c (Thermo Scientific, UK) spectrophotometer.

2.4.3. Quantification of plasmid DNA

DNA concentrations were determined using a Nanodrop 2000c (Thermo Scientific, UK) spectrophotometer. The DNA concentration was established based on its ability to absorb UV light, according to the Beer-Lambert-Bouguer Law (Abitan et al., 2008). The higher the amount of light absorbed the more concentrated the sample. DNA sample absorbance was measured at three wavelengths, 230, 260 and 280 nm. At 260 nm an optical density (OD) of 1 corresponds to 50 µg/ml of double stranded DNA (dsDNA) (Orkin, 1990). The OD ratios of the absorbances at different wavelengths allows the purity of the DNA sample to be assessed. The DNA was 30-500 ng/µl depending on the amount of tissue used. This depended on the number of ear clips obtained from the mouse (i.e. one or two, for identification purposes).

2.4.4. Genotyping

Heterozygous TMEM16A-KO samples were identified due to the presence of the neomycin cassette, which was used during the generation of the mutant mouse strain to select for murine stem cells containing the modified gene. Therefore, detection of the neomycin cassette was used to differentiate the homozygous TMEM16A-KO from the wild-type mice, as the wild-type mice did not endogenously contain this DNA sequence.

PCR was used to detect the presence of the TMEM16A gene and the neomycin cassette. Detection of the TMEM16A gene alone was observed in the wild-type, while detection of both the TMEM16A gene and the neomycin cassette indicated a heterozygous KO animal. The HotStarTaq Master Mix kit (Qiagen, UK) was used per the manufacturer's instructions. Briefly, genomic DNA from individual samples was mixed with HotStarTaq

Master Mix, which contained HotStarTaq DNA Polymerase in PCR Buffer containing $MgCl_2$ and nucleoside triphosphate (dNTP), forward and reverse primers, and ddH_2O. This resulted in a total PCR reaction volume of 10 μl (tables 2.15 and 2.16).

Table 2.15. TMEM16A and Neomycin primers for PCR genotyping reaction.

Gene	Direction	Sequence
TMEM16A	Fw	5'- CCTATGACTGCCAGGGACGCCC-3'
	Rv	5'- TGTTCCTGTCCCTGCAATGCGG-3'
Neomycin	Fw	5'- GACGCCCTCCATTGACCC-3'
	Rv	5'- GGAGTAGAAGGTGGCGCGAAG-3'

Table 2.16. Contents of genotyping PCR reaction.

Component	Volume (μL)
HotStarTaq Master Mix	5
ddH_2O	3
Fw Primer	0.5
Rv primer	0.5
Sample DNA	1

The PCR reaction involved an initial denaturing step of 94 °C for five minutes, before 38 cycles involving brief steps for denaturing, annealing, and amplification. This was followed by a final elongation period of five minutes at 72 °C. The exact duration and conditions are reported in tables 2.17 and 2.18.

Table 2.17. TMEM16A PCR genotyping protocol

Temperature (°C)	Time (min)	Cycles
94	5	1
94	0.5	
61	0.5	38
72	0.75	
72	7	1
4	Hold	-

Table 2.18. Neomycin PCR genotyping protocol

Temperature (°C)	Time (min)	Cycles
94	5	1
94	0.5	
57	0.5	38
72	0.75	
72	7	1
4	Hold	-

PCR products were mixed with 5x loading dye (Qiagen, UK) before running on a 1 % agarose gel supplemented with 0.005 % ethidium bromide (EtBr) at 90 mV for 45-60 minutes in tris-actetate EDTA (TAE) buffer (EMD Millipore). EtBr is a fluorescent DNA intercalator which increases its fluorescence ~25 fold upon binding dsDNA. In aqueous solutions, EtBr is excited at 526 nm, and emits at a wavelength of 590 nm (Severini and Morgan, 1991, Bechtol et al., 1994). DNA within the agarose gel was therefore visualised by exposure to ultraviolet light. Both wild-type and heterozygous TMEM16A-KO PCR

products produced a band of ~300 base pairs (bp). Heterozygous TMEM16A-KO mice produced a PCR product for both TMEM16A and Neomycin PCR reactions at ~300 bp and ~400 bp, respectively.

2.5. Cell preparation

2.5.1. Cell culture and transfection

Human embryonic kidney 293T (HEK-293T) cells were obtained from American Type Culture Collection (ATCC). HEK-293T cells are derived from HEK-293 cells, and are widely used as a heterologous expression system for ion channel research (Adomaviciene et al., 2013, Ta et al., 2016). They are particularly well suited to Cl^- channel experiments as there are no or very limited endogenous Cl^- channels expressed (Adomaviciene et al., 2013). The "T" in HEK-293T refers to the expression of Simian Virus 40 (SV40) large T-antigen which increases transfection efficiency of viral plasmids containing SV40 origin of replication (Lin et al., 2014). This T-antigen binds to cell cycle inhibitor proteins, which forces the cell to enter the cell cycle more frequently and therefore increases the amplification of transfected plasmids, thus creating a greater transfection efficiency (Lin et al., 2014).

HEK-293T cells were cultured in Dulbecco's Modified Eagle's Medium F-12 (Sigma-Aldrich, UK) supplemented with 10% Foetal Bovine Serum (FBS) (Sigma-Aldrich, UK) and 0.5% Gentamicin (Sigma-Aldrich, UK). Cells were grown at 37 °C and 5% CO_2, in a humidified atmosphere. The media was replaced every two days and cells were passaged at a confluence of ~80%.

HEK-293T cell passaging protocol for growth in T25 flasks (Corning, UK).

1. HEK-293T cells were washed with 5 ml Dulbecco's Phosphate-Buffered Saline

solution (DPBS) (Thermo Fisher Scientific, UK).

2. Cells were incubated with 1 ml trypsin (Sigma-Aldrich, UK) at 37 °C for 30 seconds.
3. Once cells were detached from the bottom of the flask, 4 ml culture medium was added to deactivate the trypsin.
4. Cells were dispersed and then centrifuged at 0.2 G for 3 minutes.
5. The pellet was then resuspended in 4 ml culture medium.
6. Flasks were seeded in a 1:4 or 1:8 ratio for flasks ready for culturing in 2 or 3 days, respectively.
7. Cells for use in patch-clamp experiments were counted using a haemocytometer.
8. Approximately 50,000 cells were seeded in 35 mm tissue culture dishes (Corning, UK), and cultured for 24 hours prior to transfection.

Transient transfection was used to induce expression of the gene of interest. Each dish of HEK-293T cells were transfected with 0.6 – 1 µg plasmid DNA for a given TMEM16x isoform, and 0.2 µg CD8 using FUGENE HD (Promega, UK) transfection reagent. FUGENE HD is a lipid-based method of transfection, which enables the DNA to be enveloped in a monolayer of lipids and is taken up into the cell by endocytosis (Jacobsen et al., 2004). DNA and FUGENE HD were mixed in 50 µl culture medium. Every 1 µg of total DNA transfected required 1.5 µl of FUGENE HD. The culture medium, DNA, and transfection reagent mixture were added to HEK-293T cells plated 24 hours previously. After incubation for 14 to 20 hours, cell were washed with extracellular solution and exposed to 0.6 µl Dynabeads, which are anti-CD8 antibody coated beads (Invitrogen, UK). Anti-CD8 antibody coated beads bind to cells expressing the transfected CD8 membrane

antigen, which is a marker for likely co-transfection of the gene of interest (Jurman et al., 1994).

2.6. Isolation of native VSMCs

Wild-type C57BL6 mice at age 8-10 weeks were culled by cervical dislocation as outlined in section 2.3. The chest was opened at the diaphragm, and the ribcage opened at the sternum. The heart and lungs were moved and the descending aorta was dissected, and immediately submerged in ice-cold PSS (table 2.12). The isolated aorta was cleaned of connecting tissue and perivascular fat, using fine forceps and scissors under a stereo-microscope (Leica, zoom 2000). The cleaned aorta was cut longitudinally, and then laterally. The pieces of aorta were then washed with ice-cold PSS and transferred into DM (table 2.12).

The pieces of aorta were incubated at 4 °C for 1 hour in DM containing 1.5 mg/ml papain (Sigma-Aldrich, UK) to allow the papain to diffuse into the tissue. Papain is a cysteine protease that becomes activated when the sulphydryl groups are reduced. It was then activated during an incubation for 5 minutes at 37 °C, with 0.5 mg/ml of the reducing agent dithiothreitol (DTT). The artery pieces were then transferred to DM containing 1.4 mg/ml of collagenase Type 1 from Clostridium histolyticum at 37 °C for 4 minutes. Collagenase has endopeptidase activity that breaks down collagen in the connective tissue. The aortic pieces were then washed twice in DM at room temperature, and then triturated using a polished glass pipette to liberate the aortic VSMCs. VSMCs were stored in DM on ice for use in electrophysiological experiments on the same day.

A drop of cell suspension was placed on a 35 mm tissue culture dish (Corning, UK), and left for ~5 minutes to allow cells to adhere. Appropriate extracellular solution was

added, and VSMCs were used in patch-clamp electrophysiology experiments as described in 2.8.2.

2.7. Molecular biology

2.7.1. Amplification of plasmid DNA

All DNA constructs were subcloned into a vector containing an antibiotic-resistant DNA sequence which allowed selection of bacteria cells that contained the DNA-vector construct of interest (table 2.3). The plasmid DNA was transformed into a 50 µl aliquot of Subcloning Efficiency DH5α Competent Cells (Invitrogen, UK), a strain of Escherichia Coli that have been modified to become non-infectious to humans (Hanahan, 1983). To summarise, ~100 ng of plasmid was added to the DH5α cells, which were subsequently incubated on ice for 30 minutes. The plasmid and cells were then heat-shocked at 42°C for 20 seconds to enable DNA uptake by the bacteria. The transformed bacterial cells were incubated with super optimal broth with catabolite repression (SOC medium) in a shaker at 3000 rpm and 37 °C for an hour (Benchtop Shaking Incubator 222DS, Labnet International). These cells were then evenly spread on a lysogeny broth (LB)-ampicillin agar plate and incubated at 37 °C overnight. Only cells that had incorporated the plasmid were therefore antibiotic-resistant and grew on the plate. A single colony of bacteria was inoculated into a 5 or 100 ml of LB-broth containing ampicillin and incubated in 37 °C shaker (at 3000 rpm, Benchtop Shaking Incubator 222DS, Labnet International) for ~16 hours. Bacteria expanded in this way were used for DNA purification as described below. Plasmids utilised in this thesis are summarised in table 2.3.

2.7.2. Extraction and purification of plasmid DNA

Plasmid DNA was extracted and purified using either QIAprep Spin Miniprep kit (Qiagen, UK) or HiSpeed Plasmid Midi Kit (Qiagen, UK), which allow extraction of 30 μg/ml or 600 μg/ml, respectively. Briefly, the bacterial cells were lysed with alkaline detergents and pelleted via centrifugation. The lysate containing DNA was neutralised and adsorbed onto a silica membrane in high salt solution. The membrane was washed with ethanol to remove any contamination. The DNA was eluted with a buffer containing Tris and EDTA to solubilise DNA. DNA was using a Nanodrop 2000c (Thermo Scientific, UK) spectrophotometer (described fully in section 2.4.3).

2.7.3. Site directed mutagenesis

TMEM16A and TMEM16B chimeras were produced in order to assess potential residues involved in PIP_2 binding. TMEM16A residues involved in PIP_2 binding were identified by Remco Jongkind (Tammaro group) in collaboration with Dr Phill Stansfeld (Departmemt of Biochemistry, University of Oxford). A brief account of the work of Remco Jongkind is given below.

The crystal structure of the fungal nhTMEM16 protein (a TMEM16A structural homologue) was elucidated in 2014, at a resolution of 3.3 Å (Brunner et al., 2014). It was therefore used as a template for generating a homology model of TMEM16A. The sequence alignment was manually adjusted to achieve the best possible fit of the crystal structure. Multiple homology models were generated and evaluated based on a set of pre-defined criteria. A total of 16 viable TMEM16A homology models were generated, and evaluated based on the following criteria. Root-Mean-Square deviation (RMSD) was applied to the crystal structure template, stability, energy minimisation and the absence

of stereochemically persisting errors. The model with the lowest RMSD, highest stability, lowest Gibbs free energy after energy minimisation, and no stereochemically persisting errors was selected. The homology model that best satisfied these pre-defined criteria was selected for use in this study.

Molecular dynamic simulations were executed using Gromacs (version 4.5.3) (Hess et al., 2008). Self-assembly coarse grain simulations in mixed lipid bilayer systems were run at 323 K for 1.1 μs using an adapted version (Bond et al., 2008) of the MARTINI force field (Marrink et al., 2007, Monticelli et al., 2008). Coarse grain resolution was favoured over atomistic resolution, as for protein lipid interaction accuracy is similar, and computational costs are lower (Stansfeld and Sansom, 2011). Initial 100 ns of the simulation were not included in the analysis to allow assembly and stabilisation of the phospholipid bilayer. The lipids constituting the phospholipid bilayer in the simulations were: 1-Palmitoyl-2-oleoylphophatidylcholine (POPC), palmitoyl-oleoyl phosphatidylserine (POPS), 1-palmitoyl-2-oleoyl-sn-glycero-3-phosphoethanolamine (POPE), cholesterol. and PIP_2. These molecules were in the ratio 10:15:40:25:10.

PIP_2 interactions with TMEM16A residues were quantified using the amount of time PIP_2 resided within a 6 Å proximity of a given residue. Analysis of the interaction times between the residues and the protein was conducted with Gromacs, SciPy (Millman and Aivazis, 2011), and NumPy (van der Walt et al., 2011). ScipPy, NumPy and PyMol were used to generate a 3D model showing the intensity of PIP_2 interaction with the TMEM16A homology model.

PIP_2-intracting TMEM16A residues of interest were identified, and found to be clustered in two main sites: TMEM16A residues LRxQ in “Site 1” and KQR in “Site 2” (positions

776, 777, 779 and 791,792,793), and TMEM16B residues DExE in “Site 1” and PEQ in “Site 2” (positions 710, 711, 713 and 725,726,727).

During my project, “site 1” was mutated in TMEM16A and TMEM16B using a chimera of 15 amino acids, which included the sites of interest, but had residues flanking either side. It was therefore necessary to use a TMEM16A and TMEM16B megaprimer (Sarkar and Sommer, 1990), to swap this region from one gene to the other. A megaprimer is the first step in a two-step polymerase chain reaction (PCR), which amplifies a section of DNA containing the sequence to be swapped e.g. TMEM16B flanked by two short primers complementary for the DNA backbone e.g. TMEM16A. The PCR product was separated from the plasmid backbone using a 1% agar gel and electrophoresis. The band containing the megaprimer was extracted from the gel using the QIAquick Gel Extraction Kit (Qiagen, UK), per manufacturer’s instructions. The second step is the amplification of the purified megaprimer with the plasmid of the DNA backbone of interest. Site 1 was also studied using an alanine scanning approach in TMEM16A, however as three non-consecutive residues were mutated only one PCR reaction was required.

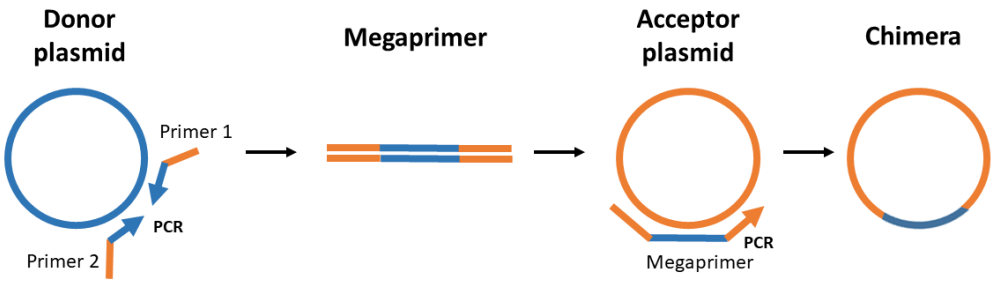

Figure 2.1. Creation of a megaprimer for constructing a chimeric DNA plasmid

The site 2 chimera was short, comprising three consecutive residues. A two-step PCR approach was therefore required to ensure the sequences would have sufficient homology for primer annealing. Therefore, for TMEM16A mutagenesis, residues in positions 791 and 793 were mutated in the initial PCR. Primers with site 792 mutation were designed, and amplified using the DNA plasmid product from the first round of PCR. For TMEM16B mutagenesis, residues 725 and 727 were initially mutated. As with TMEM16A residue 726 was subsequently mutated using the PCR product from the initial reaction.

2.7.4. Design of primers

Primers were designed using Primer3web (Whitehead Institute and Howard Hughes Medical Institute) and sequences aligned using the Basic Local Alignment Search Tool (BLAST, NCBI). Primers were ordered from IDT Technologie (Belgium). Sequencing was performed by GATC Biotech (Germany).

Table 2.19. Primers designed for construction of TMEM16A and TMEM16B chimeras and TMEM16A alanine scanning

Mutation	PCR step	Direction	Sequence
Site 1 16A into 16B	1 Megaprimer	Fw	5'- TATCTTTGAGATTGGAGT CCCGAAGATGAAAAAGTTCATCCGC-3'
		Rv	5'- CTGCGCAGACAGAGCCCC GAAAGTGACCCTGACCACTCAAAAC -3'
	2	Fw	*Megaprimer PCR product*
		Rv	*Megaprimer PCR product*

Site 1 16B into 16A	1 Megaprimer	Fw	5'- TCTCTTCGAGATTGGCAT CCCGAAGCTAAAGAAACTCTTTCGG -3'
		Rv	5'- GATGAGACAGAGCCTGGA TCAGACCGTGAAGAGTACGTGAAGC -3'
	2	Fw	*Megaprimer PCR product*
		Rv	*Megaprimer PCR product*
Site 1 16A Alanine scanning	1	Fw	5'- ATCCGCTACCTGAAGGCG GCCAGAGCGAGCCCCTCAGACCGTGAA-3'
		Rv	5'- TTCACGGTCTGAGGGGCT CGCTCTGGCCGCCTTCAGGTAGCGGAT -3'
Site 2 16A into 16B	1	Fw	5'- *CCTGACCACTCAAAACGT* AAGGAGCGC*TGGGACCTGGACCACAGC*-3'
		Rv	5'- CCTGACCACTCAAAACGT AAGGAGCGCTGGGACCTGGACCACAGC-3'
	2	Fw	5'- *CCTGACCACTCAAAACGT* AAGCAGCGC*TGGGACCTGGACCACAGC* -3'
		Rv	5'- CCTGACCACTCAAAACGT AAGCAGCGCTGGGACCTGGACCACAGC -3'
Site 2 16B into 16A	1	Fw	5'- *GAAGAGTACGTGAAGCGG* CCACAGCAG*TATGAGGTGGACTTCAAC* -3'
		Rv	5'- GTTGAAGTCCACCTCATAC TGCTGTGGCCGCTTCACGTACTCTTC -3'
	2	Fw	5'- *GAAGAGTACGTGAAGCGG* CCAGAGCAG*TATGAGGTGGACTTCAAC* -3'
		Rv	5'- GTTGAAGTCCACCTCATA CTGCTCTGGCCGCTTCACGTACTCTTC -3'

2.8. Patch-clamp electrophysiology

Patch-clamp electrophysiology is a technique that involves the use of microelectrodes (a glass pipette and a reference electrode) to study the electrical properties of cell membranes (Hamill et al., 1981). The experiments for this thesis were carried out in whole-cell and inside-out patch-clamp techniques in the voltage-clamp configuration. In the voltage-clamp configuration, the membrane *Vm* was held at a specified value by constantly injecting a compensatory current (Molleman, 2002). This current therefore reflected the ionic movement occurring due to changes in membrane resistance, for example due to changes in ion channel gating.

2.8.1. Experimental set-up for patch-clamp electrophysiology

An Olympus IX51 inverted microscope (Olympus, UK) and micromanipulator (Scientifica, UK) were positioned on an anti-vibration air table (Newport, USA) and surrounded by a Faraday cage to provide mechanical stability and electrical shielding (Molleman, 2002). Optimal electrical shielding was obtained by connecting the individual items of the set-up to a single ground point, avoiding current loops between the instruments (Molleman, 2002).

All recordings were performed at room temperature using a HEKA amplifier controlled by PULSE/PULSEFIT electrophysiology software (HEKA Elektronik, Harvard Bioscience, UK). All currents were low-pass filtered at 2-5 kHz and sampled at 10 kHz (unless otherwise stated). Whole-cell capacitance and series resistance were compensated by 70% for during voltage clamp, using the HEKA amplifier in-built compensation circuits.

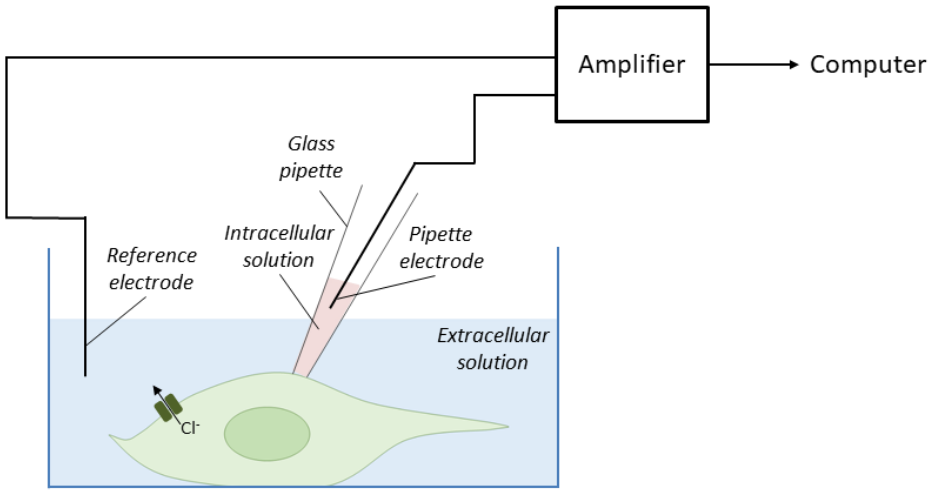

Figure 2.2. Patch-clamp electrophysiology setup.

Pipettes were pulled daily from borosilicate glass capillaries using a two-stage vertical puller (Narishige, UK) and had resistances between 2 and 3.5 MΩ in the working solutions. The pipette resistance was recorded when the reference electrode and pipette electrode were immersed in the extracellular bath solution. The resistance was calculated by dividing 10 mV by the current amplitude elicited in response to a 10 ms, 10 mV voltage pulse. This value was also displayed on the user interface of the recording software.

The bath solution was grounded through an Ag–AgCl reference electrode. An Ag^-/AgCl electrode was also used for the pipette electrode and connected to the headstage controlled by the micromanipulator. The AgCl electrodes consist of a silver wire (0.01 mm diameter) that has an outer coating of AgCl. The ionic current from the cell is converted to an electrical current within the metal wire according to the following reaction:

$$Cl^- + Ag \leftrightarrow AgCl + e^-$$

which occurs at the interface between the liquid and the metal. This reaction is reversible, which minimises the solid-liquid junction potential caused by redox reaction (electron transfer) between the metal electrodes and the salt solutions. A liquid junction potential between two electrodes was caused by the unequal mobility of the ions in the pipette and bath solution (Barry and Lynch, 1991, Neher, 1992).

2.8.2. Patch-clamp configurations

To establish whole-cell and inside-out patch-clamp configurations, the tip of the pipette is first gently pressed on the cell membrane and suction is applied to obtain a high resistance (>1 GΩ) seal (GΩ seal).

The whole-cell patch-clamp configuration can be achieved following the formation of the GΩ seal, when additional suction is applied to rupture the membrane and enable the pipette solution to come in contact with the cell interior (Fig. 2.3). Whole-cell patch-clamp configuration allows recording of the overall activity of all the open ion channels on the cell membrane. As soon as the whole-cell configuration was obtained, cells were lifted and held at 0 mV for 3 minutes, prior to commencement of the experiment. This facilitated the intracellular solution in patch-pipette to enter the cell and fully equilibrate with the intracellular environment.

To obtain the inside-out configuration, the patch of the cell membrane that is in contact with the tip of the pipette was excised after formation of the GΩ seal, by pulling the pipette diagonally away from the membrane. In this way, the cytosolic side of the cell membrane was exposed to the bath solution while the extracellular side was facing the pipette solution. The inside-out configuration was used to study the effect of modulators applied to the intracellular side of the membrane.

In the whole-cell configuration, capacitance is present as the cell membrane can store charge and act as a capacitor. The series resistance refers to the sum of the access resistance and pipette resistance in series with the membrane capacitator (Molleman, 2002)**.** Membrane resistance and cell capacitance need to be overcome to control the *Vm* and therefore needs to be compensated. Because larger cell membranes can store more charge, the cell capacitance also reflects the size of the cell. To compare currents from cells of different sizes, the current (expressed in pA) was normalised for cell capacitance (expressed in pF) and thus, the current density data is given as pA/pF.

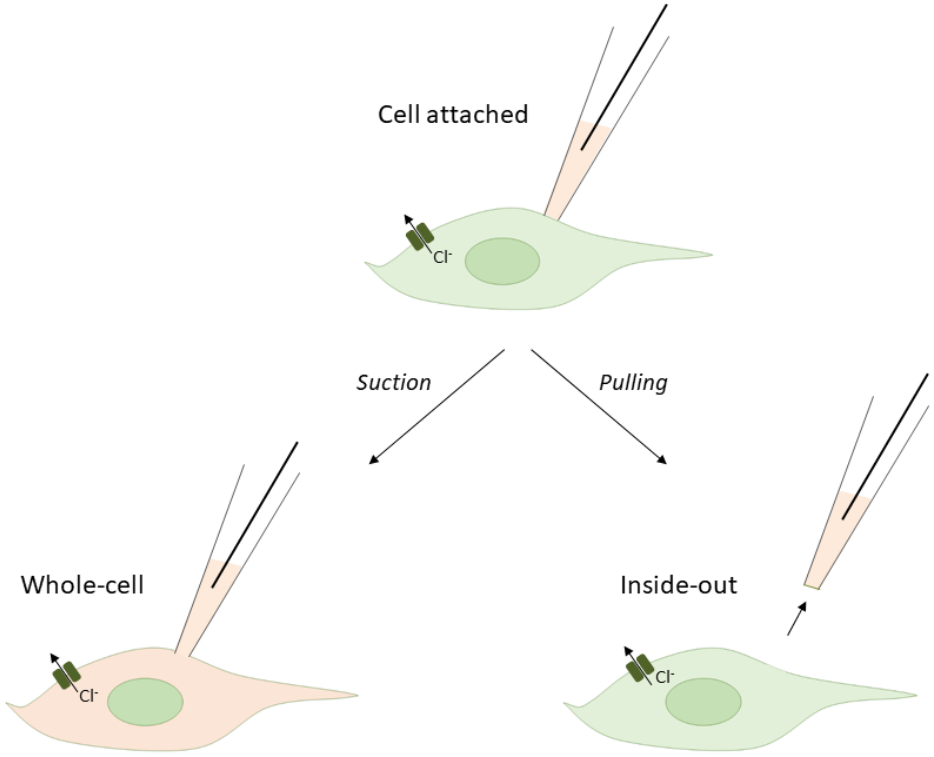

Figure 2.3. Patch-clamp electrophysiology recording configurations used in this thesis.

2.8.3. Perfusion system

Some experiments required the cell or excised patch to be exposed to various modulators. The exchange of solutions was achieved by using a gravity-driven local perfusion system consisting of eight tubes of 1.2 mm diameter. Each tube could contain a different solution for perfusion. The perfusion system was then lowered into the bath solution, and the cell or excised patch attached to the tip of the patch pipette moved in front of a tube. Solution was perfused via gravity flow, and changes of solution was achieved via manually moving the tubes.

2.8.4. Stimulation protocols

A variety of stimulation protocols were used in this thesis. The main features of these protocols are described in this section, although specific variations of these protocols are discussed in the relevant chapter.

Main stimulation protocols:

1. **IV-ramp protocol**: A ramp protocol was used to study TMEM16A current within a broad range of *Vm*. Ramps of 1 s duration ran between -100 mV and 100 mV, with V_{hold} maintained at 0 mV. Currents were measured every 10 mV and divided by the Cm to obtain current density vs *Vm* relationships.
2. **TMEM16A current *versus* ligand relationship**: Currents were measured at 70 mV in the presence of TMEM16A modulators such as diC8-PIP_2 or DHA. The current was measured at 70 mV during inside-out or whole-cell patch-clamp while the excised patch or cell was exposed to solutions containing various [ligand]. The current measured in the presence of various [ligand] was

normalised for the current measured in the absence of the ligand and plotted *versus* [ligand]. The resulting dose response relationships were fitted with modified Hill equations for ligands that produced activation (equation 2.1) or inhibition (equation 2.2), respectively. These equations take the form of:

$$\frac{\mathrm{I_{ligand}}}{\mathrm{I_0}} = \frac{\mathrm{A_{max}} - 1}{1 + \left(\frac{[\mathrm{ligand}]}{\mathrm{EC_{50}}}\right)^{h}} \quad [2.1]$$

Where A_{max} is the maximal TMEM16A current activation, EC_{50} is the [ligand] at which activation is half-maximal and *h* is the Hill coefficient.

$$\frac{\mathrm{I_{ligand}}}{\mathrm{I_0}} = \frac{1}{1 + \left(\frac{[\mathrm{ligand}]}{\mathrm{IC_{50}}}\right)^{h}} \quad [2.2]$$

Where IC_{50} is the [ligand] at which activation is half-maximal and *h* is the Hill coefficient.

3. **IV-tail protocol (Current *versus* *Vm* relationship)**: Current versus *Vm* relationships were constructed by measuring currents in response to *Vm* steps of 1 s duration (test pulses) from −100 to 140 mV in 40 mV increments. Each test pulse was preceded by a *Vm* step to 70 mV of 1 s duration (pre-pulse). Pulses were elicited every 2 s from a holding *Vm* of 0 mV. Steady-state currents were measured at the end of the test pulses. For determination of the current reversal potential (E_{rev}), instantaneous currents were estimated from extrapolation of

single exponential fits of the test-pulse currents to the beginning of each test pulse. These instantaneous current values were plotted as a function of the *Vm*.

4. **IV-Steps**: Cells were held at 0 mV, before the test pulse induced a *Vm* of 70 mV for 1.5 s. *Vm* was then held at -70 mV for 0.5 s, and returned to the holding *Vm* between sweeps. Time between sweeps varied between experiments, as appropriate.
5. **IV-CaCC**: Current versus *Vm* relationships were constructed by measuring currents in response to *Vm* steps of 1 s duration from −100 to 100 mV in 20 mV increments. Following each test pulse, *Vm* was set to -60 mV for 0.5 s. Pulses were elicited every 2 s from a holding *Vm* of 0 mV.
6. **Double-pulse protocol - recovery of TMEM16A currents from DrVSP-mediated inhibition**: A double-pulse protocol was used to determine the time required for the response of TMEM16A current to recover following DrVSP activation during a 4 s pulse to 100 mV (conditioning pulse). The conditioning pulse was followed by a varying recovery period (3 s to 55 s) at -50 mV and a subsequent 4 s test pulse to 100 mV. The effect of DrVSP was assessed by measuring the difference between the peak (Ip) and the steady-state (Iss) current elicited by each depolarising pulse (Ip-Iss). The extent of recovery was expressed as the ratio of Ip-Iss measured during a test pulse relative to that measured during the conditioning pulse. Time constant of recovery (τ_r) was obtained by fitting a single exponential function to the relationship between extent of recovery and the duration of the recovery period.
7. **Ca_V current voltage protocol**: The current vs voltage relationship for Ca_V channels was obtained by applying 0.2 s pulses from -70 mV to 60 mV in 10 mV

steps from a holding potential of -60 mV. The peak current (divided by Cm) at each *Vm* was measured and plotted *versus Vm*.

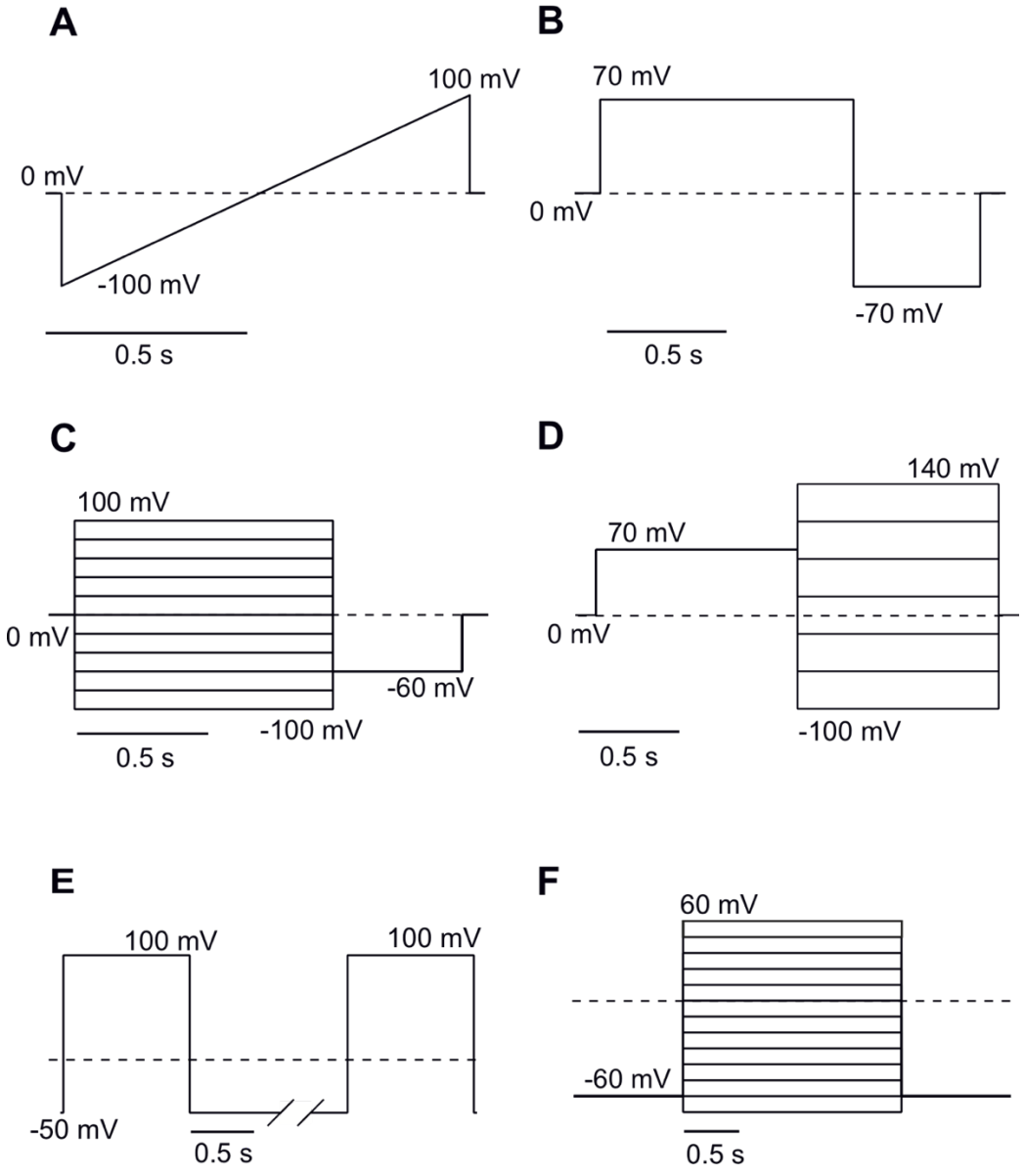

Figure 2.4. Patch-clamp recording voltage stimulation protocols.

(A) IV-ramp voltage protocol (2.8.4.1); (B) IV-steps voltage protocol (2.8.4.4); (C) IV-CaCC voltage protocol (2.8.4.5); (D) IV-tail voltage protocol (2.8.4.3); (E) Double-pulse voltage protocol (2.8.4.6); (F) Ca_V voltage protocol (2.8.4.7). Dotted lines represent 0 mV level.

2.8.5. Stationary noise analysis

Stationary noise analysis was used to assess TMEM16A open probability (Po), single channel conductance (i), and number of channels (N), in the absence and presence of PIP_2 (Chapter 4). Stationary noise analysis (DeFelice, 1981) assumes that there are N independent and identical channels with a single conducting level, i. The macroscopic current (I) is given by:

$$I = iNP_o \quad [2.3]$$

From binomial theory, the variance, σ^2, is related to I by:

$$\sigma^2 = iI + \frac{I^2}{N} \quad [2.4]$$

Lengths (1-5 s duration) of stationary currents were measured at 70 mV and in different $[Ca^{2+}]_i$ in both the absence and presence of diC8-PIP_2. For each tract of current, the σ^2 and mean I, were calculated. Background variance and current measured in 0 $[Ca^{2+}]_i$ were subtracted, and the σ^2-I plot was fitted with equation 2.4 with i and N as free parameters. Single channel conductance (γ) was calculated by dividing i by the *Vm* at which the experiment was conducted. The σ^2 and I measured at each $[Ca^{2+}]_i$ were subsequently normalised for the estimated maximal current (I_{max}), corresponding to P_o=1), and averaged. In this way, the y axis represents σ^2/I_{max} and the x-axis represents Po.

2.9. Wire myography

Myograph, from 'myo' meaning muscle in latin, can be used to measure, or 'graph' the isometric tension of a wide variety of blood vessels. Wire myography was used to assess the function of rings of thoracic aorta isolated from wild-type or heterozygous TMEM16A-KO mice. In this technique two wires attached to fixed jaws are fed through the arterial lumen. The jaws are subsequently moved apart to induce vessel stretch so that changes in vessel tension can be detected via a force transducer.

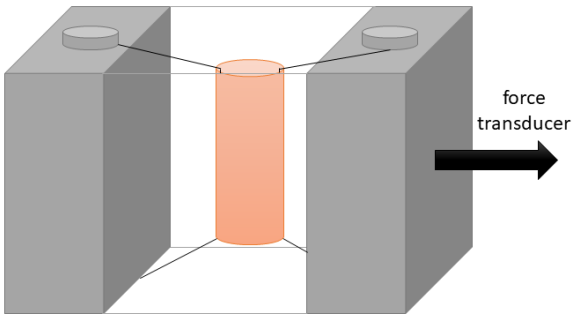

Figure 2.5. Wire myography experimental setup

Following cervical dislocation the thoracic aorta was immediately removed and cleaned of all perivascular fat and connective tissue in ice cold PSS. The arteries were cut into rings, ~2 mm in length and mounted onto the jaws of a small vessel dual wire myograph 410A system (Danish MyoTechnology, DMT, Denmark) using 40 µm gold-plated tungsten wire (Goodfellow, UK). One of the myograph jaws was connected to a micrometer that allowed manual adjustment of the distance between the two jaws, and therefore control of basal artery stretch. The other jaw was connected to a force

transducer allowing the tension produced by the artery ring to be measured. The myograph chamber was split into two independent 5 ml bath chambers which were maintained at 37 °C.

2.9.1. Theory of normalisation procedure

The magnitude of contraction and sensitivity of a vessel to agonists varies depending on the extent of stretch applied to that vessel. It is therefore necessary to apply an equal amount of stretch to all vessels regardless of vessel length, animal sex or genotype so that vessel responses can be accurately compared with each other (Mulvany and Halpern, 1977). The aim of the normalisation procedure was to identify the micrometer reading, i.e. distance between the jaws, necessary to produce the internal circumference (IntCir) that the vessel would have if relaxed under 90 % of 100 mmHg transmural pressure (Mulvany and Halpern, 1977), this was termed the $IntCir_{100}$.

In order to normalise the amount of stretch applied to the vessel segments to the appropriate IntCir, a computer program was written by Dr Paolo Tammaro and Dr Hannah Garnet which implemented the algorithm determined by Mulvany and Halpern (Mulvany and Halpern, 1977) into the IGOR (Wavemetrics, USA) platform. This programme was termed the normalisation procedure script. The normalisation procedure script is underpinned by the LaPlace law:

$$Pi = \frac{Tension}{\left(\frac{IC}{2\pi}\right)} \quad [2.5]$$

In which Pi is the effective pressure for each vessel segment and Tension is the force (in mN) divided by the vessel length x2 (in mm). The Pi is an estimate of the pressure needed to stretch the vessel to the measured $IntCir_{100}$.

2.9.2. Normalisation procedure

To acclimatise the artery rings to the wire myograph, ice cold PSS (see table 2.4.) was replaced with PSS warmed to 37 °C immediately after mounting and vessels left to stabilise for ~30 minutes. The stretch of the vessel was then increased step-wise by increasing the distance between the myograph jaws in 100 µm increments. The normalisation procedure script takes the jaw measurement and tension values at each step as inputs, alongside the vessel length and wire thickness to calculate the jaw measurement that must be applied to create the desired transmural pressure, which is at 90 % of measured $IntCir_{100}$ for the aorta.

2.9.3. Myography experimental design

Isometric tension measurements were recorded using an AD/DA converter (USB-6221, National Instruments, UK) and Chart v5 (Strathclyde University, UK) software. All experiments were performed at 37 °C. Functional viability of vessels was assessed after normalisation by ensuring the contractile response to 55 mM KCl remained consistent over three repeats. Each KCl treatment lasted 6 minutes. Between additions vessel tension was relaxed back to baseline by washing with PSS pre-warmed to 37°C. All data was normalised to percentage change from maximum PE-induced constriction to allow for variation in overall contractile force.

2.9.4. [PE]-tension relationship analysis

Contractility of aortic rings was measured in response to increasing doses of L-phenylephrine hydrochloride (PE). Dose response data was based on cumulative additions of the drug (diluted in PSS) to the bath solution. TMEM16A modulators, such as DHA or Bumetanide, were pre-incubated with the aortic rings for 25 minutes prior to adding the first dose of PE. Data was normalised to the third 55 mM KCl contractile response to allow for variation in overall contractile force.

Experiments requiring removal of the Cl^- component of vessel contractility, K-methanesulfonate was used to induce aortic ring contraction in the presence and absence of other modulators. In this case, KCl was still used to assess viability of vessels and for normalisation of data.

2.10. Study design and statistical analysis

The work in this thesis adheres to the Animal Research: Reporting of *In Vivo* Experiments (ARRIVE) guidelines set by the National Centre for the Replacement, Refinement, and Reduction of Animals in Research (NC3Rs).

2.10.1. Randomisation

Randomisation was carried out as effectively as possible throughout this thesis. Experiments involving transfected HEK-293T cells were identified using anti-CD8 beads, and then selected at random for patch-clamp electrophysiology. Data was generated using at least three independent transfections for each condition, and cells with 1-2 anti-CD8 beads attached were selected in order to minimise variation in transfection levels.

Patch-clamp electrophysiology experiments using native cells also relied on cells being selected at random. For myography experiments, the thoracic aorta was dissected and then freshly isolated aortic rings were chosen at random for experimentation. All experiments involving primary cells or tissues used at least five animals per data set. In experiments using two or more different treatments randomisation was achieved by changing the order of application of the agents.

2.10.2. Operator blinding

Blinding is a useful approach in the collection and analysis of data that could involve a bias in the collection of data, or a degree of qualitative interpretation of the results. Objective methods of analysis, such as automated analysis procedures were used for each experiment type, with methods of analysis devised prior to execution of the experiment.

Myography experiments could not be blinded as for most experiments both myography chambers contained aortic rings obtained from either wild-type or mutant mice that were previously genotyped by the operator. Automated analysis of tension at selected time points ensured no user bias during data analysis occurred.

2.10.3. Statistical analysis

Statistical significance was determined with paired or unpaired t-tests, or two-way ANOVA with Bonferroni's post-test, as appropriate. For all statistical tests, $P<0.05$ was considered significant. Significance is denoted on figures as follows: * $P<0.05$, ** $P<0.005$, *** $P<0.0005$.

2.11. Contribution to work

Unless otherwise stated, all experiments in this thesis were designed by Kathryn Acheson and Dr Paolo Tammaro, and executed and analysed by Kathryn Acheson.

Lara Scofano contributed to the collection of data presented in figures 3.8, 4.7, and 4.8.

Chau My Ta contributed to the collection of data presented in figures 4.1, 4.2, 4.4, and 4.14. As outlined in section 2.7.4, the location of the putative PIP_2 binding site was elucidated by Dr Phill Stansfeld and Remco Jonkind.

Chapter 3

Pharmacology of cloned and native TMEM16A channels

Chapter 3 - Pharmacology of cloned and native TMEM16A channels

Research within the Tammaro group has demonstrated that TMEM16A is the major component of CaCC current in VSMCs (Manoury et al., 2010). It has been proposed that TMEM16A current in VSMCs has a profound role in blood vessel contraction (Pedemonte and Galietta, 2014, Manoury et al., 2010), via activation of the Gq-PCR signalling cascade. This chapter aims to define and characterise the most suitable compound for use in further studies in this thesis.

This chapter is divided into three main parts. The first provides a basic biophysical characterisation of TMEM16x family members, followed by a brief overview of the current pharmacology of cloned TMEM16A channels, to identify a suitable small-molecule modulator of TMEM16A for use as a tool compound in subsequent studies.

The second part of this chapter focuses on the effect of the small molecule inhibitor of TMEM16A, Ani9. This is the most selective and potent blocker of TMEM16A, and reported to be potent in the nanomolar range and be selective for TMEM16A, while not affecting TMEM16B (Seo et al., 2016). The study by Seo et al. (2016) remains the only instance in the literature where Ani9 has been tested on cloned TMEM16A and TMEM16B channels. Alongside TMEM16A and TMEM16B, TMEM16F is the only other plasma-membrane localised member of the TMEM16x family to conduct Cl^-. Therefore, the effect of Ani9 on cloned TMEM16A, TMEM16B, and TMEM16F channels was studied. The selectivity of Ani9 for native TMEM16A was then explored, including testing of Ani9 on a varitey of other native VSMC currents, in order to assess whether Ani9 was a suitable pharmalogical tool for subsequent studies presented in this thesis.

In the third part of this chapter, the TMEM16A heterozygous KO model (TMEM16A-Het-KO) and Ani9 were used in order to test whether genetic and pharmacological methods

of reducing TMEM16A are comparable, and therefore to assess whether Ani9 is a suitable pharmacological tool for use in subsequent studies involving isolated aortic rings. In addition to this, the role of TMEM16A in isolated ventricular cardiomyocytes was studied using Ani9.

In summary, the work presented in this chapter confirms that TMEM16A is expressed in VSMCs, and is a key depolarising force in blood vessel contractility. This introductory results chapter also provides a solid foundation of control experiments for subsequent studies in this thesis, which involve the modulation of TMEM16A by lipids.

3.1 Electrophysiological profiles of cloned TMEM16x channels

3.1.1. TMEM16A and TMEM16B calcium sensitivity

TMEM16A and TMEM16B are the only two members of the TMEM16x family to form plasma membrane localised CaCCs (Pedemonte and Galietta, 2014, Hartzell et al., 2009). TMEM16A and TMEM16B have differing sensitivity to $[Ca^{2+}]_i$ (Adomaviciene et al., 2013). In order to define appropriate $[Ca^{2+}]_i$ for experiments presented in later chapters of my thesis, this study started by testing the Ca^{2+}-sensitivity of cloned TMEM16A and TMEM16B.

The inside-out patch-clamp technique was used to examine the effect of a range of $[Ca^{2+}]_i$ on cloned TMEM16A and TMEM16B channels. Patches were excised from HEK-293T cells expressing TMEM16A or TMEM16B, and were subsequently held at 70 mV. Current (I) was measured in the presence of various $[Ca^{2+}]_i$. The current was then normalised to maximal current (I_{max}) recorded at 78 μM $[Ca^{2+}]_i$. The I/I_{max} relationship was plotted against $[Ca^{2+}]_i$, and fitted with the Hill equation (equation 2.1, Fig. 3.1). TMEM16A was ~1.5-fold more sensitive to $[Ca^{2+}]_i$ than TMEM16B. TMEM16A currents were characterised by an EC_{50} value of 1.03 ± 19.11 μM and an *h* value of 2.39 ± 0.09 (n=7), compared to an EC_{50} of 1.57 ± 86.5 μM and an *h* value of 2.14 ± 0.25 (n=5) for TMEM16B.

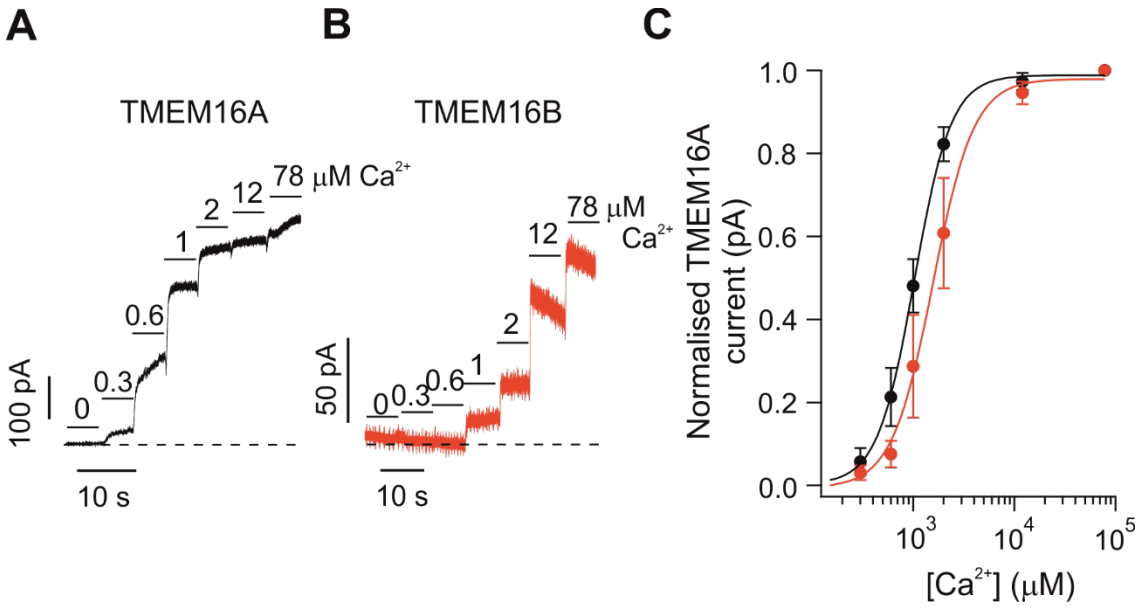

Figure 3.1. TMEM16A and TMEM16B Ca^{2+}-dependence

(A) Current recorded using the inside-out patch-clamp technique, from a patch excised from HEK-293T cells expressing TMEM16A. The Vm was maintained at 70 mV, and $[Ca^{2+}]_i$ was varied as indicted. Dotted line represents zero-current level.

(B) Current recorded using the inside-out patch-clamp technique, from a patch excised from HEK-293T cells expressing TMEM16B. The Vm was maintained at 70 mV, and $[Ca^{2+}]_i$ was varied, as indicted. Dotted line represents zero-current level.

(C) Mean TMEM16A (black, n=7) or TMEM16B (red, n=5) current versus $[Ca^{2+}]_i$ relationships. Currents were normalised to the current achieved at 78 µM $[Ca^{2+}]_i$. Data was fitted using the Hill equation (equation 2.1).

3.1.2. TMEM16A and TMEM16B IV-relationship

Experiments in the previous section assessed the extent to which TMEM16A and TMEM16B respond to $[Ca^{2+}]_i$. The next experiment aimed to study the response of these channels to *Vm* at a fixed $[Ca^{2+}]_i$.

The current *versus* voltage (IV) relationship of cloned TMEM16A and TMEM16B channels were studied in order to assess current density and activation and deactivation kinetics.

The whole-cell patch-clamp technique was used to study HEK-293T cells expressing cloned TMEM16A or TMEM16B channels. TMEM16A currents were recorded in the presence of 0.3 μM $[Ca^{2+}]_i$. Conversely, TMEM16B currents were recorded in the presence of 0.6 μM $[Ca^{2+}]_i$. Based on data presented in figure 3.1, different $[Ca^{2+}]_i$ were used to ensure the same extent of activation for the two channels. The IV-relationship was studied using the "IV-CaCC" voltage protocol (Fig. 3.2).

TMEM16A and TMEM16B currents measured at each *Vm* were normalised to the Cm and plotted against the *Vm* to construct the IV-relationship (Fig. 3.2). Non-transfected (NT) HEK-293T cells were used as a control. In NT cells, small endogenous currents were 5.69 ± 0.45 (pA/pF) (n=12) at 100 mV. TMEM16A and TMEM16B currents had a strongly outwardly rectifying IV-relationship, with more outward current at positive *Vm* than inward current at negative *Vm*. TMEM16A currents at 100 mV were 320.07 ± 62.57 (pA/pF) (n=9), and 70.19 ± 15.16 (pA/pF) (n=9) for TMEM16B at the same *Vm*.

Visual inspection of the currents shown in figure 3.2 suggested the rate of activation of TMEM16A and TMEM16B currents differed. The time-course of the increase in current as the *Vm* was stepped from 0 mV to a given test pulse was quantified in terms to time taken to reach half-maximal current ($\tau_{a0.5}$). The time-course of the current decay

(deactivation, $\tau_{d0.5}$) during repolarisation to -60 mV was also expressed as the time required to reach 50% of the decay in current.

For TMEM16A currents, as the *Vm* increased, the $\tau_{a0.5}$ also increased, resulting in a $\tau_{a0.5}$ of 69.39 ± 3.46 ms at 40 mV, and 77.35 ± 7.78 ms at 100 mV (n=8, Fig.3.2). TMEM16B channels had a more rapid activation, with a $\tau_{a0.5}$ of 7.05 ± 0.63 ms at 60 mV, and 8.69 ± 0.32 at 100 mV ms (n=5, Fig.3.2). TMEM16B $\tau_{a0.5}$ was not measured at 40 mV as the fast kinetics precluded accurate measurements of $\tau_{a0.5}$. Tail currents representing deactivation of TMEM16A and TMEM16B channels were measured during repolarisation to -60 mV. The $\tau_{d0.5}$ for TMEM16A channel closure was 44.15 ± 2.97 ms when preceded by channel activation to 100 mV. For TMEM16B this was 3.09 ± 0.37 ms (Fig.3.2). Overall, TMEM16B activation was found to occur ~8.9-fold faster than TMEM16A at 100 mV. Deactivation of TMEM16B was also faster than TMEM16A, by ~14.3-fold.

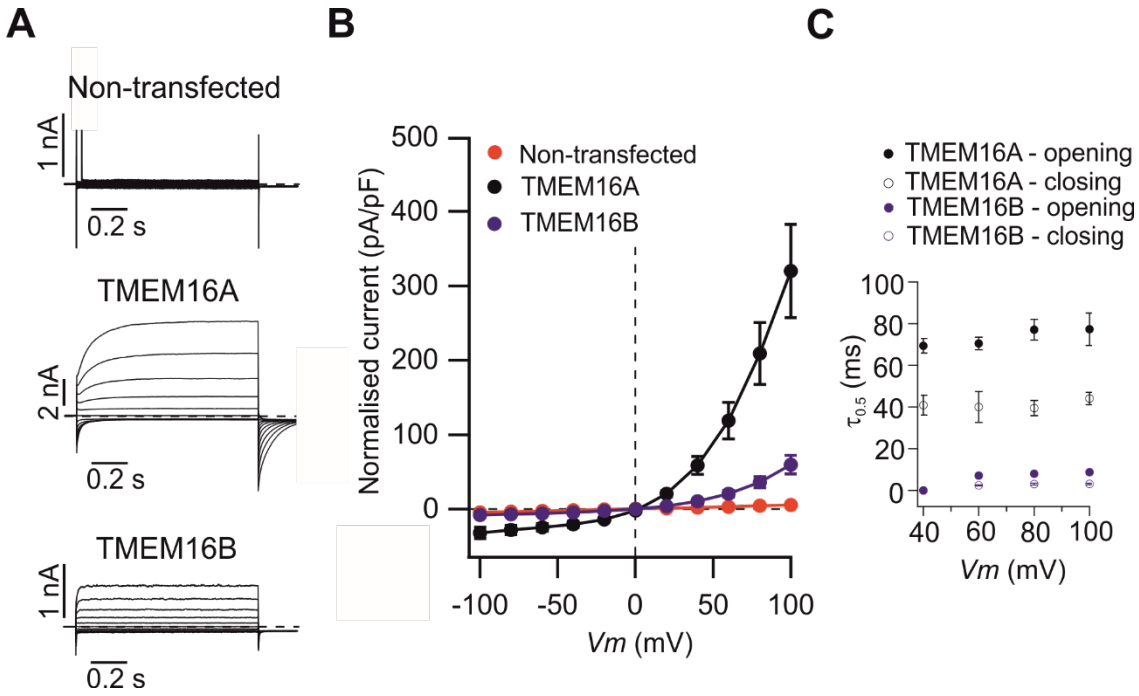

Figure 3.2. Cloned TMEM16A and TMEM16B channel IV-relationship

(A) Non-transfected (NT), TMEM16A, and TMEM16B transfected HEK-293T cells were studied in the whole-cell patch-clamp configuration. Solutions contained 0.3 μM $[Ca^{2+}]_i$ for recordings of NT and TMEM16A currents, and 0.6 μM $[Ca^{2+}]_i$ for TMEM16B currents. Currents were recorded using the "IV-steps" voltage protocol, which induced 1 s test pulses between -100 mV and 100 mV in 20 mV increments, followed by -60 mV for 0.5 s. Holding potential was 0 mV. Dotted line represents zero-current level.

(B) Mean whole-cell current vs Vm relationships, measured at the end of the test pulses.

(C) Mean $\tau_{a0.5}$ (filled symbols) and $\tau_{d0.5}$ (open symbols) for TMEM16A (black), and TMEM16B (blue) currents. Number of experiments were NT (n=12), TMEM16A (n=9), and TMEM16B (n=9).

3.1.3. TMEM16F current versus voltage relationship

In addition to CaCCs, the TMEM16x family includes the Cl^- channel and phospholipid scramblase TMEM16F (Pedemonte and Galietta, 2014, Hartzell et al., 2009, Acheson, 2016). TMEM16F channels have a characteristic whole-cell Cl^- current that increases in amplitude over time (Pedemonte and Galietta, 2014, Hartzell et al., 2009, Acheson, 2016). The time course of the development of the whole-cell TMEM16F current was therefore defined at this stage of the project, before any further pharmacological testing was carried out.

To observe TMEM16F activity, $[Ca^{2+}]_i$ was elevated to 78 μM, as previous reports have shown that TMEM16F is active at high $[Ca^{2+}]_i$ (Ye et al., 2018, Acheson, 2016). HEK-293T cells expressing TMEM16F were studied using the whole-cell patch-clamp technique. Whole-cell TMEM16F currents were examined using the "IV-CaCC" voltage protocol. Experiments were run every 2 minutes from the establishment of the whole cell configuration (defined as t=0 minutes).

TMEM16F current increased over time (Fig. 3.3), with an outwardly-rectifying IV-relationship similar to that of the TMEM16A and TMEM16B currents described above (Fig. 3.2). At 100 mV TMEM16F current was 8.29 ± 0.76 pA/pF at t=0 min, increasing to 12.24 ± 1.44 pA/pF at t=2 min, 16.36 ± 1.47 pA/pF at t=4 min, and 27.58 ± 3.50 pA/pF at t=6 min (n=4) (Fig. 3.3).

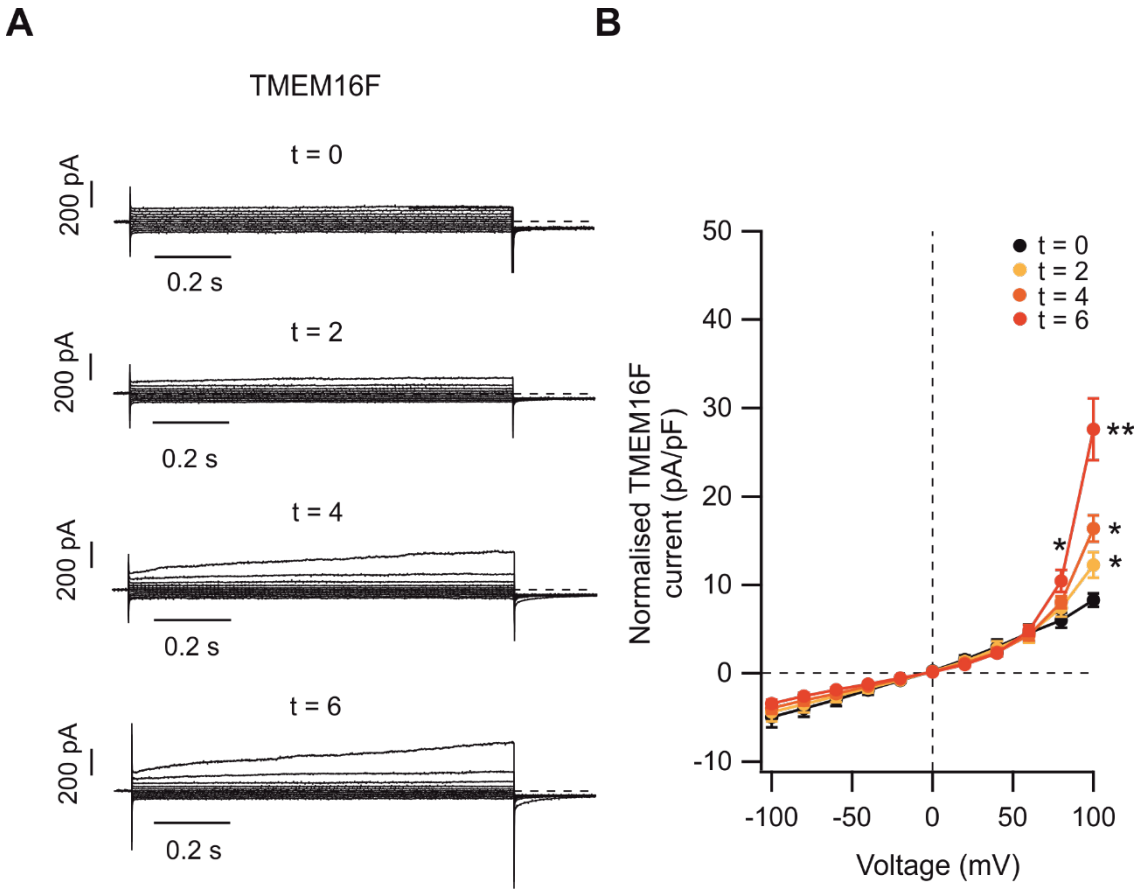

Figure 3.3. TMEM16F IV-relationship and time course

(A) TMEM16F expressing HEK-293T cells were studied in the whole-cell patch-clamp configuration. Solutions contained 78 μM $[Ca^{2+}]_i$. Currents were recorded at two-minute intervals using the "IV-steps" voltage protocol. Holding potential was 0 mV. Dotted line represents zero-current level.

*(B) Mean whole-cell IV-relationships, measured at the end of the test pulses (n=4). *P<0.05, **P<0.005 (two-way ANOVA).*

3.2. Pharmacology of cloned TMEM16A channels

The following experiments aimed to test pharmacological modulators from the literature using our experimental setup. Overall, this section aimed to identify a pharmacological modulator of TMEM16A that could be used as a tool for studying native TMEM16A channels later in this thesis.

TMEM16A currents were measured in the whole-cell patch-clamp configuration in the presence of 0.3 μM $[Ca^{2+}]_i$. The "IV-tails" voltage protocol was used as with this protocol the pre-pulse triggers channel opening, while the subsequent test-pulses at various *Vm* allow the study of TMEM16A modulators on the open channel at various *Vm*. Each experimental protocol was executed under perfusion conditions, first with control extracellular solution, followed by solutions containing appropriate concentrations of the compound of interest. Currents were analysed during the steady-state phase of the test pulse and normalised to the Cm.

3.2.1. Effect of Eact on cloned TMEM16A currents

Eact is described in the literature as an activator of TMEM16A with an EC_{50} of 10 μM when applied extracellularly during whole-cell patch clamp (Namkung et al., 2011a). The effect of Eact on TMEM16A was studied using the experimental design is described above (section 3.2). Here, it was found that TMEM16A current was unaffected by Eact (10 μM, table 3.1), and slightly inhibited when [Eact] was increased to 100 μM (n=7) (Fig. 3.4). These data demonstrates that Eact has a significantly ($P<0.05$) different effect on TMEM16A to that stated in the literature.

Table 3.1. Effect of Eact on TMEM16A currents

	TMEM16A current at 140 mV (pA/pF)
Control	232.81 ± 63.27
10 μM Eact	234.46 ± 67.50
100 μM Eact	156.65 ± 50.07
n	7

"Control", "10 μM Eact", and "100 μM Eact" refer to the TMEM16A current obtained at 140 mV. "n" refers number of experiments.

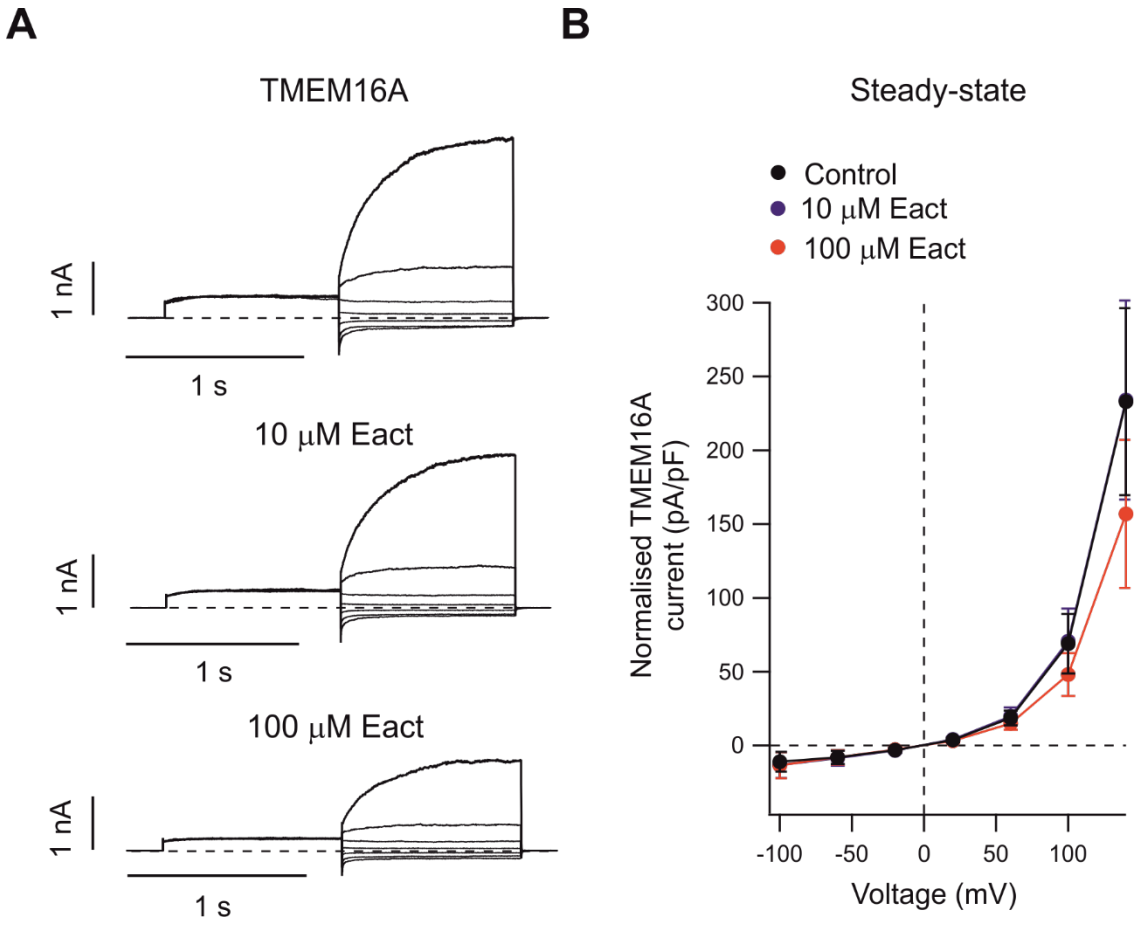

Figure 3.4. TMEM16A currents in response to Eact

(A) TMEM16A expressing HEK-293T cells were studied in the whole-cell patch-clamp configuration, in response to the "IV-tail" protocol. Solutions contained 0.3 μM $[Ca^{2+}]_i$. Eact (10 μM or 100 μM) was applied as indicated. Dotted lines represent the zero-current level.

(B) Mean steady-state TMEM16A current versus Vm relationships measured in the absence (control) or presence of Eact (10 μM or 100 μM), as indicated (n=7, N.S. P>0.05 two-way ANOVA).

3.2.2. Effect of MONNA on cloned TMEM16A currents

MONNA is a reported blocker of TMEM16A, with an IC_{50} of 0.08 μM (Oh et al., 2013). The effect of MONNA on TMEM16A was studied using the experimental design is described in section 3.2. Normalised TMEM16A currents were reduced by ~1.4-fold in the presence of 1 μM MONNA (Fig. 3.5, table 3.2). This current was blocked further by ~1.9-fold compared to the control in the presence of 5 μM MONNA (n=5). This effect was statistically significant at *Vm* of 60 mV and above. This data suggests that MONNA is a blocker of TMEM16A, however we find it to be less potent than reported by Oh et al. (2013).

Table 3.2. Effect of MONNA on TMEM16A currents

	TMEM16A current at 140 mV (pA/pF)
Control	684.53 ± 103.01
1 μM MONNA	496.74 ± 68.49
5 μM MONNA	352.37 ± 37.57
n	5

"Control", "1 μM MONNA", and "5 μM MONNA" refer to the TMEM16A current obtained at 140 mV. "n" refers number of experiments.

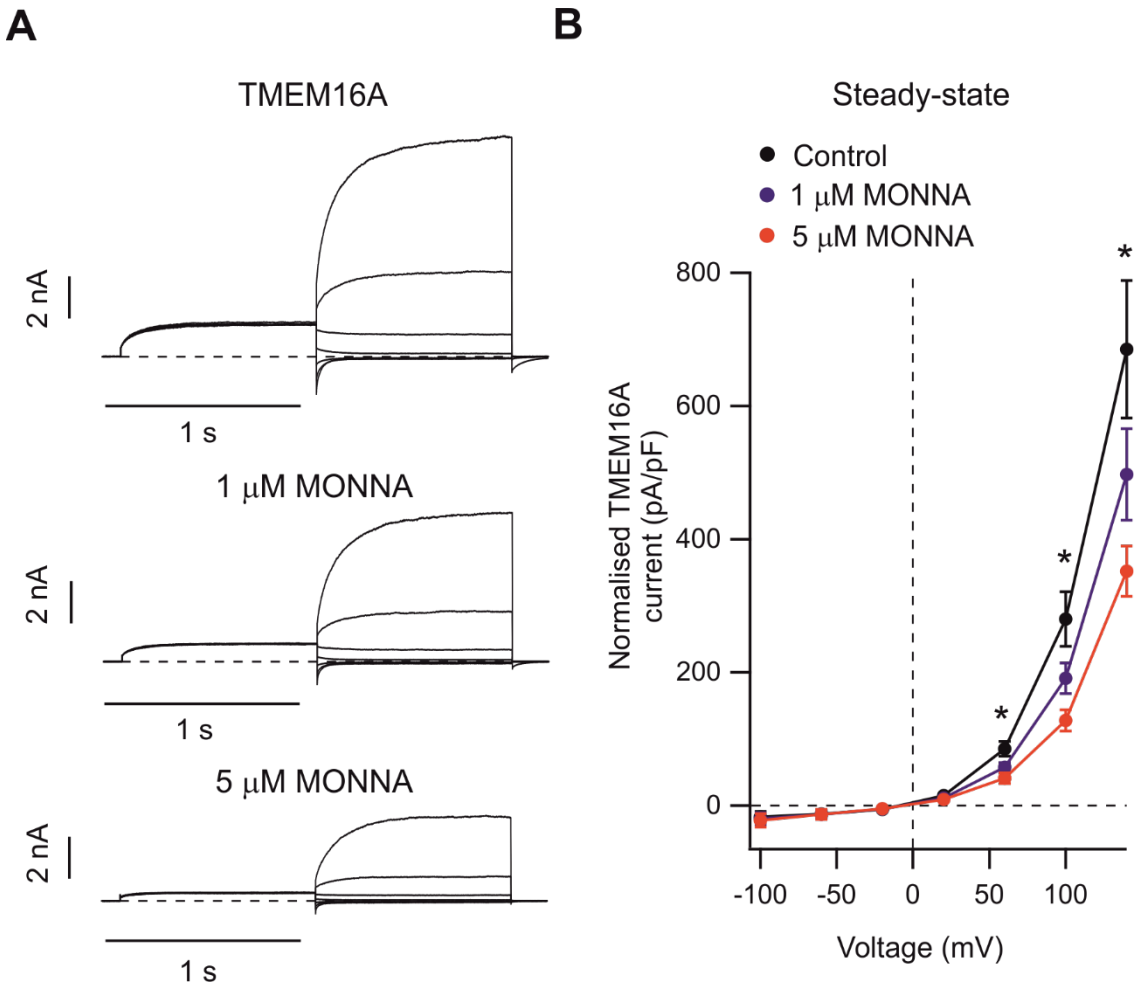

Figure 3.5.TMEM16A currents in response to MONNA

(A) TMEM16A expressing HEK-293T cells were studied in the whole-cell patch-clamp configuration, in response to the "IV-tail" protocol. Solutions contained 0.3 μM $[Ca^{2+}]_i$. MONNA (1 μM or 5 μM) was applied as indicated. Dotted lines represent the zero-current level.

*(B) Mean steady-state TMEM16A current versus Vm relationships measured in the absence (control) or presence of MONNA (1 μM or 5 μM), as indicated (n=5, * P<0.05 two-way ANOVA).*

3.2.3. Effect of bumetanide on cloned TMEM16A currents

Bumetanide is a potent blocker of the NKCC1 exchanger (Ben-Ari, 2017). Bumetanide can be used experimentally in order to modulate $[Cl^-]_i$ in primary cells and tissues. Experiments presented later in this thesis (chapter 5) require a reduction in $[Cl^-]_i$ in the SM of isolated aortic rings. In order to ensure bumetanide does not directly interact with TMEM16A, bumetanide was tested on cloned TMEM16A channels.

TMEM16A expressing HEK-293T cells were studied using the experimental design is described in section 3.2, in the presence of bumetanide. TMEM16A currents were normalised to the Cm, and mean data was analysed at the steady-state phase of the test-pulse (Fig. 3.6). Bumentanide did not significantly reduce ($P<0.05$) TMEM16A current at 10 μM or 40 μM (n=5) (Fig. 3.6, table 3.3). Bumetanide is therefore a suitable tool for modulating $[Cl^-]_i$ without directly affecting TMEM16A channel activity.

Table 3.3. Effect of bumetanide on TMEM16A currents

	TMEM16A current at 140 mV (pA/pF)
Control	638.39 ± 202.86
10 μM bumetanide	578.25 ± 180.48
40 μM bumetanide	470.29 ± 119.31
n	5

"Control", "10 μM bumetanide", and "40 μM bumetanide" refer to the TMEM16A current obtained at 140 mV. "n" refers number of experiments.

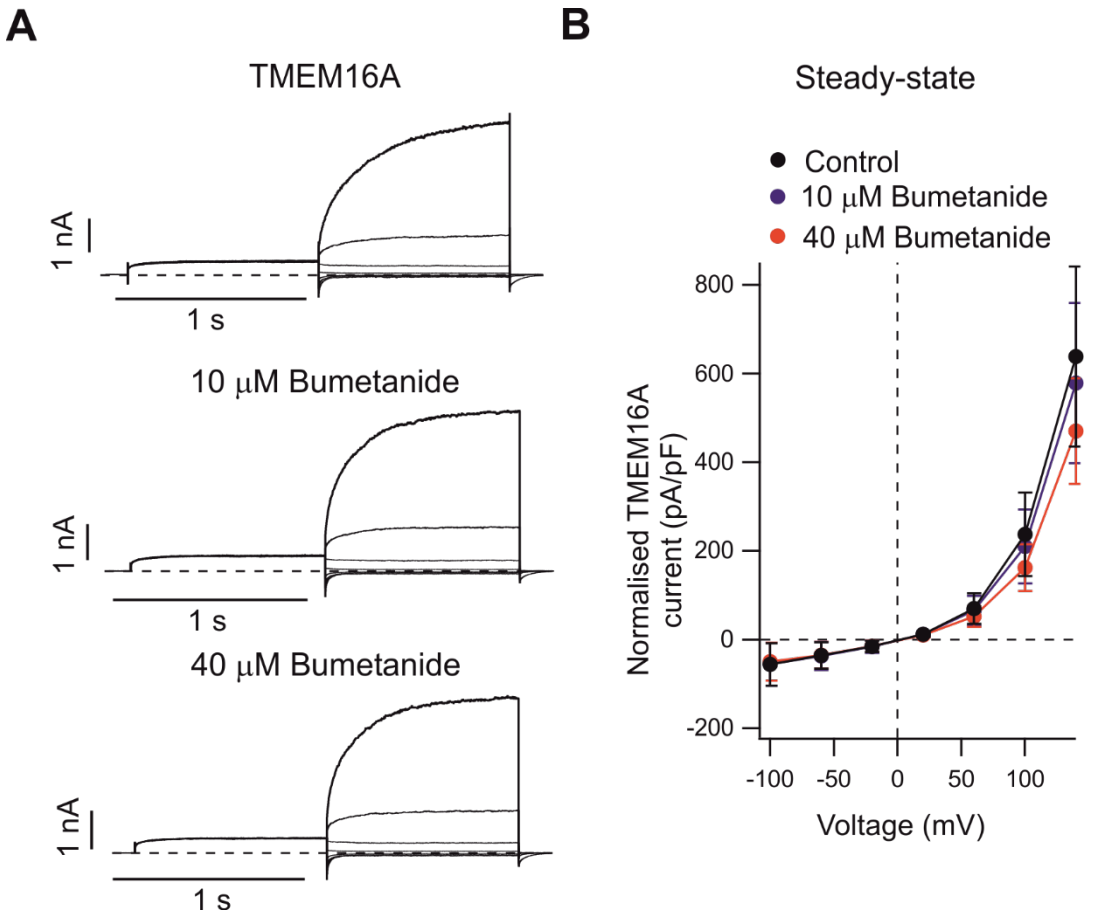

Figure 3.6. TMEM16A currents in response to the NKCC1 blocker Bumetanide

(A) TMEM16A expressing HEK-293T cells were studied in the whole-cell patch-clamp configuration, in response to the "IV-tail" protocol. Solutions contained 0.3 μM $[Ca^{2+}]_i$. Bumetanide (10 μM or 40 μM) was applied as indicated. Dotted lines represent the zero-current level.

(B) Mean steady-state TMEM16A current versus Vm relationships measured in the absence (control) or presence of Bumetanide (10 μM or 40 μM), as indicated (n=5, N.S. P>0.05 two-way ANOVA).

3.2.4. Effect of Ani9 on cloned TMEM16A currents

In 2016, Ani9 was reported to potently inhibit TMEM16A, with an IC_{50} of 100 nM (Seo et al., 2016). Ani9 was also reported to have a negligible effect on TMEM16B channels, and other anion channels, such as CFTR and ENaC (Seo et al., 2016).

The effect of Ani9 on TMEM16A was studied using the experimental design as described in section 3.2. TMEM16A currents were reduced by ~2.8-fold in the presence of 100 nM Ani9 (n=7, Fig. 3.7). In the presence of 3 μM Ani9, TMEM16A currents were reduced by ~13-fold at 100 mV (Table 3.4). The effect of Ani9 on TMEM16A current was statistically significant at all *Vm* tested. As this study demonstrates Ani9 to be a potent inhibitor of the TMEM16A channel, it was studied further to determine its suitability as a tool compound for the rest of this thesis.

Table 3.4. Effect of Ani9 on TMEM16A currents

	TMEM16A current at 140 mV (pA/pF)
Control	484.84 ± 91.03
100 nM Ani9	174.10 ± 43.81
3 μM Ani9	37.38 ± 8.39
n	7

"Control", "100 nM Ani9", and "3 μM Ani9" refer to the TMEM16A current obtained at 140 mV. "n" refers number of experiments.

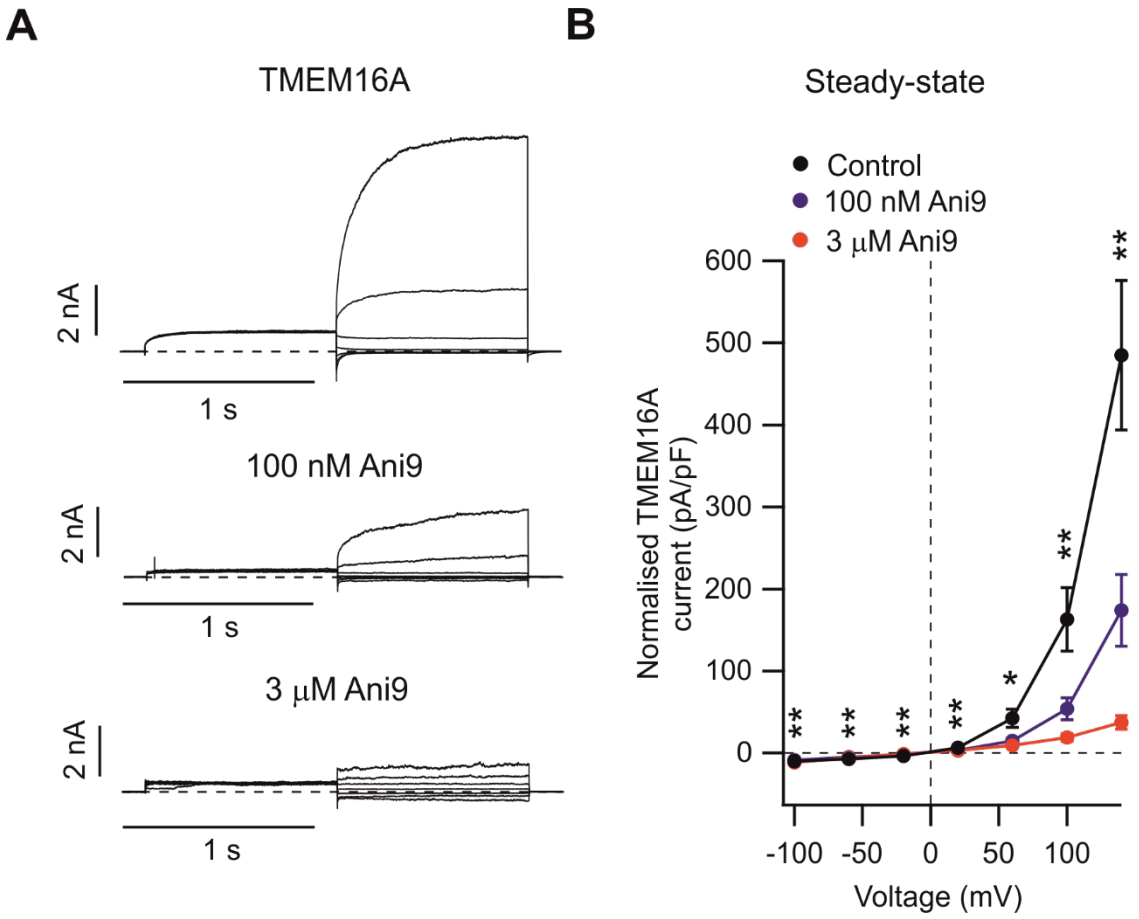

Figure 3.7. TMEM16A currents in response to Ani9

(A) TMEM16A expressing HEK-293T cells were studied in the whole-cell patch-clamp configuration, in response to the "IV-tail" protocol. Solutions contained 0.3 μM $[Ca^{2+}]_i$. Ani9 (100 nM or 3 μM) was applied as indicated. Dotted lines represent the zero-current level.

*(B) Mean steady-state TMEM16A current versus Vm relationships measured in the absence (control) or presence of Ani9 (100 nM or 3 μM), as indicated (n=7, two-way ANOVA, *P<0.05, ** P<0.005).*

3.3. Functional characterisation of Ani9 on cloned TMEM16x channels

3.3.1. Ani9 modulation of TMEM16A in high $[Ca^{2+}]_i$

A full characterisation of the effects of Ani9 on TMEM16A has not yet been published. In the following experiments, the effect of Ani9 on TMEM16A currents during conditions of high $[Ca^{2+}]_i$ (1 μM) were assessed. TMEM16A current was elicited using the "IV-tail" voltage protocol.

On addition of Ani9 (3 μM) the TMEM16A currents were only partially inactivated (Fig. 3.8). TMEM16A currents in high $[Ca^{2+}]_i$ were 1544.60 ± 450.75 pA/pF in control, and reduced to 306.03 ± 112.51 pA/pF in the presence of Ani9 (3 μM) (n=8). TMEM16A currents were measured at the end of the test pulse and normalised for the Cm (Fig. 3.8).

The mean TMEM16A currents measured in standard $[Ca^{2+}]_i$ (0.3 μM, Fig. 3.7) were also plotted in figure 3.8 for comparison (dashed lines). In low $[Ca^{2+}]_i$ (0.3 μM), Ani9 (3 μM) produced a near full block of TMEM16A (Fig. 3.7). However, in high $[Ca^{2+}]_i$ (1 μM), Ani9 inhibits TMEM16A but leaves a residual, unblocked, TMEM16A current ~8.2-fold greater. This suggests Ani9 is a less potent inhibitor of TMEM16A when $[Ca^{2+}]_i$ is increased.

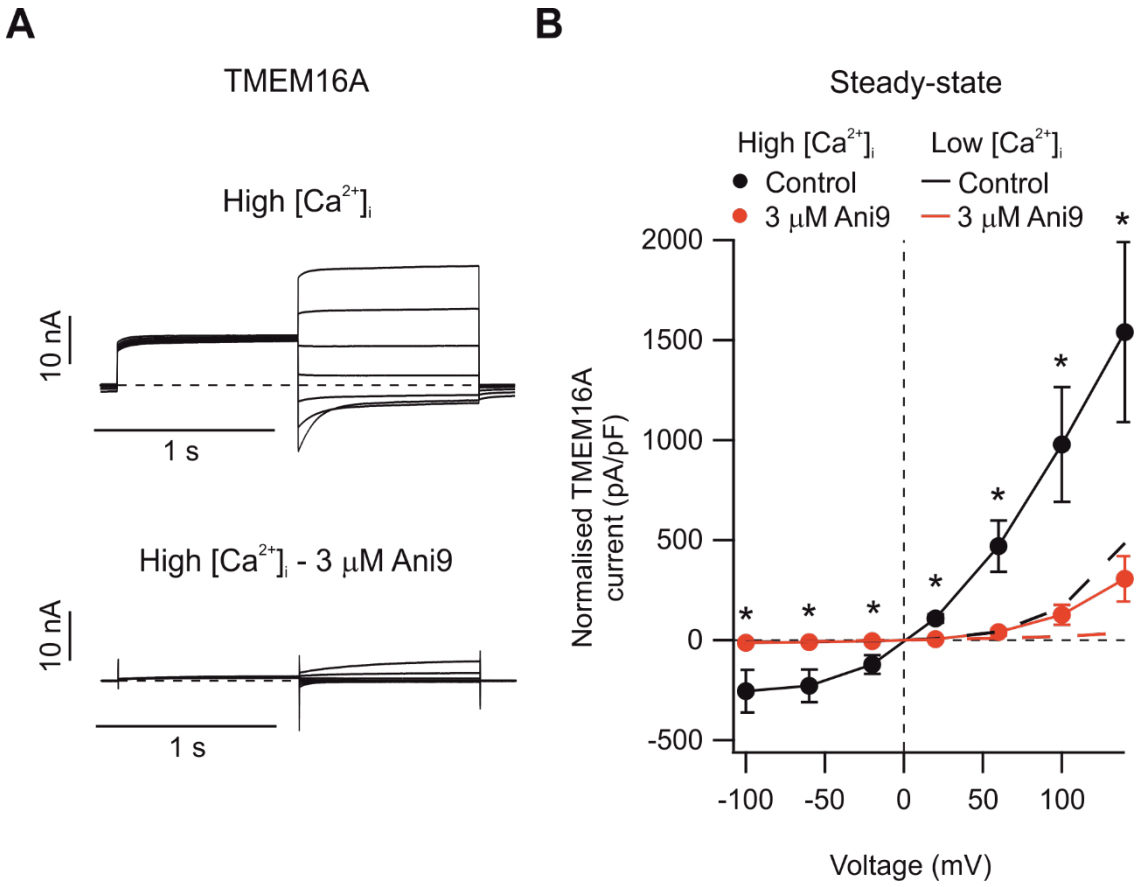

Figure 3.8. Ani9 modulation of TMEM16A at high $[Ca^{2+}]_i$

(A) TMEM16A expressing HEK-293T cells were studied in the whole-cell patch-clamp configuration, in response to the "IV-tail" protocol. High intracellular Ca^{2+} CaCC solutions contained 1 μM free $[Ca^{2+}]_i$. Ani9 (3 μM) was applied as indicated. Currents were analysed at the end of the test-pulse. Dotted lines represent the zero-current level.

*(B) Mean steady-state TMEM16A current versus Vm relationships measured in low and high Ca^{2+} solutions. TMEM16A currents were recorded in the absence or presence of Ani9 (3 μM), as indicated. Dashed mean TMEM16A current vs Vm relationships represent mean TMEM16A currents in low Ca^{2+} from figure 3.7, in the absence or presence of Ani9 (3 μM), as indicated. Number of experiments was (n=8). Statistical comparison of Ani9 in high $[Ca^{2+}]_i$ (two-way ANOVA, *P<0.05).*

3.3.2. Ani9 modulation of TMEM16B

Unlike TMEM16A, TMEM16B was reported to be unaffected by Ani9 (Seo et al., 2016). However, this has not been confirmed by other research groups. As the current set of experiments aim to test whether Ani9 is selective for TMEM16A, the following experiments were designed to confirm whether TMEM16B is modulated by Ani9.

Whole-cell TMEM16B currents were studied using the whole-cell patch-clamp technique in the presence of 0.6 μM $[Ca^{2+}]_I$, using the "IV-steps" voltage protocol. TMEM16B currents were measured at the end of the test pulse, and normalised to the Cm. There was no significant difference to between the TMEM16B control current and TMEM16B in the presence of Ani9 (10 μM), which resulted in a normalised TMEM16B current of 1.01 ± 0.01 (n=4) (Fig. 3.9). It was therefore confirmed that Ani9 does not modulate TMEM16B, a finding that is in line with the original publication (Seo et al., 2016).

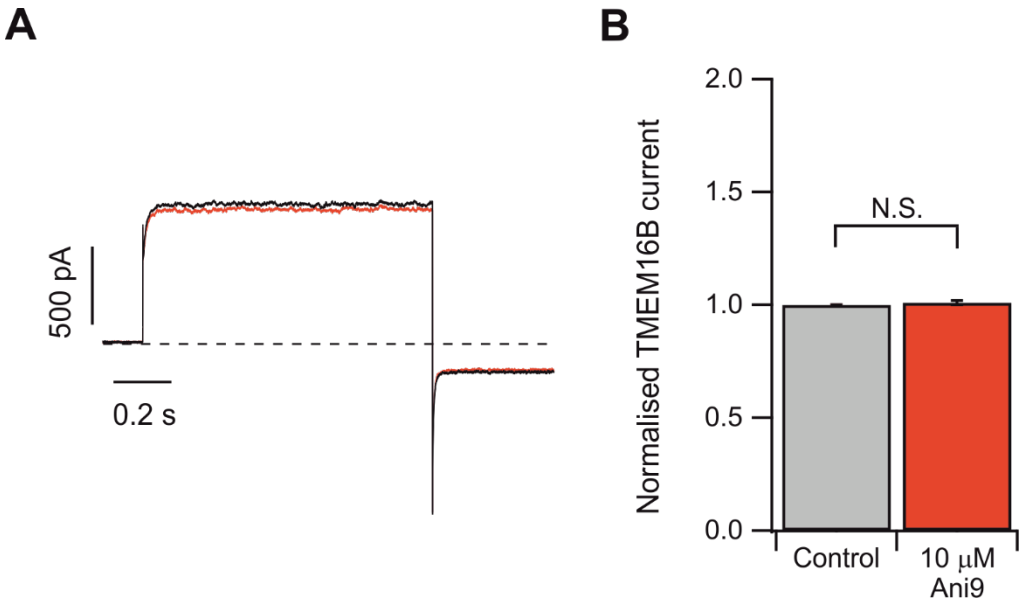

Figure 3.9. TMEM16B currents in response to Ani9

(A) TMEM16B expressing HEK-293T cells were studied in the whole-cell patch-clamp configuration, in response to the "IV-tail" protocol. Solutions contained 0.6 μM free $[Ca^{2+}]_i$. Ani9 (10 μM) was applied as indicated. Dotted line represents zero-current level.

(B) Mean normalised TMEM16B current at 70 mV in the absence (control) and presence of Ani9 (10 μM). TMEM16B current was analysed during the steady-state, and normalised to control conditions. N.S. P>0.05 (paired t-test, n=4).

3.3.3. Ani9 modulation of TMEM16F

TMEM16F behaves as a CaCC and a phospholipid scramblase (Pedemonte and Galietta, 2014, Hartzell et al., 2009, Acheson, 2016). There are currently no reported synthetic, small-molecule pharmacological modulators of TMEM16F. The following experiment explores the effect of Ani9 on TMEM16F currents.

Whole-cell TMEM16F currents were elicited using the "IV-steps" voltage protocol in the presence of 78 μM $[Ca^{2+}]_i$. High $[Ca^{2+}]_i$ was required as TMEM16F has reduced Ca^{2+} sensitivity (Pedemonte and Galietta, 2014, Hartzell et al., 2009, Acheson, 2016). TMEM16F currents were recorded six minutes after establishing the whole-cell configuration, as TMEM16F current slowly activates during whole-cell patch-clamping (Fig. 3.3).

It was found that TMEM16F was profoundly activated by Ani9. TMEM16F current was 13.48 ± 4.16 pA/pF at 70 mV, which increased to 63.61 ± 12.21 pA/pF (n=5) on addition of Ani9 (10 μM) (Fig. 3.10). At 70 mV Ani9 (10 μM) therefore increased TMEM16F current by ~4.7-fold.

To examine the possibility that Ani9 activates an endogenous currents in HEK-293T cells under conditions of high $[Ca^{2+}]_i$, NT cells were exposed to Ani9 (10 μM). NT cells containing 78 μM $[Ca^{2+}]_i$ were unaffected by Ani9 (10 μM), with control currents of 9.32 ± 3.62 pA/pF at 70 mV, and 8.35 ± 3.47 pA/pF in the presence of Ani9 (10 μM) (n=5) (Fig. 3.10).

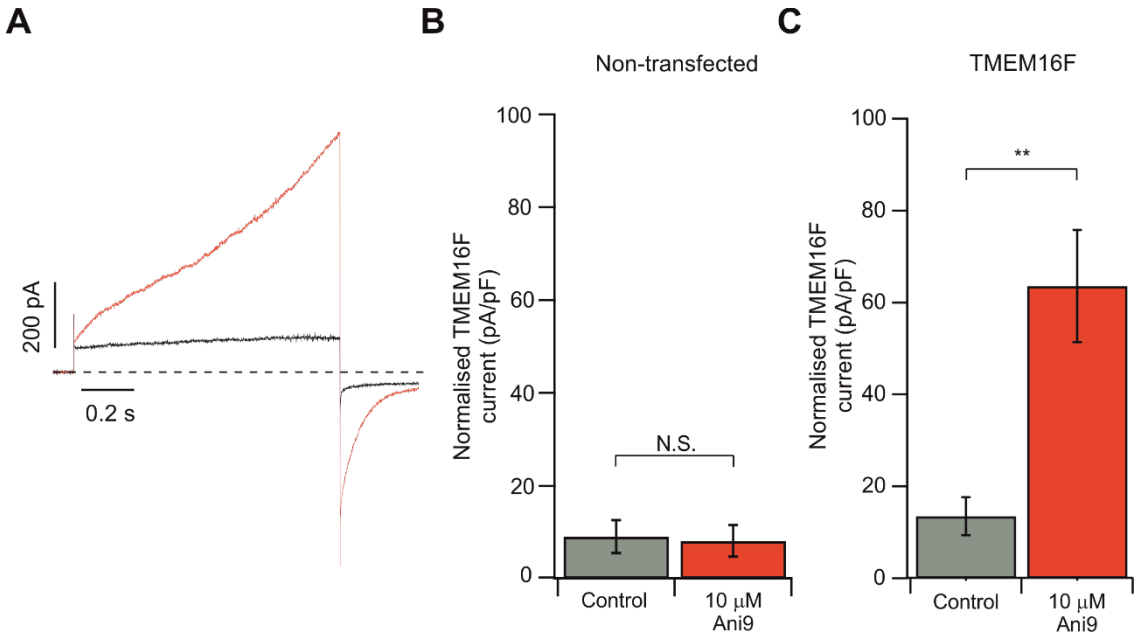

Figure 3.10. Effect of Ani9 on TMEM16F currents

(A) TMEM16F expressing HEK-293T cells were studied in the whole-cell patch-clamp configuration, in response to the "IV-tail" protocol. Solutions contained 78 μM free $[Ca^{2+}]_i$. Ani9 (10 μM) was applied as indicated. Dotted line represents zero-current level.

(B) Mean non-transfected HEK-293T cell current at 70 mV in the absence (control) and presence of Ani9 (10 μM). Current was analysed at the end of the voltage step, and normalised to control conditions. N.S. P>0.05 (paired t-test, n=5).

*(C) Mean normalised TMEM16F current at 70 mV in the absence (control) and presence of Ani9 (10 μM). TMEM16F current was analysed at the end of the voltage step, and normalised to control conditions. ** P<0.005 (paired t-test, n=5).*

3.4. Native currents in isolated VSMCs

Previous experiments in this chapter have confirmed that Ani9 is a potent blocker of TMEM16A in our experimental setup. The following experiments were designed to study the effect of Ani9 on native TMEM16A currents, and the effect of genetic deletion of one TMEM16A allele (TMEM16A heterozygous KO model). In addition, the effect of Ani9 on cationic currents in VSMCs was tested in order to define the selectivity of Ani9 for TMEM16A.

3.4.1. Effect of TMEM16A genetic depletion VSMCs

TMEM16A currents were studied in aortic VSMCs obtained from mice with a heterozygous knock-out for the TMEM16A gene (TMEM16A-Het-KO). VSMCs obtained from TMEM16A homozygous knock-out mice were not available, as this genetic deletion is embryonically lethal (Rock et al., 2008).

Wild-type and TMEM16A-Het-KO VSMCs were studied using patch-clamp electrophysiology. Solutions containing 0.6 μM $[Ca^{2+}]_i$, and the "IV-CaCC" voltage protocol was used to elicit whole-cell TMEM16A currents. Currents were analysed at the end of the test-pulse, and were normalised to the Cm (Fig.3.11). At 100 mV, TMEM16A currents were 45.16 ± 6.46 pA/pF (n=3). In TMEM16A-Het-KO VSMCs, TMEM16A current was reduced by ~1.9-fold to 23.85 ± 2.78 pA/pF (n=5). This effect was statistically significant at *Vm* below -80 mV and above 40 mV.

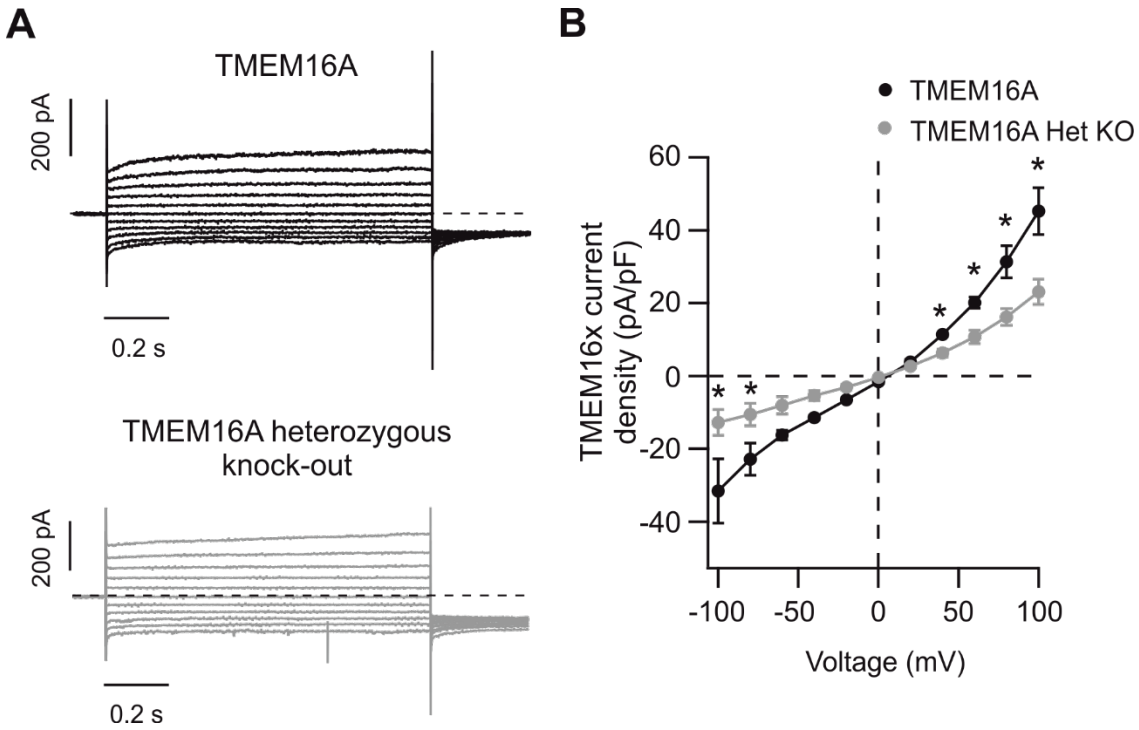

Figure 3.11. Effect of TMEM16A-Het-KO in VSMCs

(A) Whole-cell patch-clamp TMEM16A currents recorded using VSMCs isolated from a wild-type and TMEM16A-Het-KO mice. Solutions contained 0.6 µM $[Ca^{2+}]_i$. The "IV-CaCC" protocol was used to elicit TMEM16A currents in the wild-type (control, shown in black) or TMEM16A-Het-KO (grey) VSMCs.

*(B) Mean whole-cell current measured between -100 mV and 100 mV in 20 mV increments, in wild-type (n=3) or TMEM16A-Het-KO (n=5) VSMCs (two-way ANOVA, *P<0.05).*

3.4.2. Effect of Ani9 on native TMEM16A currents in VSMCs

The previous experiment confirms a role of TMEM16A in VSMCs, via heterozygous deletion of the TMEM16A gene. In order to assess whether Ani9 would be able to replicate this effect via inhibition of TMEM16A, Ani9 was tested on native TMEM16A in VSMCs.

VSMCs were studied using whole-cell patch-clamp electrophysiology. Solutions contained 0.6 μM $[Ca^{2+}]_i$, and whole-cell TMEM16A current was generated using the "IV-ramp" protocol. TMEM16A currents were normalised using the Cm and plotted against the *Vm*. At -95 mV, TMEM16A current was reduced by ~1.4-fold in the presence of Ani9 (1 μM) compared to the control (Fig. 3.12). At 95 mV, TMEM16A current was reduced by ~2.3-fold in the presence of Ani9 (1 μM) compared to the control (Table 3.5). This data demonstrates that Ani9 (1 μM) blocks native TMEM16A currents in VSMCs at all *Vm* tested, except from at -5 mV which is a *Vm* close to the E_{rev}.

Table 3.5. Effect of Ani9 on native TMEM16A currents in VSMCs

	Control (pA/pF)	Ani9 (pA/pF)
-95 mV	-9.63 ± 1.59	-6.99 ± 1.46
95 mV	24.61 ± 3.62	10.90 ± 1.08
n	9	9
N	6	6

"-95 mV" and "95 mV" refer to the current obtained at these Vm. "n" refers number of experiments, "N" is number of animals.

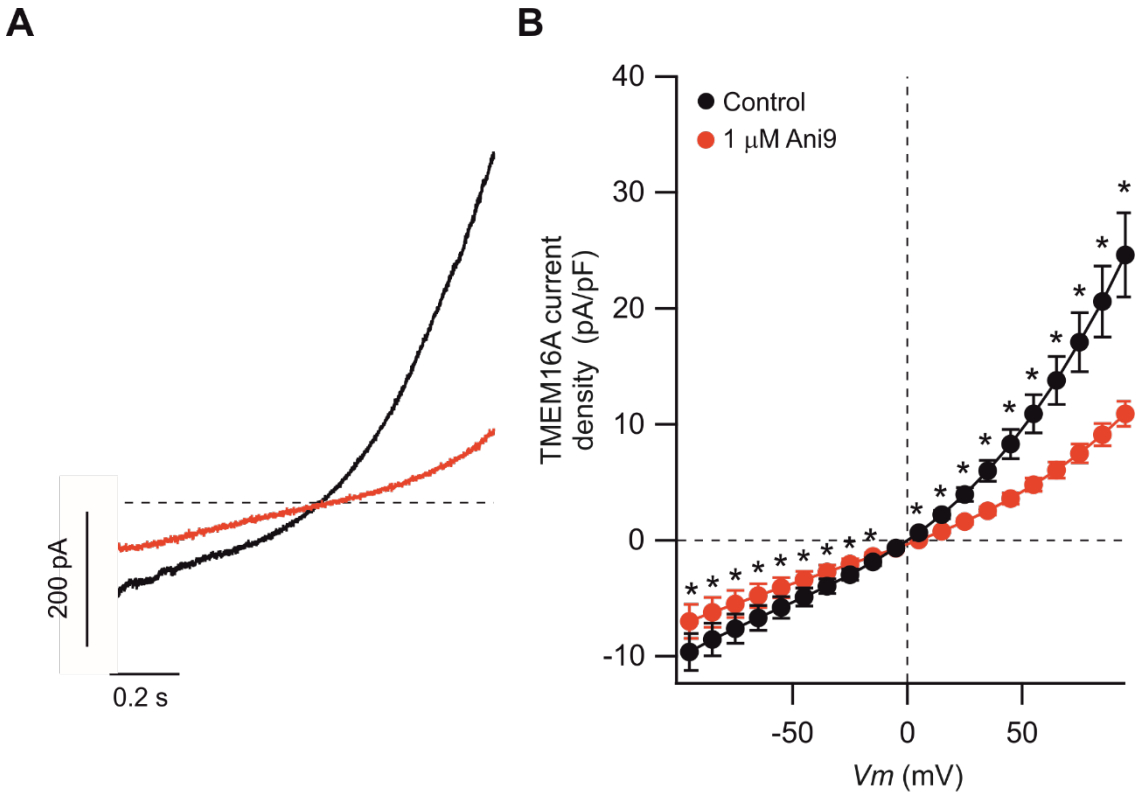

Figure 3.12. Ani9 effect on TMEM16A current in VSMCs.

(A) Whole-cell patch-clamp native TMEM16A currents recorded in isolated VSMCs. Solutions contained 0.6 μM $[Ca^{2+}]_i$, and the "IV-ramp" protocol was used to elicit TMEM16A currents in the absence (control, shown in black) or presence (red) of Ani9 (1 μM).

*(B) Mean whole-cell current measured from -95 mV to 95 mV in 10 mV increments, in the absence (black, control), or presence of Ani9 (red), *P<0.05 (two-way ANOVA, n=9).*

3.4.3. Effect of Ani9 on cationic currents in VSMC

The previous experiment (Fig. 3.12) demonstrates that Ani9 blocks native TMEM16A in VSMCs at all *Vm* tested. In order for Ani9 to be used as a blocker of TMEM16A in intact isolated aorta contraction studies, we first needed to establish the specificity of Ani9 in VSMCs. As little is known about the specificity of Ani9, it was studied here using solutions favourable for cationic VSMC currents.

Isolated VSMCs were studied using the whole-cell patch clamp technique in the presence of "cationic solutions" (Tables 2.8 and 2.9). These solutions were designed to include physiological concentrations of ions in the VSMCs, but to not favour TMEM16A activity, as $[Ca^{2+}]_i$ is maintained low (<10 nM) to prevent TMEM16A channel activation. The "IV-ramp" protocol was used to assess the VSMC cationic current at a range of *Vm* between -100 mV and 100 mV. VSMC cationic currents were normalised for the Cm. Under these conditions, Ani9 (1 μM) did not affect VSMC cationic currents at any *Vm* tested (Fig 3.13, Table 3.6). This suggests Ani9 does not modulate any large-current cationic ion channels expressed in VSMCs.

Table 3.6. Effect of Ani9 on cationic currents in VSMCs

	Control (pA/pF)	Ani9 (pA/pF)
-95 mV	-9.85 ± 2.37	-9.28 ± 2.21
95 mV	171.87 ± 42.44	188.44 ± 49.25
n	5	5
N	5	5

"-95 mV" and "95 mV" refer to the current obtained at these Vm. "n" refers number of experiments, "N" is number of animals.

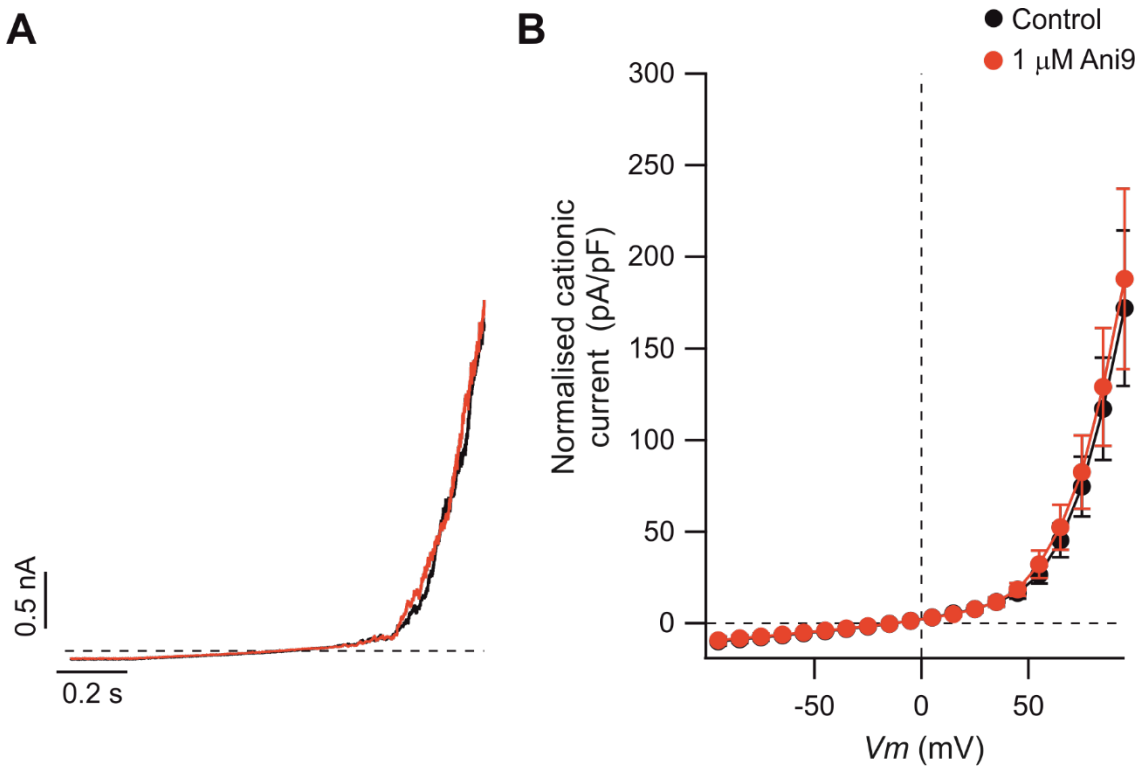

Figure 3.13. Ani9 effect on cationic currents in VSMCs.

(A) Whole-cell patch-clamp recordings of cationic currents from isolated VSMCs. "Cationic solutions" in combination with the "IV-ramp" protocol were used to elicit cationic VSMC currents in the absence (control, shown in black) or presence (red) of Ani9 (1 μM).

(B) Mean whole-cell current measured from -95 mV to 95 mV in 10 mV increments, in the absence (black, control), or presence of Ani9 (red), N.S. P>0.05 (two-way ANOVA, n=5).

3.4.4. Effect of Ani9 on Ca_V currents in VSMCs

The experiments in the previous section demonstrate that Ani9 does not modulate cation currents in VSMCs. The solutions used in these experiments, in spite of being suitable to reveal K^+ and non-selective cation currents (such as those mediated by TRP channels), may not enable detection of Ca_V currents. As Ca_V currents present activation and inactivation components, recording of Ca_V currents requires the *Vm* to be maintained for a sufficiently long duration (rendering the "IV-ramp" protocol in fig. 3.13 unsuitable). Furthermore, Ca_V currents can be amplified with solutions containing Ba^{2+} (Tables 2.10 and 2.11).

Whole-cell patch-clamp electrophysiology of VSMCs was conducted using "Ca_V solutions" and the "IV-Ca_V" voltage protocol, in order to record VSMC Ca_V currents in the presence and absence of Ani9. Ca_V currents were normalised to Cm, and measured at the peak of each *Vm* (Fig. 3.14). Overall, this experiment demonstrates that Ca_V currents were unaffected by Ani9 (1 μM, table 3.7). Taken together, the VSMC electrophysiology experiments using Ani9 therefore demonstrate that Ani9 is specific for TMEM16A.

Table 3.7. Effect of Ani9 on cationic currents in VSMCs

	Control (pA/pF)	Ani9 (pA/pF)
10 mV	-4.26 ± 0.79	-4.18 ± 0.98
n	8	8
N	5	5

"10 mV" refers to the current obtained at this Vm. "n" refers number of experiments, "N" is number of animals.

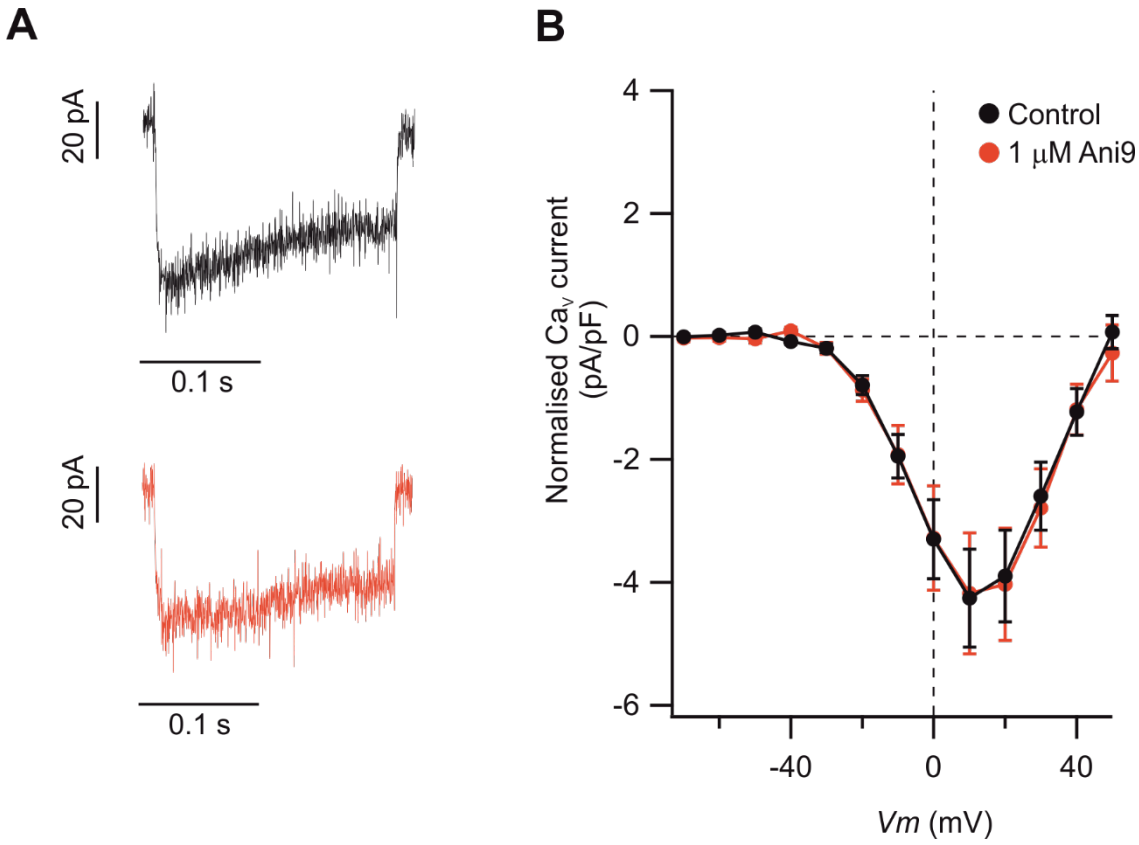

Figure 3.14. Effect of Ani9 on Ca_V currents in VSMCs.

(A) Whole-cell patch-clamp Ca_V currents recorded using isolated VSMCs. "Ca_V solutions" in combination with the "Ca_V" voltage protocol were used to elicit Ca_V currents in the absence (control, shown in black) or presence (red) of Ani9 (1 μM). Representative traces result from the 10 mV test-pulse. Dotted line represents zero current level.

(B) Mean whole-cell current measured from -95 mV to 95 mV in 10 mV increments, in the absence (black, control), or presence of Ani9 (red), N.S. P>0.05 (two-way ANOVA, n=8).

3.5. Effect of TMEM16A inhibition in isolated aortic rings

TMEM16A accounts for the CaCC component in VSMCs, and is implicated in agonist-induced blood vessel contraction (Matchkov et al., 2015, Pedemonte and Galietta, 2014). This section aims to gain an initial understanding of the role of TMEM16A in agonist-induced blood vessel contraction, using Ani9 to reduce TMEM16A activity, and genetic reduction of TMEM16A currents using the TMEM16A-Het-KO.

Myography was used to study freshly isolated murine aortic rings. The mounting and normalisation procedures for myography experiments is described fully in chapter 2. Phenylephrine (PE) was used as the contractile agonist for these experiments.

3.5.1. Effect of Ani9 on isolated aortic rings

Ani9 has been demonstrated to be a potent blocker of cloned TMEM16A channels (Fig. 3.7), and native TMEM16A channels in VSMCs (Fig. 3.12). Ani9 therefore represents an experimental tool to investigate the role of TMEM16A in agonist-induced contraction.

The isolated aortic rings were incubated in the presence of Ani9 (1 μM), or left untreated (control) for 20 minutes, prior to addition of increasing concentrations of PE. The tension obtained at various [PE] was normalised for the tension evoked by 55 mM KCl (detailed in section 2.9.2), and plotted *versus* [PE] (Fig. 3.15). The tension *versus* [PE] experiments were fitted with the Hill equation (Table 3.8). Aortic contraction was significantly reduced ($P<0.05$) in the presence of Ani9 (1 μM), with a ~2.2-fold reduction compared to the control.

Table 3.8. Overview of blood vessel contraction in the presence or absence of Ani9.

	Control	Ani9
10 μM PE	0.60 ± 0.03	0.29 ± 0.06
Plateau of fit	0.61 ± 0.01	0.30 ± 0.01
PE EC_{50}	0.16 ± 0.01	0.13 ± 0.01
h	1.12 ± 0.05	0.19 ± 0.08
n	7	7
N	7	7

"10 μM PE" is the tension obtained in the presence of this [PE], and normalised for the tension measured in 55 mM KCl. "Plateau of fit" is the maximal value of aortic contraction determined via the Hill fit of the data (equation 2.2). The "PE EC_{50}" is the value of [PE] required to reach half maximal contraction. The "h" value is the Hill coefficient and represents the slope of the Hill fit. "n" is number of experiments, "N" is number of animals.

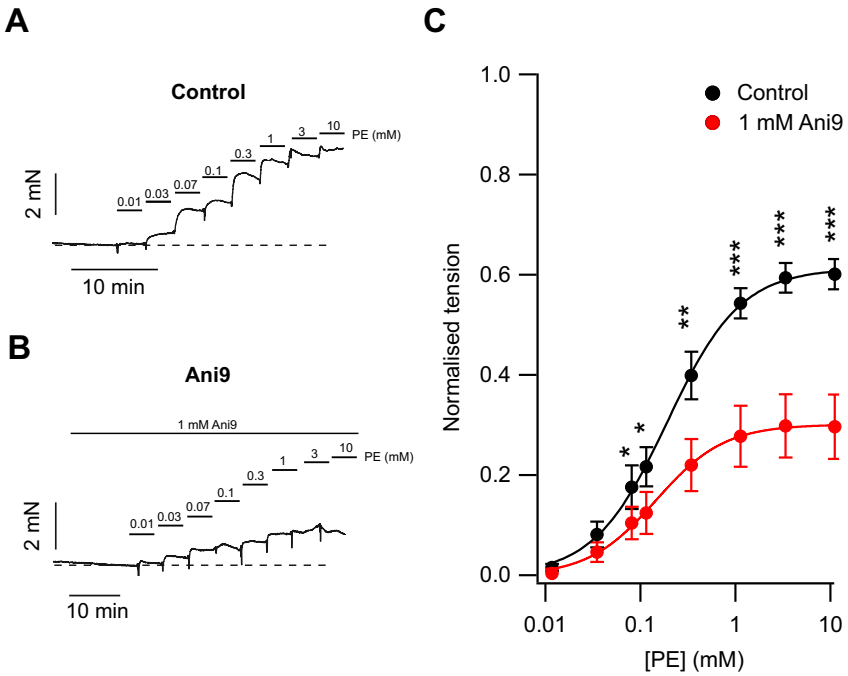

Figure 3.15. Effect of Ani9 on PE-mediated contraction of aortic rings

(A) Representative change in isometric tension of control aortic rings in response to increasing [PE], as indicated. Dotted lines represent baseline tension.

(B) Representative change in isometric tension of control aortic rings in response to increasing [PE] in the presence of Ani9 (1 μM), as indicated. Dotted lines represent baseline tension.

*(C) Mean tension vs [PE] relationship of control (n=7), and Ani9 (1 μM) (n=7) aortic rings. *P<0.05, **P<0.005, ***P<0.0005 (two-way ANOVA).*

3.5.2. TMEM16A heterozygous knock-out

Aortic rings obtained from TMEM16A-Het-KO mice were utilised in order to assess how a reduction in TMEM16A expression affects agonist-induced constriction of isolated aortic rings.

The tension obtained at various [PE] was normalised for the tension evoked by 55 mM KCl (detailed in section 2.9.2), and plotted *versus* [PE] (Fig. 3.16). PE-mediated aortic contraction was reduced by ~1.8-fold in the TMEM16A-Het-KO model. This effect was found to be statistically significant ($P<0.05$) on addition of [PE] at 0.1 μM PE and above.

Table 3.9. Overview of TMEM16A-Het-KO vs wild-type blood vessel contraction.

	Control	TMEM16A-Het-KO
10 μM PE	0.60 ± 0.07	0.36 ± 0.08
Plateau of fit	0.62 ± 0.01	0.37 ± 0.01
PE EC_{50}	0.15 ± 0.01	0.17 ± 0.01
h	1.13 ± 0.06	1.14 ± 0.07
n	7	7
N	7	7

"10 μM PE" is the tension obtained in the presence of this [PE], and normalised for the tension measured in 55 mM KCl. "Plateau of fit" is the maximal value of aortic contraction determined via the Hill fit of the data (equation 2.2). The "PE EC_{50}" is the value of [PE] required to reach half maximal contraction. The "h" value is the Hill coefficient and represents the slope of the Hill fit. "n" is number of experiments, "N" is number of animals.

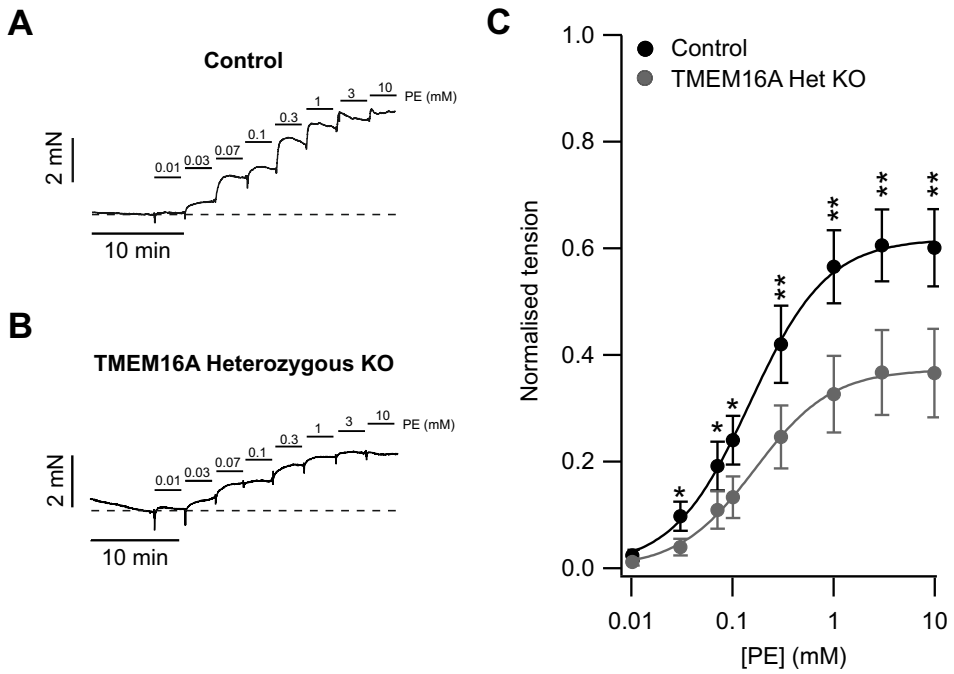

Figure 3.16. PE-mediated contraction of aortic rings in wild-type and TMEM16A-Het-KO

(A) Representative change in isometric tension of control aortic rings in response to increasing [PE]. Dotted lines represent baseline tension.

(B) Representative change in isometric tension of TMEM16A-Het-KO aortic rings in response to increasing [PE]. Dotted lines represent baseline tension.

*(C) Mean tension vs [PE] relationship of control (n=7), and TMEM16A-Het-KO (n=7) aortic rings. *P<0.05, **P<0.005 (two-way ANOVA).*

3.6. Calcium-activated chloride channels in isolated ventricular cardiomyocytes

To gain an understanding of whether TMEM16A functions in ventricular cardiomyocytes and therefore affects the vascular system indirectly, the whole-cell currents of murine isolated ventricular cardiomyocytes were studied. Ventricular cardiomyocytes were isolated from wild-type mice within the Lei/Terrar groups, and were generously donated for these experiments. Whole-cell patch-clamp experiments were conducted in the presence of "standard CaCC solutions" (Tables 2.4 and 2.5) containing 0.6 μM $[Ca^{2+}]_i$ (Table 2.6), using the "IV-ramp" voltage protocol.

Ani9 (1 μM) produced no significant reduction in whole-cell current, with a control current of 1112.58 ± 143.06 nA at 95 mV, and a current of 933.58 ± 125.13 nA in the presence of Ani9 (1 μM, Fig. 3.17). Overall, this data demonstrates that Ani9 does not affect whole-cell current in isolated ventricular cardiomyocytes. This suggests that TMEM16A is not responsible for a large anion current in this cell type. Alternatively, Ca^{2+} in the vicinity of TMEM16A channels is sufficiently high to reduce the effect of Ani9, as data in figure 3.8 demonstrates that Ani9 potency is reduced in the presence of high $[Ca^{2+}]_i$.

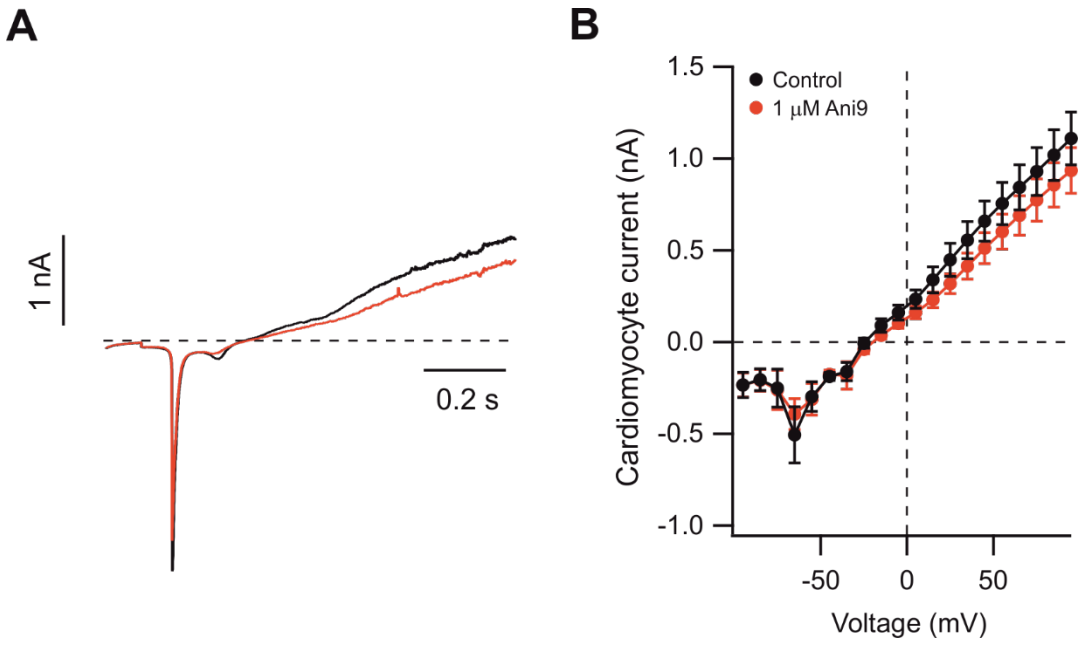

Figure 3.17. Effect of Ani9 on whole-cell currents in isolated ventricular cardiomyocytes

(A) Whole-cell patch-clamp whole-cell currents recorded from isolated ventricular cardiomyocytes from a wild-type mouse. Solutions contained 0.6 μM $[Ca^{2+}]_i$, and the "IV-ramp" protocol was used to elicit whole-cell currents in the absence (control, shown in black) or presence (red) of Ani9 (1 μM).

(B) Mean whole-cell current measured between -95 mV to 95 mV in 10 mV increments, in the absence (black, control), or presence of Ani9 (red, n=5). N.S. P>0.05 (two-way ANOVA).

3.7. Discussion

This chapter has elucidated the key electrophysiological properties of cloned TMEM16A in a heterologous expression system, and also native TMEM16A currents in VSMCs obtained from murine aorta and ventricular cardiomyocytes. CaCC currents in VSMCs are thought to be primarily mediated by TMEM16A, as the expression of TMEM16B is low in the thoracic aorta (Schreiber et al., 2010). The IV-relationship of cloned TMEM16F was also explored in this chapter, however it is unlikely to contribute to the Cl^- current in VSMCs due to the prolonged high $[Ca^{2+}]_i$ required for its activation.

Current pharmacology of TMEM16A channels was explored, with a particular focus on Ani9. Subsequently, the functional role of native TMEM16A in VSMCs was assessed using Ani9, a pharmacological blocker of TMEM16A, and the TMEM16A-Het-KO. The effect of TMEM16A inhibition was also assessed in isolated aortic rings.

3.7.1. Cloned and native TMEM16x channels

This chapter studied some of the electrophysiological properties of cloned TMEM16A, TMEM16B and TMEM16F. This was to confirm that these cloned channels had similar electrophysiological profiles to that stated in the literature, so that appropriate comparisons of these results could be made. Furthermore, Ca^{2+}-sensitivity of TMEM16A and TMEM16B were defined, so that the extent of channel activation at a range of $[Ca^{2+}]_i$ could be defined for experiments.

Isolated VSMCs were studied using solutions favourable for eliciting TMEM16A currents. Native TMEM16A VSMC current was found to demonstrate a similar outwardly-rectifying IV-relationship to cloned TMEM16A channels, in agreement with TMEM16A studies both within the research group and the wider TMEM16A literature

(Adomaviciene et al., 2013, Manoury et al., 2010, Heinze et al., 2014, Jensen et al., 2018). This VSMC current was also blocked by Ani9, suggesting that TMEM16A is responsible for this current. This VSMC current was unlikely to be mediated by TMEM16B or TMEM16F, as TMEM16B has low expression in VSMCs (Schreiber et al., 2010), and TMEM16F requires very high $[Ca^{2+}]_i$ for activation (Pedemonte and Galietta, 2014).

3.7.2. TMEM16A pharmacology

TMEM16A pharmacology remains in early stages of development. In this chapter, examples of pharmacological modulators from the literature were studied. It was found that reported TMEM16A potentiators such as Eact were unable to modulate TMEM16A activity, and the TMEM16A blocker MONNA was found to be less potent than reported (Oh et al., 2013).

In order to provide a suitable control for myography experiments involving bumetanide detailed in chapter 5, bumetanide was tested on cloned TMEM16A channels. As bumetanide is a potent blocker of the NKCC1 exchanger (Ben-Ari, 2017), it was used experimentally to modulate $[Cl^-]_i$. It was therefore necessary to establish whether bumetanide pharmacologically alters TMEM16A activity, to ensure that any changes seen in myography results were due to reduced $[Cl^-]_i$, and not as a result of direct TMEM16A modulation. It was found that bumetanide does not modulate cloned TMEM16A channel activity, and was therefore concluded to be a suitable tool for modulating $[Cl^-]_i$ in myography experiments.

The remainder of this chapter focused on TMEM16A modulation by Ani9, as it is reported to be a potent and selective blocker of TMEM16A (Seo et al., 2016). The

modulatory effect of Ani9 on TMEM16A has not been well characterised in the literature. This chapter has started to investigate the effect of Ani9 on TMEM16A under conditions of high $[Ca^{2+}]_i$, and the effect of Ani9 on TMEM16B and TMEM16F.

Results presented in this chapter confirmed that Ani9 is a potent blocker of cloned TMEM16A channels, and has no effect on TMEM16B. Ani9 showed a strong potentiation of the Cl^- current mediated by the phospholipid scramblase TMEM16F, however this effect was demonstrated under conditions of high $[Ca^{2+}]_i$ over a timescale of minutes, so this modulation may have no physiological relevance. It was beyond the scope of this project to study whether Ani9 effects phospholipid scrambling of TMEM16F, however as the phospholipid scramblase pathway and Cl^--conduction pathway are shared (Suzuki et al., 2014), it could be speculated that both functions would be affected.

These results suggest that Ani9 requires more testing in order to assess its suitability as a clinical candidate for targeting TMEM16A, as off-target modulation of TMEM16F could cause increased phospholipid scrambling in cells such as platelets, and therefore cause vascular disease such as blood clotting (Bricogne et al., 2019, Gilbert et al., 2015). These findings provide a strong case for directing research efforts into finding additional potent and selective modulators of TMEM16A activity.

3.7.3. TMEM16A in VSMC agonist induced contraction

Two approaches were taken in order to define the role of TMEM16A in VSMC agonist induced contraction. Firstly, the role of native TMEM16A was elucidated in isolated VSMCs using patch-clamp electrophysiology. Subsequently, the role of native

TMEM16A in isolated aortic rings was studied using myography. Both of these approaches used the TMEM16A-Het-KO, and the potent TMEM16A blocker Ani9.

This chapter has provided evidence that there is a TMEM16A component to the global VSMC current. In "standard CaCC solutions" (Tables 2.4 and 2.5), the $[Ca^{2+}]_i$ was 0.6 μM (Table 2.6), higher than the concentration used when cloned TMEM16A currents were studied in HEK-293T cells. This is because native TMEM16A expression is lower in VSMCs (Dam et al., 2014, Jensen et al., 2018). Ani9 was found to block TMEM16A currents in VSMCs, however in solutions that favour cation currents Ani9 had no effect. This result was in agreement with the original Ani9 publication, which also found Ani9 to be selective for TMEM16A when tested on a selection ion channel types (Seo et al., 2016). VSMCs obtained from the TMEM16A-Het-KO had reduced TMEM16A currents compared to the wild-type.

A similar result was observed in isolated aortic rings, with the TMEM16A-Het-KO reducing PE-mediated aortic contraction. This effect was replicated using Ani9 on wild-type aortic rings. This data is in agreement with a study by Heinze et al., which studied the effects of complete genetic deletion of TMEM16A in systemic arteries, and observed reduced aortic contraction (Heinze et al., 2014).

3.7.4. The role of TMEM16A in isolated ventricular cardiomyocytes

TMEM16A is expressed in the heart, and has been found to have a role in ischemia-induced arrhythmias, via disruption of the repolarisation of cardiomyocytes during an action potential (Ye et al., 2015). Experiments in this chapter were carried out using "standard CaCC solutions" (Tables 2.4 and 2.5) in order to begin to understand the role of TMEM16A in isolated cardiomyocytes, and to minimise the effect of other ion

channels during recording. At around -60 to -65 mV the *Vm* reaches a threshold during the activation phase of the cardiac action potential that triggers a depolarising Na^+ current (Herring and Paterson, 2018), which was observed at this *Vm* in our recordings (Fig. 3.17). In our experimental setup, Ani9 was unable to block any whole-cell currents recorded. We hypothesise that this does not necessarily correlate with a lack of TMEM16A activity, but could be a result of the size of cardiomyoctes. If the cardiomyoctes are too large for the $[Ca^{2+}]_i$ to be clamped, it could be present in a higher concentration than expected. This would result in a lower potency of Ani9, similar to that demonstrated earlier in this chapter on experiments studying the effect of Ani9 on cloned TMEM16A channels at high $[Ca^{2+}]_i$ (Fig. 3.8).

3.7.5. Physiological significance

The experiments in this chapter demonstrate that Ani9 is a potent blocker of cloned and native TMEM16A. The proximity of the TMEM16A pore to the plasma membrane has evoked interest in the lipid regulation of TMEM16A (Dang et al., 2017, Paulino et al., 2017). Once this has been fully characterised, this could provide an avenue into clinical targeting of TMEM16A.

This chapter also demonstrates that reduction of TMEM16A currents by genetic or pharmacological methods reduces PE-induced vascular contractility. It could therefore be speculated that mutations in TMEM16A could lead to clinical vascular disease, and therefore be an underlying cause of idiopathic vascular disease.

Chapter 4

Understanding the PIP_2 regulation of TMEM16A

Chapter 4 – Understanding the PIP_2 regulation of TMEM16A

Phosphatidylinositol-4,5-bisphosphate (PIP_2) is a ubiquitous signalling lipid located in the inner leaflet of the plasma membrane. PIP_2 is formed in an ATP-dependent process involving phosphorylation of phosphatidylinositol-4-phosphate (PIP) by PIP 5-kinase (PIPK), and it is cleaved by PLC following activation of the Gq-PCR signalling cascade (Loew, 2007). The importance of ion channel modulation by PIP_2 has been widely explored, and PIP_2 has been demonstrated to modulate a variety of ion channel types (Suh and Hille, 2008, Hille et al., 2015). For channels such as KCNQ1, PIP_2 is reported to be mandatory for channel function (Zhang et al., 2003, Loussouarn et al., 2003, Zaydman et al., 2013, Royal et al., 2017).

This chapter investigates the PIP_2 modulation of cloned TMEM16A. Pritchard *et al.* (2014) demonstrated that PIP_2 has an inhibitory effect on native I_{CaCC} current in rat isolated pulmonary VSMCs (Pritchard et al., 2014). However, the effect of PIP_2 modulation of cloned TMEM16A channels was not explored in this paper. The study described in this chapter therefore aims to begin to examine the regulation of cloned TMEM16A channels by PIP_2, in order to reveal the mechanism of this modulation.

The modulation of TMEM16A in response to a water-soluble analogue of PIP_2 (diC8-PIP_2) was initially tested, in order to understand whether cloned TMEM16A currents were affected by PIP_2. To explore the effect of endogenous PIP_2 on cloned TMEM16A channels, a voltage-sensitive phosphatase (VSP) or the α1-adrenergic receptor were co-transfected with TMEM16A in order to deplete endogenous PIP_2 in the plasma membrane. Subsequently, TMEM16A pharmacology when endogenous PIP_2 was depleted was assessed, in order to understand whether the response of TMEM16A to pharmacological agents could be disrupted during Gq-PCR activation and associated

PIP_2 depletion from the plasma membrane. Finally, a mutagenesis strategy was taken in order to explore a potential PIP_2 binding site.

4.1. Sensitivity of TMEM16A channels to diC8-PIP_2

The direct modulation of TMEM16A by diC8-PIP_2 analogue was tested during inside-out patch-clamp recording, so that the intracellular side of the TMEM16A could be directly exposed to diC8-PIP_2. This patch-clamp configuration also allows the effect of diC8-PIP_2 on TMEM16A to be studied independent of the intracellular environment. Patches were excised from non-transfected HEK-293T cells, and cells expressing cloned TMEM16A channels. In these experiments, *Vm* was kept constant at 70 mV, and $[Ca^{2+}]_i$ was 0.6 µM. The first observation was that patches excised from non-transfected cells had very small current amplitudes. This small endogenous current was unaffected by addition of diC8-PIP_2 (Fig 4.1). This excluded the possibility that endogenous diC8-PIP_2-sensitive currents existed in the patches. When diC8-PIP_2 was applied to the intracellular side of the patch obtained from cells transfected with TMEM16A, the TMEM16A current increased in a dose-dependent manner up to a factor of 1.26 ± 0.04 (n=12) in 100 µg/ml (117 µM) diC8-PIP_2. The Hill equation of the relationships between the TMEM16A current and [diC8-PIP_2] yielded a EC_{50} of 45 µg/ml (53 µM) and *h* of 1.2.

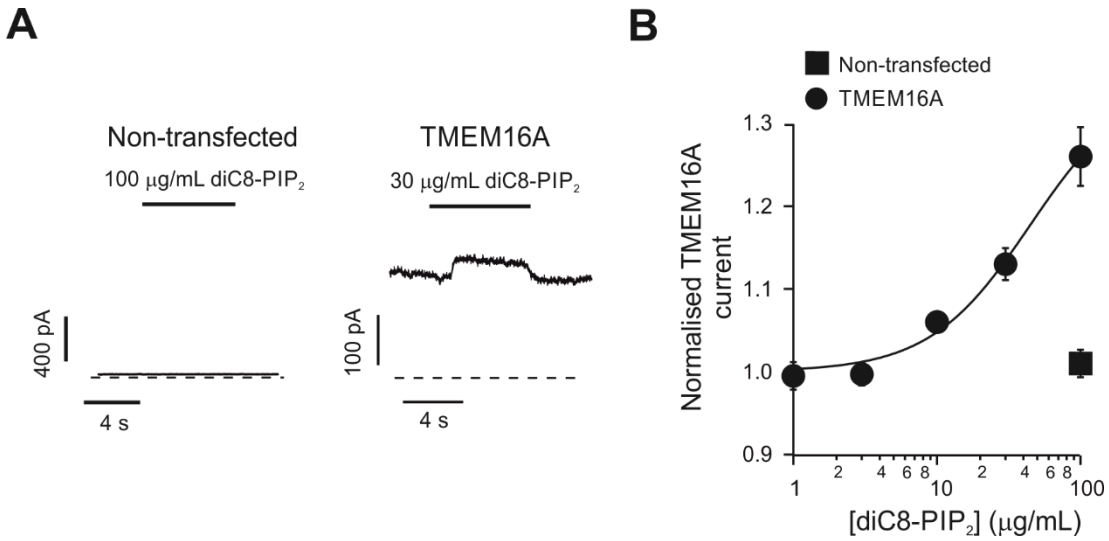

Figure 4.1. Effect of diC8-PIP_2 on TMEM16A currents

(A) Currents recorded from inside-out patches excised from NT HEK-293T cells, or cells expressing TMEM16A. The water-soluble PIP_2 analogue diC8-PIP_2 was applied to the intracellular side of the patch, as indicated by the horizontal bars. The Vm was maintained at 70 mV for the duration of the recordings, and free $[Ca^{2+}]_i$ was 0.6 μM. Dashed lines represent zero-current levels.

(B) Mean relationships between diC8-PIP_2 concentration ([diC8-PIP_2]) and TMEM16A currents, expressed relative to the current measured in the absence of diC8-PIP_2 (n=12). The smooth curves through the points represent the best fits of the data using the Hill equation (equation 2.1).

4.2. Effects of intracellular Ca^{2+} on the sensitivity of TMEM16A channels to diC8-PIP_2

Intracellular Ca^{2+} levels are dynamically regulated in living cells. It was therefore studied whether the effects of diC8-PIP_2 on cloned TMEM16A channels varied depending on $[Ca^{2+}]_i$.

TMEM16A currents were recorded from inside-out patches exposed to different $[Ca^{2+}]_i$ in the absence or presence of 100 μg/ml (117 μM) diC8-PIP_2 (Fig. 4.2). In these experiments, *Vm* was maintained at 70 mV, and $[Ca^{2+}]_i$ was initially 0, and then incrementally increased to 78 μM $[Ca^{2+}]_i$. TMEM16A currents were normalised for control currents observed in the presence of 78 μM $[Ca^{2+}]_i$ as this $[Ca^{2+}]_i$ maximally activates TMEM16A channels (Adomaviciene et al., 2013, Scudieri et al., 2012).

In the presence of 0.3 μM $[Ca^{2+}]_i$, diC8-PIP_2 increased the currents by a factor of 5.27 ± 1.29 (n=15). In contrast, in the presence of 0.6 μM $[Ca^{2+}]_i$, diC8-PIP_2 caused an increase of the currents by a factor of 1.44 ± 0.17 (n=15) while in 2 μM $[Ca^{2+}]_i$, there was no significant current activation by diC8-PIP_2 (Fig. 4.3).

To assess whether diC8-PIP_2 was able to modulate TMEM16A activity under conditions of maximal activation, experiments described above were repeated with 78 μM $[Ca^{2+}]_i$. *Vm* was kept constant at 70 mV, and patches were exposed to 78 μM $[Ca^{2+}]_i$ in the absence and presence of 100 μg/ml (117 μM) diC8-PIP_2 (Fig. 4.2). Normalised TMEM16A currents were unaffected by 100 μg/ml (117 μM) PIP_2 under these $[Ca^{2+}]_i$ conditions (Fig. 4.2). Collectively, the experiments described above demonstrate that the effect of diC8-PIP_2 on TMEM16A currents is strongly $[Ca^{2+}]_i$-dependent, particularly at low $[Ca^{2+}]_i$.

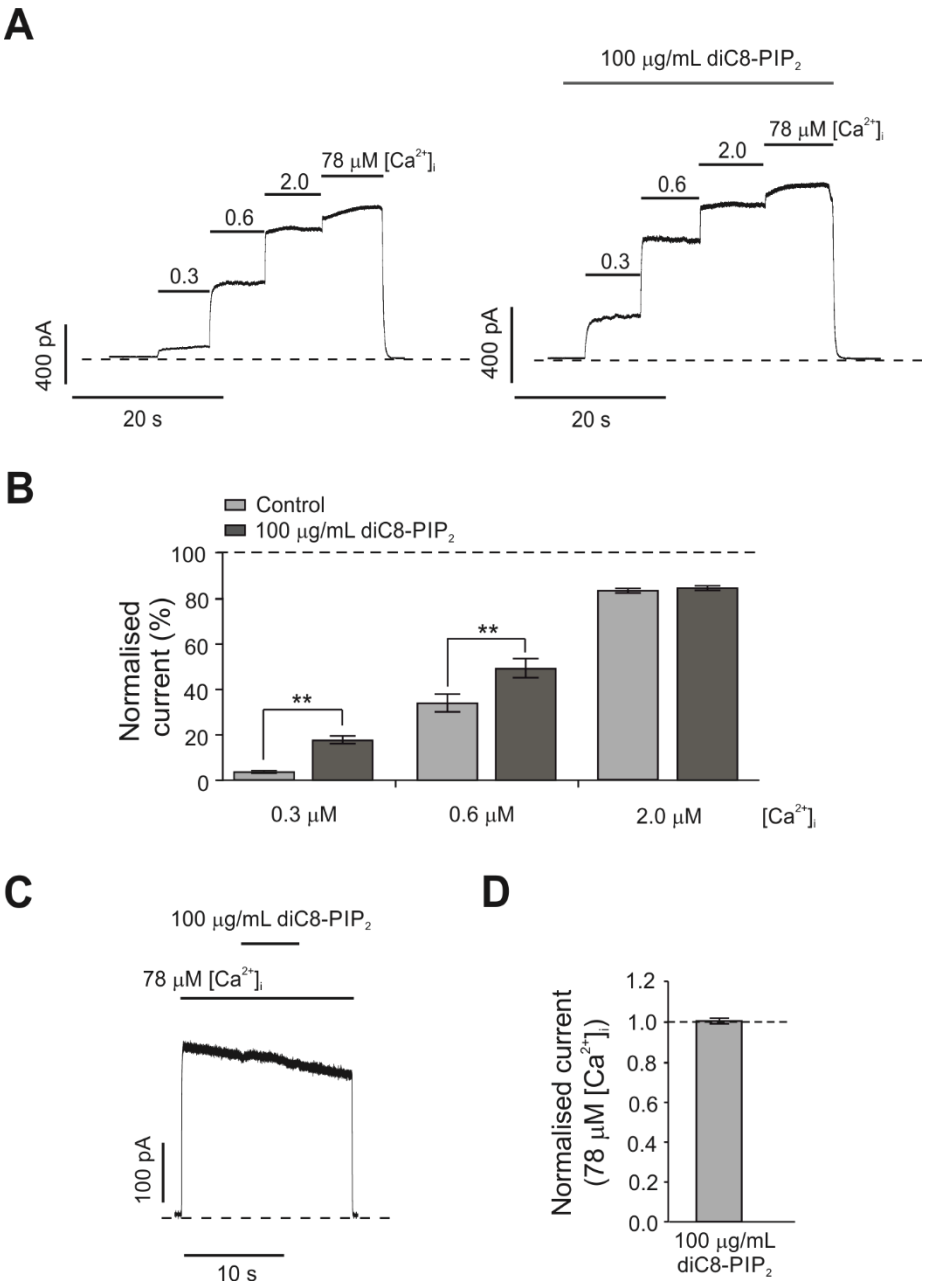
A
100 μg/mL diC8-PIP2
78 μM [Ca2+]i
2.0
0.6
0.3
400 pA
20 s
B
Control
100 μg/mL diC8-PIP2
Normalised current (%)
100
80
60
40
20
0
**
**
0.3 μM
0.6 μM
2.0 μM
[Ca2+]i
C
100 μg/mL diC8-PIP2
78 μM [Ca2+]i
100 pA
10 s
D
Normalised current (78 μM [Ca2+]i)
1.2
1.0
0.8
0.6
0.4
0.2
0.0
100 μg/mL diC8-PIP2

Figure 4.2. Effect of $[Ca^{2+}]_i$ on the sensitivity of TMEM16A currents to intracellular diC8-PIP_2

(A) Currents recorded from an inside-out patch excised from a TMEM16A expressing HEK-293T cell in response to various $[Ca^{2+}]_i$, as indicated. diC8-PIP_2 (100 μg/ml (117 μM)) was applied to the intracellular side of the patch, as indicated. The Vm was maintained at 70 mV for the entire duration of the experiment. Dashed lines represent zero-current levels.

*(B) Mean TMEM16A current amplitudes measured in the absence (control) or presence of diC8-PIP_2 and various $[Ca^{2+}]_i$. Currents measured at each $[Ca^{2+}]_i$ were normalised to the current measured in 78 μM $[Ca^{2+}]_i$. ** P<0.005 (paired t-test, n=15).*

(C) Currents recorded from inside-out patches excised from HEK-293T cells expressing TMEM16A. DiC8-PIP_2 (100 μg/ml (117 μM)) was applied as indicated. $[Ca^{2+}]_i$ was 78 μM. The Vm was 70 mV for the entire duration of the recordings. The dashed line represents the zero-current level.

(D) TMEM16A current measured in the presence of diC8-PIP_2 normalised to current measured in 78 μM $[Ca^{2+}]_i$. N.S. P>0.05 (paired t-test, n=8).

Changes in macroscopic current amplitude are caused by changes in i, P_o or N (Hille, 2001). These factors are related as described in equations 2.3 and 2.4. Experiments were therefore carried out in order to understand which one of these factor(s) is affected by PIP_2. Changes in N cannot occur in our experimental conditions (inside-out patch-clamp) because channel trafficking will not occur when the patch is excised from its normal cellular environment. Stationary noise analysis revealed that application of diC8-PIP_2 (100 μg/ml (117 μM)) caused an increase in Po of TMEM16A channels (Fig. 4.3). This increase was Ca^{2+}-dependent: P_o was increased by 5.90 ± 1.20 (n=15) fold in the presence of 0.3 μM $[Ca^{2+}]_i$. In contrast, in the presence of 0.6 μM $[Ca^{2+}]_i$ P_o increased only by a factor of 1.63 ± 0.17 (n=15) and there was no detectable change in ≥2 μM $[Ca^{2+}]_i$ (Fig. 4.3). Notably, γ of the TMEM16A channel was not affected by diC8-PIP_2, being ~2.5 pS in both the absence and presence of the lipid. Therefore, the changes in TMEM16A current amplitudes caused by diC8-PIP_2 were due to changes in channel gating, while γ was not affected.

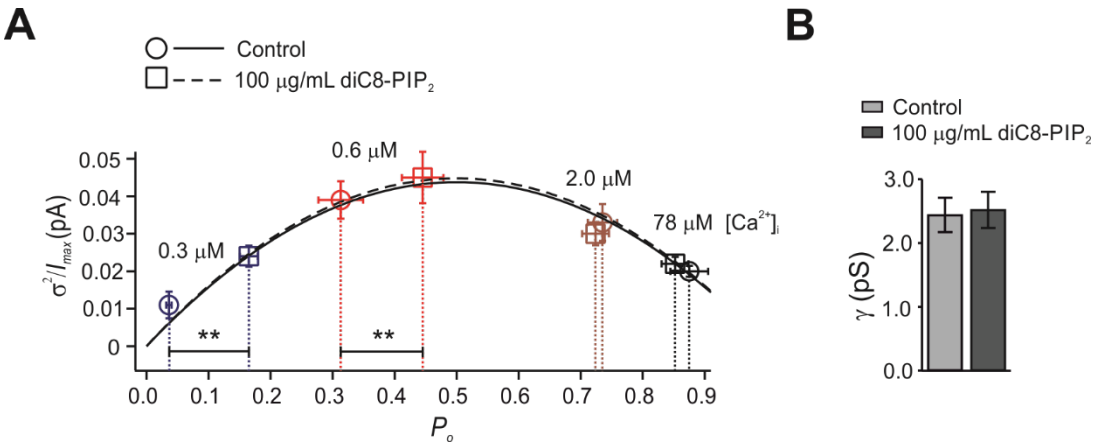

Figure 4.3. Stationary noise analysis of the effect of $[Ca^{2+}]_i$ on the sensitivity of TMEM16A currents to intracellular diC8-PIP_2

(A) TMEM16A current variance (σ^2) normalised for the maximal current (I_{max}) and plotted against the P_o for tracts of stationary currents recorded in the presence of various $[Ca^{2+}]_i$ and in the absence or presence of diC8-PIP_2. The parabolic lines are the best fit of the data using a quadratic function.

(B) Mean TMEM16A single channel conductance (γ) obtained from stationary noise analysis conducted in the presence or absence of diC8-PIP_2 (100 µg/ml (117 µM)).

*** P<0.005 (paired t-test, n=15).*

4.3. Effect of *Vm* on the sensitivity of TMEM16A channels to diC8-PIP_2

The next set of experiments aimed to define the effects of diC8-PIP_2 at various *Vm*. During inside-out patch-clamp, a pre-pulse of 70 mV was used to open TMEM16A channels followed by a series of test-pulses, during the "IV-tail" voltage protocol (Fig. 4.4). TMEM16A currents were recorded in the presence of 0.3 µM $[Ca^{2+}]_i$, chosen due to the pronounced effect of diC8-PIP_2 on TMEM16A at this $[Ca^{2+}]_i$ (Fig. 4.2). It was first noted that the intracellular diC8-PIP_2 did not alter the E_{rev} of TMEM16A current (assessed using instantaneous tail-currents). In the absence and presence of 100 µg/ml (117 µM) diC8-PIP_2 in the intracellular solution, the E_{rev} of TMEM16A current was 3.1 ± 1.1 mV (n=9), very close to the expected E_{rev} values for Cl^- in our recording conditions (~1 mV). Therefore, diC8-PIP_2 did not alter the TMEM16A channel selectivity to ions. It is noteworthy that the diC8-PIP_2 promoted an increase in TMEM16A steady-state current at all tested *Vm* (Fig. 4.4).

Initially, we examined the requirement of intracellular Ca^{2+} in the development of the effect of diC8-PIP_2 on TMEM16A currents. It was found that in the absence of intracellular Ca^{2+} (nominally Ca^{2+}-free intracellular solution), diC8-PIP_2 exhibited no effect on the TMEM16A currents at all *Vm* tested (Fig. 4.4). This indicated that diC8-PIP_2 does not result in activation of TMEM16A channel in the absence of intracellular Ca^{2+}.

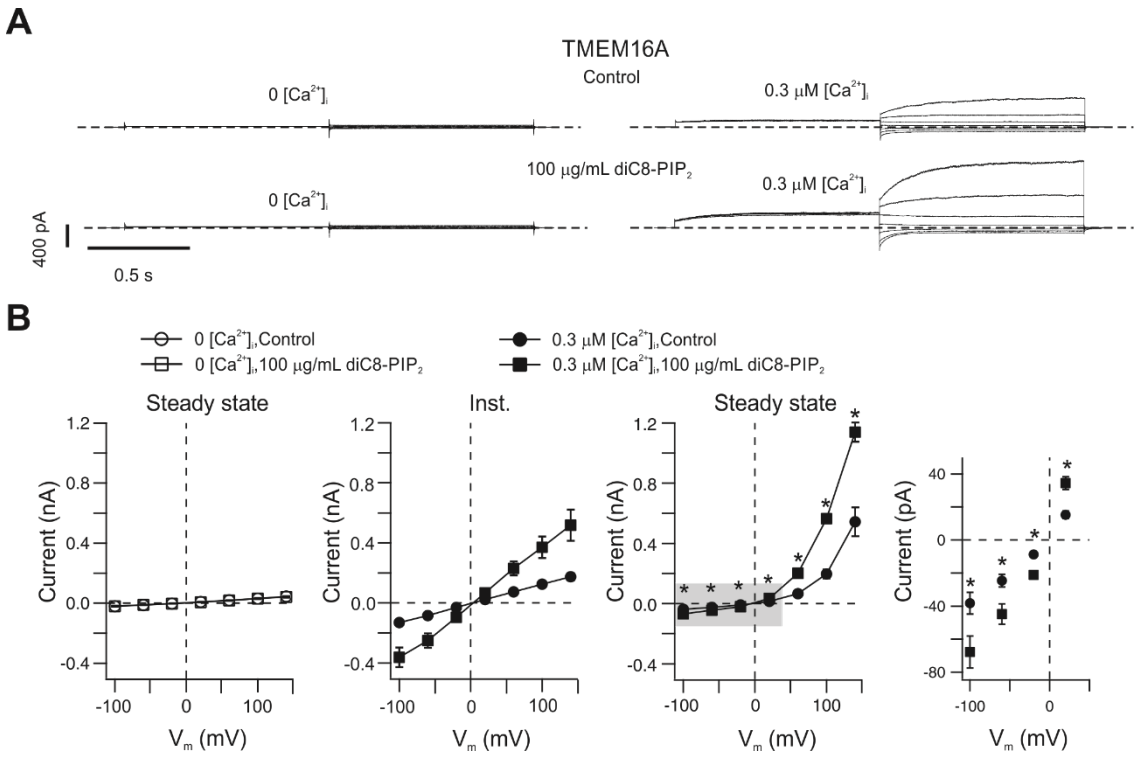

Figure 4.4. Effects of Vm on the sensitivity of TMEM16A currents to intracellular diC8-PIP_2

(A) Currents recorded from inside-out patches excised from HEK-293T cells expressing TMEM16A. DiC8-PIP_2 (100 µg/ml (117 µM)) was applied to the intracellular side of the patch, as indicated. Dashed horizontal lines represent zero-current level. $[Ca^{2+}]_i$ was 0 or 0.3 µM, as indicated.

*(B) Mean instantaneous and steady-state TMEM16A current versus Vm relationships measured in the absence (control) or presence of diC8- PIP_2 (100 µg/ml (117 µM)), as indicated. The rightmost panel represents an expansion of the area highlighted in grey in the steady-state current versus Vm relationship panel. The number of experiments conducted in 0 $[Ca^{2+}]_i$, and 0.3 µM $[Ca^{2+}]_i$ was (n=6) and (n=9), respectively. * P<0.05 (two-way ANOVA).*

4.4. Sensitivity of TMEM16A channels to endogenous PIP_2

The experiments described above involved an exogenous synthetic analogue of PIP_2 (diC8- PIP_2). To test whether endogenous PIP_2 modulates TMEM16A current, cells were co-transfected with TMEM16A channels in conjunction with the membrane-localised protein *danio rerio* voltage-sensitive phosphatase (DrVSP), which depletes endogenous PIP_2 content. This is achieved by activating a phosphatase domain in DrVSP via membrane depolarisation, which in turn dephosphorylates endogenous PIP_2 (Okamura et al., 2009). Initial control experiments were carried out in the absence of DrVSP. Under this condition, when *Vm* was stepped to 100 mV for 4 s from the holding potential of -100 mV, large TMEM16A whole-cell currents were elicited that reached a stable steady-state value (Fig. 4.5, table 4.1).

When cells were co-transfected with TMEM16A and DrVSP, the holding *Vm* was -100 mV to maintain DrVSP in the inactive state. In these experiments, the depolarising step to 100 mV elicited a whole-cell TMEM16A current with an unusual morphology, as it decreased in amplitude over the course of the depolarising step. This is likely to be due to depletion of endogenous PIP_2 by DrVSP, that occurs only at depolarising *Vm* (Okamura et al., 2009). Subsequent depolarising pulses did not produce this effect, as endogenous PIP_2 was already depleted. During the first depolarising step, the TMEM16A current was reduced by ~1.4-fold from the initial peak to the steady-state current measured at the end of the test pulse (Fig. 4.5, table 4.1).

To confirm the DrVSP-mediated inhibition of TMEM16A current was due to depletion of endogenous PIP_2, an inactive mutant of DrVSP was used in the following set of experiments. In this mutant DrVSP, the cysteine in position 302 was replaced by a serine (DrVSP(C302S)). This modification removes PIP_2 dephosphorylation activity of DrVSP

(Imai et al., 2012). Co-expression of DrVSP(C302S) with TMEM16A produced currents that have similar kinetics to TMEM16A currents in the absence of DrVSP (Fig. 4.5, table 4.1). Collectively, these experiments demonstrate that endogenous PIP_2 is a potent regulator of TMEM16A function.

Table 4.1. Effect of DrVSP-mediated depletion of plasma membrane PIP_2 on TMEM16A currents

	TMEM16A	TMEM16A + DrVSP	TMEM16A + DrVSP(C302S)
Peak (pA/pF)	473 ± 70	187 ± 53	355 ± 140
Steady-state (pA/pF)	473 ± 69	136 ± 39	363 ± 144
n	8	14	5

"Peak" refers to the maximal TMEM16A current obtained at 100 mV. "Steady-state" refers to the plateau of the TMEM16A current obtained at 100 mV. "n" refers number of experiments.

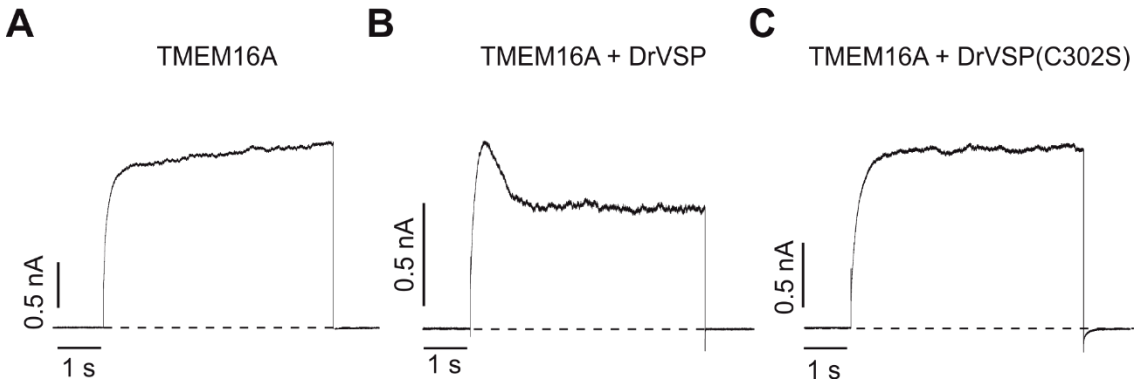

Figure 4.5. Effect of DrVSP activation on TMEM16A currents

(A) Whole-cell currents recorded from HEK-293T cells expressing TMEM16A, in response to the "IV-steps" voltage protocol. $[Ca^{2+}]_i$ was 0.3 µM (n=8). Dashed lines represent zero-current levels.

(B) Whole-cell currents recorded from HEK-293T cells co-expressing TMEM16A and DrVSP, in in response to the "IV-steps" voltage protocol. $[Ca^{2+}]_i$ was 0.3 µM (n=14). Dashed lines represent zero-current levels.

(C) Whole-cell currents recorded from HEK-293T cells co-expressing TMEM16A and DrVSP(C302S), in response to the "IV-steps" voltage protocol. $[Ca^{2+}]_i$ was 0.3 µM (n=5). Dashed lines represent zero-current levels.

4.5. Recovery of the DrVSP-mediated inhibition of TMEM16A channels

It was hypothesised that if DrVSP-mediated inhibition of TMEM16A currents was caused by active depletion of PIP_2 from the plasma membrane, this inhibition could be replicated if enough time was allowed for PIP_2 synthesis to take place in the cells. This possibility was tested using the "double-pulse" voltage protocol during whole-cell recordings in cells co-expressing TMEM16A and DrVSP (Fig. 4.6). In these experiments, Mg-ATP (1 mM) was included in the intracellular solution to enable PIP_2 synthesis by endogenous PIPK. Furthermore, the holding potential was maintained at -50 mV, which is close to the resting membrane potential in HEK-293T cells, while also being sufficient to maintain DrVSP inactivated (Okamura et al., 2009). DrVSP-mediated modulation of TMEM16A current was completely restored after ~50 s "recovery" period at -50 mV. However, in the absence of Mg-ATP this restoration of the effect did not take place (Fig. 4.6). The relationship between the extent of recovery of the current *versus* the duration of the time interval spent at -50 mV was fitted with a single exponential function and characterised by a time constant of recovery (τ_r) of 7.2 ± 0.7 s (n=11). This data demonstrates that in the presence of Mg-ATP, cellular PIP_2 can be re-synthesised by PIPK and restore current amplitude.

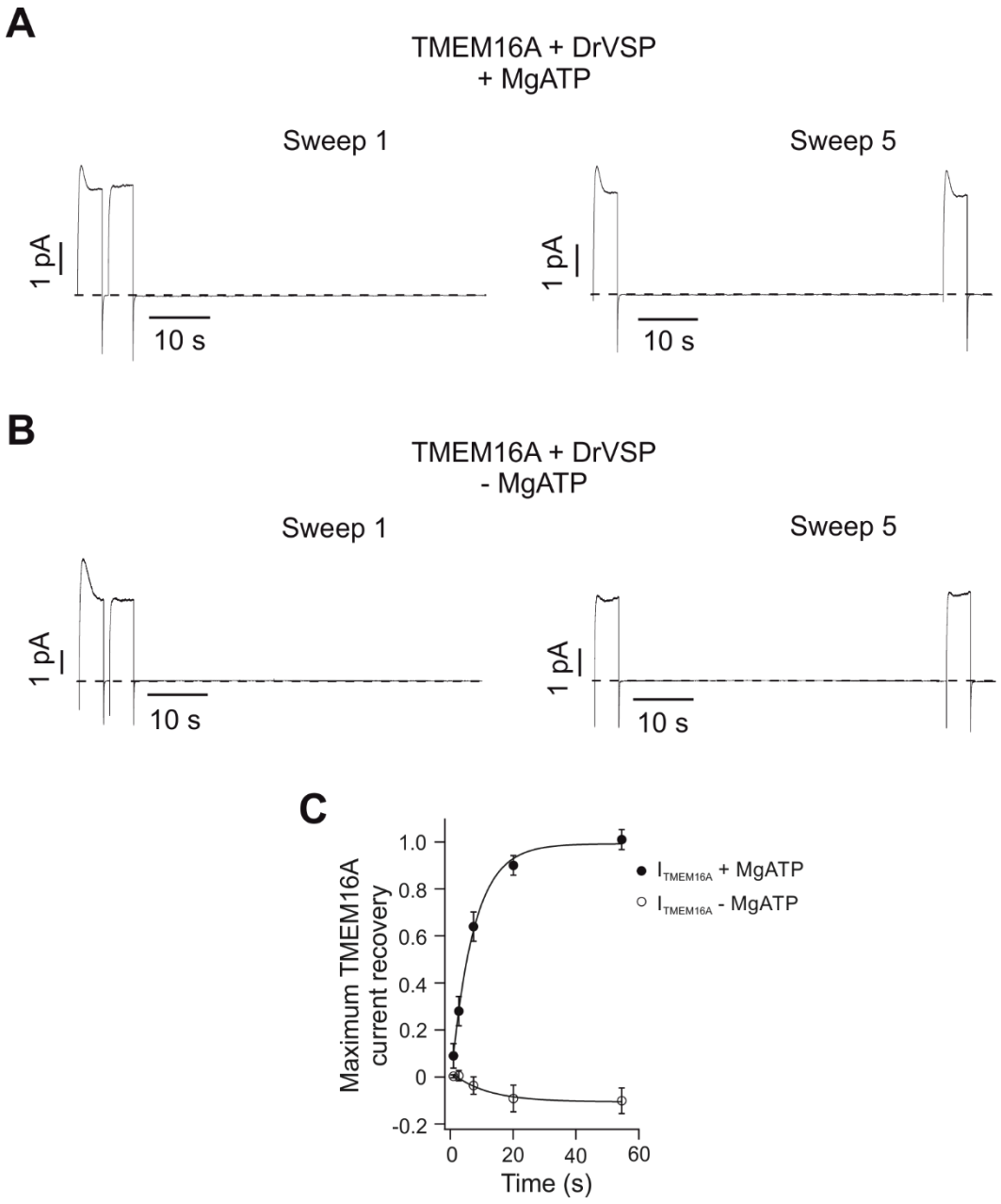
A
TMEM16A + DrVSP
+ MgATP
Sweep 1
Sweep 5
1 pA
10 s
1 pA
10 s
B
TMEM16A + DrVSP
- MgATP
Sweep 1
Sweep 5
1 pA
10 s
1 pA
10 s
C
Maximum TMEM16A current recovery
1.0
0.8
0.6
0.4
0.2
0
-0.2
0
20
40
60
Time (s)
I TMEM16A + MgATP
I TMEM16A - MgATP

Figure 4.6. Effects of DrVSP recovery on the kinetics of TMEM16A currents

(A) Whole-cell currents recorded from HEK-293T cells expressing TMEM16A co-transfected with DrVSP. $[Ca^{2+}]_i$ was 0.3 µM, and the intracellular solution contained 1 mM Mg-ATP. The "double-pulse" voltage protocol is described in 2.6.5. Dashed line represents zero-current levels.

(B) Whole-cell currents recorded from HEK-293T cells expressing TMEM16A co-transfected with DrVSP. $[Ca^{2+}]_i$ was 0.3 µM, and intracellular solution did not contain 1 mM Mg-ATP. Dashed line represents zero-current levels.

(C) Mean relationship between the extent of recovery of the DrVSP-mediated modulation of the currents and the recovery time. The smooth curves through the points represent the best fit of the data with single exponential functions. In the presence of Mg-ATP (n=11), in the absence of Mg-ATP (n=11).

4.6. TMEM16A pharmacology following PIP_2 depletion

During the Gq-PCR signalling cascade, PIP_2 in the plasma membrane is depleted and $[Ca^{2+}]_i$ increases. As TMEM16A Ca^{2+}-sensitivity is tightly regulated by PIP_2, the relationship between PIP_2 modulation and TMEM16A pharmacology is a key consideration especially because the action of TMEM16A modulators (such as Ani9, chapter 3) may vary depending on channel gating.

These experiments therefore explore whether pharmacological potency and efficacy differs when endogenous PIP_2 had been depleted. Two modulators were tested, Ani9 (Seo et al., 2016) and A9C (Ta et al., 2016). These were chosen as they have differing effects on TMEM16A. Ani9 is the most potent blocker of TMEM16A, and is used as a tool compound in this thesis. It is therefore important for further studies to understand whether this inhibition is altered by the local abundance of endogenous PIP_2. A9C is a compound that can block and activate TMEM16A (Ta et al., 2016). It was therefore tested in this study in order to gain an understanding of whether PIP_2 can modulate the activity of the blockage or activatory component of this regulation.

4.6.1. Effect of Ani9 on TMEM16A following PIP_2 depletion

HEK-293T cells were either transfected with TMEM16A alone or co-transfected with TMEM16A and DrVSP. Transfected cells were then patch-clamped in the whole-cell configuration using standard CaCC solutions with 0.3 μM $[Ca^{2+}]_i$. Endogenous PIP_2 was depleted using a 5 s depolarisation pulse to 100 mV (Fig. 4.7). The *Vm* was subsequently held at 70 mV to activate the cloned TMEM16A channels. Two concentrations of Ani9 were used (50 nM and 100 nM) to assess the effect of Ani9 providing a partial block of TMEM16A currents, as the IC_{50} is reported to be 50-100 nM (Seo et al., 2016). TMEM16A currents were normalised to TMEM16A currents in the absence of Ani9. The lower [Ani9] of 50 nM resulted in a decreased normalised TMEM16A current to 0.52 ± 0.07 (n=9), and 0.44 ± 0.05 (n=8) in cells co-expressing TMEM16A and DrVSP. 100 nM Ani9 resulted in a normalised TMEM16A current of 0.29 ± 0.05 (n=9) and 0.24 ± 0.03 (n=8) for normalised TMEM16A current when co-expressing with DrVSP (Fig. 4.7). Therefore, there was no significant difference in Ani9 inhibition of TMEM16A in the presence or absence of PIP_2.

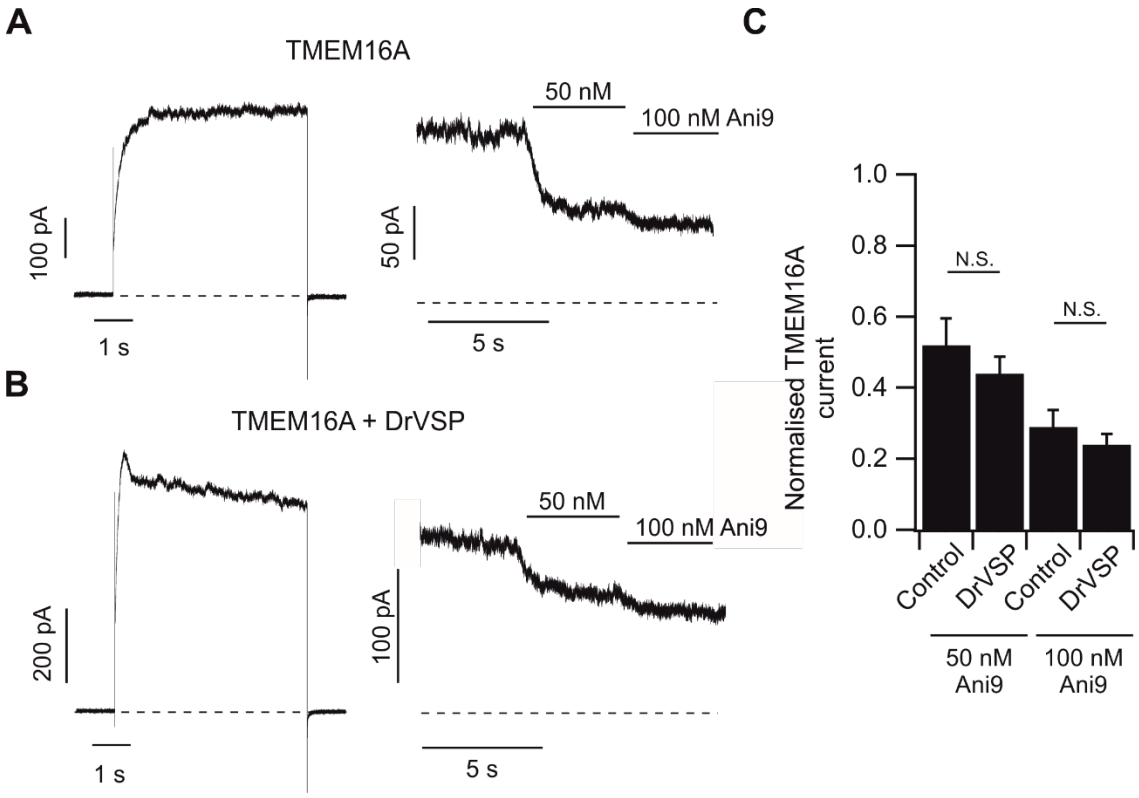

Figure 4.7. Effect of Ani9 on TMEM16A following endogenous PIP_2 depletion by DrVSP

(A) Whole-cell currents recorded from HEK-293T cells expressing TMEM16A. $[Ca^{2+}]_i$ was 0.3 µM. Left-hand panel represents the current elicited by the initial 5 s voltage pulse from -100 mV to 100 mV. Right-hand panel represents currents elicited at 70 mV in the presence of 50 nM Ani9, and 100 nM Ani9, as indicated. Dashed lines represent zero-current levels.

(B) Whole-cell currents recorded from HEK-293T cells expressing TMEM16A co-transfected with DrVSP. $[Ca^{2+}]_i$ was 0.3 µM. Left-hand panel represents the current elicited by the initial 5 s voltage pulse from -100 mV to 100 mV. Right-hand panel represents currents elicited at 70 mV in the presence of 50 nM Ani9, and 100 nM Ani9. Dashed lines represent zero-current levels.

(C) Mean TMEM16A current (n=9) or current obtained from cells co-expressing DrVSP (n=8) current amplitudes, measured in the absence (control) or presence of 50 µM or 100 µM Ani9. Currents measured at each [Ani9] were normalised to the current measured in the absence of Ani9. NS P>0.05 (unpaired t-test).

4.6.2. Effect of A9C on TMEM16A following PIP_2 depletion

A9C has an activatory and inhibitory effect on TMEM16A (Ta et al., 2016, Bradley et al., 2014). The following experiments were designed to test how PIP_2 modulation of TMEM16A effects the pharmacology of A9C, during both the activatory and inhibitory phases in order to assess of both of these effects.

The "IV-tails" protocol was used to study the effects of pharmacological modulators on open TMEM16A channels at a range of *Vm*. HEK-293T cells expressing TMEM16A alone or co-expressing TMEM16A and DrVSP were studied using patch-clamp electrophysiology in the whole-cell configuration in the presence of 0.3 μM $[Ca^{2+}]_i$. Endogenous PIP_2 was depleted using a 1 s depolarisation pulse to 100 mV. The "IV-tails" voltage protocol was then triggered in the presence or absence of 300 μM A9C, as this concentration provides both the activation and inhibition response in TMEM16A (Fig. 4.8). Instantaneous TMEM16A current was measured, as A9C modulation has the most profound effect at this point.

In the presence of 300 μM A9C, at -100 mV normalised TMEM16A current was -9.04 ± 0.85 nA/pF (n=10), however normalised TMEM16A current in the presence of DrVSP was -4.97 ± 1.07 nA/pF (n=6), a ~1.8-fold reduction (Fig. 4.8). There was no significant difference at positive *Vm*. Depletion of endogenous PIP_2 therefore affects the pharmacology of the activatory effect of A9C at negative *Vm*, but does not affect the inhibitory effect of A9C.

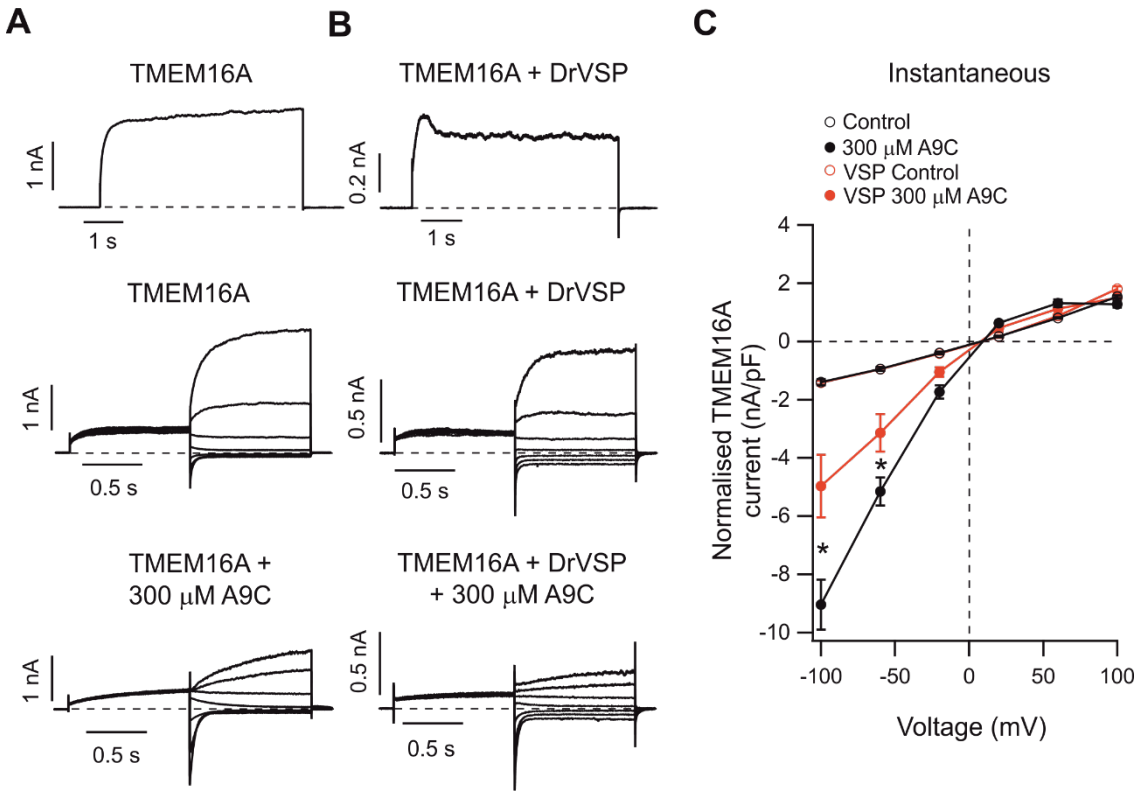

Figure 4.8. Effect of A9C on TMEM16A following endogenous PIP_2 depletion by DrVSP

(A) Whole-cell currents recorded from HEK-293T cells expressing TMEM16A. $[Ca^{2+}]_i$ was 0.3 μM. The initial row represents the current elicited by the initial 5 s voltage pulse from -100 mV to 100 mV to activate DrVSP. The second row represents control "IV-tail" protocol recordings in the absence of A9C. The third row represents TMEM16A currents elicited in the presence of 300 μM A9C. Dashed lines represent zero-current levels.

(B) Whole-cell currents recorded from HEK-293T cells expressing TMEM16A co-transfected with DrVSP. $[Ca^{2+}]_i$ was 0.3 μM. The initial row represents the current elicited by the initial 5 s voltage pulse from -100 mV to 100 mV to activate DrVSP. The second row represents control "IV-tail" protocol recordings in the absence of A9C. The third row represents TMEM16A currents elicited in the presence of 300 μM A9C. Dashed lines represent zero-current levels.

*(C) Mean instantaneous TMEM16A current (n=10) current obtained from cells co-expressing DrVSP (n=6) current amplitudes, measured in the absence or presence of 300 μM A9C. Currents measured at each Vm were normalised to the Cm and plotted versus Vm, * P<0.05 (two-way ANOVA).*

4.7. Alpha1-adrenergic receptor mediated modulation of TMEM16A channels

The α1-adrenergic receptor is a Gq-PCR that activates the PIP_2 pathway, and is expressed in VSMCs. Previous experiments in this chapter have depleted plasma membrane PIP_2 using DrVSP. Voltage sensitive phosphatases (VSP) are expressed in many different species, and are mainly found to be expressed in the reproductive tissue of humans (Sutton et al., 2012, Tapparel et al., 2003). As this thesis focuses on TMEM16A in murine VSMCs, we wanted to study TMEM16A sensitivity to PIP_2 using a more physiologically relevant control mechanism. The following experiments use the co-expression of the α1-adrenergic receptor and TMEM16A in order for us to study the effect of PIP_2 depletion on TMEM16A activity during the Gq-PCR signalling cascade.

In order to dissect the effect of Ca^{2+}-release from intracellular stores from the effect of PIP_2 depletion in the plasma membrane, two intracellular solutions were used. These intracellular solutions only differed in their EGTA concentrations. EGTA is the main Ca^{2+} chelating agent in the intracellular solution used in the patch-clamp electrophysiology experiments. "Low EGTA CaCC intracellular solution" (Table 2.7) was used to observe $[Ca^{2+}]_i$ increase, after IP_3 mediated Ca^{2+} release from intracellular stores. "Standard CaCC intracellular solution" (Table 2.4) contained nominally "high" EGTA, and is sufficient to quickly buffer the released Ca^{2+} (Naraghi, 1997). This prevents modulation of TMEM16A by increased $[Ca^{2+}]_i$, therefore allows the effect of depletion of PIP_2 on the channel to be observed.

HEK-293T cells expressing the α1-adrengergic receptor alone, or co-expressing the α1-adrengergic receptor and TMEM16A, were recorded in the whole-cell patch-clamp configuration, using the "IV-ramp" protocol. Control TMEM16A currents were recorded before the addition of phenylephrine (PE, 1 μM). Cells expressing the α1-adrenergic

receptor alone demonstrated a very small whole-cell current that did not significantly change ($P<0.05$) when PE (1 μM) was added, removing the possibility that endogenously expressed channels are activated by α1-adrenergic receptor mediated pathways, or by PE directly. On addition of PE (1 μM) in the "low" EGTA solution, cells co-expressing the α1-adrenergic receptor and TMEM16A, had an increased TMEM16A current by ~3.4-fold at 95 mV (Fig. 4.9, Table 4.2). The current increase reached a maximum after ~5 s exposure to PE, after which the TMEM16A current decreased (Fig. 4.9). TMEM16A current in the "high" EGTA solution (which rapidly buffered $[Ca^{2+}]_i$ released in response to IP_3) decreased by ~3.4-fold at 95 mV in response to PE (1 μM). The decrease in TMEM16A activity in a high $[Ca^{2+}]_i$ buffering conditions suggests that depletion of PIP_2 in the α1-adrenergic receptor signalling cascade reduces TMEM16A activity. These results align with the finding shown in figure 4.5 that depletion of endogenous PIP_2 by DrVSP reduces TMEM16A current. Together, these data implicate PIP_2 to be the factor in the Gq-PCR signalling cascade that modulates TMEM16A.

Table 4.2. Effect of Gq-PCR signalling cascade activation on TMEM16A currents.

	α1-adrenergic receptor alone (pA/pF)		TMEM16A current in low EGTA (pA/pF)		TMEM16A current in high EGTA (pA/pF)	
	Control	PE	Control	PE	Control	PE
-95 mV	-9.86 ± 3.60	-12.19 ± 3.88	-16.28 ± 4.48	-120.45 ± 40.74	-6.74 ± 2.60	-8.13 ± 1.22
95 mV	10.02 ± 3.62	14.7 ± 5.35	109.94 ± 25.43	371.26 ± 66.86	39.54 ± 6.51	11.70 ± 2.16
n	7		10		4	

"-95 mV" and "95 mV" refer to the current obtained at these Vm. "n" refers number of experiments.

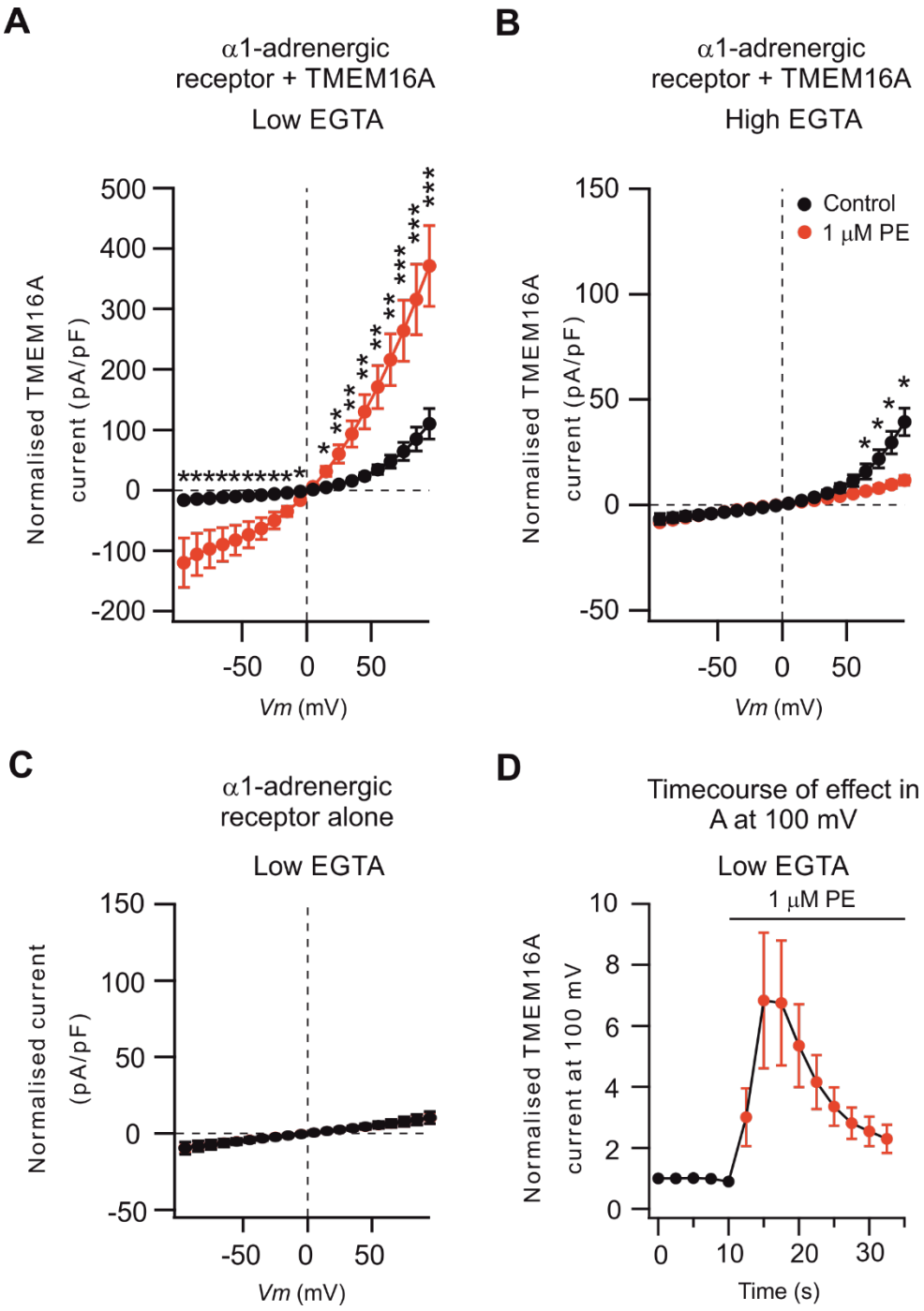
A
α1-adrenergic
receptor + TMEM16A
Low EGTA
Normalised TMEM16A
current (pA/pF)
500
400
300
200
100
0
-100
-200
-50
0
50
Vm (mV)
B
α1-adrenergic
receptor + TMEM16A
High EGTA
Control
1 μM PE
Normalised TMEM16A
current (pA/pF)
150
100
50
0
-50
-50
0
50
Vm (mV)
C
α1-adrenergic
receptor alone
Low EGTA
Normalised current
(pA/pF)
150
100
50
0
-50
-50
0
50
Vm (mV)
D
Timecourse of effect in
A at 100 mV
Low EGTA
1 μM PE
Normalised TMEM16A
current at 100 mV
10
8
6
4
2
0
0
10
20
30
Time (s)

Figure 4.9. Alpha1-adrenergic receptor mediated regulation of TMEM16A channels

(A) Whole-cell currents recorded from HEK-293T cells co-expressing TMEM16A and the α1-adrenergic receptor. TMEM16A current was elicited in response to the "IV-ramp" voltage protocol, using CaCC solutions containing in low intracellular EGTA (n=12). 1 µM phenylephrine (PE) was added as indicated (red).

(B) Whole-cell currents recorded from HEK-293T cells co-expressing TMEM16A and the α1-adrenergic receptor. TMEM16A current was elicited in response to the "IV-ramp" voltage protocol, using standard CaCC solutions, which contained high [EGTA] (n=4). 1 µM phenylephrine (PE) was added as indicated (red).

(C) Whole-cell currents recorded from HEK-293T cells expressing the α1-adrenergic receptors, elicited in response to the "IV-ramp" voltage protocol (n=7). 1 µM phenylephrine (PE) was added as indicated (red).

*(D) Time-course of the TMEM16A current increase in response to PE in cells co-expressing TMEM16A and the α1-adrenergic receptor. TMEM16A currents were normalised to currents measured in the absence of 1 μM PE (red). *P<0.05, **P<0.005, ***P<0.0005 (two-way ANOVA).*

4.8. PIP_2 modulation of TMEM16A on depletion of plasma-membrane cholesterol.

Cholesterol is a crucial component of the plasma-membrane, where it has major roles in membrane fluidity and lipid rafts (Simons and Ehehalt, 2002). Cholesterol has been identified to modulate a number of ion channels (Levitan et al., 2014, Levitan et al., 2010), including TMEM16A (De Jesus-Perez et al., 2018, Sones et al., 2010). It has been reported that depletion of plasma membrane cholesterol disrupts the PIP_2 modulation of KCNQ and other ion channel types (Chun et al., 2010). These experiments were therefore designed to test whether plasma membrane composition has a role in the regulation of TMEM16A by PIP_2.

Plasma-membrane cholesterol can be depleted experimentally using β-cyclodextrin (Ohtani et al., 1989). β-cyclodextrin is a cyclic heptameric molecule of glucose, which is able to sequester cholesterol from the plasma membrane due to the lipophilicity of the space inside the β-cyclodextrin ring (Sharma and Janis, 1991). β-cyclodextrin does not incorporate into cells, and is effective on a timescale of minutes (Ohtani et al., 1989). It is therefore a useful tool for studying the effect of cholesterol depletion on ion channels using patch-clamp electrophysiology.

Inside-out patches excised from cells expressing TMEM16A were recorded in the presence of 0.6 μM $[Ca^{2+}]_i$. TMEM16A currents were elicited using the "IV-steps" protocol. This voltage protocol was repeated every 10 seconds for 3 minutes, during which time the patch was perfused with β-cyclodextrin (3 mg/ml). TMEM16A currents were measured at the end of the test-pulse and normalised to the current observed in the absence of β-cyclodextrin (3 mg/ml). There was an increase in TMEM16A current in the presence of β-cyclodextrin (3 mg/ml) (Fig. 4.10). Normalised TMEM16A current increased to ~1.7-fold (n=4) after 3 minutes of exposure to β-cyclodextrin (3 mg/ml).

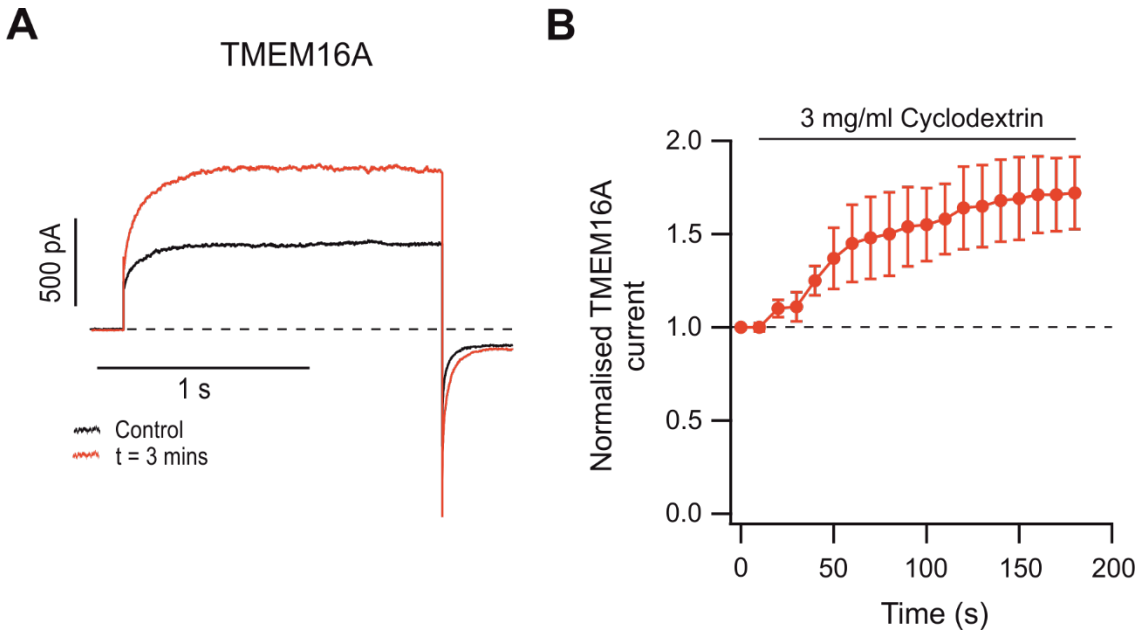

Figure 4.10. Effect of β-cyclodextrin on cloned TMEM16A channels

(A) TMEM16A expressing HEK-293T cells were studied in the inside-out patch-clamp configuration. Solutions contained 0.6 μM $[Ca^{2+}]_i$, in combination with the "IV-steps" protocol. Patches were perfused for 10 s with control intracellular solution, and then three minutes with of β-cyclodextrin (3 mg/ml). Dotted line represents zero-current level.

(B) Mean normalised TMEM16A current at 70 mV in the absence (sweeps one and two) and presence of β-cyclodextrin (3 mg/ml). Dotted line represents TMEM16A current prior to treatment with diC8-PIP_2. (n=4).

Experiments depicted in figure 4.10 confirm that depletion of plasma membrane cholesterol by β-cyclodextrin (3 mg/ml) increases TMEM16A current. TMEM16A-expressing HEK-293T cells were recorded using solutions containing 0.6 μM $[Ca^{2+}]_i$, in the inside-out patch-clamp configuration. Cells were pre-treated with β-cyclodextrin (3 mg/ml) to deplete plasma membrane cholesterol. Subsequently, patches were perfused with diC8-PIP_2 (30 μg/ml) at a fixed *Vm* of 70 mV. In parallel, experiments were carried out in non-pre-treated patches as a control.

Similar to the effect of diC8-PIP_2 on TMEM16A observed in figure 4.1, normalised control TMEM16A current increased by ~1.4-fold (n=7). Conversely, diC8-PIP_2 perfusion over β-cyclodextrin treated TMEM16A patches resulted in a decrease in normalised TMEM16A current, by ~0.8-fold (Fig. 4.11).

The opposing effect of diC8-PIP_2 on untreated or β-cyclodextrin treated patches expressing TMEM16A provides evidence that plasma-membrane composition can have a significant effect on TMEM16A activity.

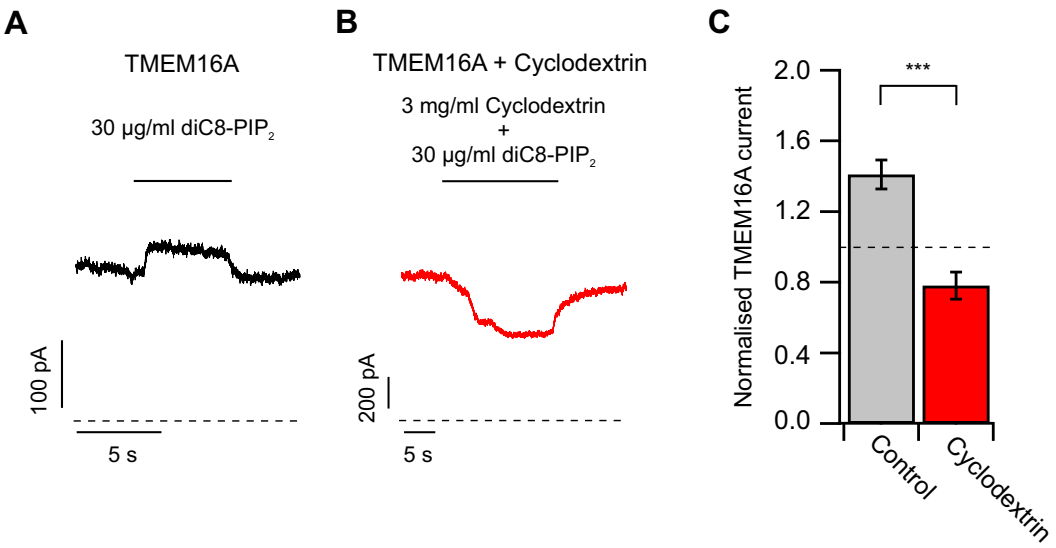

Figure 4.11. Effect of diC8-PIP_2 on TMEM16A following pre-treatment with β-cyclodextrin

(A) TMEM16A-expressing HEK-293T cells were studied in the inside-out patch-clamp configuration. $[Ca^{2+}]_i$ was 0.6 µM, and Vm was maintained at 70 mV. Patches were perfused for three minutes with intracellular solution before diC8-PIP_2 was applied to the intracellular side of the patch, as indicated by the horizontal bars. Dotted line represents zero-current level.

(B) TMEM16A-expressing HEK-293T cells were studied in the inside-out patch-clamp configuration. $[Ca^{2+}]_i$ was 0.6 µM, and Vm was maintained at 70 mV. Patches were perfused for three minutes with intracellular solution in the presence of β-cyclodextrin (3 mg/ml). DiC8-PIP_2 was applied to the intracellular side of the pre-treated patch, as indicated by the horizontal bars. Dotted line represents zero-current level.

*(C) Mean relationships between TMEM16A and diC8-PIP_2, under conditions of control or pre-treated with β-cyclodextrin (3 mg/ml). Normalised to TMEM16A current in before treatment with diC8-PIP_2. Dotted line represents TMEM16A current prior to treatment with diC8-PIP_2. Control (n=7), pre-treated (n=4), ***P<0.0005 (unpaired t-test).*

4.9. TMEM16A and TMEM16B - chimeric approach to understanding the PIP_2 binding site.

Studies presented so far in this chapter have demonstrated that TMEM16A activity is increased in the presence of PIP_2. It is important to locate the TMEM16A binding site of PIP_2 in order to clarify the mechanism of action of PIP_2. Once elucidated, the PIP_2 binding site could also form the basis for targeted drug discovery. Work in the Tammaro group (in collaboration with Dr Phill Stansfeld, Department of Biochemistry) has resulted in the proposition of two possible binding sites of PIP_2 (fully described in section 2.7.4). Although this initial computational work allowed us to formulate a hypothesis, this was not tested experimentally at the time of identification.

The mutagenesis strategy was based on the finding from the Tammaro group, that while TMEM16A currents are potentiated by diC8-PIP_2 (Fig. 4.2), TMEM16B currents are inhibited by PIP_2. TMEM16A and TMEM16B share a ~55% sequence homology, and are in these studies presumed to have an analogous structure (Picollo et al., 2015, Scudieri et al., 2012). Therefore a chimeric mutagenesis approach was taken to explore this proposed PIP_2 binding site of TMEM16A and TMEM16B (Fig. 4.12).

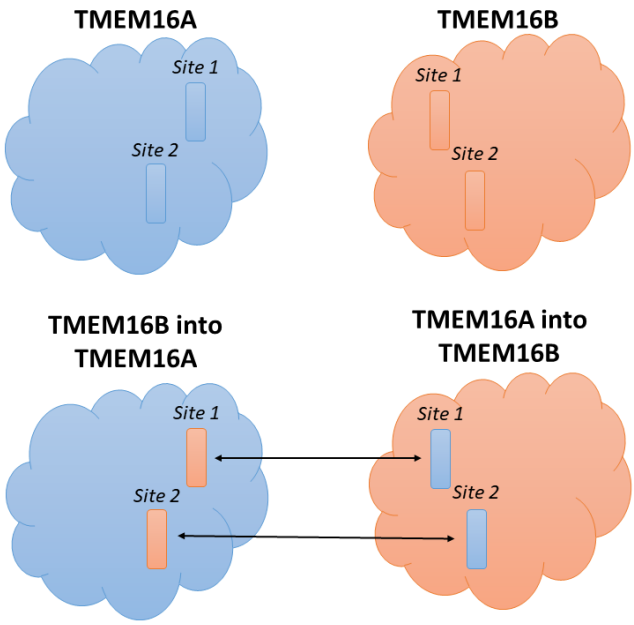

Figure 4.12. Chimeric TMEM16A and TMEM16B mutagenesis strategy.
Diagrammatic representation of the mutagenesis strategy taken. Blue and orange clouds represent TMEM16A and TMEM16B, respectively. Rectangles represent regions of residues to be exchanged between the proteins.

Computational studies of the TMEM16A and TMEM16B PIP_2 binding sites were carried out using a model based on the crystal structure of the fungal nhTMEM16. NhTMEM16 is a structural homologue of the TMEM16A protein (Brunner et al., 2014). In the transmembrane domain areas, nhTMEM16A and TMEM16A share a sequence homology of 42% (Brunner et al., 2014). The sequence alignment was manually adjusted to achieve the best possible fit of the crystal structure. Multiple homology models were generated and evaluated based on a set of pre-defined criteria (described fully in section 2.7.4). The homology model that best satisfied these pre-defined criteria was selected for use in this project. Coarse grain molecular dynamic simulations were then conducted on the chosen TMEM16A homology model, in order to identify a potential PIP_2 interaction site. 15 simulations of 1.1 ms were performed. The percentage time

that each PIP_2 molecule spent within a 6 Å proximity of each residue was calculated. Residues that had a minimum of 90% interaction with PIP_2 during the simulations were selected as residues of interest for this project.

4.9.1. Design of TMEM16A and TMEM16B chimeras

The TMEM16A PIP_2 binding site residues of interest were identified by Dr Phill Stansfeld (Department of Biochemistry) and Remco Jonkind (described in section 2.7.4), and found to be localised in two areas of interest, which will be the focus of this study. These PIP_2 binding site regions of interest will be described as "site 1" and "site 2".

In TMEM16A, "site 1" is 15 residues long and starts at amino acid position 767. TMEM16B "site 2" is also 15 residues long and starts at position 501. The "site 2" mutations span three consecutive residues in both TMEM16A and TMEM16B, which start at residues 791 and 725, respectively. For the "site 1" and "site 2" mutations, chimeras were produced where corresponding regions were swapped between the two proteins. Site 1 and site 2 mutations are described by the section swapped into the backbone, for example "16B into 16A" is a TMEM16A backbone with a TMEM16B putative PIP_2 binding site. Conversely, "16A into 16B" is a TMEM16B backbone with a TMEM16A putative binding site (Fig. 4.12).

During *in silico* analysis, three residues were identified as being particularly crucial for PIP_2 binding in TMEM16A "site 1". These identified residues were mutated to alanine residues for alanine scanning mutagenesis experiments. This approach exchanges charged residues for inert, non-reactive alanine residues (Weiss et al., 2000).

4.9.2. Effect of diC8-PIP_2 on TMEM16B currents

The inhibitory effect of diC8-PIP_2 on TMEM16B channel activity was studied here. These experiments were designed to establish whether the inhibition of TMEM16B by diC8-PIP_2 was profound enough to be suitable for use in the following mutagenesis studies. These results provide the basis for the chimeric TMEM16A and TMEM16B approach taken in order to search for the PIP_2 binding site (Fig. 4.12).

Inside-out patch-clamp electrophysiology was used to study the effect of diC8-PIP_2 on TMEM16B. Solutions contained 1 μM $[Ca^{2+}]_i$ to activate the TMEM16B channels, and the TMEM16B-expressing patch was perfused with increasing concentrations of diC8-PIP_2. TMEM16B was inhibited by 100 μg/ml diC8-PIP_2 in a dose dependent manner to a maximum of 0.82 ± 0.02 of the normalised TMEM16B current (Fig. 4.13). The TMEM16B currents versus [diC8-PIP_2] relationship was fitted with the Hill equation (equation 2.2), which resulted in an IC_{50} value of 39 ± 2 μg/ml and *h* value of 1.1 ± 0.1 (n=9).

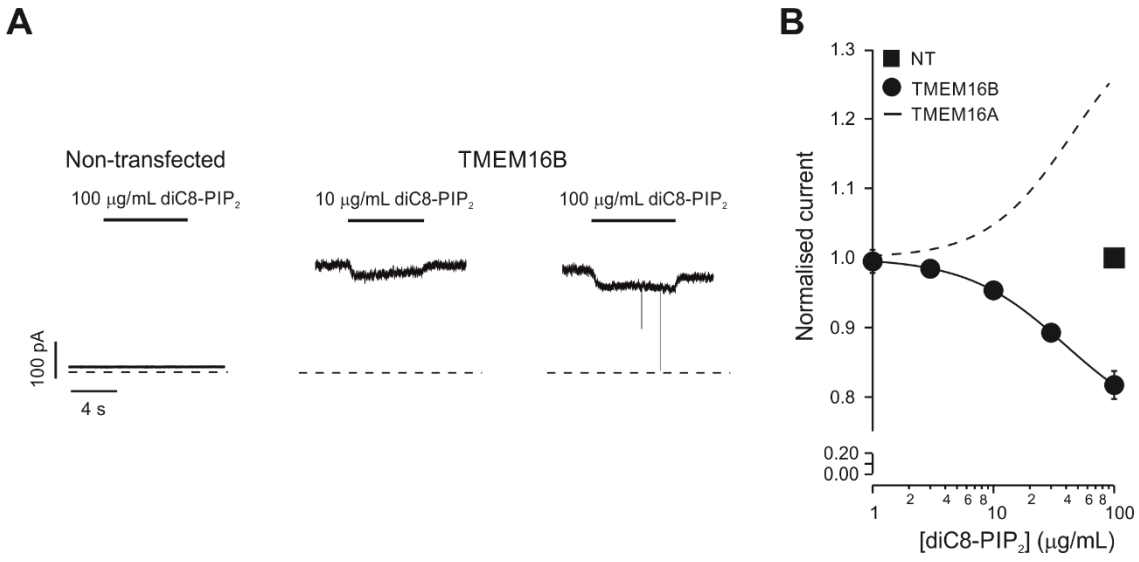

Figure 4.13. Effect of diC8-PIP_2 on TMEM16B currents.

(A) TMEM16B currents recorded from inside-out patches excised from HEK-293T cells in NT HEK-293T cells, or cells expressing TMEM16B. DiC8-PIP_2 was applied to the intracellular side of the patch, as indicated by the horizontal bars. Vm was maintained at 70 mV for the duration of the recordings. $[Ca^{2+}]_i$ was 1 μM. Dashed lines represent zero-current levels.

(B) Mean relationships between diC8-PIP_2 concentration ([diC8-PIP_2]) and TMEM16B currents, expressed relative to the current measured in the absence of diC8-PIP_2 (n=9). Dotted line represents the effect of diC8-PIP_2 on TMEM16A, for comparison. The smooth curve through the points represents the best fit of the data using the Hill equation (equation 2.2).

4.9.3. Voltage sensitivity of site 1 TMEM16A and TMEM16B chimeras

Initial experiments were conducted in order to assess the whole-cell electrophysiological properties of the TMEM16A or TMEM16B chimeras. Currents elicited from TMEM16A and "site 1 16B into 16A" were recorded in the presence of 0.3 μM $[Ca^{2+}]_i$, as this mutation was generated using the TMEM16A construct. TMEM16B and "site 1 16A into 16B" constructs were recorded in the presence of 0.6 μM $[Ca^{2+}]_i$, as this mutation was generated onto the TMEM16B construct.

As reported in chapter 3, TMEM16A and TMEM16B produced outwardly rectifying current-voltage relationships, with currents of 404.73 ± 63.64 pA/pF (n=6) and 102.79 ± 14.90 pA/pF (n=5) at 100 mV, respectively (Fig. 4.14).

The "site 1 16B into 16A" mutant channel was observed to have a reduced current, which more similar to TMEM16B than TMEM16A, with a current of 102.68 ± 27.73 pA/pF (n=6) at 100 mV.

The time-course of activation of the "site 1 16B into 16A" mutant channel also appeared to be different to that of TMEM16A. The "site 1 16B into 16A" were characterised by a slower $\tau_{a0.5}$ than TMEM16A at 40 mV, with a $\tau_{a0.5}$ of 46.07 ± 5.97 for "site 1 16B into 16A", and 69.39 ± 3.46 for TMEM16A. This effect was also observed at 60 mV, however, this effect was not statistically significant at 80 mV or 100 mV. The $\tau_{d0.5}$ was more pronounced, with "site 1 16B into 16A" producing a significantly faster inactivation ($P<0.05$) than TMEM16A at all *Vm* tested.

The "site 1 16A into 16B" had a current density significantly larger ($P<0.05$) than TMEM16B at depolarised *Vm*, with a current of 165.37 ± 23.01 pA/pF (n=6) at 100 mV (Fig. 4.14).

TMEM16B and “site 1 16A into 16B” mutant channel activation and deactivation rates were also assessed. These were studied at *Vm* of 60 mV, 80 mV, and 100 mV. Unlike TMEM16A, TMEM16B was not studied at 40 mV, as the fast kinetics precluded accurate measurements of $\tau_{a0.5}$. The “site 1 16A into 16B” had a faster $\tau_{a0.5}$ than TMEM16B at 80 mV and 100 mV. At 100 mV, $\tau_{a0.5}$ was 11.99 ± 0.61 for “site 1 16A into 16B”, and 8.69 ± 0.32 from TMEM16B. The $\tau_{d0.5}$ not significantly different ($P<0.05$) between TMEM16B and “site 1 16A into 16B” at any *Vm* tested.

These data suggest that swapping “site 1” between TMEM16A and TMEM16B alters the voltage sensitivity of the channels, with the “site 1 16B into 16A” resulting in a channel that has a voltage sensitivity more similar to TMEM16B, and the “site 1 16A into 16B” producing a channel with voltage sensitivity more similar to TMEM16A. Overall, “Site 1” mutations did not have IV-relationships consistent with the TMEM16A or TMEM16B wild-type proteins.

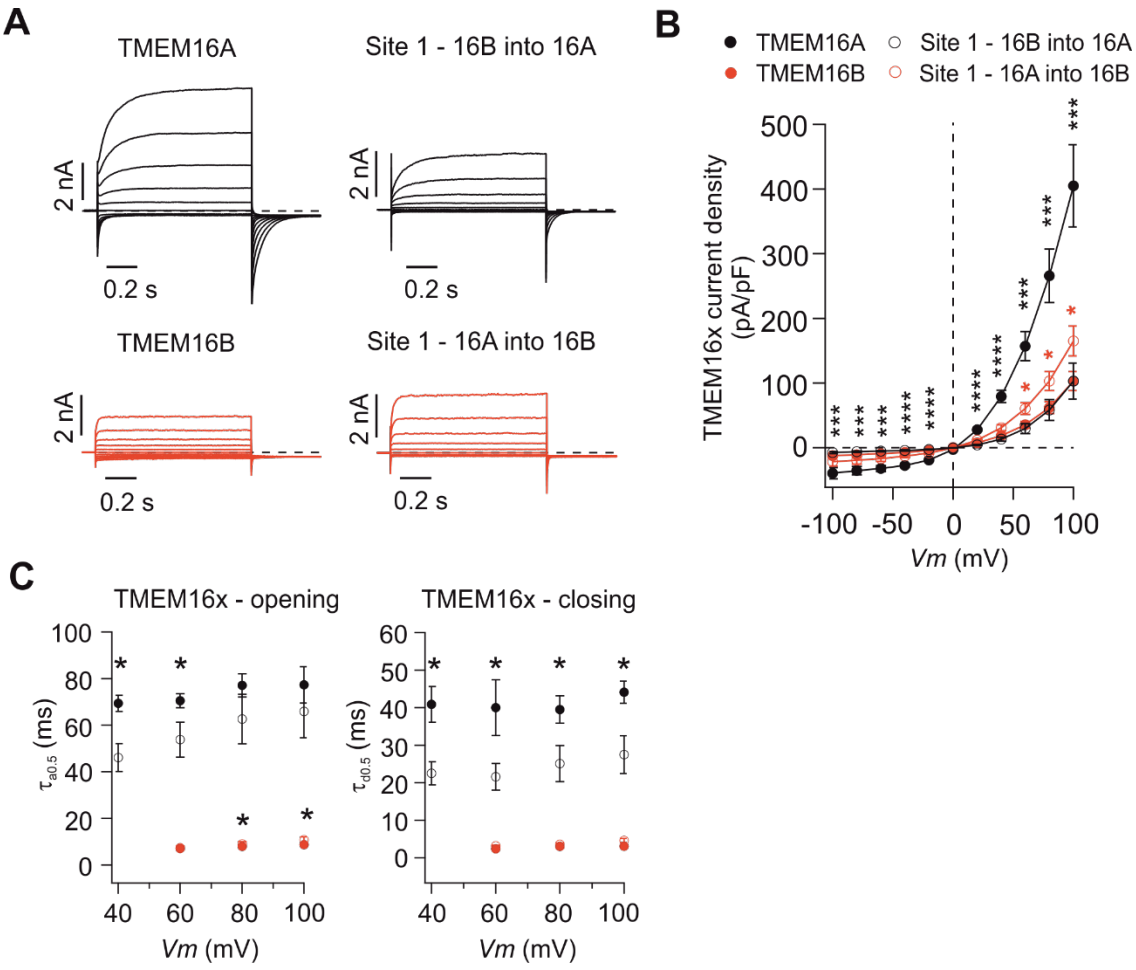

Figure 4.14. Current-voltage relationship of TMEM16A and TMEM16B and chimeras in site 1.

(A) TMEM16A, "site 1 16B into 16A", TMEM16B, and "site 1 16A into 16B" expressing HEK-293T cells were studied in the whole-cell patch-clamp configuration, using the "IV-steps" voltage protocol. Solutions contained 0.3 μM $[Ca^{2+}]_i$ for recordings of TMEM16A and "site 1 16B into 16A" currents (traces depicted in black). $[Ca^{2+}]_i$ was 0.6 μM for TMEM16B and "site 1 16A into 16B" (traces depicted in red). Dotted line represents zero-current level.

*(B) Mean relationships between Vm and TMEM16A (control), TMEM16B (control), "site 1 16B into 16A", and "site 2 16B into 16A" currents. *P<0.05 (two-way ANOVA, n=6, 5, 6, 6, respectively).*

*(C) Mean $\tau_{a0.5}$ and $\tau_{d0.5}$ of TMEM16A (black filled circles), "site 1 16B into 16A" (black open circles), TMEM16B (red filled circles), and "site 1 16A into 16B" (red open circles). *P<0.05 (unpaired t-test).*

4.9.4. Voltage sensitivity of site 1 TMEM16A alanine scanning mutagenesis

Alanine scanning is a mutagenesis technique that involves swapping residues of interest with alanine residues. Residues hypothesised to be involved in binding to PIP_2 were substituted for alanine, as it is a non-charged, non-polar amino acid. It can therefore be thought of as inert, as it may not form electrostatic interactions with the PIP_2, or other ligands in the proposed binding site. Alanine scanning in "site 1" was therefore intended to disrupt the PIP_2 binding site.

During the *in silico* simulations, the amount of time PIP_2 spent in close proximity to residues was quantified. Three residues in site 1 were identified as being especially important in PIP_2 binding to TMEM16A. These were in TMEM16A positions 776, 777, 779, which correspond to leucine, arginine, and glutamine. All three residues were substituted for alanine, to determine whether they interacted with PIP_2 during PIP_2 modulation of TMEM16A.

HEK-293T cells expressing TMEM16A or the triple alanine scanning TMEM16A mutant were studied using whole-cell patch-clamp. Solutions contained 0.3 μM $[Ca^{2+}]_i$, and the "IV-CaCC" voltage protocol was used to assess current density of the wild-type and mutant channels.

Alanine scanning mutagenesis of TMEM16A in "site 1" did not have a significantly different ($P<0.05$) current density to that of wild-type TMEM16A. TMEM16A and the alanine scanning TMEM16A had respective current of 150.75 ± 72.24 (n=3) and 159.38 ± 92.09 (n=4) at 100 mV (Fig. 4.15). Alanine scanning in "site 1" did not significantly ($P<0.05$) affect the current density of TMEM16A, or have a significant impact ($P<0.05$) on $\tau_{a0.5}$ or $\tau_{d0.5}$ (Fig. 4.15).

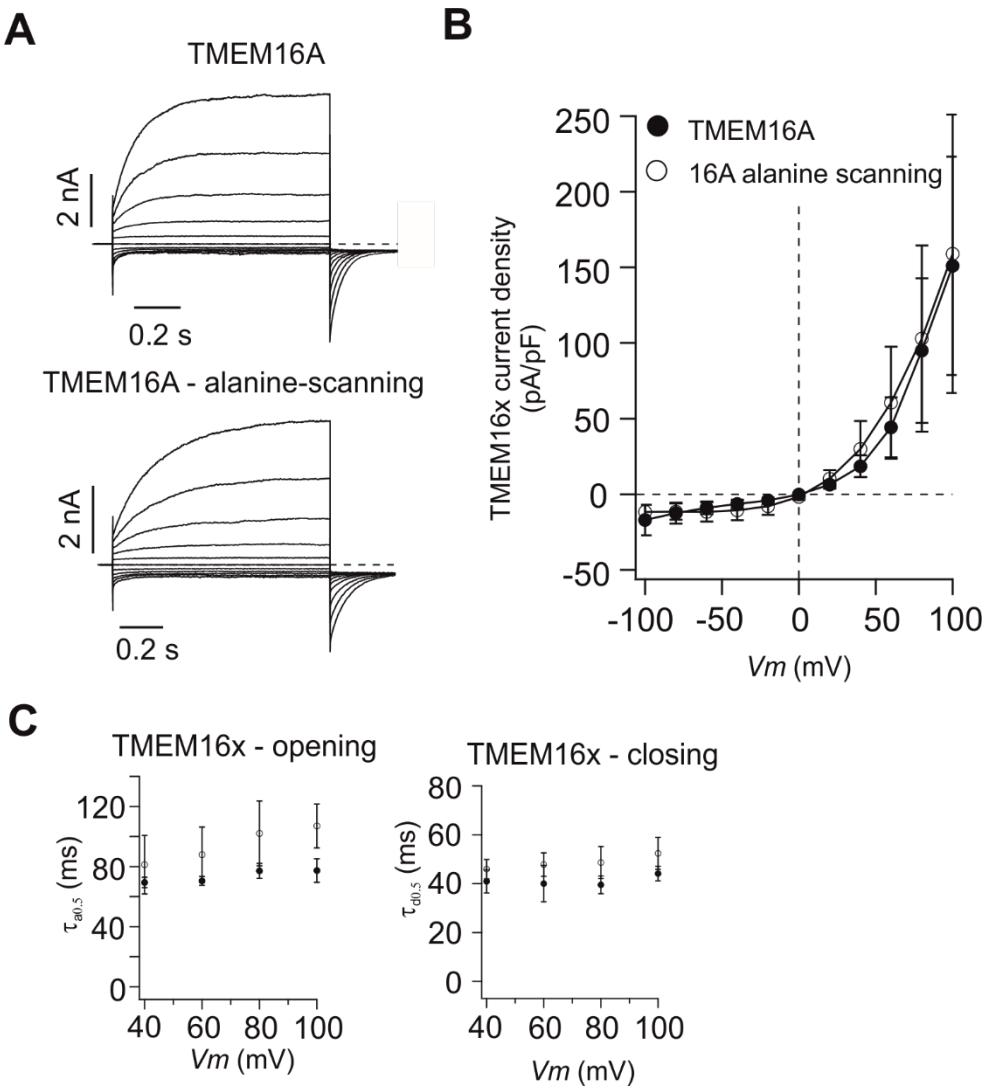

Figure 4.15. Current-voltage relationship of TMEM16A triple alanine-scanning mutants in site 1

(A) TMEM16A and alanine-scanning TMEM16A transfected HEK-293T cells were studied in the whole-cell patch-clamp configuration, using the "IV-steps" voltage protocol. Solutions contained 0.3 μM $[Ca^{2+}]_i$. Dotted line represents zero-current level.

(B) Mean relationships between Vm and TMEM16A and alanine-scanning TMEM16A, n=3 and 4, respectively. N.S. P>0.05 (two-way ANOVA).

(C) Mean $\tau_{a0.5}$ and $\tau_{d0.5}$ of TMEM16A (black filled circles) and TMEM16A alanine scanning (black open circles). N.S. P>0.05 (unpaired t-test).

4.9.5. Voltage sensitivity of site 2 TMEM16A and TMEM16B chimeras

TMEM16A and TMEM16B were also mutated in "site 2", a shorter downstream site also identified to be involved in PIP_2 binding. TMEM16A "site 2" is located at residues 791, 792, and 793, and TMEM16B "site 2" is located at 725, 726, and 727. As with site 1 mutagenesis, the regions of interest were exchanged between TMEM16A and TMEM16B.

Voltage sensitivity for "site 2" was assessed using the same methodology as for "site 1". In contrast to "site1", where the inserted sequence conferred properties to the backbone channel, in "site 2" voltage sensitivity of the channels were not significantly altered ($P<0.05$). TMEM16A had a current density of 150.75 ± 72.24 (n=3), not significantly different ($P<0.05$) to the current density of "site 2 16B into 16A" 150.75 ± 72.24 (n=4) (Fig. 4.16). TMEM16B and "site 2 16A into 16B" also did not differ significantly ($P<0.05$) between each other, with a current density of 29.44 ± 3.41 (n=4) and 21.91 ± 3.03 (n=4), respectively (Fig. 4.16).

The TMEM16A "site 2" mutant channel activation and deactivation rates were also assessed, and were not found to be significantly different ($P<0.05$) at any *Vm* tested. TMEM16A and "site 2 16B into 16A" had a $\tau_{a0.5}$ of 77.35 ± 7.78, and 92.27 ± 20.66 at 100 mV, respectively. The $\tau_{d0.5}$ of TMEM16A was 44.15 ± 2.97 at 100 mV, and 47.95 ± 8.23 for "site 2 16B into 16A" (Fig. 4.16). The TMEM16B "site 2" kinetics could not be studied as the "site 2 16A into 16B" currents were small and therefore could not be fitted with a single exponential function (Fig. 4.16).

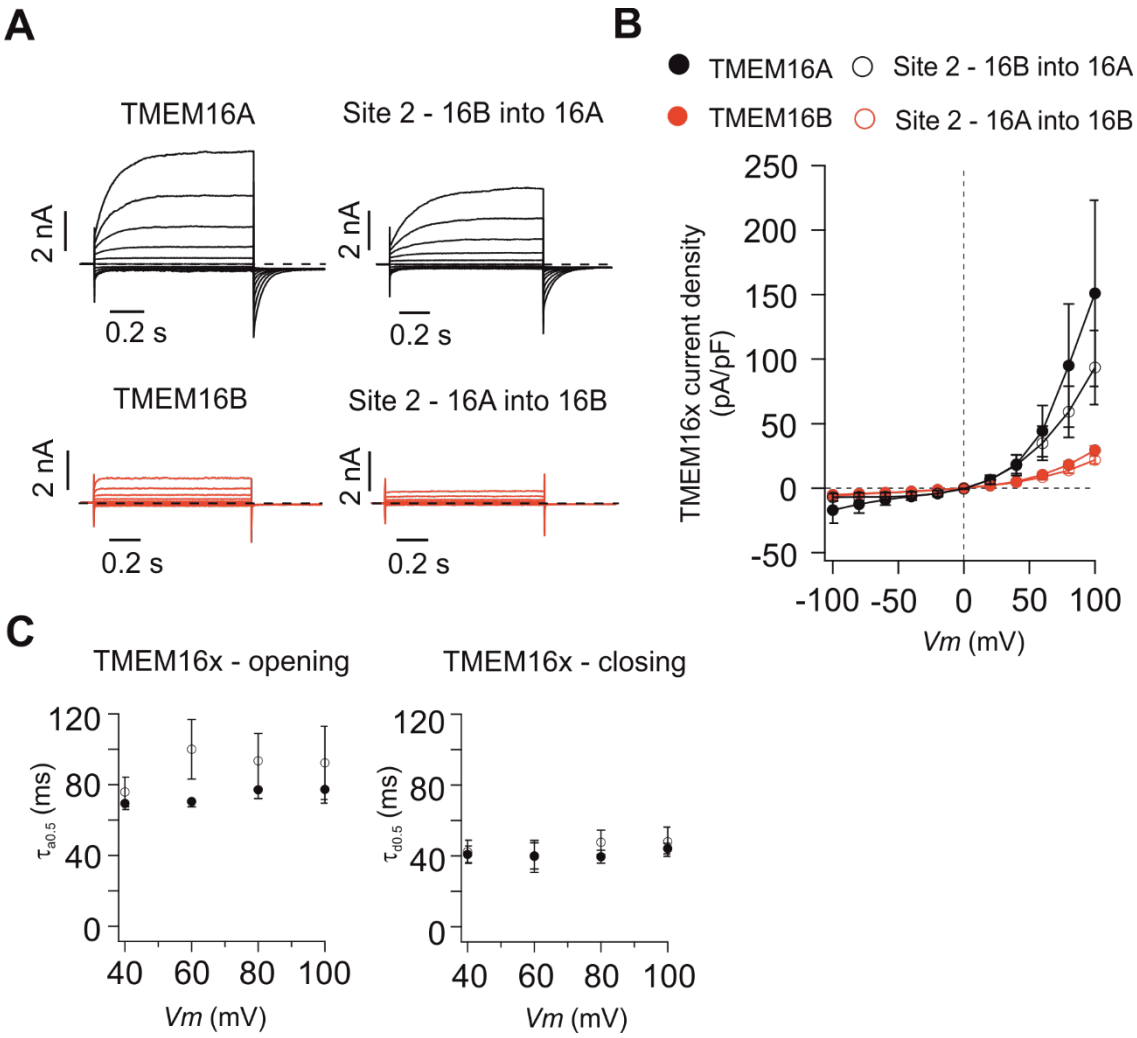

Figure 4.16. Current-voltage relationship of TMEM16A and TMEM16B mutants in site 2

(A) TMEM16A, "site 2 16B into 16A", TMEM16B, and "site 2 16A into 16B" transfected HEK-293T cells were studied in the whole-cell patch-clamp configuration, using the "IV-steps" voltage protocol. Solutions contained 0.3 μM $[Ca^{2+}]_i$ for recordings of TMEM16A and "site 2 16B into 16A" currents (traces depicted in black). $[Ca^{2+}]_i$ was 0.6 μM for TMEM16B and "site 2 16A into 16B" (traces depicted in red). Dotted line represents zero-current level.

(B) Mean relationships between Vm and TMEM16A (control), TMEM16B (control), "site 2 16B into 16A", and "site 2 16B into 16A" currents were n= 3, 3, 4, and 4, respectively. N.S. P>0.05 (two-way ANOVA).

(C) *Mean $\tau_{a0.5}$ and $\tau_{d0.5}$ of TMEM16A (black filled circles) and "site 2 16B into 16A" (black open circles). N.S. P>0.05 (unpaired t-test).*

4.9.6. Effect of diC8-PIP_2 on TMEM16A mutants

In the TMEM16A and TMEM16B "site 1" and "site 2" chimera studies, it was observed that the current of the TMEM16A and TMEM16B mutants was disrupted in "site 1", but not in "site 2". This could have been as a result of altered sensitivity to PIP_2. Subsequent experiments aim to study whether PIP_2 modulation of these channels has been affected by mutations.

In order to assess whether the PIP_2 binding site on TMEM16A has been disrupted by mutagenesis, diC8-PIP_2 was perfused over inside-out patches (Fig. 4.17). Three mutations were tested, all of which were made on the TMEM16A construct. Therefore, for inside-out patch-clamp experiments the solutions 0.6 μM $[Ca^{2+}]_i$ were used. Patches were excised from cells transiently expressing TMEM16A, "site 1 16B into 16A", alanine scanning TMEM16A, and "site 2 16B into 16A". Currents were recorded with the *Vm* maintained at 70 mV. Excised patches were then perfused with diC8-PIP_2 (30 μg/ml) for 5 s.

In patches expressing wild-type TMEM16A, when perfused with 30 μg/ml diC8-PIP_2 an increase of 1.36 ± 0.08 (n=8) was observed (Fig. 4.17). The "site 1 16B into 16A", mutation was not significantly affected ($P<0.05$) when diC8-PIP_2 was perfused over, with an increase in normalised current to 1.41 ± 0.34 (n=3, fig. 4.17). Similarly, alanine scanning in the same site did not significantly reduce ($P<0.05$) the effect of diC8-PIP_2, resulting in an increase in current to 1.19 ± 0.18 (n=4, fig. 4.17). When TMEM16A is mutated in "site 2 16B into 16A", there is again no significant reduction in potentiation of current compared to the wild-type, with an increased normalised TMEM16A current of 1.32 ± 0.14 (n=7, fig. 4.17). Taken together these results suggest that PIP_2 binding is a complicated process, that may not result from interaction of residues at one site.

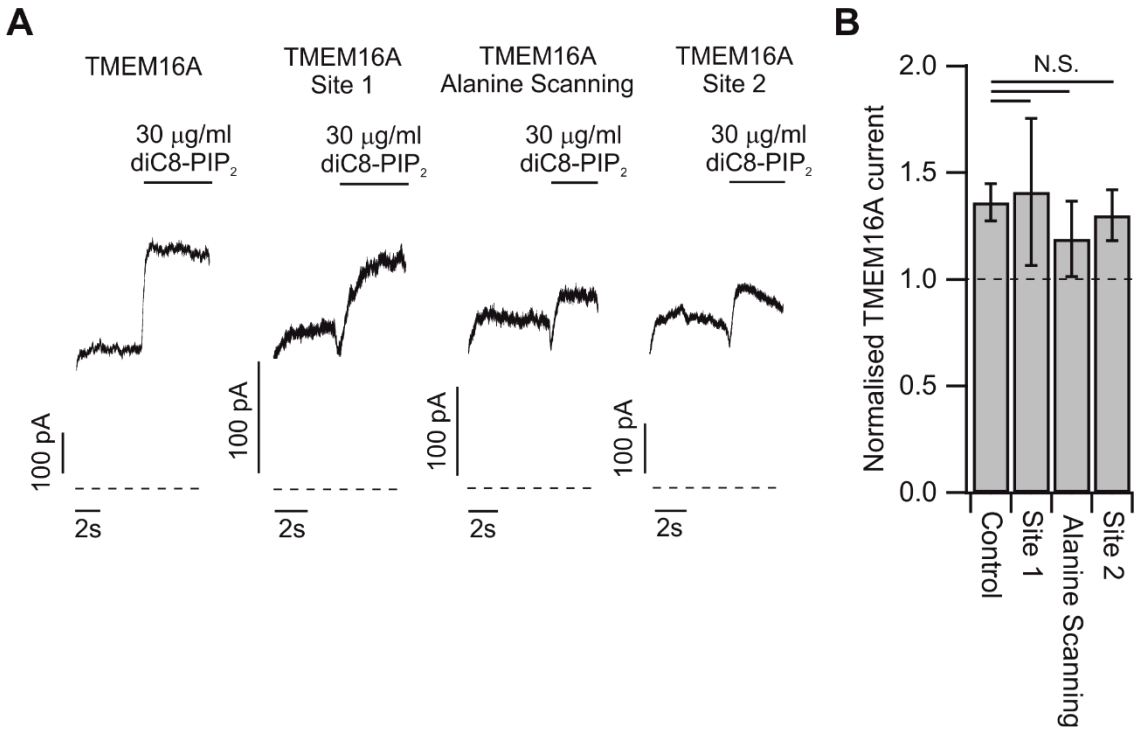

Figure 4.17. Effect of diC8-PIP_2 on TMEM16A and mutant TMEM16A currents

(A) Patches were excised from HEK-293T cells expressing TMEM16A (control), "site 1 16B into 16A", alanine scanning TMEM16A, or "site 2 16B into 16A". Currents were recorded in the inside-out patch-clamp configuration. Solutions contained 0.6 μM free $[Ca^{2+}]_i$ for all experiments. The water-soluble PIP_2 analogue diC8-PIP_2 was applied to the intracellular side of the patch, as indicated by the horizontal bars. The Vm was maintained at 70 mV for the entire duration of the recordings. Dashed lines represent zero-current levels.

(B) Mean relationships between [diC8-PIP_2] and TMEM16A (control), "site 1 16B into 16A", alanine scanning TMEM16A, or "site 2 16B into 16A" currents, expressed relative to the current measured in the absence of diC8-PIP_2, represented by the dotted line. TMEM16A (control), "site 1 16B into 16A", alanine scanning TMEM16A, or "site 2 16B into 16A" were n= 8, 3, 4, and 7, respectively. N.S. P>0.05 (unpaired t-test).

4.10. Discussion

This study demonstrates that PIP_2 modulates TMEM16A channels. The potentiating effect of PIP_2 occurred in a concentration range similar to that causing modulation of other ion channel types such as KCNQ (Li et al., 2011, Zhang et al., 2003), K_v (Rodriguez-Menchaca et al., 2012), and TRPC1 (Saleh et al., 2009) channels. The concentration range of diC8-PIP_2 that modulated the TMEM16A currents (1-100 µg/ml, 1.17-117 µM) is similar to the reported concentrations of physiological PIP_2, which spans from ~2 µM in cultured cell lines (McLaughlin et al., 2002) to 200 µM in platelets in the resting state (Hartwig et al., 1995).

The extent of PIP_2 modulation of TMEM16A current varied significantly depending on $[Ca^{2+}]_i$. Furthermore, the effects of PIP_2 on TMEM16A current were observable at all *Vm* tested. This suggests that *in vivo* modulation of TMEM16A currents by PIP_2 may occur under resting conditions as well as at depolarised *Vm*.

4.10.1 Modulation of TMEM16A by endogenous PIP_2

The voltage-sensitive phosphatase, DrVSP, was used to determine the sensitivity of the TMEM16A channel to endogenous PIP_2. DrVSP is a phosphoinositide 5-phosphatase transmembrane protein that enables depletion of PIP_2 content in intact cells when *Vm* is brought to depolarised values (Okamura et al., 2009). Here, it was found that DrVSP activation reduced the amplitude of TMEM16A currents. The kinetics of PIP_2 depletion by DrVSP have been investigated using fluorescence resonance energy transfer (FRET) imaging of PIP_2 levels in HEK-293T cells (Itsuki et al., 2014).

It was shown that within ~1 s of activation of the phosphatase, PIP_2 in the membrane was significantly depleted (Itsuki et al., 2014). This time course of alteration of plasma

membrane PIP_2 content is consistent with the changes in current amplitude we observed in cells co-expressing TMEM16A channels and DrVSP. The DrVSP-dependent modulation of TMEM16A currents were fully re-established after ~55 seconds at -50 mV. This duration corresponds to the estimated time of PIP_2 re-synthesis by endogenous PIPK (Itsuki et al., 2014, Falkenburger et al., 2010b, Loew, 2007). Endogenous PIPK required the addition of ATP in order for PIP_2 to be re-synthesised. Following the depletion of PIP_2, in the absence of ATP DrVSP-dependent modulation of TMEM16A currents were not re-established.

The α1-adrenergic receptor was co-expressed with TMEM16A in order for physiological PIP_2 regulation to be observed. "High" and "low" concentrations of the intracellular Ca^{2+} buffering agent EGTA were used to dissect the contributions of changes in $[Ca^{2+}]_i$ and endogenous PIP_2, to modulation of the TMEM16A channel. In solutions containing "high" EGTA, α1-adrenergic receptor stimulation with PE displayed a decrease in current. We interpret this to be as a result of plasma membrane PIP_2 depletion during the Gq-PCR mediated signalling cascade. This suggests that PIP_2 could be of great importance in regulating TMEM16A activity in conditions of low intracellular Ca^{2+}, where we observed the PIP_2 modulation to be most pronounced.

4.10.2. Effect of plasma membrane composition on PIP_2 modulation of TMEM16A

The recent elucidation of the TMEM16A structure has provided evidence that the TMEM16A pore is in close proximity to the plasma membrane (Dang et al., 2017, Paulino et al., 2017). This evidence is indicative that the plasma membrane composition is a strong regulator of TMEM16A activity.

Cholesterol is a major regulator of ion channel function (Levitan et al., 2010). Plasma-membrane composition, and therefore cholesterol levels, vary between cell types (Bolz, 2013). Cholesterol has been implicated in the localisation and metabolism of PIP_2, via cholesterol-rich lipid rafts (Hong et al., 2012). Lipid rafts are involved in the regulation of Gq-PCR mediated signalling, and therefore have a role in the control of PIP_2 hydrolysis (Allen et al., 2007).

Cholesterol has been observed to reduce TMEM16A activity, as depletion of plasma membrane cholesterol increases TMEM16A current (De Jesus-Perez et al., 2018, Sones et al., 2010). In contrast to previous results demonstrated in this chapter, we observed that following depletion of plasma membrane cholesterol, PIP_2 decreases TMEM16A activity. This finding resembles the reversal of the PIP_2 effect by cholesterol depletion observed on the Mg^{2+}-inhibitory cation channel (MIC), human ether-a-go-go-related gene (hERG), and KCNQ channels (Chun et al., 2010). This study concluded that cholesterol modulates ion channel activity via long-term regulation of PIP_2 levels (Chun et al., 2010). However, experiments shown in this chapter demonstrate an acute effect of the interplay between cholesterol and PIP_2 on TMEM16A activity.

4.10.3. TMEM16A pharmacology following depletion of endogenous PIP_2

Pharmacological interception of the Gq-PCR (e.g. α1-adrenergic receptor) pathway may be a useful tool in the regulation of blood vessel tone, especially for vascular diseases in which TMEM16A has been implicated, such as hypertension (Papp et al., 2019).

VSP-mediated depletion of PIP_2 in the plasma membrane allowed the effect of PIP_2 on TMEM16A pharmacology to be assessed. We found that a reduction in endogenous PIP_2

had no effect on the potency of the TMEM16A blocker Ani9, but facilitated an increase in the activatory effect of A9C on TMEM16A at negative *Vm*.

Previous studies in the Tammaro group have demonstrated that A9C interacts with TMEM16A in the pore region (Ta et al., 2016). As endogenous PIP_2 is plasma membrane-bound, and the TMEM16A pore is partially exposed to the plasma membrane, it is feasible that PIP_2 and A9C both interact with TMEM16A in a similar "activator" region. It was therefore interesting to begin to study the PIP_2 binding site.

4.10.4. PIP_2 binding site mutagenesis studies

The differential effect of PIP_2 on TMEM16A and TMEM16B channels was the basis for PIP_2 binding-site mutagenesis. Residues of interest were suggested by Remco Jongkind in collaboration with Dr Phill Stansfeld, and were found to be clustered around two main areas. "Site 1" chimeras had an altered sensitivity to voltage compared to wild-type TMEM16A or TMEM16B. We hypothesise this is due to an altered sensitivity to PIP_2. "Site 2" chimeras were unaffected in their sensitivity to voltage, and none of the mutant tested significantly interfered with diC8-PIP_2-binding. We conclude that mutation of each of these sites alone is not sufficient to interfere with PIP_2 interaction with TMEM16A. This could be because the residues exchanged between TMEM16A and TMEM16B both do correspond to the PIP_2 binding site, and that the differential PIP_2 effect on these proteins is because of differences in transduction. An additional possible explanation for this is differences between the homology model used and the actual TMEM16A cryo-EM structure (Paulino et al., 2017, Dang et al., 2017). As the PIP_2 binding site *in silico* simulations were carried out before the TMEM16A cryo-EM structure had been elucidated, they were created using the TMEM16A homology model

(nhTMEM16). The TMEM16A homology model mutations made in TMEM16A for experimental testing did not perfectly align. The locations of the proposed and actual mutations are depicted in figure 4.18.

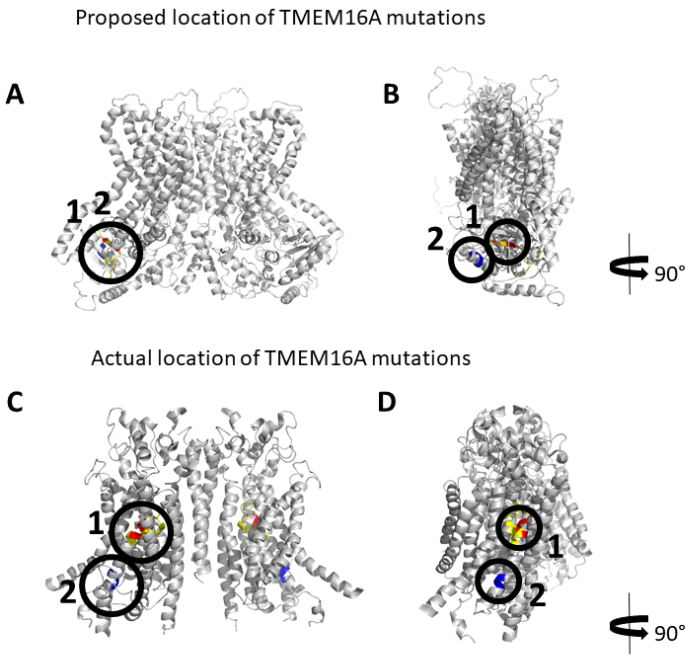

Figure 4.18. TMEM16A model of PIP_2 binding site locations.

Model created using PyMol software. Yellow and red residues represent the location of the "site 1" chimera, with red residues representing residues selected for alanine scanning. "Site 2" residues are represented in blue. Sites 1 and 2 are shown using black circles.

(A) PyMol diagram of the proposed location of the TMEM16A mutations, using the nhTMEM16x based TMEM16A homology model.

(B) PyMol model from (A), rotated 90°.

(C) PyMol diagram of the actual location of the TMEM16A mutations, using the cryo-EM structure of TMEM16A.

(D) PyMol model from (C), rotated 90°.

It could therefore be suggested that the sites of interest may have favourable pockets of residues for PIP_2-binding but are not as accessible for free or membrane bound PIP_2-interactions. In addition to this, due to the nature of course grain molecular simulations, it is only possible to assess proximity of lipids to specific residues. This means affinity of the proposed binding pocket of PIP_2 is not studied. However, this has shown to be closely correlated for previous studies on lipid-protein interactions (Marrink et al., 2007, Bond et al., 2008).

Recently, the TMEM16F PIP_2 binding site has been elucidated. PIP_2 binds to a cluster of positively charged residues near the TMEM16F N-terminus by electrostatic interaction. The authors suggest that due to lack of similarity between TMEM16F and TMEM16A in this region, a different mechanism of action could be responsible (Ye et al., 2018).

4.10.5. Physiological significance of TMEM16A regulation by PIP_2

The extent to which PIP_2 modulation of TMEM16A channels affects the cell electrical activity may vary depending on the cell type. There are multiple factors that could contribute to the impact of this modulation on cell electrical activity. The proximity of TMEM16A channels to lipid rafts or cellular mechanisms that determine local plasma membrane PIP_2 content (such as PLC or PIPK) may vary between cell types.

This study has started to define the regulation of TMEM16A by the endogenous lipids PIP_2 and cholesterol. Availability and proximity of endogenous lipids to ion channels is defined by the local plasma membrane composition, which can be in the form of lipid rafts and is cell type specific. Targeting the plasma membrane clinically, for example modulating the lipid composition to increase membrane fluidity, could be a potential method of TMEM16A modulation, as it could result in a differing degree of PIP_2 or

cholesterol availability for TMEM16A modulation. Membrane fluidity in VSMCs could be modulated using components like cholesterol, which influence lateral membrane fluidity (Wydro, 2011, Ramstedt and Slotte, 2002). This could result in increased PIP_2 lateral movement. Dietary intervention, for example a diet high in PUFAs which incorporate into the membrane (Shaikh et al., 2015), can also be used to modulate cell membrane fluidity.

Chapter 5

Modulation of TMEM16A channels by docosahexaenoic acid (DHA)

Chapter 5 - Modulation of TMEM16A channels by docosahexaenoic acid (DHA)

DHA is an omega-3 dietary polyunsaturated fatty acid (PUFA). Omega-3 refers to the position of the first carbon double bond, when counting from the carboxyl group. PUFAs have established beneficial effects on the cardiovascular system, with DHA reported to have potent vasodilatory effects (Bonaa et al., 1990, Nestel et al., 2002, Goodfellow et al., 2000, Mori et al., 2000). Specifically, dietary supplementation with DHA reportedly decreases systolic blood pressure (SBP) in humans (Miller et al., 2014, Sveinsdottir et al., 2016). The mechanisms underlying DHA effect on vascular tone and blood pressure are not fully defined. In this chapter, the effects of DHA on murine isolated VSMCs and isolated aortic rings were studied, to elucidate the mechanisms by which omega-3 PUFAs act in the vasculature. Here, it is hypothesised that inhibition of TMEM16A by DHA may promote vasodilation. This hypothesis is based on the notion that the pore region of TMEM16A is reported to be in close proximity to the plasma membrane (Paulino et al., 2017, Dang et al., 2017). Therefore, the TMEM16A pore region may be sensitive to DHA in addition to other lipids, such as PIP_2 (chapter 4). DHA-mediated vasodilation is also consistent with altered activity of other ion channels, such as inhibition of non-selective cation channels (NSCCs), activation of K^+ channels, and inhibition of Ca_V channels. Therefore, the possibility that DHA affects these channels in VSMCs is also examined in this chapter.

Data presented in this chapter provides evidence that cloned and native TMEM16A channels are potently inhibited by DHA. DHA also caused significant vascular relaxation of isolated mouse aortic rings, an effect found to be mimicked by pharmacological

inhibition of TMEM16A by Ani9. Myography experiments using altered extracellular Cl^- ($[Cl^-]_e$) demonstrated a role for Cl^- channels in this response. Specifically, increasing the Cl^- electrochemical gradient by lowering $[Cl^-]_e$ strongly enhanced contraction of aortic rings, revealing a role for Cl^- channels in this response. However, DHA profoundly reduced the effect of low Cl^-. Native NSCCs and K^+ channels were found to be modulated by DHA, however this modulation occurred outside the physiological range of *Vm*. In contrast, DHA inhibited native TMEM16A and Ca_V channels at all *Vm* tested.

Overall, the work in this chapter demonstrates that cloned and native TMEM16A channels are blocked by DHA. DHA regulates aortic tone, at least in part, via attenuation of the aortic response to agonist-induced contraction, through prevention of TMEM16A and Ca_V channel activation. This results in reduced VSMC contraction.

5.1. DHA modulation of cloned TMEM16A channels

This study was started by testing the effect of DHA on cloned TMEM16A channels. TMEM16A currents expressed in HEK-293T cells were studied using whole-cell patch clamp electrophysiology, in the presence of increasing extracellular concentrations of DHA ($[DHA]_e$). *Vm* was maintained at 70 mV and $[Ca^{2+}]_i$ was buffered to 0.3 μM. Exposure of cells to various [DHA] resulted in a concentration-dependent decrease in TMEM16A current. DHA inhibition occurred rapidly and the TMEM16A current was measured as the effect reached the steady-state for each [DHA]. The resultant data was normalised to the Cm. The currents measured in the presence of DHA were normalised to the current measured in the absence of DHA.

A decrease in the current at positive *Vm* is consistent with the block of TMEM16A. However, this could also be due to the activation of an endogenous inward current that could reduce the overall current at positive *Vm*. To test whether DHA activates endogenous currents in HEK-293T cells, non-transfected (NT) cells were exposed to various $[DHA]_e$ during whole-cell patch-clamp. In the NT cells normalised currents on addition of DHA (70 μM) were 1.01 ± 0.06. DHA therefore had no effect on NT cells at all concentrations tested (Fig. 5.1). In TMEM16A transfected cells, DHA inhibited cloned TMEM16A channels in a dose dependent manner, with normalised mean TMEM16A current in the presence of DHA (70 μM) of 0.17 $\pm$ 0.02 (n=10) (Fig. 5.1). Mean data was fitted with the hill equation (Equation 2.2, fig. 5.1). This resulted in an IC_{50} of 15.4 ± 1.5, and an *h* of 1.14 ± 0.13 (n=10).

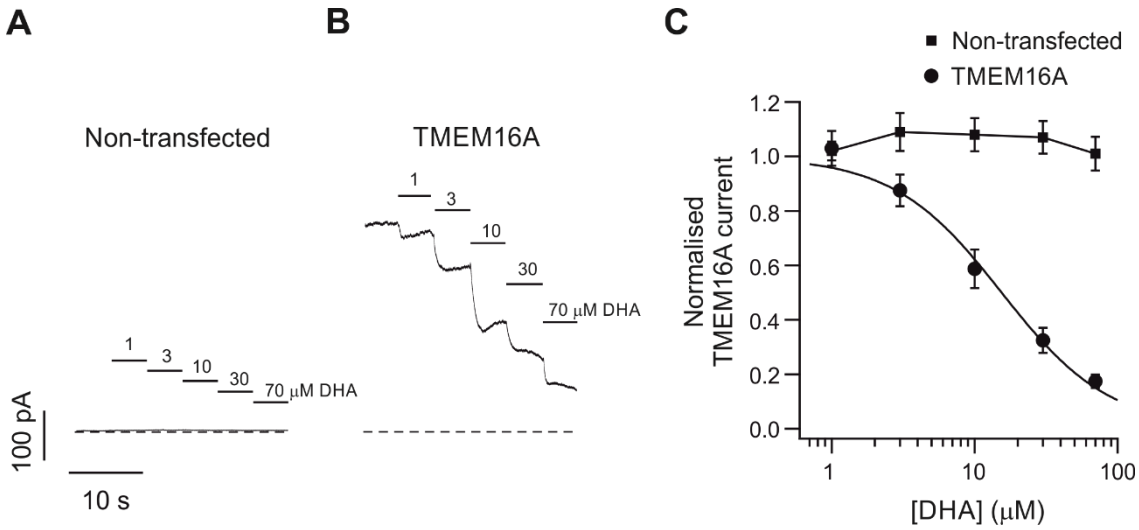

Figure 5.1. Effect of DHA on cloned TMEM16A currents.

(A) Current recorded from NT HEK-293T cells in the whole-cell patch-clamp configuration. DHA was applied extracellularly as indicated by the horizontal bars. Vm was maintained at 70 mV for the duration of the recording, $[Ca^{2+}]_i$ was 0.3 μM. Dashed lines represent zero-current levels.

(B) Current recorded from TMEM16A-expressing HEK-293T cells in the whole-cell patch-clamp configuration. DHA was applied extracellularly as indicated by the horizontal bars. Vm was maintained at 70 mV for the duration of the recording, $[Ca^{2+}]_i$ was 0.3 μM. Dashed lines represent zero-current levels.

(C) Mean relationships between DHA concentration ([DHA]) and TMEM16A currents, expressed relative to the current measured in the absence of DHA. The smooth curve through the points represents the best fit of the data using the Hill equation (equation 2.2). Number of experiments was (n=5) for NT and (n=10) for DHA.

Experiments in figure 5.1 were conducted at a fixed *Vm* and a fixed $[Ca^{2+}]_i$. However, *in vivo*, TMEM16A currents are typically triggered by activation of a Gq-PCR, which results in dynamic changes in $[Ca^{2+}]_i$ and *Vm*. To achieve this in our experimental system, the α1-adrenergic receptor was co-transfected with TMEM16A in HEK-293T cells.

Whole-cell patch-clamp electrophysiology was used to study HEK-293T cells co-expressing TMEM16A and the α1-adrenergic receptor. "Low EGTA CaCC intracellular solution" (Table 2.7) was used to observe TMEM16A activity as Ca^{2+} was liberated from intracellular Ca^{2+} stores. This solution contained a lower concentration of the Ca^{2+} chelating agent EGTA (Table 2.7) than "standard CaCC intracellular solution" (Table 2.4). In these experiments, the α1-adrenergic receptor was activated by exposing the cell to PE (1 μM).

TMEM16A currents were elicited in response to the "IV-ramp" protocol. TMEM16A currents were normalised for the Cm and plotted against the *Vm* (Fig. 5.2). In the absence of PE, the TMEM16A current displayed characteristic outward rectification. When PE was applied for ~5 s, the current amplitude increased substantially at all *Vm* tested. For example, at -95 mV TMEM16A current increased by ~10.6-fold, while at 95 mV the TMEM16A current increased by ~5.3-fold (Table 5.1). When the experiment was repeated in the presence of DHA (70 μM), the exposure to PE failed to produce a TMEM16A current increase. This effect is consistent with the inhibiting action of DHA on cloned TMEM16A channels. Overall, the TMEM16A current was unaffected at negative *Vm*, and there was a slight decrease at 95 mV.

Table 5.1. Electrophysiological characterisation of TMEM16A currents evoked by activation of the Gq-PCR signalling cascade, in the presence or absence of DHA.

	Control (pA/pF)	PE (pA/pF)	PE & DHA (pA/pF)
-95 mV	-11.39 ± 2.98	-120.45 ± 40.74	-11.98 ± 3.31
95 mV	70.25 ± 18.94	371.26 ± 66.86	37.26 ± 13.96
n	17	10	7

"-95 mV" and "95 mV" refer to the current obtained at these Vm. "n" refers number of experiments.

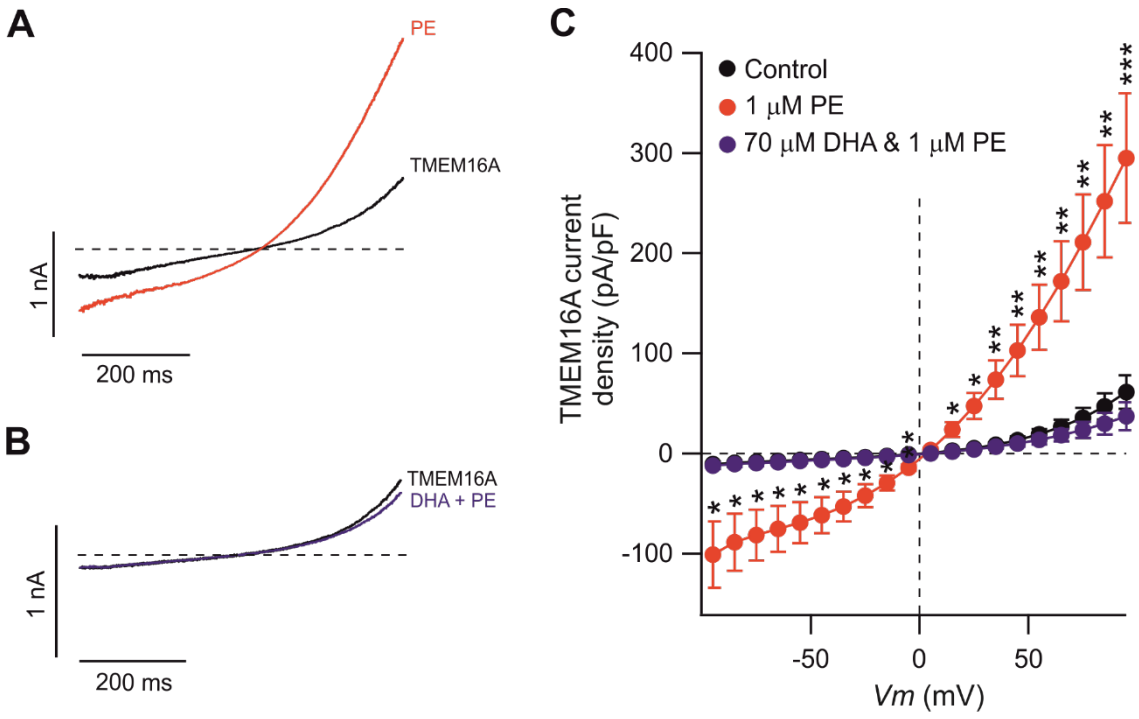

Figure 5.2. Alpha1-adrenergic receptor mediated activation of TMEM16A in the presence of DHA

(A) Representative whole-cell currents recorded from HEK-293T cells expressing TMEM16A co-transfected with the α1-adrenergic receptor in the absence (black) or presence (red) of PE (1 μM). Low EGTA solutions contained 0.21 μM $[Ca^{2+}]_i$. The "IV-ramp" voltage protocol was used to elicit TMEM16A currents.

(B) Representative whole-cell currents recorded from HEK-293T cells expressing TMEM16A co-transfected with the α1-adrenergic receptor in the absence (black) or presence (blue) of PE (1 μM) and DHA (70 μM). Low EGTA solutions contained 0.21 μM $[Ca^{2+}]_i$. The "IV-ramp" voltage protocol was used to elicit TMEM16A currents.

*(C) Mean TMEM16A current versus voltage relationship obtained in the absence (control, n=17) ore presence of PE (1 μM, n=10), or in the presence of both PE (1 μM) and DHA (70 μM, n=7). Statistical analysis between PE alone and PE and DHA, *P<0.05, **P<0.005, ***P<0.0005 (two-way ANOVA).*

5.2. Effect of PIP_2 on DHA modulation of TMEM16A currents

The TMEM16A current activation in response to PE, and its lack of activation in the presence of DHA described in the previous section, are consistent with the increase in $[Ca^{2+}]_i$ triggered by the activation of the α1-adrenergic receptor. However, activation of the α1-adrenergic receptor also causes a reduction in PIP_2 levels in the plasma membrane. As discussed in chapter 4, PIP_2 influences TMEM16A channel function. The relationship between DHA and PIP_2 is explored in the next set of experiments.

In these experiments, HEK-293T cells co-expressing TMEM16A and DrVSP (TMEM16A-DrVSP) were used. As outlined in chapter 4, DrVSP enables PIP_2 in the plasma membrane to be depleted. DrVSP(C302S) is a mutant form of DrVSP, which has an inactive phosphatase domain, and is therefore unable to effectively deplete endogenous PIP_2. HEK-293T cells co-expressing TMEM16A and DrVSP(C302S) (TMEM16A-DrVSP(C302S)) was therefore used as a control.

In order to activate the DrVSP, a 5 s voltage step to 100 mV was triggered. This voltage protocol was used for both TMEM16A-DrVSP, and TMEM16A-DrVSP(C302S).

In TMEM16A-DrVSP expressing cells TMEM16A current was reduced as endogenous PIP_2 was depleted by DrVSP (chapter 4). TMEM16A-DrVSP currents were normalised to the peak TMEM16A current. The remaining fractional steady-state current was 0.79 ± 0.04 (n=6, Fig. 5.3). This inhibition was observed in analogous experiments shown in chapter 4. In TMEM16A-DrVSP(C302S) expressing cells, TMEM16A current was not reduced by activation of the mutant DrVSP.

Following the initial PIP_2-depleting step, *Vm* was maintained at 70 mV, and increasing $[DHA]_e$ were perfused over the TMEM16A-DrVSP or TMEM16A-DrVSP(C302S) expressing cells (Fig. 5.3). Mean currents measured in various $[DHA]_e$ were plotted

against [DHA] and fitted with the Hill equation (Equation 2.2, fig. 5.3). This resulted in an IC_{50} of 15.92 $\pm$ 3.94 μM, and an *h* of 0.49 $\pm$ 0.03 (n=7) for TMEM16A-DrVSP(C302S), and an IC_{50} of 16.71 $\pm$ 1.02 μM, and an *h* of 0.47 $\pm$ 0.94 (n=6) for TMEM16A-DrVSP. These experiments demonstrate that the effect of DHA on TMEM16A channel activity is independent of the endogenous PIP_2 regulation of TMEM16A channel activity.

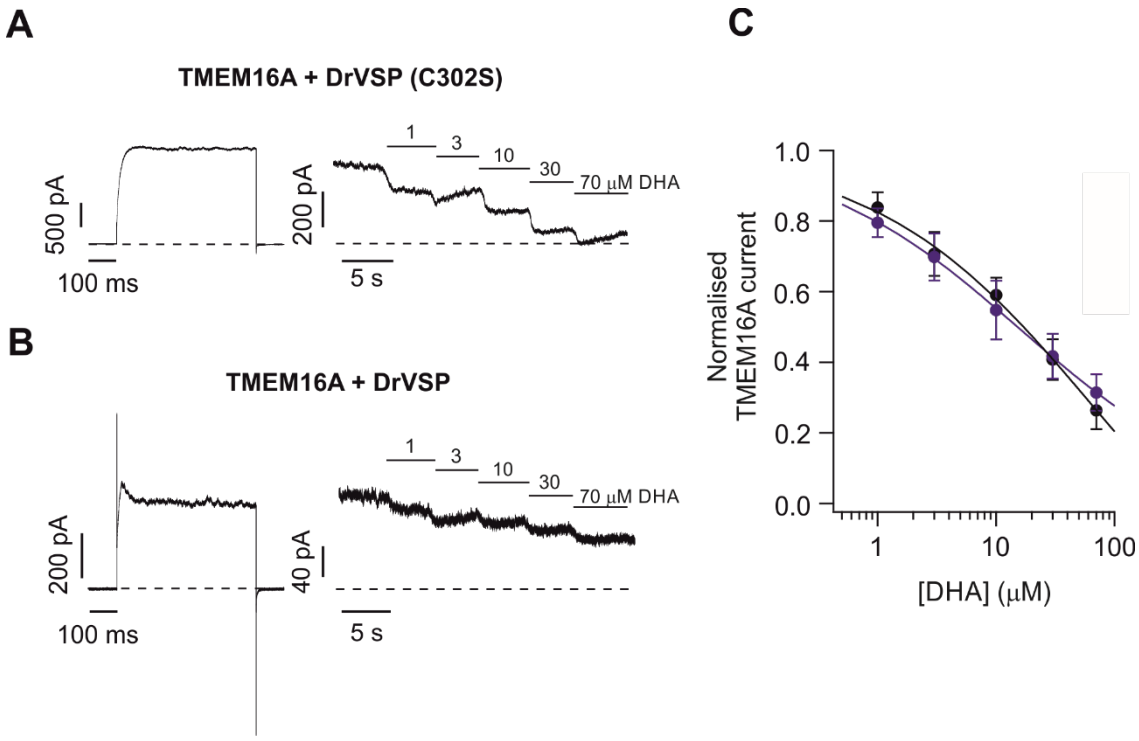

Figure 5.3. DHA modulation of TMEM16A under conditions of PIP_2 depletion.

(A) Whole-cell currents recorded from HEK-293T cells expressing TMEM16A co-transfected with DrVSP(C302S). Solutions contained 0.3 μM $[Ca^{2+}]_i$. The left panel is the current elicited by a 5 s depolarisation to 100 mV. The right panel represents currents measured at 70 mV. Various [DHA] were added, as indicated by horizontal bars. Dotted lines represent zero-current levels.

(B) Whole-cell currents recorded from HEK-293T cells expressing TMEM16A co-transfected with DrVSP. Solutions contained 0.3 μM $[Ca^{2+}]_i$. The left panel is the current elicited by a 5 s depolarisation to 100 mV. The right panel represents currents measured at 70 mV. Various [DHA] were added, as indicated by horizontal bars. Dotted lines represent zero-current levels.

(C) Mean relationships between DHA concentration ([DHA]) and TMEM16A currents in the presence of DrVSP(C302S) (control, n=6) or DrVSP (n=7). TMEM16A currents are expressed relative to the current measured in the absence of DHA. Data were fitted using the Hill equation (equation 2.2). N.S. P>0.05 (unpaired t-test).

5.3. Effect of DHA on isolated VSMCs

Experiments presented in this chapter so far have demonstrated the inhibition of cloned TMEM16A channels by DHA. This inhibition was observed at physiological *Vm* and $[Ca^{2+}]_i$, during α1-adrenergic receptor activation. This suggests that inhibition of TMEM16A by DHA may also have a physiological role in regulating the activity of native TMEM16A in VSMCs. The following experiments aimed to test this possibility.

Whole-cell currents were recorded from isolated VSMCs using "CaCC solutions" (Tables 2.4 and 2.5) with 0.6 μM $[Ca^{2+}]_i$, and the "IV-ramp" protocol (Fig. 5.4). TMEM16A currents were normalised for the Cm. At -95 mV, addition of DHA resulted in a ~1.2-fold reduction in TMEM16A current, which increased to a ~1.7-fold reduction in TMEM16A current at 95 mV (Fig. 5.4, table 5.2). TMEM16A current in the presence of DHA is significantly smaller ($P<0.05$) than the TMEM16A control current at all voltages tested, with the exception of -5 mV which is close to the E_{rev} for TMEM16A in these solutions. These data demonstrate that DHA (70 μM) blocks TMEM16A current at physiologically relevant *Vm* (Knot and Nelson, 1998, Nelson et al., 1990b).

Table 5.2. TMEM16A currents evoked in VSMCs in the presence or absence of DHA.

	Control (pA/pF)	DHA (pA/pF)
-95 mV	-9.63 ± 1.59	-8.27 ± 1.46
95 mV	24.61 ± 3.62	14.40 ± 1.90
n	9	9
N	7	7

"-95 mV" and "95 mV" refer to the current obtained at these Vm. "n" refers number of experiments, "N" is number of animals.

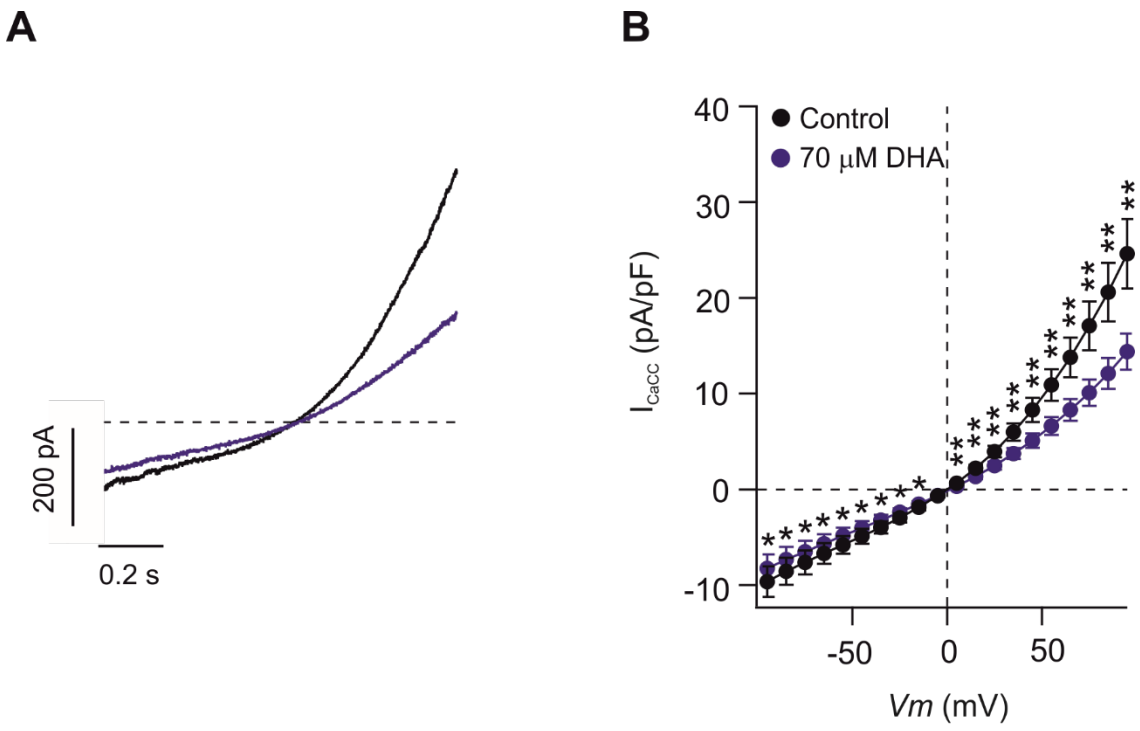

Figure 5.4. Effect of DHA on the native TMEM16A current in isolated VSMCs.

(A) Whole-cell patch-clamp TMEM16A currents recorded from isolated murine VSMCs. $[Ca^{2+}]_i$ was 0.6 μM. The "IV-ramp" protocol was used to elicit TMEM16A currents in the absence (control, shown in black) or presence (blue) of DHA (70 μM).

*(B) Mean whole-cell TMEM16A current measured from -95 mV to 95 mV in 10 mV increments, in the absence (black, control, n=9), or presence of DHA (blue, n=9). *P<0.05, **P<0.005 (two-way ANOVA).*

5.4. Effect of DHA on isolated aortic rings

Experiments shown in chapter 3 demonstrated, using both pharmacology and genetic deletion techniques, that TMEM16A is a crucial depolarising force in agonist-induced blood vessel contraction. The next set of experiments aimed to define whether TMEM16A inhibition may underlie the DHA-mediated vasodilation in aortic rings.

The isolated aortic rings were incubated with DHA (70 μM), or left untreated (control) for 20 minutes prior to the addition of various [PE]. In control conditions, the tension generated by the aortic rings increased as [PE] was increased. The tension measured in the presence of each [PE] was normalised to the tension evoked by 55 mM KCl (Fig. 5.5). The calculated tension was plotted *versus* [PE] and the relationship fitted with the Hill equation (equation 2.2). This fit revealed that the plateau was significantly reduced in the presence of DHA (70 μM), with a ~2.5-fold reduction in vascular contractility in the presence of DHA (table 5.3). This effect was statistically significant ($P<0.05$) at all [PE] tested, apart from the lowest concentration (0.01 μM).

Table 5.3. Overview of blood vessel contraction in the presence or absence of DHA.

	Control	DHA
10 μM PE	0.61 ± 0.01	0.25 ± 0.06
Plateau of fit	0.61 ± 0.01	0.26 ± 0.01
PE EC_{50}	0.15 ± 0.01	0.17 ± 0.01
h	1.16 ± 0.05	1.23 ± 0.07
n	7	7
N	9	9

"10 μM PE" is the tension obtained in the presence of this [PE], and normalised for the tension measured in 55 mM KCl. "Plateau of fit" is the maximal value of aortic contraction determined via the Hill fit of the data (equation 2.2). The "PE EC_{50}" is the value of [PE] required to reach half maximal contraction. The "h" value is the Hill coefficient and represents the slope of the Hill fit. "n" is number of experiments, "N" is number of animals.

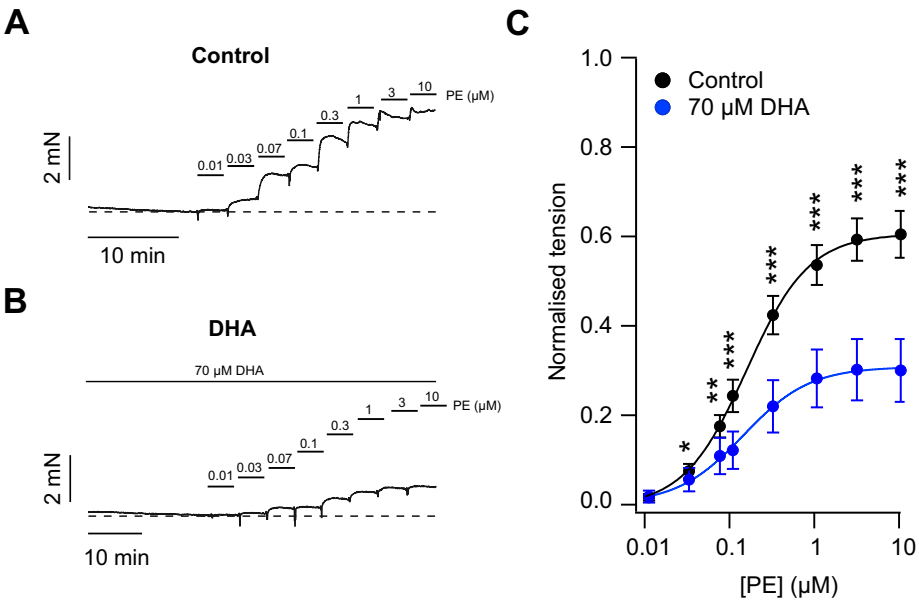

Figure 5.5. PE-mediated contraction of aortic rings in the presence of DHA

(A) Representative change in isometric tension of control aortic rings in response to increasing concentrations of PE. Dotted lines represent baseline tension. Control is replotted from data in fig 3.15.

(B) Representative change in isometric tension of aortic rings in response to increasing concentrations of PE, in the presence of DHA (70 μM), as indicated. Dotted lines represent baseline tension.

*(C) Mean tension vs [PE] relationship of control (n=7), and DHA (70 μM, n=7) aortic rings. *P<0.05, **P<0.005, ***P<0.0005 (two-way ANOVA).*

It was next assessed whether TMEM16A inhibition by DHA is the primary cause of the DHA-mediated reduction in blood vessel contraction. In chapter 3, Ani9 blocked TMEM16A currents in VSMCs, but had no modulatory effect on cationic currents. This data suggests that in isolated aortic rings Ani9 will be selective for TMEM16A. Therefore, the effect of Ani9 on blood vessel contractility can be attributed to inhibition of TMEM16A currents. The following experiments aimed to establish whether Ani9 and DHA produced a similar reduction in agonist-induced blood vessel contraction. Ani9 was tested at a concentration of 1 μM in these experiments to produce a complete inhibition of TMEM16A channels (Seo et al., 2016).

The isolated aortic rings were incubated with Ani9 (1 μM) for 20 minutes, or left untreated for the same length of time (control). Subsequently, aortic rings were exposed to increasing [PE]. Tension *versus* [PE] relationships were constructed as described above, and fitted with the Hill equation (Equation 2.2). The plateau of the PE-mediated aortic contraction fit was significantly reduced ($P<0.05$) in the presence of Ani9 (1 μM), with a ~2.2-fold reduction in contraction compared to the untreated aortic rings (Fig. 5.6, Table 5.4). This effect was statistically significant at all [PE] tested ($P<0.05$), apart from the lowest two concentrations (0.01 μM and 0.03 μM).

Table 5.4. Overview of blood vessel contraction in the presence or absence of Ani9.

	Control	Ani9
10 μM PE	0.60 ± 0.03	0.29 ± 0.06
Plateau of fit	0.61 ± 0.01	0.30 ± 0.01
PE EC_{50}	0.16 ± 0.01	0.13 ± 0.01
h	1.12 ± 0.05	0.19 ± 0.08
n	7	7
N	7	7

"10 μM PE" is the tension obtained in the presence of this [PE], and normalised for the tension measured in 55 mM KCl. "Plateau of fit" is the maximal value of aortic contraction determined via the Hill fit of the data (equation 2.2). The "PE EC_{50}" is the value of [PE] required to reach half maximal contraction. The "h" value is the Hill coefficient and represents the slope of the Hill fit. "n" is number of experiments, "N" is number of animals.

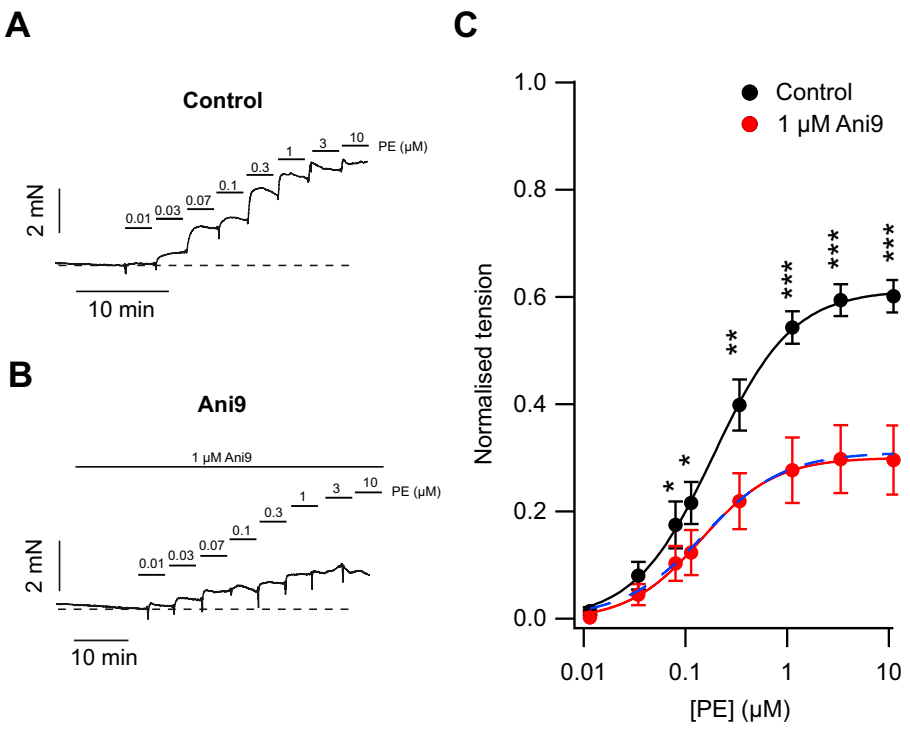

Figure 5.6. PE-mediated contraction of aortic rings in the presence of Ani9 vs DHA.

Control and Ani9 myography data initially presented in figure 3.15.

(A) Representative change in isometric tension of aortic rings in response to increasing concentrations of PE, in the presence of Ani9 (1 μM), as indicated. Dotted lines represent baseline tension.

*(B) Mean tension vs [PE] relationship of control (n=7), and Ani9 (1 μM, n=7) aortic rings. Dotted blue line represents aortic contraction in the presence of 70 μM DHA (Fig. 5.5). *P<0.05, **P<0.005, ***P<0.0005 (two-way ANOVA).*

5.4.1. Use of Cl^- to understand the role of TMEM16A in myography

Experiments testing the effect of DHA on isolated aortic rings have demonstrated a role of DHA in reduction of agonist-induced vascular constriction. Ani9 mimics this effect, which suggests that the effect of DHA on aortic tone could be due to TMEM16A inhibition. To test this idea, the role of Cl^- channels in this response were tested using two methodologies. First, myography experiments in the presence of bumetanide were carried out in order to achieve reduced $[Cl^-]_i$. The rationale for this is that TMEM16A currents would be reduced as the E_{Cl} would be pushed towards a more negative *Vm* (Fig 5.7). Subsequently myography experiments using high $[Cl^-]_e$ were carried out in order to increase TMEM16A mediated current and restore the response to PE (Fig. 5.7).

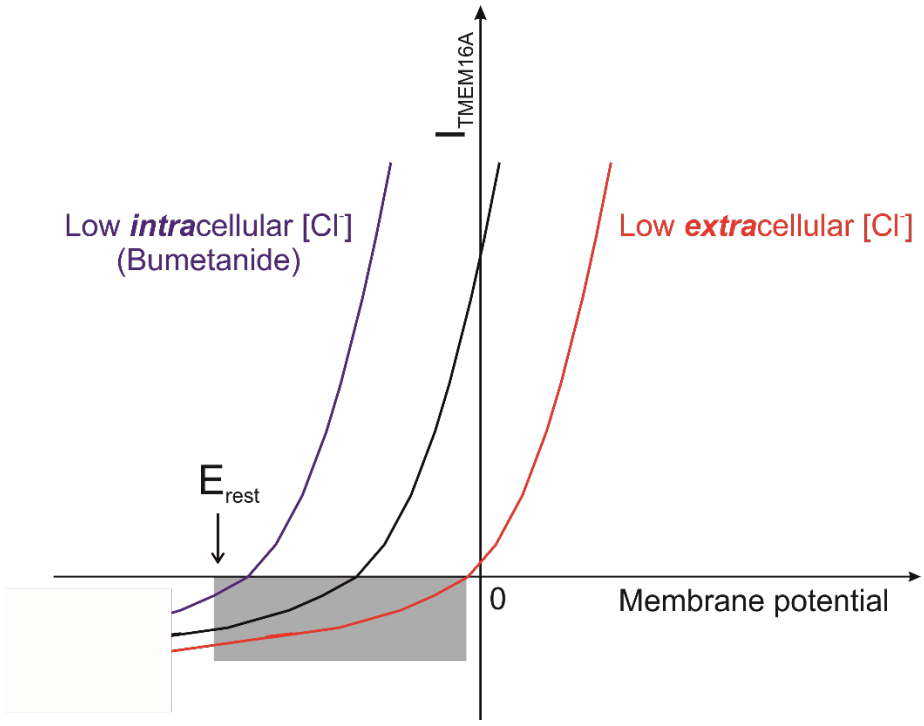

Figure 5.7. Diagram depicting the effect of electrochemical gradient for Cl^- in VSMCs. Black line represents model TMEM16A current. In conditions of low $[Cl^-]_i$, such as on addition of bumetanide, the E_{Cl} shifts to a more negative Vm (blue). In conditions of low $[Cl^-]_e$, the E_{Cl} shifts to a less negative Vm (red). The shaded box represents physiologically relevant range of Vm.

5.4.2. Effect of reducing VSMC $[Cl^-]_i$ on aortic contraction

Bumetanide is an NKCC1 transporter blocker (Ben-Ari, 2017), clinically used for treatment of oedema and hypertension (Ward and Heel, 1984, Handler et al., 1981). It is also an effective experimental tool to enable inhibition of NKCC1 and consequent reduction of $[Cl^-]_i$ in VSMCs (Orlov et al., 2012, Garg et al., 2007). This experiment used bumetanide to reduce VSMC intracellular Cl^- concentration ($[Cl^-]_i$) in isolated aortic rings during myography experiments. Experiments presented in chapter 3 demonstrated that bumetanide has no direct effect on cloned TMEM16A currents (Fig. 3.6), which excludes the possibility of non-specific effects of this compound on TMEM16A channels.

The isolated aortic rings were incubated in the presence of bumetanide (40 μM) for 20 minutes, or left untreated for the same length of time (control). Various [PE] were then added to each aorta. The calculated tension was plotted *versus* [PE] and the relationship fitted with the Hill equation (Equation 2.2). This fit revealed that the plateau was significantly ($P<0.05$) reduced in the presence of bumetanide (40 μM), with a ~3.2-fold reduction in vascular contraction (Table 5.5).

This effect was significantly significant at all [PE] tested ($P<0.05$). This experiment demonstrates that a reduction in $[Cl^-]_i$ in VSMCs reduces the agonist-induced contraction in isolated aortic rings. This is in agreement with results in figure 5.6, which demonstrate that blocking TMEM16A using Ani9 reduces Cl^--mediated contraction of aortic rings, and also reduces agonist-induced contraction in isolated aortic blood vessels. DHA has the same effect (Fig. 5.5) which suggests that it acts as a mediator of blood vessel relaxation via TMEM16A.

Table 5.5. Overview of blood vessel contraction in the presence of bumetanide.

	Control	Bumetanide
10 μM PE	0.63 ± 0.03	0.20 ± 0.03
Plateau of fit	0.64 ± 0.01	0.20 ± 0.01
PE EC_{50}	0.15 ± 0.01	0.28 ± 0.01
h	1.13 ± 0.03	1.36 ± 0.06
n	22	10
N	10	10

"10 μM PE" is the tension obtained in the presence of this [PE], and normalised for the tension measured in 55 mM KCl. "Plateau of fit" is the maximal value of aortic contraction determined via the Hill fit of the data (equation 2.2). The "PE EC_{50}" is the value of [PE] required to reach half maximal contraction. The "h" value is the Hill coefficient and represents the slope of the Hill fit. "n" is number of experiments, "N" is number of animals.

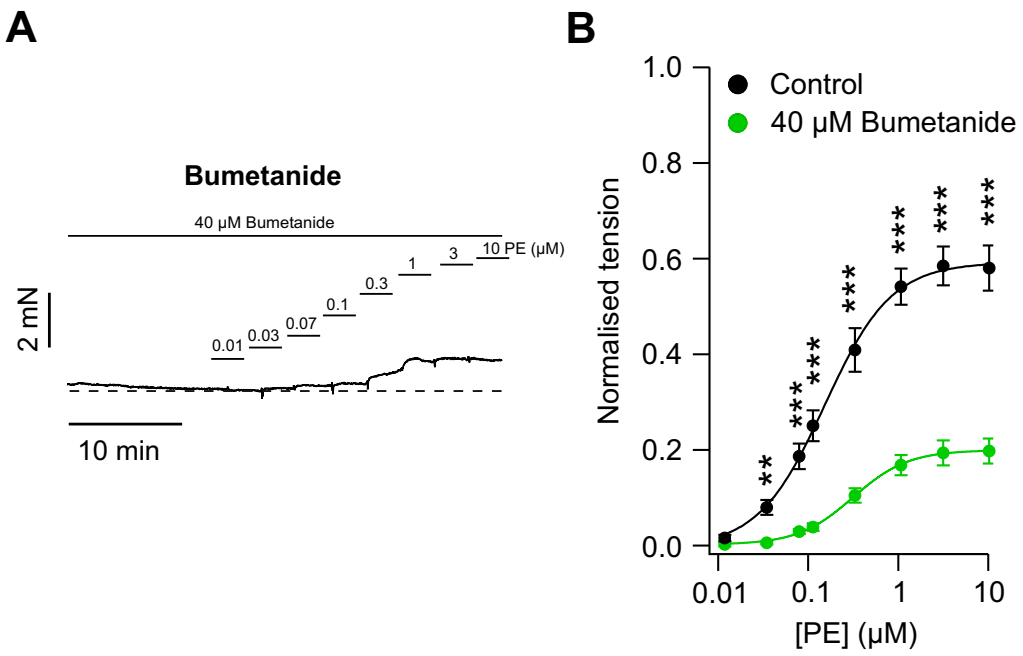

Figure 5.8. PE-mediated contractility of aortic rings in the presence of bumetanide vs DHA

(A) Isometric tension of aortic rings in response to increasing concentrations of PE, in the presence of 40 µM bumetanide. Dotted line represents baseline tension.

*(B) Mean tension vs [PE] relationship of control (n=10), and Bumetanide (40 µM, n=10) aortic rings. *P<0.05, **P<0.005, ***P<0.0005 (two-way ANOVA).*

5.4.3. Effect of reducing $[Cl^-]_e$ in VSMCs on isolated aortic rings

The previous experiments are consistent with a role of TMEM16A in the DHA modulation of aortic contraction. The following experiments aimed to define this more fully by increasing the electrochemical gradient for Cl^- in VSMCs. We predict that low $[Cl^-]_e$ will cause aortic contraction, because a shift in E_{Cl} amplifies TMEM16A currents. If DHA acts via TMEM16A, we expect this low $[Cl^-]_e$-mediated contraction in aortic rings to be reduced in the presence of DHA.

Prior to exchange of "standard PSS" (Table 2.13) with "low Cl^- PSS" (Table 2.14), TMEM16A channels were activated by exposure to PE. Different concentrations of PE were required to elicit the same amount of blood vessel constriction in the absence and presence of DHA (70 μM). Therefore, based on the data shown in figure 5.5, concentrations of PE were selected that produced a ~50% activation in the absence of DHA and in the presence of DHA. The concentrations of PE selected for these experiments were 0.1 μM for the control and 1 μM in the presence of DHA.

Isolated aortic rings were incubated in presence of DHA (70 μM) for 20 minutes, or left untreated for the same length of time (control). PE was then added to each aortic ring to activate TMEM16A channels (Fig 5.9). Contraction of the aortic rings in low Cl^- PSS was normalised to the contraction observed in standard PSS.

Agonist-induced contraction was significantly reduced ($P<0.05$) in the presence of DHA (70 μM), with a ~1.9-fold reduction observed. This suggests that agonist-induced contraction is Cl^- mediated, and that the effect of DHA on blood vessels is mediated via TMEM16A.

Table 5.6. Effect of DHA on aortic contraction in conditions of low $[Cl^-]_e$.

	Low $[Cl^-]_e$	Low $[Cl^-]_e$ and DHA
Normalised plateau value	9.41 ± 2.19	4.97 ± 1.40
n	8	8
N	8	8

"Normalised plateau value" is the tension obtained in the presence of low Cl^-, normalised for the tension measured in response to PE in standard PSS. "n" is number of experiments, "N" is number of animals.

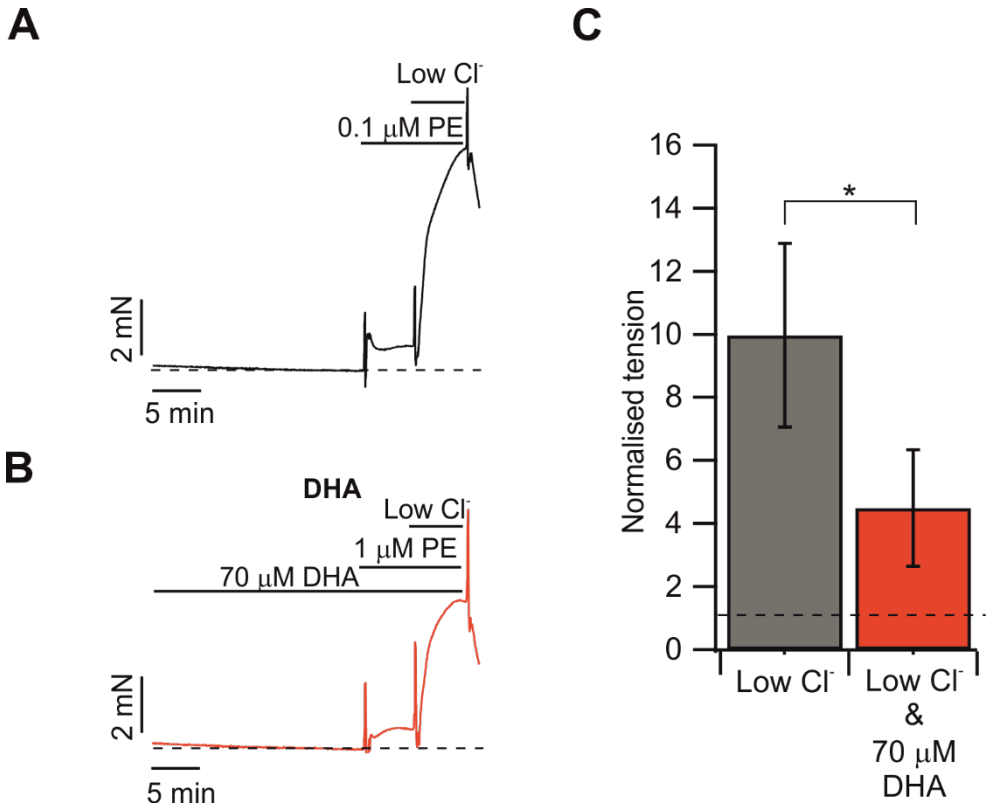

Figure 5.9. PE-mediated contraction of aortic rings in the presence of Low $[Cl^-]_e$ and DHA

(A) Representative change in isometric tension of control aortic rings in response to PE and low $[Cl^-]_e$ conditions. Dotted lines represent baseline tension.

(B) Representative change in isometric tension of aortic rings in response to PE and low $[Cl^-]_e$ conditions in the presence of DHA (70 μM). Dotted lines represent baseline tension.

*(C) Mean normalised aortic ring tension vs [PE] in low $[Cl^-]_e$ conditions, in the absence (control) (n= 8), and presence of DHA (70 μM, n=8). *P<0.05 (unpaired t-test).*

5.4.4. Effect of DHA on K^+-mediated depolarisation of aortic rings

The effect of DHA on aortic ring contraction mediated by elevation of extracellular K^+ concentration ($[K^+]_e$) was studied next. It is well established that increasing $[K^+]_e$ causes depolarisation and contraction of VSMCs (Tammaro et al., 2004, Manoury et al., 2009, Eid et al., 2018). Therefore, the depolarising action of TMEM16A would be bypassed in this case, in favour of depolarisation induced by $[K^+]_e$. Specifically, increasing $[K^+]_e$ results in a depolarising shift of the E_K with consequential *Vm* depolarisation. This activates the L-type Ca_V channels, which causes an increase in $[Ca^{2+}]_i$, and results in blood vessel contraction (Nelson et al., 1990b). In order for this K^+-mediated blood vessel contraction to be independent of changes in $[Cl^-]_e$, K-methanesulfonate was used instead of KCl. Increasing $[K^+]_e$ is expected to cause depolarisation and direct activation of Ca_V channels, in a TMEM16A-independent manner. This is because methanesulfonate does not permeate through Cl^- channels. The rationale for this experiment was that if channels other than TMEM16A are modulated by DHA or Ani9, these agents would affect contraction under conditions in which TMEM16A channels are not taking part in the depolarisation of VSMCs.

The isolated aortic rings were incubated in the presence of DHA (70 μM), Ani9 (1 μM), or alone under identical conditions (control) for 20 minutes, prior to the addition of increasing concentrations of K-methanesulfonate (Fig. 5.10). In the presence of DHA (70 μM), aortic contraction induced by 100 mM K-methanesulfonate was reduced by ~1.3-fold. At the same [K-methanesulfonate], in the presence of Ani9 (1 μM) aortic contraction was reduced by ~1.1-fold (Table 5.7).

Isolated aortic ring contraction evoked by K-methanesulfonate was only marginally effected by DHA and Ani9, at the highest two concentrations tested. It is hypothesised

that this could be due to small activation of TMEM16A by the increase in *Vm*. Overall, this data suggests that DHA-mediated attenuation of PE-induced contraction requires a modulation of TMEM16A. This is due to the loss of the significant reduction ($P<0.05$) in contraction with DHA or Ani9 in the absence of TMEM16A-mediated contraction.

Table 5.7. Effect of DHA and Ani9 effect on aortic contraction in the presence of 100 mM K-methanesulfonate.

	Control	DHA (70 μM)	Ani9 (1 μM)
100 mM K-methanesulfonate	1.21 ± 0.02	0.89 ± 0.08	1.09 ± 0.04
n	10	5	5
N	5	5	5

"100 mM K-methanesulfonate" is the tension obtained in the presence of this [K-methanesulfonate], normalised for the tension measured in 55 mM KCl. "n" is number of experiments, "N" is number of animals.

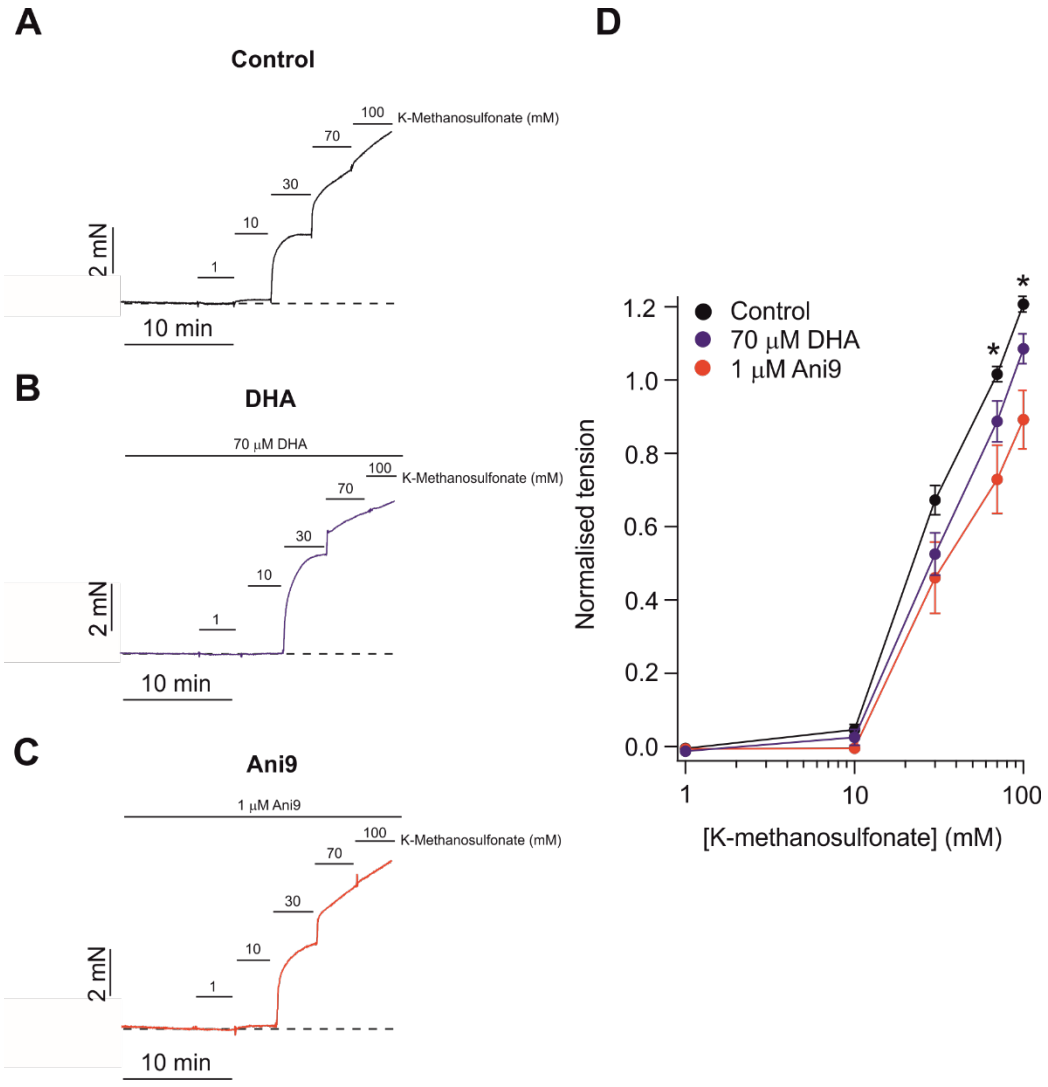

Figure 5.10. K-methanesulfonate-mediated aortic contraction in the presence of DHA and Ani9

(A) Representative change in isometric tension of control aortic rings in response to increasing concentrations of K-methanesulfonate, indicated by black lines. Dotted lines represent baseline tension.

(B) Representative change in isometric tension of aortic rings in response to increasing concentrations of K-methanesulfonate, indicated by black lines in the presence of DHA (70 μM). Dotted lines represent baseline tension.

(C) Representative change in isometric tension of aortic rings in response to increasing concentrations of K-methanesulfonate, indicated by black lines, in the presence of Ani9 (1 μM), as indicated. Dotted lines represent baseline tension.

*(D) Mean tension vs [K-methanesulfonate] relationship of control (n=10), and DHA (70 μM, n=5), or Ani9 (1 μM, n=5) aortic rings. *P<0.05 (two-way ANOVA).*

5.5. DHA effect on cationic currents in VSMCs

Experiments shown so far in this chapter implicate TMEM16A inhibition in the vasodilatory effect of DHA. However, DHA is reported to modulate other ion channels, such as K^+, TRP, and Ca_V channels (reviewed in (Elinder and Liin, 2017)). The possibility that DHA-mediated vasodilation also involves modulation of these channels was therefore examined.

The whole-cell patch-clamp technique was used to record whole-cell VSMC currents in the presence of "cationic solutions", using the "IV-ramp" voltage protocol in VSMCs. The *Vm* was held at -50 mV between sweeps. DHA (70 μM) was found to increase VSMC current at depolarised *Vm*, with an increase in cationic current by ~7.1-fold at 95 mV (Fig. 5.11). The time course of this effect was defined as the amount of time taken for the DHA effect to plateau in each cell at 100 mV (Fig 5.11.C). Overall, DHA activated whole-cell cationic currents in VSMCs (Table 5.8). This activation occurred only at positive Vm, and was only statistically significant at a *Vm* of ~55 mV or higher.

Table 5.8. Cationic currents evoked in VSMCs in the presence or absence of DHA.

	Control (pA/pF)	DHA (pA/pF)
-95 mV	-13.91 ± 2.67	-14.19 ± 2.16
95 mV	111.02 ± 19.78	792.48 ± 140.46
n	6	6
N	6	6

"-95 mV" and "95 mV" refer to the current obtained at these Vm. "n" refers number of experiments, "N" is number of animals.

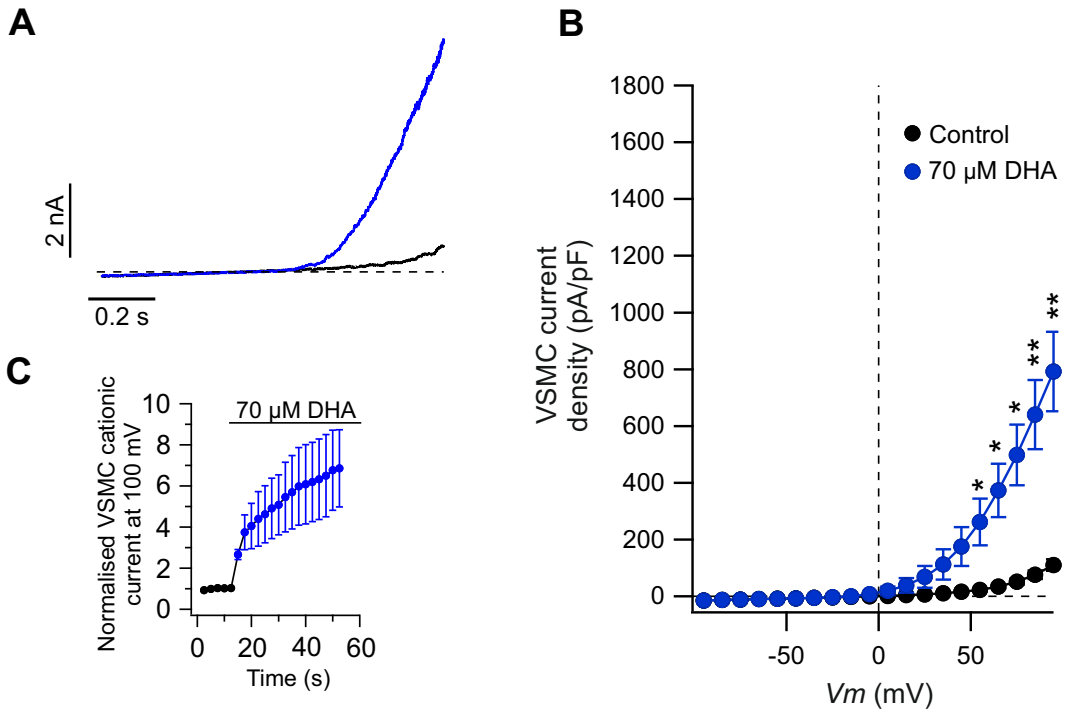

Figure 5.11. Effect of DHA on isolated VSMCs

(A) Whole-cell patch-clamp cationic currents recorded from isolated murine VSMCs. Cationic solutions and the "IV-ramp" protocol were used to elicit cationic currents in the absence (control, shown in black) or presence (blue) of DHA (70 µM).

*(B) Mean whole-cell current measured from -95 mV to 95 mV in 10 mV increments, in the absence (black, control, n=6), or presence of DHA (blue, n=6). Data analysed at plateau of DHA effect in that cell. *P<0.05, **P<0.005 (two-way ANOVA).*

(C) Time course of the effect of DHA on VSMC cationic currents at 100 mV on addition of DHA (70 µM). Data was normalised to control currents at 100 mV in the absence of DHA.

5.5.1. Study of the effect of DHA on K^+ and TRP channels

Experiments in figure 5.11 show that DHA activates cationic currents in VSMCs at positive *Vm*. The following experiments aimed to identify the current subtypes responsible for this increase in cationic current.

The effect of DHA on TMEM16A was tested in the presence of pharmacological blockers of individual cation channels. Clotrimazole, glibenclamide, and paxilline were selected for these experiments as they inhibit TRPM2 channels (Hill et al., 2004), K_{ATP} channels (Pompermayer et al., 2005), and BK_{Ca} channels (Zhou and Lingle, 2014), respectively. The concentrations used were selected in order to result in a full inhibition of these channels.

Whole-cell patch-clamp experiments recorded VSMC cationic currents using the "IV-ramp" voltage protocol. VSMC currents were recorded for 5 sweeps of the voltage protocol under control conditions, followed by 10 sweeps with the pharmacological blocker (e.g. clotrimazole), DHA (70 μM) was then added. The time course of this effect was defined as the amount of time taken for the DHA effect to plateau in each cell at 100 mV (Fig 5.12).

Clotrimazole (10 μM) was found to have no effect on whole-cell cationic current in VSMCs, and also did not affect the DHA-mediated increase in current (Fig. 5.12). At -95 mV, cationic currents in VSMC were unaffected by addition of clotrimazole (10 μM) and DHA (70 μM). At 95 mV, currents were unaffected by clotrimazole (10 μM). However, on addition of clotrimazole (10 μM) and DHA (70 μM) VSMC cationic currents increased by ~5.3-fold (Table 5.9). The effect of DHA addition was statistically significant ($P<0.05$) at *Vm* of 35 mV or greater.

Glibenclamide (10 μM) did not have an effect the whole-cell cationic current in VSMC, however it did result in an increased DHA-mediated whole-cell cationic current (Fig. 5.12) compared to that of DHA alone (Fig. 5.11). At -95 mV and 95 mV, VSMC cationic currents were unaffected by addition of glibenclamide (10 μM). However, on addition of DHA (70 μM), the cationic currents increased by ~13.8-fold at 95 mV. This DHA effect was not statistically significant ($P<0.05$) at -95 mV (Table 5.10). The effect of DHA addition was statistically significant at *Vm* of 55 mV or greater.

Paxilline (1 μM) was revealed to inhibit the VSMC whole-cell VSMC cationic current, and addition of DHA (70 μM) had no effect on this blocked current (Fig. 5.12). At -95 mV VSMC cationic currents were unaffected by both paxilline alone, and addition of DHA. At 95 mV paxilline (1 μM) blocked the VSMC cationic currents by ~5.6-fold. This block was then not affected by the addition of DHA (70 μM) (Table 5.11). The effect of DHA addition was statistically significant ($P<0.05$) at *Vm* of -5 mV or greater.

Table 5.9. Cationic currents evoked in VSMCs in the presence or absence of the TRP channel blocker clotrimazole and DHA.

		Clotrimazole	
	Control (pA/pF)	Clotrimazole (10 μM) (pA/pF)	DHA (70 μM) & clotrimazole (10 μM) (pA/pF)
-95 mV	- 19.72 ± 9.89	-16.55 ± 7.16	-15.68 ± 6.05
95 mV	147.36 ± 50.74	169.52 ± 43.70	776.01 ± 181.07
n		5	
N		5	

"-95 mV" and "95 mV" refer to the current obtained at these Vm. "n" refers number of experiments, "N" is number of animals.

Table 5.10. Cationic currents evoked in VSMCs in the presence of the K^+ channel blocker glibenclamide and DHA.

	Glibenclamide		
	Control (pA/pF)	Glibenclamide (10 μM) (pA/pF)	DHA (70 μM) & glibenclamide (10 μM) (pA/pF)
-95 mV	-16.22 ± 3.24	-16.27 ± 3.56	-30.53 ± 7.74
95 mV	93.65 ± 16.45	106.07 ± 19.13	1288.44 ± 324.75
n		6	
N		4	

"-95 mV" and "95 mV" refer to the current obtained at these Vm. "n" refers number of experiments, "N" is number of animals.

Table 5.11. Cationic currents evoked in VSMCs in the presence of the K^+ channel blocker paxilline and DHA.

	Paxilline		
	Control (pA/pF)	Paxilline (1 μM) (pA/pF)	DHA (70 μM) & paxilline (1 μM) (pA/pF)
-95 mV	-5.96 ± 1.58	-4.99 ± 1.37	-4.92 ± 1.39
95 mV	90.48 ± 15.95	16.07 ± 3.36	13.71 ± 2.71
n		8	
N		5	

"-95 mV" and "95 mV" refer to the current obtained at these Vm. "n" refers number of experiments, "N" is number of animals.

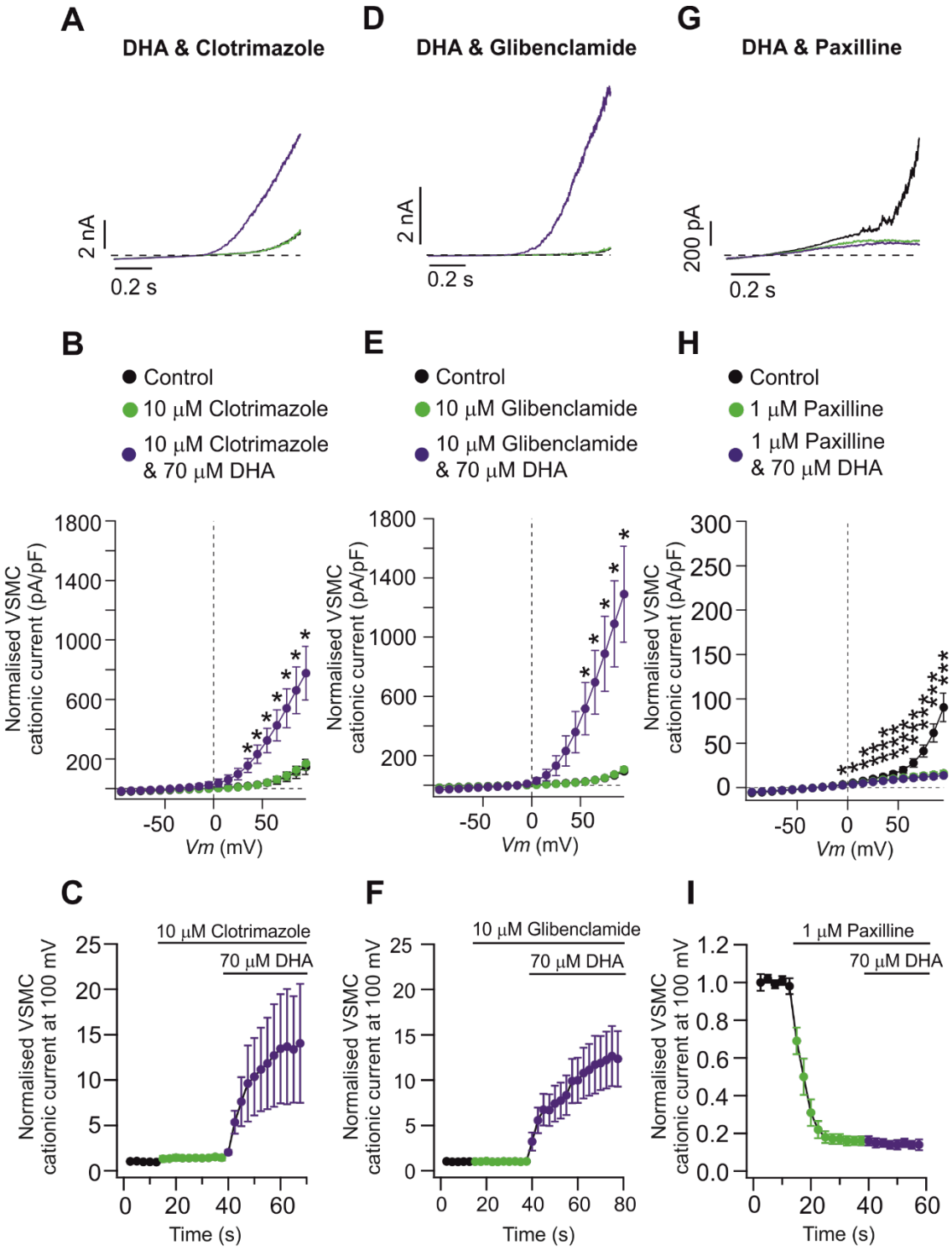
A
DHA & Clotrimazole
2 nA
0.2 s
D
DHA & Glibenclamide
2 nA
0.2 s
G
DHA & Paxilline
200 pA
0.2 s
B
Control
10 μM Clotrimazole
10 μM Clotrimazole & 70 μM DHA
E
Control
10 μM Glibenclamide
10 μM Glibenclamide & 70 μM DHA
H
Control
1 μM Paxilline
1 μM Paxilline & 70 μM DHA
Normalised VSMC cationic current (pA/pF)
Vm (mV)
C
F
I
10 μM Clotrimazole
10 μM Glibenclamide
1 μM Paxilline
70 μM DHA
Normalised VSMC cationic current at 100 mV
Time (s)

Figure 5.12. Effect of DHA on isolated VSMCs in the presence of a variety of ion channel blockers.
(A) Representative whole-cell patch-clamp currents recorded from isolated VSMCs. "Standard cationic" solutions and the "IV-ramp" protocol were used to elicit VSMC cationic currents in the absence (control, shown in black) and presence (green) of clotrimazole (10 µM). DHA (70 µM, blue) was subsequently added in each experiment.
*(B) Mean whole-cell current in the presence of clotrimazole (10 µM) were measured from -95 mV to 95 mV in 10 mV increments (n=5). Data analysed at plateau of pharmacological effect in that cell. *P<0.05 (two-way ANOVA).*
(C) Time course of the effect of clotrimazole (10 µM) and DHA (70 µM) on VSMC cationic currents at 100 mV. Data was normalised to control currents at 100 mV in the absence of clotrimazole and/or DHA.
(D) Representative whole-cell patch-clamp currents recorded from isolated VSMCs. "Standard cationic" solutions and the "IV-ramp" protocol were used to elicit VSMC cationic currents in the absence (control, shown in black) and presence (green) of glibenclamide (10 µM). DHA (70 µM, blue) was subsequently added in each experiment.
*(E) Mean whole-cell current in the presence of glibenclamide (10 µM) were measured from -95 mV to 95 mV in 10 mV increments (n=6). Data analysed at plateau of pharmacological effect in that cell. *P<0.05 (two-way ANOVA).*
(F) Time course of the effect of glibenclamide (10 µM) and DHA (70 µM) on VSMC cationic currents at 100 mV. Data was normalised to control currents at 100 mV in the absence of glibenclamide and/or DHA.
(G) Representative whole-cell patch-clamp currents recorded from isolated VSMCs. "Standard cationic" solutions and the "IV-ramp" protocol were used to elicit VSMC cationic currents in the absence (control, shown in black) and presence (green) of paxilline (1 µM). DHA (70 µM, blue) was subsequently added in each experiment.
*(H) Mean whole-cell current measured from -95 mV to 95 mV in 10 mV increments (n=8). Data analysed at plateau of pharmacological effect in that cell. *P<0.05, **P<0.005, ***P<0.0005 (two-way ANOVA).*
(I) Time course of the effect of paxilline (1 µM) and DHA (70 µM) on VSMC cationic currents at 100 mV. Data was normalised to control currents at 100 mV in the absence of paxilline and/or DHA.

DHA is reported to activate BK_{Ca} channels in VSMCs (Qian et al., 2018, Hoshi et al., 2013, Wang et al., 2011). BK_{Ca} channels are activated by an increase in $[Ca^{2+}]_i$, which causes *Vm* hypopolarisation and therefore VSMC relaxation (Dopico et al., 2018, Jackson, 2017). In this way, these channels provide negative feedback on the contraction that an increase in $[Ca^{2+}]_i$ induces via TMEM16A channels.

Paxilline is a potent blocker of BK_{Ca} channels, which was found to reduce the activatory effect of DHA on a cationic current in VSMCs (Fig. 5.12). The following myography experiments were designed to dissect the role of BK_{Ca} channels in DHA mediated vasodialation. Paxilline was added to isolated aortic rings in order to remove the contribution of BK_{Ca} channels to agonist-induced contraction.

The isolated aortic rings were left untreated (control), or incubated with paxilline (1 μM), or paxilline (1 μM) and DHA (70 μM), for 20 minutes prior to addition of increasing [PE]. Paxilline (1 μM) alone increased the PE-induced contraction (Fig. 5.13, table 5.12). DHA reduced the PE-mediated contraction in the presence of paxilline (1 μM), with a ~3.7-fold decrease compared to paxilline at 10 μM PE, and a ~2.4-fold reduction in contraction compared to the control at 10 μM PE (Table 5.12). PE-mediated aortic contractility in the presence of paxilline and DHA was significantly reduced ($P<0.05$) at all concentrations compared to both the control conditions and paxilline alone. Overall, this demonstrates that the contribution of BK_{Ca} channels to the DHA effect on vascular tone is minimal. This is because when BK_{Ca} channels are pharmacologically blocked using paxilline, the DHA and paxilline effect on the tone of aortic rings is not significantly different ($P<0.05$) to the effect of DHA alone.

Table 5.12. Overview of blood vessel contraction in the presence of paxilline with and without DHA.

	Control	Paxilline (1 μM)	Paxilline (1 μM) & DHA (70 μM)
10 μM PE	0.58 ± 0.03	0.97 ± 0.19	0.26 ± 0.61
Plateau of fit	0.59 ± 0.01	0.98 ± 0.01	0.25 ± 0.01
PE EC_{50}	0.15 ± 0.01	0.18 ± 0.01	0.15 ± 0.01
h	1.11 ± 0.05	1.17 ± 0.06	1.6 ± 0.13
n	7	7	7
N	7	7	7

"10 μM PE" is the tension obtained in the presence of this [PE], and normalised for the tension measured in 55 mM KCl. "Plateau of fit" is the maximal value of aortic contraction determined via the Hill fit of the data (equation 2.2). The "PE EC_{50}" is the value of [PE] required to reach half maximal contraction. The "h" value is the Hill coefficient and represents the slope of the Hill fit. "n" is number of experiments, "N" is number of animals.

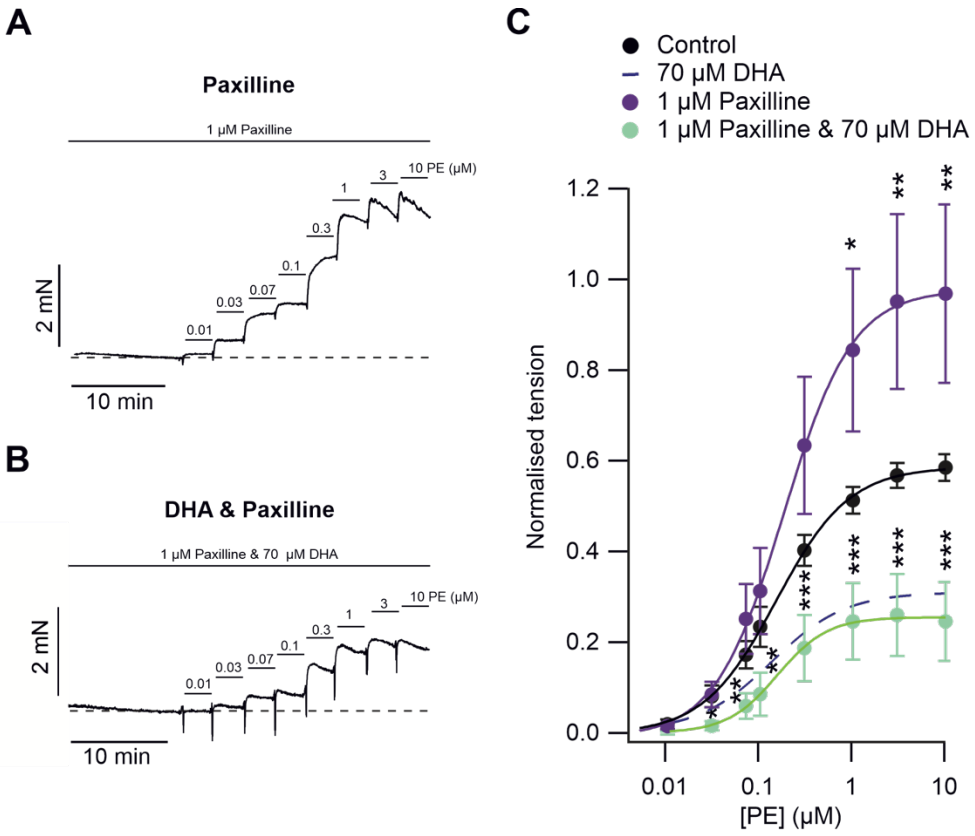

Figure 5.13. PE-mediated aortic contraction in the presence of paxilline and DHA.

(A) Representative change in isometric tension of aortic rings in response to increasing [PE], in the presence of paxilline (1 μM). Dotted line represents baseline tension.

(B) Representative change in isometric tension of aortic rings in response to increasing [PE], in presence of paxilline (1 μM) and DHA (70 μM). Dotted line represents baseline tension.

*(C) Mean tension vs [PE] relationship of control (n=7), and paxilline (1 μM, n=7), or paxilline (1 μM) and DHA (70 μM, n=7) aortic rings. Dotted blue line represents aortic contraction in the presence of DHA (70 μM) from figure 5.5. Statistics compare control data to respective test conditions, *P<0.05, **P<0.005, ***P<0.0005 (two-way ANOVA).*

5.5.2. Study of the effect of DHA on Ca_V channels

L-type Ca_V channels are reported to be blocked by a range of dietary PUFAs (Elinder and Liin, 2017), and are reported to be blocked by DHA in rat cardiac ventricular myocytes (Pepe et al., 1994, Ferrier et al., 2002), guinea-pig tracheal smooth muscle cells (Hazama et al., 1998), and VSMCs in hypertensive rats (Engler and Engler, 2000). These experiments were designed in order to understand whether DHA-mediated relaxation of aortic rings involves Ca_V channels in VSMCs. The Ca_V channel blocker nifedipine was also tested in order to establish an appropriate concentration for subsequent studies (Godfraind, 2017, Striessnig et al., 2015).

Whole-cell patch-clamp electrophysiology of VSMCs was conducted using "Ca_V solutions", and the "IV-Ca_V" voltage protocol. The peak Ca_V current at each *Vm* tested was plotted *versus* the *Vm*. The resulting IV-relationship was characterised by a maximum at 10 mV. In the presence of DHA (70 μM), the overall IV-relationship was attenuated. For example, at 10 mV the current was reduced by ~3.2-fold.

Nifedipine (10 nM) blocked Ca_V channels to the same extent as DHA (70 μM). Control Ca_V currents were perfused with nifedipine (10 nM) at 10 mV, and were found to be reduced by ~3.4-fold compared to the control (Fig. 5.14). Mean DHA inhibition from figure 5.14.A is depicted using blue dashed line for comparison. 10 nM nifedipine was found to produce Ca_V current inhibition to a similar extent as that of 70 μM DHA. A nifedipine concentration of 10 nM was subsequently used in isolated blood vessel studies to selectively mimic the effect of DHA blockage of Ca_V currents, allowing the effect of DHA on Ca_V currents to be modelled independent of the DHA effect on other ion channels.

Table 5.13. Ca_V currents evoked in VSMCs in the presence of nifedipine and DHA.

	Control (pA/pF)	DHA (70 μM) (pA/pF)	Nifedipine (100 nM) (pA/pF)
10 mV	-4.26 ± 0.79	-1.33 ± 0.4	-1.25 ± 0.29
n	13	7	6
N	13	7	6

"10 mV" refers to the current obtained at this Vm. "n" refers number of experiments, "N" is number of animals.

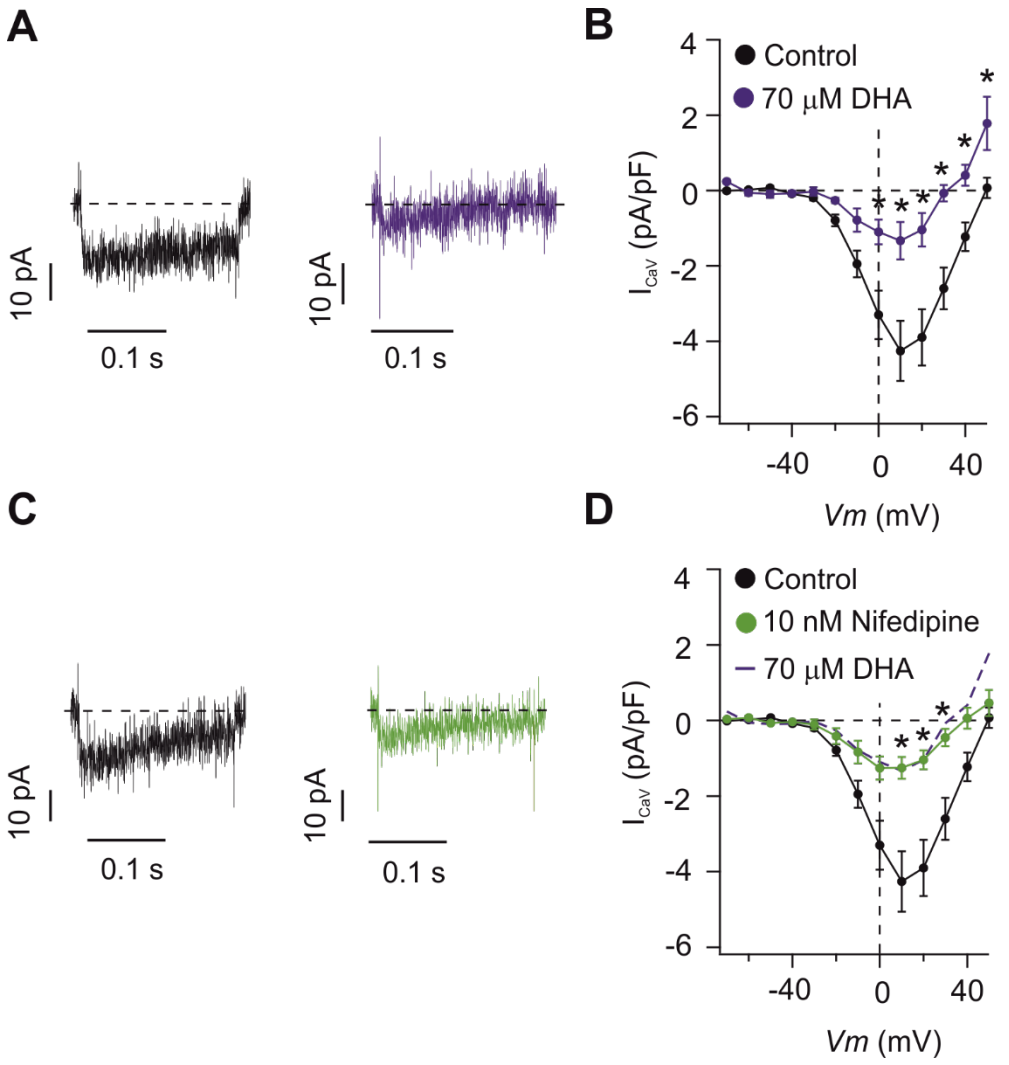

Figure 5.14. DHA and nifedipine effect on endogenous Ca_V channels in isolated VSMCs

(A) Whole-cell patch-clamp Ca_V currents recorded from isolated murine VSMCs. "Ca_V solutions" in combination with the "Ca_V" voltage protocol were used to elicit Ca_V channel currents at 10 mV in the absence (control, shown in black) or presence (blue) of 70 μM DHA.

*(B) Mean whole-cell Ca_V current measured at between -70 mV and 50 mV in 10 mV increments, in the absence (black, control, n=13), or presence of DHA (blue, n=7), *P<0.05 (two-way ANOVA).*

(C) Whole-cell patch-clamp Ca_V currents recorded from isolated VSMCs from a wild-type mouse. "Ca_V solutions" in combination with the "Ca_V" protocol were used to elicit Ca_V currents at 10 mV in the absence (control, shown in black) or presence (green) of 10 nM nifedipine.

*(D) Mean whole-cell Ca_V current measured at between -70 mV and 50 mV in 10 mV increments, in the absence (black, control, n=13), or presence of nifedipine (green, n=6), DHA data from (B) is denoted by the blue dotted line. *P<0.05 (two-way ANOVA).*

The following myography experiment was designed to study the contribution of Ca_V channels to DHA-mediated vasorelaxation in isolated aortic rings. In the previous experiment, a concentration of nifedipine (10 nM) that blocks Ca_V channels to the same extent as DHA (70 μM) in VSMCs was identified. Therefore, 10 nM nifedipine was tested on isolated aortic rings.

The isolated aortic rings were left untreated (control), or incubated in the presence of nifedipine (10 nM), for 20 minutes prior to addition of increasing [PE] (Fig. 5.15). The tension versus [PE] experiments were fitted with the Hill equation (Equation 2.1). The plateau of the fit of the aortic ring contraction in the presence of nifedipine (10 nM) was reduced by ~1.5-fold compared to the control (Table. 5.14). The control aortic contraction was significantly different ($P<0.05$) to the vessel preincubated with nifedipine at all [PE] tested. Overall, this data suggests that Ca_V channels play an important role in DHA-mediated vasodilation.

Table 5.14. Overview of aortic contraction in the presence of nifedipine.

	Control	Nifedipine (10 nM)
10 μM PE	0.65 ± 0.07	0.41 ± 0.07
Plateau of fit	0.66 ± 0.01	0.41 ± 0.01
IC_{50}	0.11 ± 0.01	0.17 ± 0.02
h	1.16 ± 0.06	1.05 ± 0.11
n	9	9
N	9	9

"10 μM PE" is the tension obtained in the presence of this [PE], and normalised for the tension measured in 55 mM KCl. "Plateau of fit" is the maximal value of aortic contraction determined via the Hill fit of the data (equation 2.2). The "PE EC_{50}" is the value of [PE] required to reach half maximal contraction. The "h" value is the Hill coefficient and represents the slope of the Hill fit. "n" is number of experiments, "N" is number of animals.

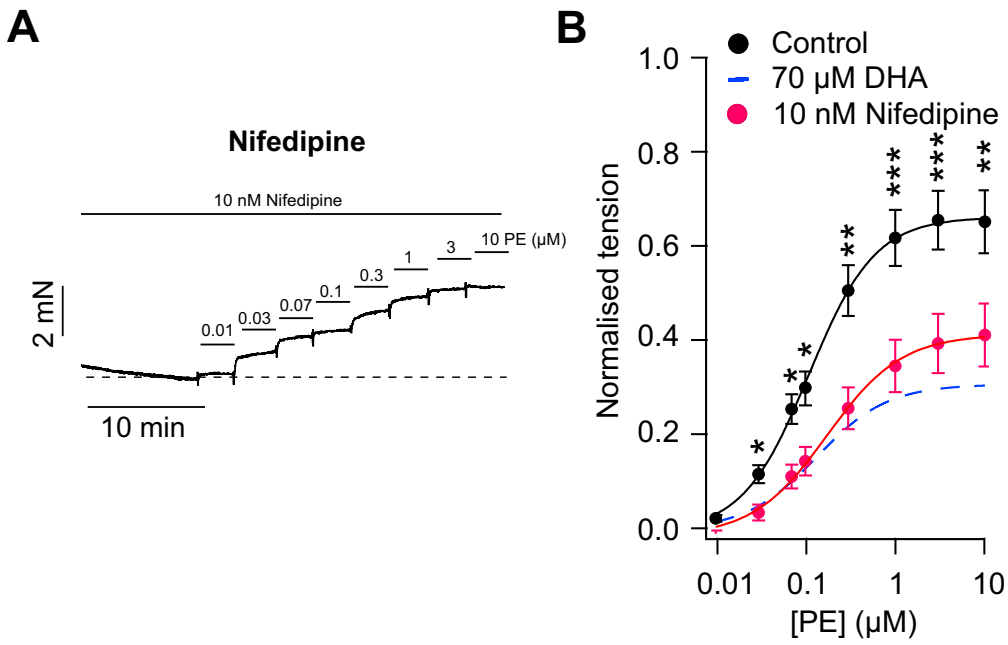

Figure 5.15. PE-mediated contraction of aortic rings in the presence of nifedipine and DHA

(A) Representative change in isometric tension of aortic rings in response to increasing concentrations of PE, in the presence of nifedipine (10 nM). Dotted line represents baseline tension.

*(B) Mean tension vs [PE] relationship of control (n=22), and nifedipine (10 nM, n=9) aortic rings. Dotted blue line represents aortic contraction in the presence of DHA (70 μM) from figure 5.5. *P<0.05, **P<0.005, ***P<0.0005 (two-way ANOVA).*

5.6. Role of TMEM16A channels in endothelial cells in the vasodilatory effect of DHA

Previous experiments in this chapter have explored the role of DHA modulation of ion channels expressed in VSMCs. The following experiment aims to understand this regulation in the absence of the locally produced vasodilator nitric oxide (NO), via blockage of NO-synthase by L-NAME (Pechanova et al., 2004). NO is a potent vasodilator produced by NO-synthase in the endothelial cells. NO diffuses to VSMCs, and acts via the guanylate cyclase (cGMP) pathway (Duarte and Ferreira, 2000). Blocking NO-synthase with L-NAME results in reduced bioavailability of NO. This generally causes an increase in tone in a variety of artery types both at rest and in the presence of contractile agonists (Edvinsson et al., 2016, Buchwalow et al., 2002). TMEM16A is reported to be expressed in the endothelium (Nilius and Droogmans, 2001). To gain an understanding as to whether inhibition of TMEM16A channels in the endothelium is involved in DHA-mediated vasodilation, experiments were carried out when the NO effect was impaired using L-NAME.

The isolated aortic rings were left untreated (control), or incubated with L-NAME (100 μM), or L-NAME (100 μM) and DHA (70 μM), for 20 minutes prior to addition of increasing [PE]. Normalised tension of aortic rings on addition L-NAME (100 μM) was increased by ~3.0-fold (Fig. 5.16). In the presence of L-NAME (100 μM) and DHA (70 μM) normalised tension was increased by ~2.1-fold compared to the control, and reduced by ~1.4-fold compared to L-NAME (Table 5.15). For comparison, normalised tension of aortic rings incubated with DHA (70 μM) was reduced by ~2.2-fold on addition of 10 μM PE (Fig. 5.5). The tension versus [PE] experiments were fitted with the Hill equation

(Equation 2.2). PE-mediated aortic contractility in the presence of L-NAME and DHA was significantly reduced ($P<0.05$) compared to in the presence of L-NAME alone.

Overall, DHA reduced aortic contraction by a similar extent in the presence or absence of L-NAME. This effect may suggest that DHA acts directly via VSMCs and is independent of the endothelium, as the inhibitory effect of DHA is not attenuated in the presence of L-NAME.

Table 5.15. Overview of blood vessel contraction in the presence of L-NAME with and without DHA.

	Control	L-NAME (100 μM)	L-NAME (100 μM) & DHA (70 μM)
10 μM PE	0.60 ± 0.03	1.92 ± 0.15	1.34 ± 0.11
Plateau of fit	0.61 ± 0.01	1.78 ± 0.03	1.18 ± 0.03
PE EC_{50}	0.14 ± 0.01	0.14 ± 0.01	0.20 ± 0.02
h	1.22 ± 0.05	1.09 ± 0.07	0.99 ± 0.08
n	6	6	5
N	6	6	5

"10 μM PE" is the tension obtained in the presence of this [PE], and normalised for the tension measured in 55 mM KCl. "Plateau of fit" is the maximal value of aortic contraction determined via the Hill fit of the data (equation 2.2). The "PE EC_{50}" is the value of [PE] required to reach half maximal contraction. The "h" value is the Hill coefficient and represents the slope of the Hill fit. "n" is number of experiments, "N" is number of animals.

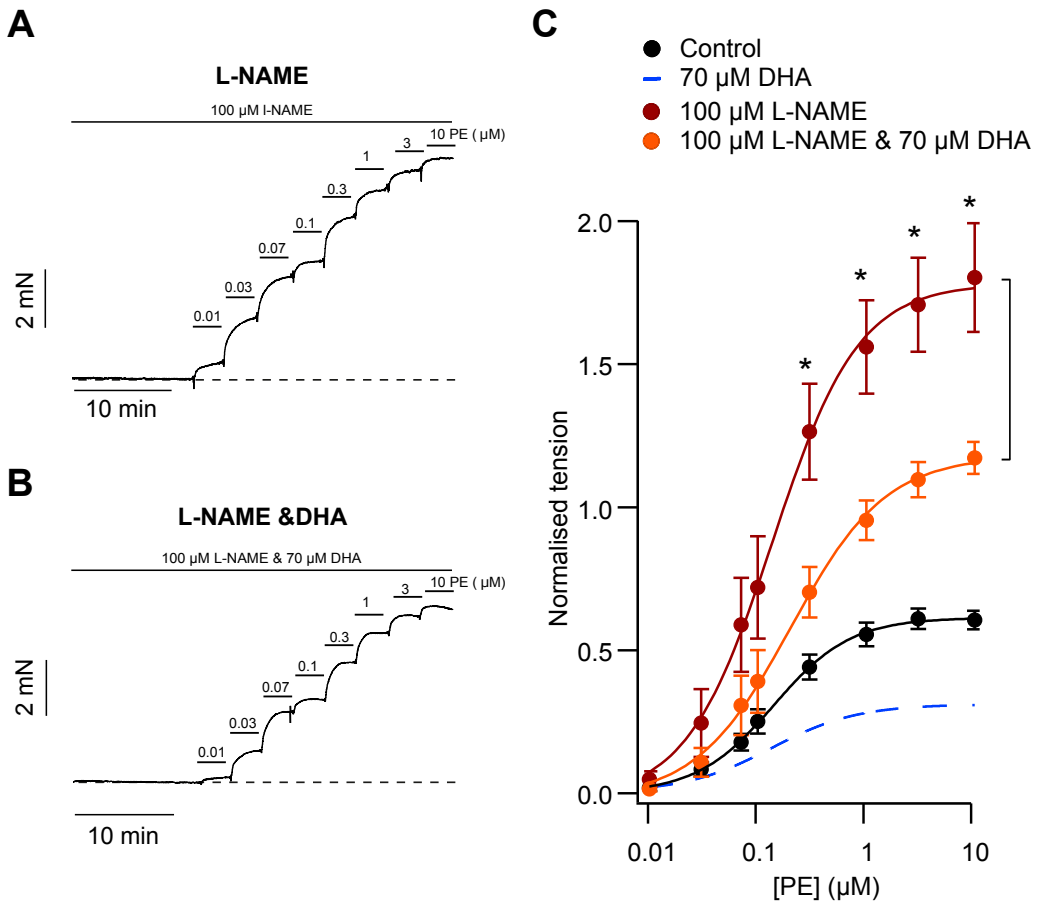

Figure 5.16. PE-mediated contraction of aortic rings in the presence of L-NAME and DHA

(A) Representative change in isometric tension of aortic rings in response to increasing [PE], in presence of L-NAME (100 µM), as indicated. Dotted line represents baseline tension.

(B) Representative change in isometric tension of aortic rings in response to increasing [PE], in the presence of L-NAME (100 µM) and DHA (70 µM), as indicated. Dotted line represents baseline tension.

*(C) Mean tension vs [PE] relationship of control (n=6), and L-NAME (100 µM, n=6), or L-NAME (100 µM) and DHA (70 µM, n=5) aortic rings. Dotted blue line represents and aortic contraction in the presence of DHA (70 µM) from figure 5.5. Statistics comparing L-NAME to L-NAME & DHA *P<0.05 (two-way ANOVA).*

5.7. Towards an understanding of the structure-function relationship of DHA-mediated inhibition of TMEM16A

Experiments presented in this chapter up to this point have demonstrated that DHA inhibits cloned and native TMEM16A channels. The following experiments aimed to gain an understanding of the structural features of DHA responsible for this effect. Therefore, the effect of eicosapentaenoic acid (EPA), and structural variants of DHA (DHA-methyl ester and acetic acid) were tested.

EPA, like DHA, is a dietary omega-3 PUFA that is reported to reduce blood pressure (Miller et al., 2014, Minihane et al., 2016). EPA was tested in this project in order to understand whether the structural differences between EPA and DHA could provide insight into the DHA inhibition of TMEM16A.

TMEM16A transfected HEK-293T cells were exposed to increasing [EPA], and studied using whole-cell patch-clamp electrophysiology. [EPA]-TMEM16A response relationships were constructed by measuring TMEM16A currents at a constant *Vm* (70 mV) while varying [EPA].

In the TMEM16A transfected cells, EPA inhibited cloned TMEM16A channels in a dose dependent manner (Fig. 5.17). The data was normalised to TMEM16A currents in the absence of EPA. Normalised TMEM16A current in the presence of EPA (1 μM) was 0.83 ± 0.04 (Fig 5.17), significantly lower ($P<0.05$) than the DHA block at 1 μM of 1.03 ± 0.06 (Fig. 5.1). Normalised TMEM16A currents in the presence of EPA (70 μM) were 0.3 ± 0.03 (n=7), significantly ($P<0.05$) less than the equivalent inhibition generated by DHA (70 μM). Mean data was plotted and fitted with the Hill equation (Fig. 5.17, equation 2.2). This resulted in an IC_{50} of 12.71 ± 1.71, and an *h* of 0.58 ± 0.02.

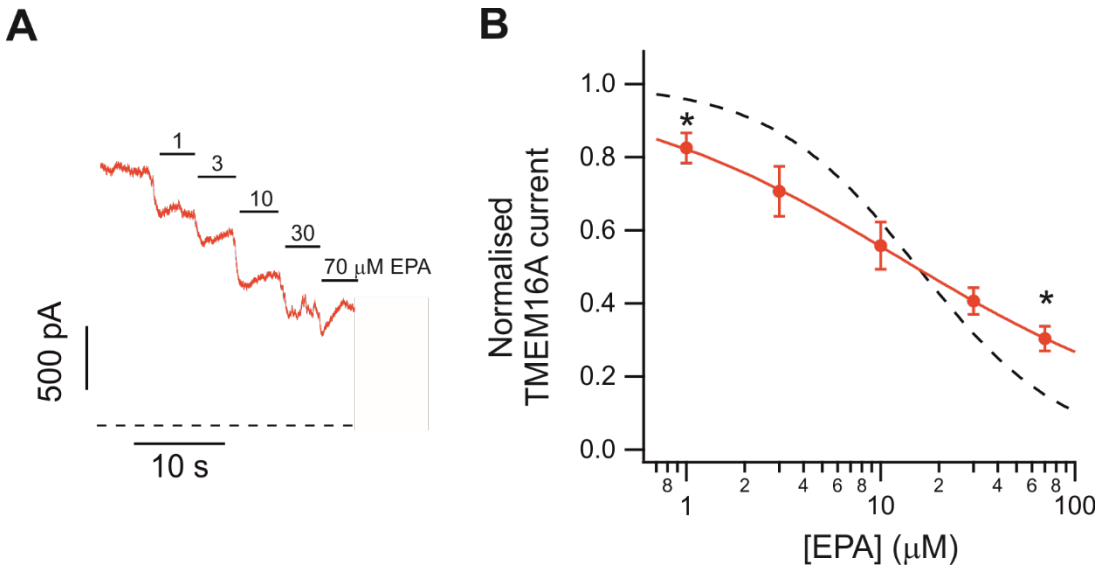

Figure 5.17. Effect of the PUFA EPA on TMEM16A

(A) TMEM16A current recorded from expressing HEK-293T cells in the whole-cell patch-clamp configuration. The PUFA EPA was applied extracellularly in increasing concentrations, as indicated by the horizontal bars. The Vm was maintained at 70 mV for the duration of the recordings, and solutions contained 0.3 μM free $[Ca^{2+}]_i$. Dashed lines represent zero-current levels.

*(B) Mean relationships between EPA concentration ([EPA]) and TMEM16A currents, expressed relative to the current measured in the absence of EPA (n=7). Data was fitted using the Hill equation (equation 2.2), which represents the best fit of the data. Dashed black line represents inhibition of TMEM16A by DHA, and is the Hill fit of data in figure 5.1. *P<0.05 (unpaired t-test).*

In order to begin to understand how DHA modulates TMEM16A, similar compounds with structural variations were tested. DHA-methyl ester has the same carbon tail, but a methyl ester group instead of the carboxyl group. Acetic acid has a carboxyl group, but a truncated carbonyl tail.

HEK-293T cells expressing TMEM16A were recorded in the whole-cell configuration in the presence of 0.3 μM $[Ca^{2+}]_i$, with *Vm* maintained at 70 mV. Increasing concentrations of DHA-methyl ester (Fig. 5.18), or acetic acid (Fig. 5.18) were perfused over the TMEM16A expressing cell.

In the TMEM16A transfected cells, DHA-methyl ester did not inhibit cloned TMEM16A channels except at 30 μM and 70 μM, which were the highest concentrations tested. Data was normalised to TMEM16A currents in the absence of DHA-methyl ester. Normalised TMEM16A currents were 0.80 ± 0.06 pA/pF (n= 12) in the presence of DHA-methyl ester (70 μM). Mean data was plotted and fitted with the Hill equation, which revealed an IC_{50} of 49.24 ± 0.09, and an *h* of 1.74 ± 0.01 (Fig. 5.18). DHA-methyl ester produces a statistically significant lower inhibition of TMEM16A than DHA at concentrations of 3 μM and above.

Acetic acid did not inhibit cloned TMEM16A channels except at 70 μM, the highest concentration tested. Normalised TMEM16A currents were 0.75 ± 0.06, and currents in the presence of 70 μM of acetic acid (n=5). Mean data was plotted, but could not be fitted with the Hill equation, due to lack of inhibition at 1-30 μM (Fig. 5.18). Acetic acid produces a statistically significant lower inhibition of TMEM16A than DHA at concentrations of 10 μM and above.

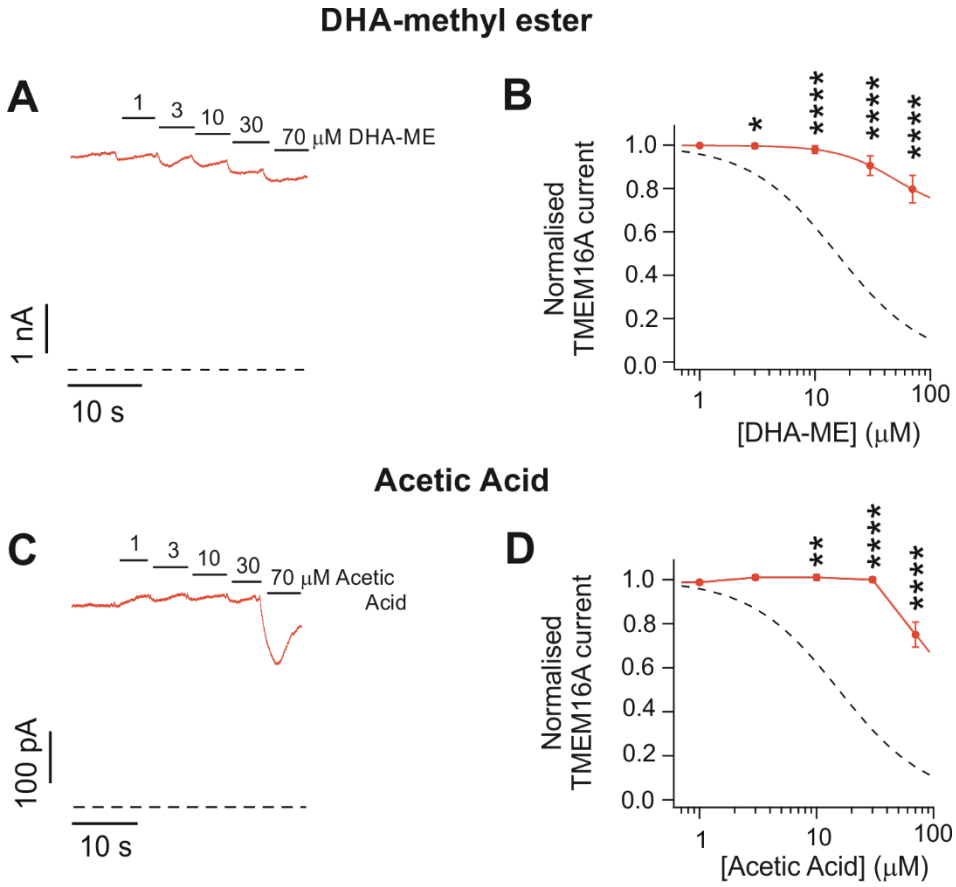

Figure 5.18. Effect of modified DHA (DHA-methyl ester and acetic acid) on TMEM16A currents

(A) TMEM16A expressing HEK-293T cells recorded in the whole-cell patch-clamp configuration. DHA-methyl ester (top panel), or Acetic acid (bottom panel) was applied extracellularly in increasing concentrations, as indicated by the horizontal bars. The Vm was maintained at 70 mV, with free $[Ca^{2+}]_i$ of 0.3 μM for all experiments. Dashed lines represent zero-current levels.

*(B) Mean relationships between DHA-methyl ester concentration ([DHA-ME]) and TMEM16A currents, expressed relative to the current measured in the absence of DHA-methyl ester (n=12). Dashed black line represents inhibition of TMEM16A by DHA, and is the Hill fit of data in figure 5.1. *P<0.05, ****P<0.00005 (paired t-test).*

(C) TMEM16A expressing HEK-293T cells recorded in the whole-cell patch-clamp configuration. Acetic acid was applied extracellularly in increasing concentrations, as indicated by the horizontal bars. The Vm was maintained at 70 mV, with free $[Ca^{2+}]_i$ of 0.3 μM for all experiments. Dashed lines represent zero-current levels.

*(D) Mean relationships between Acetic Acid concentration ([Acetic Acid]) and TMEM16A currents, expressed relative to the current measured in the absence of acetic acid (n=5). Dashed black line represents inhibition of TMEM16A by DHA, and represents the Hill fit of data in figure 5.1. **P<0.005, ****P<0.00005 (paired t-test).*

5.8. Discussion

The work presented in this chapter demonstrated that cloned TMEM16A channels are inhibited by DHA, an effect that may explain the effect of dietary PUFAs on aortic tone (Elinder and Liin, 2017, Saravanan et al., 2010). The rationale for testing the effect of DHA on cloned TMEM16A channels was the discovery that the intracellular signalling lipid PIP_2 modulates TMEM16A activity (fully described in chapter 4). As the TMEM16A pore is in close proximity to the plasma membrane (Dang et al., 2017, Paulino et al., 2017), it was hypothesised that TMEM16A may be highly sensitive to the plasma membrane composition. PUFAs are highly hydrophobic, and therefore readily incorporate into the plasma membrane (Stillwell and Wassall, 2003). In addition to this, PUFAs have been widely reported to modulate a range of voltage gated ion channels, such as K_v, BK_{Ca}, Ca_V, and TRP channels (Elinder and Liin, 2017, Boland and Drzewiecki, 2008), and therefore the contribution of DHA effect on these channels to vessel relaxation was also studied.

5.8.1. Effect of DHA on cloned TMEM16A channels

The study presented in this chapter demonstrates that DHA potently inhibits TMEM16A in a dose dependent manner, a finding that is in agreement with results published while this study was underway (De Jesus-Perez et al., 2018). DHA was tested in a concentration range of 1 μM and 70 μM, as micelles form at around 100 μM (Richieri et al., 1992, Borjesson et al., 2008). It is also a physiologically appropriate range, as PUFA concentration in the plasma is typically ~50 μM (De Caterina et al., 2000, Fraser et al., 2003, Siddiqui et al., 2008). This can increase to ~400 μM with changes in diet or dietary

supplementation (Siddiqui et al., 2008, Kuriki et al., 2002, Fraser et al., 2003, Bonaa et al., 1990, Herold and Kinsella, 1986).

DHA modulation of cloned TMEM16A channels was tested following DrVSP mediated PIP_2 depletion, as PIP_2 levels are dynamically regulated by the Gq-PCR signalling cascade (Fig. 5.3), and it was argued that variations in PIP_2 levels may affect TMEM16A inhibition by DHA. As TMEM16A is highly sensitive to the plasma membrane composition, it was important to gain an understanding of how TMEM16A is simultaneously regulated by multiple lipids. The results indicated that modulation of cloned TMEM16A was unaffected by depletion of PIP_2.

Co-transfection of cloned TMEM16A and the α1-adrenergic receptor provided a physiological means of activating the Gq-PCR signalling cascade, which in turn activates TMEM16A channels. In the presence of DHA, the inhibition of TMEM16A was sufficient to prevent an increase in TMEM16A current by the α1-adrenergic receptor. This simplified system could provide an explanation for the vasodilator effect of DHA in blood vessels, as inhibition of TMEM16A by DHA could prevent Gq-PCR mediated VSMC depolarisation.

5.8.2. DHA on VSMCs and isolated aortic rings

Initial myography experiments in chapter 3 demonstrated that reduction of TMEM16A channels through genetic deletion or pharmacological methods leads to a reduction in agonist-induced contraction. This study used this premise to hypothesise that inhibition of TMEM16A by DHA could be the underlying mechanism of vasorelaxation induced by DHA. This was tested using patch-clamp electrophysiology in isolated VSMCs and isometric contraction studies in isolated aortic rings. DHA was found to block native

TMEM16A channels in VSMC, an effect that was statistically significant at all *Vm* tested (except near the E_{rev}). DHA was also revealed to activate cationic VSMC currents. However, this effect was only statistically significant at *Vm* above 50 mV, which is outside the range of physiologically relevant *Vm* in VSMCs (Nelson et al., 1990b, Knot and Nelson, 1998). Pharmacology-based VSMC studies revealed the identified cationic currents to be BK_{Ca} and Ca_V currents.

The Ca_V channel blocker nifedipine reduced maximal isolated aortic contraction by ~1.5-fold compared to the control, while DHA alone reduced maximal aortic contraction by ~2.4-fold. This data suggests that DHA inhibition of Ca_V channels are not the most crucial factor underlying the vasorelaxation by DHA. As Ani9 reduces agonist-induced blood vessel contraction to the same extent as DHA, we can conclude that TMEM16A is not the only ion channel involved in DHA-mediated vasorelaxation, but certainly has an important role.

The crucial role of TMEM16A in DHA-mediated vasorelaxation was further confirmed using $[Cl^-]$ modification experiments. Bumetanide is an NKCC1 blocker, which can be used to reduce $[Cl^-]_i$ experimentally in VSMCs by 20-30% (Orlov et al., 1996). Incubation of the isolated vessels with bumetanide resulted in a ~3.2-fold reduction in agonist-induced contraction at the highest [PE] tested. This suggests that reduction in $[Cl^-]_i$ in VSMCs leads to a significant reduction in Cl^--mediated vascular contractility in the presence of PE, which is in agreement with the DHA and Ani9 data discussed previously. In conditions of low $[Cl^-]_e$, following activation using an appropriate [PE], aortic contraction increased ~9.4-fold. However, in the presence of DHA, this was reduced to ~5.0-fold. This data supports the hypothesis that Cl^- is a crucial depolarising force in blood vessel contractility, and that DHA is able to modulate these currents. The final

[Cl^-]-based experiment involved using K-methanesulfonate instead of KCl to provide a depolarising force to the isolated vessels, as methanesulfonate is a molecule with poor permeability through Cl^- channels (Lefevre et al., 1996). In the experiment outlined in figure 5.10, a slight inhibition for both DHA and Ani9 was observed, which can be attributed to some TMEM16A activity remaining at the highest concentrations of K-methanesulfonate tested, due to $[Cl^-]_i$ not being depleted prior to experimentation, and the PSS solution containing some free Cl^-.

Modulation of TMEM16A and Ca_V channels by DHA results in an effect of vasorelaxation during agonist-induced aortic contraction. This is the first report that suggests a crucial role of DHA-mediated inhibition of TMEM16A expressed in VSMCs, and a resultant reduction in aortic contraction.

5.8.3. Structural significance of TMEM16A regulation by DHA

It should be considered that not all PUFAs in the plasma are DHA. EPA is another common dietary PUFA, and was found at approximately the same concentrations as DHA in the plasma (Yurko-Mauro et al., 2015). Results in this chapter have demonstrated that EPA blocks TMEM16A, however this effect is significantly higher than DHA at low concentrations and significantly less than DHA at high concentrations (Fig. 5.17). This finding is in agreement with the hypothesis that dietary PUFAs act via TMEM16A, as the underlying mechanism of the vasodilator action of DHA. Next, this study utilised commercially available molecules that conferred modifications to the structure of DHA. Effective truncation of the DHA carbon tail by using acetic acid, or replacing the DHA carboxyl group with a methyl-ester to remove the charged head

group abolishes the ability of the molecule to modulate TMEM16A. Taken together, this data demonstrates that the structure of DHA is key for inhibition of TMEM16A.

5.8.4. Physiological significance and potential clinical implications

Data collected in this chapter demonstrate that TMEM16A is inhibited by DHA, and could provide a previously unexplored mechanism of action for the beneficial vascular properties of DHA. It has been demonstrated that omega-3 PUFA supplementation increases levels of DHA in the plasma (Siddiqui et al., 2008, Kuriki et al., 2002, Fraser et al., 2003, Bonaa et al., 1990, Herold and Kinsella, 1986). The recent large scale ASCEND clinical trial reported that in patients with diabetes, there was no significant reduction in serious vascular events in people who receive omega-3 PUFA dietary supplementation (Group et al., 2018). However, observational studies of Okinawa islanders and the Greenland Inuit populations have diets high in omega-3 PUFAs and a low risk of death from vascular disease (Kagawa et al., 1982, Bjerregaard et al., 2003). There is also evidence that following myocardial infarction, men show a ~30% reduction in mortality (and mortality related to cardiovascular disease) after consumption of oily fish twice a week (Burr et al., 1989). Furthermore, in patients with hypertension, high doses of omega-3 PUFAs are associated with a reduction in systemic blood pressure (Morris et al., 1993). Data shown in this chapter could provide an underlying mechanism for the reported beneficial vascular effects of omega-3 PUFAs.

The British Heart Foundation (BHF) makes lifestyle recommendations based on advice from The National Institute for Health and Care Excellence (NICE), and recommends regularly eating oily fish in order to prevent hypertension and other cardiovascular disease. The American Heart Association also recommends oily fish consumption to

prevent cardiovascular disease, and suggest omega-3 PUFA supplements to prevent coronary heart disease (Siscovick et al., 2017).

DHA inhibition of TMEM16A represents an intervention for regulation of blood vessel tone that has no reported side effects. A future research project could involve locating the binding site of DHA on the TMEM16A channel, and exploiting this knowledge to aid in the design of synthetic modulators of TMEM16A acting on this site.

Overall, it was found that DHA inhibits cloned TMEM16A channels. This effect was also observed in native TMEM16A currents in isolated VSMCs, in addition to confirming that BK_{Ca} and Ca_V channels are also modulated by DHA. This research project also illustrated that in studies involving isolated aortic rings, DHA modulation of TMEM16A current during agonist-induced contraction was found to be a crucial and novel mechanism of vasorelaxation.

Chapter 6

Concluding remarks

Chapter 6 - Concluding remarks

The overall aim of this thesis was to study the regulation of TMEM16A by lipids, and the role of this regulation in the control of vascular tone. The research in this thesis builds on previous research in the Tammaro group, which provides evidence for the expression and function of TMEM16A in VSMCs (Manoury et al., 2010). As outlined in chapter 1, TMEM16A has a role in depolarising the *Vm* in VSMCs, and represents an important pathway in agonist-induced blood vessel contraction. In this thesis, the regulation of TMEM16A by both the intracellular signalling lipid PIP_2 and the extracellular dietary PUFA DHA were studied. It was hypothesised that TMEM16A is sensitive to modulation by lipids, as the recent elucidation of the cryo-EM structure has revealed that the TMEM16A pore is partially exposed to the plasma membrane. This structural arrangement is unprecedented in ion channels, and indicates that TMEM16A may be an exceptionally lipid-sensitive ion channel. Using a combination of patch-clamp electrophysiology, molecular biology, and myography, this thesis explores the lipid regulation of cloned TMEM16A channels, and the impact of this regulation on native TMEM16A in VSMCs, and on tone of isolated aortic rings. Furthermore, the effect of DHA on a variety of other ion channel types (cationic) in VSMCs was studied.

The main findings of this thesis are:

1, The TMEM16A pharmacological modulator Ani9 was found to be a potent inhibitor of cloned TMEM16A and selective for native TMEM16A in VSMCs, as it did not modulate VSMC cationic currents, including Ca_V currents. Ani9 was then therefore used as a tool to specifically block native TMEM16A. Inhibition of native TMEM16A by Ani9 was used alongside a heterozygous knock-out of TMEM16A, which had reduced TMEM16A

expression in VSMCs. These methodologies confirmed that TMEM16A is expressed in VSMCs, and that TMEM16A has a key role in vascular contraction.

2, Intracellular application of the water-soluble analogue of PIP_2, diC8-PIP_2, was observed to potentiate TMEM16A activity. This effect was especially pronounced at physiologically relevant $[Ca^{2+}]_i$ and *Vm*. As PIP_2 is a crucial component of the Gq-PCR signalling cascade, we studied cells co-expressing TMEM16A and the α1-adrenergic receptor. On triggering the Gq-PCR signalling cascade, the rise in $[Ca^{2+}]_i$ resulted in enhanced TMEM16A activity. However, when this rise in $[Ca^{2+}]_i$ is prevented, TMEM16A activity decreased due to depletion of endogenous PIP_2. Endogenous PIP_2 was also depleted artificially using an endogenous PIP_2 phosphatase (DrVSP), which when co-expressed with TMEM16A, resulted in a TMEM16A current that reduced over time as PIP_2 was depleted. This DrVSP effect on TMEM16A could be reversed when ATP was included in the intracellular solution, as it is required for the re-synthesis of PIP_2. Depletion of PIP_2 by DrVSP was found to affect the pharmacology of TMEM16A, by reducing the activatory action of A9C. The Ani9 inhibition of TMEM16A was unaffected by the DrVSP-mediated depletion of PIP_2. Mutagenesis studies (chimeric construction and alanine scanning) were designed to identify a PIP_2 binding site. The TMEM16A and TMEM16B chimera in “site 1” demonstrated an altered IV-relationship, which could be attributed to an altered sensitivity to PIP_2. However, none of the mutant channels tested disrupted binding of diC8-PIP_2. Overall, we observe TMEM16A to be highly sensitive to the intracellular signalling lipid PIP_2.

3, The extracellular application of omega-3 PUFA DHA was found to inhibit cloned TMEM16A channels. This effect was demonstrated to be physiologically relevant, as when TMEM16A currents were recorded in the presence of DHA, the Gq-PCR signalling

cascade was insufficient to increase TMEM16A activity. DHA was also found to inhibit TMEM16A in VSMCs at all *Vm* tested, and reduce agonist-induced aortic contraction in myography experiments. A similar reduction in agonist-induced aortic contraction was also observed on addition of Ani9. Myography experiments testing the effect of DHA under conditions of modified $[Cl^-]_i$ and $[Cl^-]_e$ were used to alter the E_{Cl} in VSMCs. Low $[Cl^-]_e$ resulted in an increased TMEM16A current in VSMCs, and increased vascular contraction, which was reduced in the presence of DHA. The NKCC1 blocker bumetanide was used to reduce $[Cl^-]_i$, which led to a reduction in native TMEM16A current, and attenuated agonist-induced aortic contraction. These data confirm that Cl^- currents mediated by TMEM16A play a key role in vascular contraction, and suggests that the vasodilatory effect of DHA is mediated by block of TMEM16A. However, in isolated VSMCs, DHA was found to activate a cationic current. Pharmacological studies in VSMCs and isolated aortic myography experiments revealed this effect could be attributed to BK_{Ca} and Ca_V currents. However the modulation of BK_{Ca} channels by DHA was found to have minimal physiological relevance. Taken together, data presented in this thesis suggests a role for TMEM16A and Ca_V channels in the vasodilator effect of DHA. The role of TMEM16A in this effect is a novel finding. DHA incorporates into the plasma membrane, so this study provides evidence that TMEM16A is regulated by the composition of the plasma membrane.

Overall, this thesis provides evidence that TMEM16A is highly sensitive to modulation by lipids. As TMEM16A is expressed in VSMCs, we conclude that the regulation of TMEM16A activity by lipids is crucial in the control of blood vessel tone. Dysregulation of vascular TMEM16A could therefore provide an explanation and target for idiopathic vascular disease.

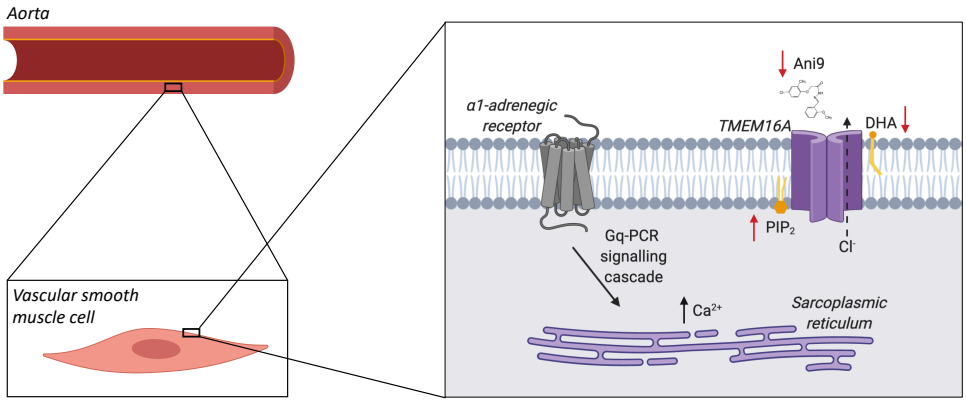

Figure 6.1. Summary schematic of research described in this thesis

Black lines represent magnified regions of areas highlighted by black boxes. Red arrows represent an increase or decrease in TMEM16A activity.

6.1. Limitations of study and future work

The British Heart Foundation and wider scientific community have recently engaged with the concept of a male bias in the study of cardiovascular disease. There is currently a higher mortality rate for women being treated for cardiovascular disease (Wilkinson et al., 2019, Lehto et al., 2012, Leifheit-Limson et al., 2015, Nguyen et al., 2018). Mice used in these studies were male. If this research was to be repeated, mice of both genders would be used to allow for sex based comparisons to be made, and to ensure this research could translate to both male and female patients.

There is scope for the work in this thesis to form the basis for further study. The study by Heinze et al. (Heinze et al., 2014) demonstrated that mice with reduced TMEM16A expression resulted in different reduction in blood vessel contraction between the aorta and other resistance blood vessels. The research in this thesis could therefore be expanded to additional blood vessel types. There is also scope for further investigation

into the TMEM16A pore region, in order to clarify whether certain residues are responsible for the lipid sensitivity of TMEM16A. This site of interest could then be targeted using pharmacology in order to identify synthetic modulators that can regulate blood vessel tone.

Publications, presentations, and posters

Publications

Acheson, K. E. 2016.

TMEM16F: function from (iso)form. *J Physiol,* 594**,** 2785-6.

Ta, C. M., **Acheson, K. E.**, Rorsman, N. J. G., Jongkind, R. C. & Tammaro, P. 2017. Contrasting effects of phosphatidylinositol 4,5-bisphosphate on cloned TMEM16A and TMEM16B channels. *Br J Pharmacol,* 174**,** 2984-2999.

Acheson, K. E. & Tammaro, P. 2019.

Inhibition of TMEM16A by docosahexaenoic acid plays a crucial role in blood vessel relaxation. Manuscript in preparation.

Presentations

Acheson, K. E. 'Inhibition of TMEM16A by docosahexaenoic acid plays a crucial role in blood vessel relaxation'

The Biophysical Society annual meeting 2019, Baltimore, USA.

Acheson, K. E. 'Lipid regulation of cloned calcium-activated chloride channels'

Flash presentation - British Pharmacological Society annual meeting 2017, London, UK. *Prize - Best flash presentation.*

Acheson, K. E. 'Lipid regulation of cloned calcium-activated chloride channels'

Postgraduate symposium in biomedical sciences 2017, University of Queensland, Australia.

Poster presentations

Acheson, K. E., Tammaro, P. 'Inhibition of TMEM16A by docosahexaenoic acid plays a crucial role in blood vessel relaxation'

British Pharmacological Society annual meeting 2018, London, UK.

Acheson, K. E., Ta, C. M., Rorsman, N. J. G., Jongkind, R. C., Tammaro, P. 'Lipid regulation of cloned calcium-activated chloride channels'

British Pharmacological Society annual meeting 2017, London, UK.

Acheson, K. E., Ta, C. M., Rorsman, N. J. G., Jongkind, R. C., Tammaro, P. 'Lipid regulation of cloned calcium-activated chloride channels'

British Heart Foundation Centre of Research Excellence conference 2017, Oxford, UK.

Acheson, K. E., Ta, C. M., Rorsman, N. J. G., Jongkind, R. C., Tammaro, P. 'Lipid regulation of cloned calcium-activated chloride channels'

OXION conference 2017, Oxford, UK.

Acheson, K. E., Ta, C. M., Rorsman, N. J. G., Jongkind, R. C., Tammaro, P. 'Lipid regulation of cloned calcium-activated chloride channels'

EMBO/FEBS meeting – Channels and Transporters 2017, Erice, Italy.

References

AARHUS, R., GRAEFF, R. M., DICKEY, D. M., WALSETH, T. F. & LEE, H. C. 1995. ADP-ribosyl cyclase and CD38 catalyze the synthesis of a calcium-mobilizing metabolite from NADP. *J Biol Chem,* 270**,** 30327-33.

ABBOTT, S. K., ELSE, P. L., ATKINS, T. A. & HULBERT, A. J. 2012. Fatty acid composition of membrane bilayers: Importance of diet polyunsaturated fat balance. *Biochimica Et Biophysica Acta-Biomembranes,* 1818**,** 1309-1317.

ABITAN, H., BOHR, H. & BUCHHAVE, P. 2008. Correction to the Beer-Lambert-Bouguer law for optical absorption. *Applied Optics,* 47**,** 5354-5357.

ACHESON, K. 2016. TMEM16F: function from (iso)form. *J Physiol,* 594**,** 2785-6.

ADOMAVICIENE, A., SMITH, K. J., GARNETT, H. & TAMMARO, P. 2013. Putative pore-loops of TMEM16/Anoctamin channels affect channel density in cell membranes. *J Physiol,* 591**,** 3487.

ALBERTS, B. 2008. *Molecular biology of the cell,* New York, Garland Science ; [London : Taylor & Francis, distributor].

ALI, H., CHRISTENSEN, S. B., FOREMAN, J. C., PEARCE, F. L., PIOTROWSKI, W. & THASTRUP, O. 1985. The ability of thapsigargin and thapsigargicin to activate cells involved in the inflammatory response. *Br J Pharmacol,* 85**,** 705-12.

ALLEN, J. A., HALVERSON-TAMBOLI, R. A. & RASENICK, M. M. 2007. Lipid raft microdomains and neurotransmitter signalling. *Nature Reviews Neuroscience,* 8**,** 128-140.

ALTHOFF, T. F. & OFFERMANNS, S. 2015. G-protein-mediated signaling in vascular smooth muscle cells - implications for vascular disease. *J Mol Med (Berl),* 93**,** 973-81.

AMBUDKAR, I. S., DE SOUZA, L. B. & ONG, H. L. 2017. TRPC1, Orai1, and STIM1 in SOCE: Friends in tight spaces. *Cell Calcium,* 63**,** 33-39.

ATILLA-GOKCUMEN, G. E., MURO, E., RELAT-GOBERNA, J., SASSE, S., BEDIGIAN, A., COUGHLIN, M. L., GARCIA-MANYES, S. & EGGERT, U. S. 2014. Dividing Cells Regulate Their Lipid Composition and Localization. *Cell,* 156**,** 428-439.

AYOUB, C., WASYLYK, C., LI, Y., THOMAS, E., MARISA, L., ROBE, A., ROUX, M., ABECASSIS, J., DE REYNIES, A. & WASYLYK, B. 2010. ANO1 amplification and expression in HNSCC with a high propensity for future distant metastasis and its functions in HNSCC cell lines. *British Journal of Cancer,* 103**,** 715-726.

BALLA, T. 2013. Phosphoinositides: tiny lipids with giant impact on cell regulation. *Physiol Rev,* 93**,** 1019-137.

BANNISTER, R. A. & BEAM, K. G. 2013. Ca(v)1.1: The atypical prototypical voltage-gated Ca2+ channel. *Biochimica Et Biophysica Acta-Biomembranes,* 1828**,** 1587-1597.

BARISH, M. E. 1983. A transient calcium-dependent chloride current in the immature Xenopus oocyte. *J Physiol,* 342**,** 309-25.

BARON, C. B., CUNNINGHAM, M., STRAUSS, J. F. & COBURN, R. F. 1984. Pharmacomechanical Coupling in Smooth-Muscle May Involve Phosphatidylinositol Metabolism. *Proceedings of the National Academy of Sciences of the United States of America-Biological Sciences,* 81**,** 6899-6903.

BARRO-SORIA, R., SCHREIBER, R. & KUNZELMANN, K. 2008. Bestrophin 1 and 2 are components of the Ca(2+) activated Cl(-) conductance in mouse airways. *Biochim Biophys Acta,* 1783**,** 1993-2000.

BARRY, P. H. & LYNCH, J. W. 1991. Liquid junction potentials and small cell effects in patch-clamp analysis. *J Membr Biol,* 121**,** 101-17.

BECHTOL, K. B., HANZEL, D. K. & LIANG, B. C. 1994. Using Dyes and Filters in a Fluorescent Imaging-System. *American Biotechnology Laboratory,* 12**,** 8-10.

BEN-ARI, Y. 2017. NKCC1 Chloride Importer Antagonists Attenuate Many Neurological and Psychiatric Disorders. *Trends Neurosci,* 40**,** 536-554.

BENEDETTO, R., OUSINGSAWAT, J., CABRITA, I., PINTO, M., LERIAS, J. R., WANITCHAKOOL, P., SCHREIBER, R. & KUNZELMANN, K. 2019. Plasma membrane-localized TMEM16 proteins are indispensable for expression of CFTR. *Journal of Molecular Medicine-Jmm,* 97**,** 711-722.

BENEDETTO, R., OUSINGSAWAT, J., WANITCHAKOOL, P., ZHANG, Y., HOLTZMAN, M. J., AMARAL, M., ROCK, J. R., SCHREIBER, R. & KUNZELMANN, K. 2017. Epithelial Chloride Transport by CFTR Requires TMEM16A. *Sci Rep,* 7**,** 12397.

BENHAM, C. D. & TSIEN, R. W. 1987. A novel receptor-operated Ca2+-permeable channel activated by ATP in smooth muscle. *Nature,* 328**,** 275-8.

BERG, I., POTTER, B. V. L., MAYR, G. W. & GUSE, A. H. 2000. Nicotinic acid adenine dinucleotide phosphate (NAADP(+)) is an essential regulator of T-lymphocyte Ca2+-signaling. *Journal of Cell Biology,* 150**,** 581-588.

BERRIDGE, M. J. 1993. Inositol trisphosphate and calcium signalling. *Nature,* 361**,** 315-25.

BERS, D. M. 2002. Cardiac excitation-contraction coupling. *Nature,* 415**,** 198-205.

BETHEL, N. P. & GRABE, M. 2016. Atomistic insight into lipid translocation by a TMEM16 scramblase. *Proceedings of the National Academy of Sciences of the United States of America,* 113**,** 14049-14054.

BILLAUD, M., DONNENBERG, V. S., ELLIS, B. W., MEYER, E. M., DONNENBERG, A. D., HILL, J. C., RICHARDS, T. D., GLEASON, T. G. & PHILLIPPI, J. A. 2017. Classification and Functional Characterization of Vasa Vasorum-Associated Perivascular Progenitor Cells in Human Aorta. *Stem Cell Reports,* 9**,** 292-303.

BJERREGAARD, P., YOUNG, T. K. & HEGELE, R. A. 2003. Low incidence of cardiovascular disease among the Inuit - what is the evidence? *Atherosclerosis,* 166**,** 351-357.

BLAUSTEIN, M. P., ZHANG, J., CHEN, L., SONG, H., RAINA, H., KINSEY, S. P., IZUKA, M., IWAMOTO, T., KOTLIKOFF, M. I., LINGREL, J. B., PHILIPSON, K. D., WIER, W. G. & HAMLYN, J. M. 2009. The Pump, the Exchanger, and Endogenous Ouabain Signaling Mechanisms That Link Salt Retention to Hypertension. *Hypertension,* 53**,** 291-U341.

BOLAND, L. M. & DRZEWIECKI, M. M. 2008. Polyunsaturated fatty acid modulation of voltage-gated ion channels. *Cell Biochem Biophys,* 52**,** 59-84.

BOLTON, T. B. 1979. Mechanisms of action of transmitters and other substances on smooth muscle. *Physiol Rev,* 59**,** 606-718.

BOLZ, S. S. 2013. Cholesterol regulation of PIP2: why cell type is so important. *Frontiers in Physiology,* 3.

BONAA, K. H., BJERVE, K. S., STRAUME, B., GRAM, I. T. & THELLE, D. 1990. Effect of eicosapentaenoic and docosahexaenoic acids on blood pressure in hypertension. A population-based intervention trial from the Tromso study. *N Engl J Med,* 322**,** 795-801.

BOND, P. J., WEE, C. L. & SANSOM, M. S. P. 2008. Coarse-Grained Molecular Dynamics Simulations of the Energetics of Helix Insertion into a Lipid Bilayer. *Biochemistry,* 47**,** 11321-11331.

BOOTMAN, M. D. & BERRIDGE, M. J. 1996. Subcellular Ca2+ signals underlying waves and graded responses in HeLa cells. *Curr Biol,* 6**,** 855-65.

BORGHI, C., ACELAJADO, M. C., GUPTA, Y. & JAIN, S. 2017. Role of nebivolol in the control and management of central aortic blood pressure in hypertensive patients. *J Hum Hypertens,* 31**,** 605-610.

BORJESSON, S. I., HAMMARSTROM, S. & ELINDER, F. 2008. Lipoelectric modification of ion channel voltage gating by polyunsaturated fatty acids. *Biophysical Journal,* 95**,** 2242-2253.

BRADLEY, E., FEDIGAN, S., WEBB, T., HOLLYWOOD, M. A., THORNBURY, K. D., MCHALE, N. G. & SERGEANT, G. P. 2014. Pharmacological characterization of TMEM16A currents. *Channels (Austin),* 8**,** 308-20.

BRAILOIU, E., RAHMAN, T., CHURAMANI, D., PROLE, D. L., BRAILOIU, G. C., HOOPER, R., TAYLOR, C. W. & PATEL, S. 2010. An NAADP-gated two-pore channel targeted to the plasma membrane uncouples triggering from amplifying Ca2+ signals. *J Biol Chem,* 285**,** 38511-6.

BRAYDEN, J. E. & NELSON, M. T. 1992. Regulation of Arterial Tone by Activation of Calcium-Dependent Potassium Channels. *Science,* 256**,** 532-535.

BRICOGNE, C., FINE, M., PEREIRA, P. M., SUNG, J., TIJANI, M., WANG, Y., HENRIQUES, R., COLLINS, M. K. & HILGEMANN, D. W. 2019. TMEM16F activation by Ca(2+) triggers plasma membrane expansion and directs PD-1 trafficking. *Sci Rep,* 9**,** 619.

BRITSCHGI, A., BILL, A., BRINKHAUS, H., ROTHWELL, C., CLAY, I., DUSS, S., REBHAN, M., RAMAN, P., GUY, C. T., WETZEL, K., GEORGE, E., POPA, M. O., LILLEY, S., CHOUDHURY, H., GOSLING, M., WANG, L., FITZGERALD, S., BORAWSKI, J., BAFFOE, J., LABOW, M., GAITHER, L. A. & BENTIRES-ALJ, M. 2013. Calcium-activated chloride channel ANO1 promotes breast cancer progression by activating EGFR and CAMK signaling. *Proc Natl Acad Sci U S A,* 110**,** E1026-34.

BROWN, D. A. & ADAMS, P. R. 1980. Muscarinic suppression of a novel voltage-sensitive K+ current in a vertebrate neurone. *Nature,* 283**,** 673-6.

BROZOVICH, F. V., NICHOLSON, C. J., DEGEN, C. V., GAO, Y. Z., AGGARWAL, M. & MORGAN, K. G. 2016. Mechanisms of Vascular Smooth Muscle Contraction and the Basis for Pharmacologic Treatment of Smooth Muscle Disorders. *Pharmacol Rev,* 68**,** 476-532.

BRUNNER, J. D., LIM, N. K., SCHENCK, S., DUERST, A. & DUTZLER, R. 2014. X-ray structure of a calcium-activated TMEM16 lipid scramblase. *Nature,* 516**,** 207-12.

BUCHWALOW, I. B., PODZUWEIT, T., BOCKER, W., SAMOILOVA, V. E., THOMAS, S., WELLNER, M., BABA, H. A., ROBENEK, H., SCHNEKENBURGER, J. & LERCH, M. M. 2002. Vascular smooth muscle and nitric oxide synthase. *FASEB J,* 16**,** 500-8.

BULLEY, S. & JAGGAR, J. H. 2014. Cl(-) channels in smooth muscle cells. *Pflugers Arch,* 466**,** 861-72.

BURR, M. L., GILBERT, J. F., HOLLIDAY, R. M., ELWOOD, P. C., FEHILY, A. M., ROGERS, S., SWEETNAM, P. M. & DEADMAN, N. M. 1989. Effects of Changes in Fat, Fish, and Fiber Intakes on Death and Myocardial Reinfarction - Diet and Reinfarction Trial (Dart). *Lancet,* 2**,** 757-761.

BYRNE, N. G. & LARGE, W. A. 1987. Action of Noradrenaline on Single Smooth-Muscle Cells Freshly Dispersed from the Rat Anococcygeus Muscle. *Journal of Physiology-London,* 389**,** 513-525.

CALCRAFT, P. J., RUAS, M., PAN, Z., CHENG, X. T., ARREDOUANI, A., HAO, X. M., TANG, J. S., RIETDORF, K., TEBOUL, L., CHUANG, K. T., LIN, P. H., XIAO, R., WANG, C. B., ZHU, Y. M., LIN, Y. K., WYATT, C. N., PARRINGTON, J., MA, J. J., EVANS, A. M., GALIONE, A. & ZHU, M. X. 2009. NAADP mobilizes calcium from acidic organelles through two-pore channels. *Nature,* 459**,** 596-U130.

CANCELA, J. M., CHURCHILL, G. C. & GALIONE, A. 1999. Coordination of agonist-induced Ca2+-signalling patterns by NAADP in pancreatic acinar cells. *Nature,* 398**,** 74-6.

CAO, E., LIAO, M., CHENG, Y. & JULIUS, D. 2013. TRPV1 structures in distinct conformations reveal activation mechanisms. *Nature,* 504**,** 113-8.

CAO, J., SCHWICHTENBERG, K. A., HANSON, N. Q. & TSAI, M. Y. 2006. Incorporation and clearance of omega-3 fatty acids in erythrocyte membranes and plasma phospholipids. *Clinical Chemistry,* 52**,** 2265-2272.

CAPUTO, A., CACI, E., FERRERA, L., PEDEMONTE, N., BARSANTI, C., SONDO, E., PFEFFER, U., RAVAZZOLO, R., ZEGARRA-MORAN, O. & GALIETTA, L. J. 2008. TMEM16A, a membrane protein associated with calcium-dependent chloride channel activity. *Science,* 322**,** 590-4.

CASTEELS, R., DROOGMANS, G. & HIMPENS, B. 1985. Excitation-Contraction Coupling in Vascular Smooth-Muscle Cells and Perivascular Nerve-Stimulation. *Journal of Cardiovascular Pharmacology,* 7**,** S9-S12.

CASTEELS, R., KITAMURA, K., KURIYAMA, H. & SUZUKI, H. 1977. The membrane properties of the smooth muscle cells of the rabbit main pulmonary artery. *J Physiol,* 271**,** 41-61.

CATTERALL, W. A. 2011. Voltage-gated calcium channels. *Cold Spring Harb Perspect Biol,* 3**,** a003947.

CATTERALL, W. A. & SWANSON, T. M. 2015. Structural Basis for Pharmacology of Voltage-Gated Sodium and Calcium Channels. *Mol Pharmacol,* 88**,** 141-50.

CHAI, R., CHEN, Y. F., YUAN, H. B., WANG, X. Z., GUO, S., QI, J. L., ZHANG, H. L., ZHAN, Y. & AN, H. L. 2017. Identification of Resveratrol, an Herbal Compound, as an Activator of the Calcium-Activated Chloride Channel, TMEM16A. *Journal of Membrane Biology,* 250**,** 483-492.

CHIPPERFIELD, A. R. & HARPER, A. A. 2000. Chloride in smooth muscle. *Prog Biophys Mol Biol,* 74**,** 175-221.

CHUN, Y. S., SHIN, S., KIM, Y., CHO, H., PARK, M. K., KIM, T. W., VORONOV, S. V., DI PAOLO, G., SUH, B. C. & CHUNG, S. 2010. Cholesterol modulates ion channels via down-regulation of phosphatidylinositol 4,5-bisphosphate. *Journal of Neurochemistry,* 112**,** 1286-1294.

CLAPPER, D. L., WALSETH, T. F., DARGIE, P. J. & LEE, H. C. 1987. Pyridine nucleotide metabolites stimulate calcium release from sea urchin egg microsomes desensitized to inositol trisphosphate. *J Biol Chem,* 262**,** 9561-8.

CONTRERAS-VITE, J. A., CRUZ-RANGEL, S., DE JESUS-PEREZ, J. J., FIGUEROA, I. A. A., RODRIGUEZ-MENCHACA, A. A., PEREZ-CORNEJO, P., HARTZELL, H. C. & ARREOLA, J. 2016. Revealing the activation pathway for TMEM16A chloride channels from macroscopic currents and kinetic models. *Pflugers Archiv-European Journal of Physiology,* 468**,** 1241-1257.

CRUZ-RANGEL, S., DE JESUS-PEREZ, J. J., ARECHIGA-FIGUEROA, I. A., RODRIGUEZ-MENCHACA, A. A., PEREZ-CORNEJO, P., HARTZELL, H. C. & ARREOLA, J. 2017. Extracellular protons enable activation of the calcium-dependent chloride channel TMEM16A. *J Physiol,* 595**,** 1515-1531.

CRUZ-RANGEL, S., DE JESUS-PEREZ, J. J., CONTRERAS-VITE, J. A., PEREZ-CORNEJO, P., HARTZELL, H. C. & ARREOLA, J. 2015. Gating modes of calcium-activated chloride channels TMEM16A and TMEM16B. *J Physiol,* 593**,** 5283-98.

CUI, J., COX, D. H. & ALDRICH, R. W. 1997. Intrinsic voltage dependence and Ca2+ regulation of mslo large conductance Ca-activated K+ channels. *Journal of General Physiology,* 109**,** 647-673.

CUI, Y., TRAN, S., TINKER, A. & CLAPP, L. H. 2002. The molecular composition of K(ATP) channels in human pulmonary artery smooth muscle cells and their modulation by growth. *American Journal of Respiratory Cell and Molecular Biology,* 26**,** 135-143.

CUNNANE, S. C., MUSA, K., RYAN, M. A., WHITING, S. & FRASER, D. D. 2002. Potential role of polyunsaturates in seizure protection achieved with the ketogenic diet. *Prostaglandins Leukot Essent Fatty Acids,* 67**,** 131-5.

CUNNINGHAM, S. A., AWAYDA, M. S., BUBIEN, J. K., ISMAILOV, II, ARRATE, M. P., BERDIEV, B. K., BENOS, D. J. & FULLER, C. M. 1995. Cloning of an epithelial chloride channel from bovine trachea. *J Biol Chem,* 270**,** 31016-26.

DAHLIN, M., HJELTE, L., NILSSON, S. & AMARK, P. 2007. Plasma phospholipid fatty acids are influenced by a ketogenic diet enriched with n-3 fatty acids in children with epilepsy. *Epilepsy Research,* 73**,** 199-207.

DAI, Y. & ZHANG, J. H. 2001. Role of Cl- current in endothelin-1-induced contraction in rabbit basilar artery. *Am J Physiol Heart Circ Physiol,* 281**,** H2159-67.

DAI, Y. & ZHANG, J. H. 2002. Manipulation of chloride flux affects histamine-induced contraction in rabbit basilar artery. *Am J Physiol Heart Circ Physiol,* 282**,** H1427-36.

DAM, V. S., BOEDTKJER, D. M., NYVAD, J., AALKJAER, C. & MATCHKOV, V. 2014. TMEM16A knockdown abrogates two different Ca(2+)-activated Cl (-) currents and contractility of smooth muscle in rat mesenteric small arteries. *Pflugers Arch,* 466**,** 1391-409.

DANG, S., FENG, S., TIEN, J., PETERS, C. J., BULKLEY, D., LOLICATO, M., ZHAO, J., ZUBERBUHLER, K., YE, W., QI, L., CHEN, T., CRAIK, C. S., JAN, Y. N., MINOR, D. L., JR., CHENG, Y. & JAN, L. Y. 2017. Cryo-EM structures of the TMEM16A calcium-activated chloride channel. *Nature,* 552**,** 426-429.

DART, C. 2010. Lipid microdomains and the regulation of ion channel function. *J Physiol,* 588**,** 3169-78.

DAVIS, A. J., FORREST, A. S., JEPPS, T. A., VALENCIK, M. L., WIWCHAR, M., SINGER, C. A., SONES, W. R., GREENWOOD, I. A. & LEBLANC, N. 2010. Expression profile and protein translation of TMEM16A in murine smooth muscle. *Am J Physiol Cell Physiol,* 299**,** C948-59.

DE CATERINA, R., LIAO, J. K. & LIBBY, P. 2000. Fatty acid modulation of endothelial activation. *Am J Clin Nutr,* 71**,** 213S-23S.

DE JESUS-PEREZ, J. J., CRUZ-RANGEL, S., ESPINO-SALDANA, A. E., MARTINEZ-TORRES, A., QU, Z., HARTZELL, H. C., CORRAL-FERNANDEZ, N. E., PEREZ-CORNEJO, P. & ARREOLA, J. 2018. Phosphatidylinositol 4,5-bisphosphate, cholesterol, and fatty

acids modulate the calcium-activated chloride channel TMEM16A (ANO1). *Biochim Biophys Acta Mol Cell Biol Lipids,* 1863**,** 299-312.

DE LA FUENTE, R., NAMKUNG, W., MILLS, A. & VERKMAN, A. S. 2008. Small-molecule screen identifies inhibitors of a human intestinal calcium-activated chloride channel. *Mol Pharmacol,* 73**,** 758-68.

DEFELICE, L. J. 1981. Introduction to Membrane Noise. *Quarterly Review of Biology,* 58**,** 287-288.

DI SALVO, J. & NELSON, S. R. 1998. Stimulation of G-protein coupled receptors in vascular smooth muscle cells induces tyrosine kinase dependent increases in calcium without tyrosine phosphorylation of phospholipase C gamma-1. *Febs Letters,* 422**,** 85-88.

DICKSON, V. K., PEDI, L. & LONG, S. B. 2014. Structure and insights into the function of a Ca2+-activated Cl- channel. *Nature,* 516**,** 213-+.

DIXIT, R., KEMP, C., KULICH, S., SEETHALA, R., CHIOSEA, S., LING, S. Z., HA, P. K. & DUVVURI, U. 2015. TMEM16A/ANO1 is differentially expressed in HPV-negative versus HPV-positive head and neck squamous cell carcinoma through promoter methylation. *Scientific Reports,* 5.

DIXON, R. E., HENNIG, G. W., BAKER, S. A., BRITTON, F. C., HARFE, B. D., ROCK, J. R., SANDERS, K. M. & WARD, S. M. 2012. Electrical Slow Waves in the Mouse Oviduct Are Dependent upon a Calcium Activated Chloride Conductance Encoded by Tmem16a. *Biology of Reproduction,* 86.

DONG, D. L., BAI, Y. L. & CAI, B. Z. 2016. Calcium-Activated Potassium Channels: Potential Target for Cardiovascular Diseases. *Adv Protein Chem Struct Biol,* 104**,** 233-261.

DOPICO, A. M., BUKIYA, A. N. & JAGGAR, J. H. 2018. Calcium- and voltage-gated BK channels in vascular smooth muscle. *Pflugers Arch,* 470**,** 1271-1289.

DUARTE, I. D. & FERREIRA, S. H. 2000. L-NAME causes antinociception by stimulation of the arginine-NO-cGMP pathway. *Mediators Inflamm,* 9**,** 25-30.

DUNNE, M. J. & PETERSEN, O. H. 1986. Intracellular Adp Activates K+ Channels That Are Inhibited by Atp in an Insulin-Secreting Cell-Line. *Febs Letters,* 208**,** 59-62.

DURAN, C., THOMPSON, C. H., XIAO, Q. H. & HARTZELL, H. C. 2010. Chloride Channels: Often Enigmatic, Rarely Predictable. *Annual Review of Physiology,* 72**,** 95-121.

DUTZLER, R., CAMPBELL, E. B., CADENE, M., CHAIT, B. T. & MACKINNON, R. 2002. X-ray structure of a CIC chloride channel at 3.0 angstrom reveals the molecular basis of anion selectivity. *Nature,* 415**,** 287-294.

DUVVURI, U., SHIWARSKI, D. J., XIAO, D., BERTRAND, C., HUANG, X., EDINGER, R. S., ROCK, J. R., HARFE, B. D., HENSON, B. J., KUNZELMANN, K., SCHREIBER, R., SEETHALA, R. S., EGLOFF, A. M., CHEN, X., LUI, V. W., GRANDIS, J. R. & GOLLIN, S. M. 2012. TMEM16A Induces MAPK and Contributes Directly to Tumorigenesis and Cancer Progression. *Cancer Research,* 72**,** 3270-3281.

DWIVEDI, R., SAHA, S., CHOWIENCZYK, P. J. & RITTER, J. M. 2005. Block of inward rectifying K+ channels (KIR) inhibits bradykinin-induced vasodilatation in human forearm resistance vasculature. *Arterioscler Thromb Vasc Biol,* 25**,** e7-9.

EARLEY, S. 2006. Molecular diversity of receptor operated channels in vascular smooth muscle: a role for heteromultimeric TRP channels? *Circ Res,* 98**,** 1462-4.

EARLEY, S. & BRAYDEN, J. E. 2015. Transient receptor potential channels in the vasculature. *Physiol Rev,* 95**,** 645-90.

EBASHI, S. 1991. Excitation-Contraction Coupling and the Mechanism of Muscle-Contraction. *Annual Review of Physiology,* 53**,** 1-16.

EDVINSSON, M. L., AHNSTEDT, H., EDVINSSON, L. & ANDERSSON, S. E. 2016. Characterization of Relaxant Responses to Natriuretic Peptides in the Human Microcirculation In Vitro and In Vivo. *Microcirculation,* 23**,** 438-46.

EDWARDS, F. R. & HIRST, G. D. S. 1988. Inward Rectification in Submucosal Arterioles of Guinea-Pig Ileum. *Journal of Physiology-London,* 404**,** 437-454.

EDWARDS, G., DORA, K. A., GARDENER, M. J., GARLAND, C. J. & WESTON, A. H. 1998. K+ is an endothelium-derived hyperpolarizing factor in rat arteries. *Nature,* 396**,** 269-272.

EGGERMONT, J., TROUET, D., CARTON, I. & NILIUS, B. 2001. Cellular function and control of volume-regulated anion channels. *Cell Biochem Biophys,* 35**,** 263-74.

EID, B. G., ABU-SHARIB, A. T., EL-BASSOSSY, H. M., BALAMASH, K. & SMIRNOV, S. V. 2018. Enhanced calcium entry via activation of NOX/PKC underlies increased vasoconstriction induced by methylglyoxal. *Biochem Biophys Res Commun,* 506**,** 1013-1018.

ELINDER, F. & LIIN, S. I. 2017. Actions and Mechanisms of Polyunsaturated Fatty Acids on Voltage-Gated Ion Channels. *Front Physiol,* 8**,** 43.

ENGLER, M. B. & ENGLER, M. M. 2000. Docosahexaenoic acid--induced vasorelaxation in hypertensive rats: mechanisms of action. *Biol Res Nurs,* 2**,** 85-95.

ESPINOSA, I., LEE, C. H., KIM, M. K., ROUSE, B. T., SUBRAMANIAN, S., MONTGOMERY, K., VARMA, S., CORLESS, C. L., HEINRICH, M. C., SMITH, K. S., WANG, Z., RUBIN, B., NIELSEN, T. O., SEITZ, R. S., ROSS, D. T., WEST, R. B., CLEARY, M. L. & VAN DE RIJN, M. 2008. A novel monoclonal antibody against DOG1 is a sensitive and specific marker for gastrointestinal stromal tumors. *American Journal of Surgical Pathology,* 32**,** 210-218.

FAHMI, M., GARCIA, L., TAUPIGNON, A., DUFY, B. & SARTOR, P. 1995. Recording of a large-conductance chloride channel in normal rat lactotrophs. *Am J Physiol,* 269**,** E969-76.

FALKENBURGER, B. H., JENSEN, J. B., DICKSON, E. J., SUH, B. C. & HILLE, B. 2010a. Phosphoinositides: lipid regulators of membrane proteins. *J Physiol,* 588**,** 3179-85.

FALKENBURGER, B. H., JENSEN, J. B. & HILLE, B. 2010b. Kinetics of PIP2 metabolism and KCNQ2/3 channel regulation studied with a voltage-sensitive phosphatase in living cells. *Journal of General Physiology,* 135**,** 99-114.

FALLAH, G., ROMER, T., DETRO-DASSEN, S., BRAAM, U., MARKWARDT, F. & SCHMALZING, G. 2011. TMEM16A(a)/anoctamin-1 Shares a Homodimeric Architecture with CLC Chloride Channels. *Molecular & Cellular Proteomics,* 10.

FAMELI, N., EVANS, A. M. & VAN BREEMEN, C. 2017. Tissue Specificity: The Role of Organellar Membrane Nanojunctions in Smooth Muscle Ca2+ Signaling. *Store-Operated Ca2+ Entry (Soce) Pathways: Emerging Signaling Concepts in Human (Patho)Physiology, 2nd Edition,* 993**,** 321-342.

FARIA, D., ROCK, J. R., ROMAO, A. M., SCHWEDA, F., BANDULIK, S., WITZGALL, R., SCHLATTER, E., HEITZMANN, D., PAVENSTADT, H., HERRMANN, E., KUNZELMANN, K. & SCHREIBER, R. 2014. The calcium-activated chloride channel Anoctamin 1 contributes to the regulation of renal function. *Kidney Int,* 85**,** 1369-81.

FAUL, F., ERDFELDER, E., LANG, A. G. & BUCHNER, A. 2007. G*Power 3: a flexible statistical power analysis program for the social, behavioral, and biomedical sciences. *Behav Res Methods,* 39**,** 175-91.

FERRERA, L., CAPUTO, A., UBBY, I., BUSSANI, E., ZEGARRA-MORAN, O., RAVAZZOLO, R., PAGANI, F. & GALIETTA, L. J. 2009. Regulation of TMEM16A chloride channel properties by alternative splicing. *J Biol Chem,* 284**,** 33360-8.

FERRIER, G. R., REDONDO, I., ZHU, J. & MURPHY, M. G. 2002. Differential effects of docosahexaenoic acid on contractions and L-type Ca2+ current in adult cardiac myocytes. *Cardiovasc Res,* 54**,** 601-10.

FESTING, M. F. 2002. The design and statistical analysis of animal experiments. *ILAR J,* 43**,** 191-3.

FESTING, M. F. & ALTMAN, D. G. 2002. Guidelines for the design and statistical analysis of experiments using laboratory animals. *ILAR J,* 43**,** 244-58.

FESTING, M. O., P.; CORTINA BORJA, M.; BERDOY, M. 2016. The Design of Animal Experiments - Reducing the use of animals in research through better experimental design.

FOSKETT, J. K., WHITE, C., CHEUNG, K. H. & MAK, D. O. 2007. Inositol trisphosphate receptor Ca2+ release channels. *Physiol Rev,* 87**,** 593-658.

FOSTER, M. N. & COETZEE, W. A. 2016. KATP Channels in the Cardiovascular System. *Physiol Rev,* 96**,** 177-252.

FRASER, D. D., WHITING, S., ANDREW, R. D., MACDONALD, E. A., MUSA-VELOSO, K. & CUNNANE, S. C. 2003. Elevated polyunsaturated fatty acids in blood serum obtained from children on the ketogenic diet. *Neurology,* 60**,** 1026-1029.

FREEMAN, J. M., VINING, E. P., PILLAS, D. J., PYZIK, P. L., CASEY, J. C. & KELLY, L. M. 1998. The efficacy of the ketogenic diet-1998: a prospective evaluation of intervention in 150 children. *Pediatrics,* 102**,** 1358-63.

GALKINA, E., KADL, A., SANDERS, J., VARUGHESE, D., SAREMBOCK, I. J. & LEY, K. 2006. Lymphocyte recruitment into the aortic wall before and during development of atherosclerosis is partially L-selectin dependent. *J Exp Med,* 203**,** 1273-82.

GANAPATHI, S. B., WEI, S. G., ZAREMBA, A., LAMB, F. S. & SHEARS, S. B. 2013. Functional regulation of ClC-3 in the migration of vascular smooth muscle cells. *Hypertension,* 61**,** 174-9.

GARG, P., MARTIN, C. F., ELMS, S. C., GORDON, F. J., WALL, S. M., GARLAND, C. J., SUTLIFF, R. L. & O'NEILL, W. C. 2007. Effect of the Na-K-2Cl cotransporter NKCC1 on systemic blood pressure and smooth muscle tone. *Am J Physiol Heart Circ Physiol,* 292**,** H2100-5.

GARLAND, C. J. & WESTON, A. H. 2011. The vascular endothelium: still amazing us 30 years on. *Br J Pharmacol,* 164**,** 837-8.

GILBERT, G. E., KRETZ, C., GINSBURG, D. & NOVAKOVIC, V. A. 2015. Platelet Phosphatidylserine Exposure, Survival and Blood Coagulation in Mice Lacking TMEM16F. *Blood,* 126.

GODFRAIND, T. 2017. Discovery and Development of Calcium Channel Blockers. *Front Pharmacol,* 8**,** 286.

GONZALEZ-PEREZ, V. & LINGLE, C. J. 2019. Regulation of BK Channels by Beta and Gamma Subunits. *Annual Review of Physiology, Vol 81,* 81**,** 113-137.

GOODFELLOW, J., BELLAMY, M. F., RAMSEY, M. W., JONES, C. J. & LEWIS, M. J. 2000. Dietary supplementation with marine omega-3 fatty acids improve systemic

large artery endothelial function in subjects with hypercholesterolemia. *J Am Coll Cardiol,* 35**,** 265-70.

GROUP, A. S. C., BOWMAN, L., MAFHAM, M., WALLENDSZUS, K., STEVENS, W., BUCK, G., BARTON, J., MURPHY, K., AUNG, T., HAYNES, R., COX, J., MURAWSKA, A., YOUNG, A., LAY, M., CHEN, F., SAMMONS, E., WATERS, E., ADLER, A., BODANSKY, J., FARMER, A., MCPHERSON, R., NEIL, A., SIMPSON, D., PETO, R., BAIGENT, C., COLLINS, R., PARISH, S. & ARMITAGE, J. 2018. Effects of n-3 Fatty Acid Supplements in Diabetes Mellitus. *N Engl J Med,* 379**,** 1540-1550.

GUAN, Y. Y., WANG, G. L. & ZHOU, J. G. 2006. The ClC-3 Cl^- channel in cell volume regulation, proliferation and apoptosis in vascular smooth muscle cells. *Trends Pharmacol Sci,* 27**,** 290-6.

GUO, D. L., RAMU, Y., KLEM, A. M. & LU, Z. 2003. Mechanism of rectification in inward-rectifier K+ channels. *Journal of General Physiology,* 121**,** 261-275.

GUO, S., CHEN, Y. F., PANG, C. L., WANG, X. Z., QI, J. L., MO, L., ZHANG, H. L., AN, H. L. & ZHAN, Y. 2017. Ginsenoside Rb1, a novel activator of the TMEM16A chloride channel, augments the contraction of guinea pig ileum. *Pflugers Archiv-European Journal of Physiology,* 469**,** 681-692.

GYOBU, S., MIYATA, H., IKAWA, M., YAMAZAKI, D., TAKESHIMA, H., SUZUKI, J. & NAGATA, S. 2016. A Role of TMEM16E Carrying a Scrambling Domain in Sperm Motility. *Mol Cell Biol,* 36**,** 645-59.

HAMILL, O. P., MARTY, A., NEHER, E., SAKMANN, B. & SIGWORTH, F. J. 1981. Improved patch-clamp techniques for high-resolution current recording from cells and cell-free membrane patches. *Pflugers Arch,* 391**,** 85-100.

HANAHAN, D. 1983. Studies on Transformation of Escherichia-Coli with Plasmids. *Journal of Molecular Biology,* 166**,** 557-580.

HANDLER, B., DHINGRA, R. C. & ROSEN, K. M. 1981. Bumetanide - a New Diuretic - Results of Clinical Efficacy and Safety in Patients with Congestive Heart-Failure. *Journal of Clinical Pharmacology,* 21**,** 691-696.

HARRIS, W. S. 1996. n-3 fatty acids and lipoproteins: comparison of results from human and animal studies. *Lipids,* 31**,** 243-52.

HARTWIG, J. H., BOKOCH, G. M., CARPENTER, C. L., JANMEY, P. A., TAYLOR, L. A., TOKER, A. & STOSSEL, T. P. 1995. Thrombin Receptor Ligation and Activated Rac Uncap Actin Filament Barbed Ends through Phosphoinositide Synthesis in Permeabilized Human Platelets. *Cell,* 82**,** 643-653.

HARTZELL, C., PUTZIER, I. & ARREOLA, J. 2005. Calcium-activated chloride channels. *Annu Rev Physiol,* 67**,** 719-58.

HARTZELL, H. C., QU, Z., YU, K., XIAO, Q. & CHIEN, L. T. 2008. Molecular physiology of bestrophins: multifunctional membrane proteins linked to best disease and other retinopathies. *Physiol Rev,* 88**,** 639-72.

HARTZELL, H. C., YU, K., XIAO, Q., CHIEN, L. T. & QU, Z. 2009. Anoctamin/TMEM16 family members are Ca^{2+}-activated Cl^- channels. *J Physiol,* 587**,** 2127-39.

HAZAMA, H., NAKAJIMA, T., ASANO, M., IWASAWA, K., MORITA, T., IGARASHI, K., NAGATA, T., HORIUCHI, T., SUZUKI, J., SOMA, M. & OKUDA, Y. 1998. Omega-3 polyunsaturated fatty acids--modulation of voltage-dependent L-type Ca2+ current in guinea-pig tracheal smooth muscle cells. *Eur J Pharmacol,* 355**,** 257-66.

HEINZE, C., SENIUK, A., SOKOLOV, M. V., HUEBNER, A. K., KLEMENTOWICZ, A. E., SZIJARTO, I. A., SCHLEIFENBAUM, J., VITZTHUM, H., GOLLASCH, M., EHMKE, H., SCHROEDER, B. C. & HUBNER, C. A. 2014. Disruption of vascular Ca2+-activated chloride currents lowers blood pressure. *J Clin Invest,* 124**,** 675-86.

HEISTAD, D. D. & MARCUS, M. L. 1979. Role of vasa vasorum in nourishment of the aorta. *Blood Vessels,* 16**,** 225-38.

HEROLD, P. M. & KINSELLA, J. E. 1986. Fish Oil Consumption and Decreased Risk of Cardiovascular-Disease - a Comparison of Findings from Animal and Human Feeding Trials. *American Journal of Clinical Nutrition,* 43**,** 566-598.

HERRING, N. & PATERSON, D. J. 2018. *Levick's Introduction to Cardiovascular Physiology,* London; New York, Boca Raton.

HESS, B., KUTZNER, C., VAN DER SPOEL, D. & LINDAHL, E. 2008. GROMACS 4: Algorithms for highly efficient, load-balanced, and scalable molecular simulation. *Journal of Chemical Theory and Computation,* 4**,** 435-447.

HIBINO, H., INANOBE, A., FURUTANI, K., MURAKAMI, S., FINDLAY, I. & KURACHI, Y. 2010. Inwardly Rectifying Potassium Channels: Their Structure, Function, and Physiological Roles. *Physiological Reviews,* 90**,** 291-366.

HILL, K., MCNULTY, S. & RANDALL, A. D. 2004. Inhibition of TRPM2 channels by the antifungal agents clotrimazole and econazole. *Naunyn Schmiedebergs Arch Pharmacol,* 370**,** 227-37.

HILL-EUBANKS, D. C., WERNER, M. E., HEPPNER, T. J. & NELSON, M. T. 2011. Calcium signaling in smooth muscle. *Cold Spring Harb Perspect Biol,* 3**,** a004549.

HILLE, B. 2001. *Ion channels of excitable membranes*, Sinauer Associates.

HILLE, B., DICKSON, E. J., KRUSE, M., VIVAS, O. & SUH, B. C. 2015. Phosphoinositides regulate ion channels. *Biochim Biophys Acta,* 1851**,** 844-56.

HILLE, B. & SCHWARZ, W. 1978. Potassium Channels as Multi-Ion Single-File Pores. *Journal of General Physiology,* 72**,** 409-442.

HIMPENS, B., DESMEDT, H., DROOGMANS, G. & CASTEELS, R. 1992. Differences in Regulation between Nuclear and Cytoplasmic Ca2+ in Cultured Smooth-Muscle Cells. *American Journal of Physiology,* 263**,** C95-C105.

HIRST, G. D. & EDWARDS, F. R. 1989. Sympathetic neuroeffector transmission in arteries and arterioles. *Physiol Rev,* 69**,** 546-604.

HOCKERMAN, G. H., JOHNSON, B. D., ABBOTT, M. R., SCHEUER, T. & CATTERALL, W. A. 1997. Molecular determinants of high affinity phenylalkylamine block of L-type calcium channels in transmembrane segment IIIS6 and the pore region of the alpha1 subunit. *J Biol Chem,* 272**,** 18759-65.

HOGAN, P. G. 2015. The STIM1-ORAI1 microdomain. *Cell Calcium,* 58**,** 357-67.

HONG, Z. K., STAICULESCU, M. C., HAMPEL, P., LEVITAN, I. & FORGACS, G. 2012. How cholesterol regulates endothelial biomechanics. *Frontiers in Physiology,* 3.

HOSHI, T., TIAN, Y. T., XU, R., HEINEMANN, S. H. & HOU, S. W. 2013. Mechanism of the modulation of BK potassium channel complexes with different auxiliary subunit compositions by the omega-3 fatty acid DHA. *Proceedings of the National Academy of Sciences of the United States of America,* 110**,** 4822-4827.

HOUSE, S. J., POTIER, M., BISAILLON, J., SINGER, H. A. & TREBAK, M. 2008. The non-excitable smooth muscle: calcium signaling and phenotypic switching during vascular disease. *Pflugers Arch,* 456**,** 769-85.

HOWARD, M., GRIMALDI, J. C., BAZAN, J. F., LUND, F. E., SANTOS-ARGUMEDO, L., PARKHOUSE, R. M., WALSETH, T. F. & LEE, H. C. 1993. Formation and hydrolysis of cyclic ADP-ribose catalyzed by lymphocyte antigen CD38. *Science,* 262**,** 1056-9.

HU, Y., ZHANG, Z., TORSNEY, E., AFZAL, A. R., DAVISON, F., METZLER, B. & XU, Q. 2004. Abundant progenitor cells in the adventitia contribute to atherosclerosis of vein grafts in ApoE-deficient mice. *J Clin Invest,* 113**,** 1258-65.

HUANG, F., ROCK, J. R., HARFE, B. D., CHENG, T., HUANG, X., JAN, Y. N. & JAN, L. Y. 2009. Studies on expression and function of the TMEM16A calcium-activated chloride channel. *Proc Natl Acad Sci U S A,* 106**,** 21413-8.

HUANG, F., WONG, X. & JAN, L. Y. 2012. International Union of Basic and Clinical Pharmacology. LXXXV: calcium-activated chloride channels. *Pharmacol Rev,* 64**,** 1-15.

HUME, J. R., WANG, G. X., YAMAZAKI, J., NG, L. C. & DUAN, D. 2010. CLC-3 chloride channels in the pulmonary vasculature. *Adv Exp Med Biol,* 661**,** 237-47.

HUSSY, N. 1992. Calcium-activated chloride channels in cultured embryonic Xenopus spinal neurons. *J Neurophysiol,* 68**,** 2042-50.

HWANG, S. J., BLAIR, P. J. A., BRITTON, F. C., O'DRISCOLL, K. E., HENNIG, G., BAYGUINOV, Y. R., ROCK, J. R., HARFE, B. D., SANDERS, K. M. & WARD, S. M. 2009. Expression of anoctamin 1/TMEM16A by interstitial cells of Cajal is fundamental for slow wave activity in gastrointestinal muscles. *Journal of Physiology-London,* 587**,** 4887-4904.

IMAI, Y., ITSUKI, K., OKAMURA, Y., INOUE, R. & MORI, M. X. 2012. A self-limiting regulation of vasoconstrictor-activated TRPC3/C6/C7 channels coupled to PI(4,5)P(2)-diacylglycerol signalling. *J Physiol,* 590**,** 1101-19.

INTAGLIETTA, M. 1991. Arteriolar vasomotion: implications for tissue ischemia. *Blood Vessels,* 28 Suppl 1**,** 1-7.

IRVINE, R. F. 2016. A short history of inositol lipids. *J Lipid Res,* 57**,** 1987-1994.

ITSUKI, K., IMAI, Y., HASE, H., OKAMURA, Y., INOUE, R. & MORI, M. X. 2014. PLC-mediated PI(4,5)P-2 hydrolysis regulates activation and inactivation of TRPC6/7 channels. *Journal of General Physiology,* 143**,** 183-201.

IWAMOTO, T., KITA, S., UEHARA, A., IMANAGA, I., MATSUDA, T., BABA, A. & KATSURAGI, T. 2004. Molecular determinants of Na+/Ca2+ exchange (NCX1) inhibition by SEA0400. *Journal of Biological Chemistry,* 279**,** 7544-7553.

JACKSON, T. R., PATTERSON, S. I., THASTRUP, O. & HANLEY, M. R. 1988. A Novel Tumor Promoter, Thapsigargin, Transiently Increases Cytoplasmic Free Ca-2+ without Generation of Inositol Phosphates in Ng115-401l Neuronal Cells. *Biochemical Journal,* 253**,** 81-86.

JACKSON, W. F. 2000. Ion channels and vascular tone. *Hypertension,* 35**,** 173-8.

JACKSON, W. F. 2017. Potassium Channels in Regulation of Vascular Smooth Muscle Contraction and Growth. *Adv Pharmacol,* 78**,** 89-144.

JACOBSEN, K. S., ZEEBERG, K., SAUTER, D. R. P., POULSEN, K. A., HOFFMANN, E. K. & SCHWAB, A. 2013. The role of TMEM16A (ANO1) and TMEM16F (ANO6) in cell migration. *Pflugers Archiv-European Journal of Physiology,* 465**,** 1753-1762.

JACOBSEN, L. B., CALVIN, S. A., COLVIN, K. E. & WRIGHT, M. 2004. FuGENE 6 Transfection Reagent: the gentle power. *Methods,* 33**,** 104-12.

JAGGAR, J. H., PORTER, V. A., LEDERER, W. J. & NELSON, M. T. 2000. Calcium sparks in smooth muscle. *Am J Physiol Cell Physiol,* 278**,** C235-56.

JANSSEN, L. J. & SIMS, S. M. 1993. Histamine activates Cl- and K+ currents in guinea-pig tracheal myocytes: convergence with muscarinic signalling pathway. *J Physiol,* 465**,** 661-77.

JENG, G., AGGARWAL, M., YU, W. P. & CHEN, T. Y. 2016. Independent activation of distinct pores in dimeric TMEM16A channels. *J Gen Physiol,* 148**,** 393-404.

JENSEN, A. B., JOERGENSEN, H. B., DAM, V. S., KAMAEV, D., BOEDTKJER, D., FUCHTBAUER, E. M., AALKJAER, C. & MATCHKOV, V. V. 2018. Variable Contribution of TMEM16A to Tone in Murine Arterial Vasculature. *Basic Clin Pharmacol Toxicol,* 123**,** 30-41.

JENTSCH, T. J. & PUSCH, M. 2018. CLC Chloride Channels and Transporters: Structure, Function, Physiology, and Disease. *Physiol Rev,* 98**,** 1493-1590.

JI, Q., GUO, S., WANG, X., PANG, C., ZHAN, Y., CHEN, Y. & AN, H. 2019. Recent advances in TMEM16A: Structure, function, and disease. *J Cell Physiol,* 234**,** 7856-7873.

JIANG, T., YU, K., HARTZELL, H. C. & TAJKHORSHID, E. 2017. Lipids and ions traverse the membrane by the same physical pathway in the nhTMEM16 scramblase. *Elife,* 6.

JIANG, Y., YU, B., YANG, H. & MA, T. H. 2016. Shikonin Inhibits Intestinal Calcium-Activated Chloride Channels and Prevents Rotaviral Diarrhea. *Frontiers in Pharmacology,* 7.

JURMAN, M. E., BOLAND, L. M., LIU, Y. & YELLEN, G. 1994. Visual identification of individual transfected cells for electrophysiology using antibody-coated beads. *Biotechniques,* 17**,** 876-81.

KAGAWA, Y., NISHIZAWA, M., SUZUKI, M., MIYATAKE, T., HAMAMOTO, T., GOTO, K., MOTONAGA, E., IZUMIKAWA, H., HIRATA, H. & EBIHARA, A. 1982. Eicosapolyenoic Acids of Serum-Lipids of Japanese Islanders with Low Incidence of Cardiovascular-Diseases. *Journal of Nutritional Science and Vitaminology,* 28**,** 441-453.

KAKEI, M., NOMA, A. & SHIBASAKI, T. 1985. Properties of adenosine-triphosphate-regulated potassium channels in guinea-pig ventricular cells. *J Physiol,* 363**,** 441-62.

KASHYAP, M. K., MARIMUTHU, A., KISHORE, C. J. H., PERI, S., KEERTHIKUMAR, S., PRASAD, T. S. K., MAHMOOD, R., RAO, S., RANGANATHAN, P., SANJEEVIAH, R. C., VIJAYAKUMAR, M., KUMAR, K. V. V., MONTGOMERY, E., KUMAR, R. V. & PANDEY, A. 2009. Genomewide mRNA profiling of esophageal squamous cell carcinoma for identification of cancer biomarkers. *Cancer Biology & Therapy,* 8**,** 36-46.

KATOH, M. & KATOH, M. 2003. FLJ10261 gene, located within the CCND1-EMS1 locus on human chromosome 11q13, encodes the eight-transmembrane protein homologous to C12orf3, C11orf25 and FLJ34272 gene products. *International Journal of Oncology,* 22**,** 1375-1381.

KINNEAR, N. P., BOITTIN, F. X., THOMAS, J. M., GALIONE, A. & EVANS, A. M. 2004. Lysosome-sarcoplasmic reticulum junctions - A trigger zone for calcium signaling by nicotinic acid adenine dinucleotide phosphate and endothelin-1. *Journal of Biological Chemistry,* 279**,** 54319-54326.

KINNEAR, N. P., WYATT, C. N., CLARK, J. H., CALCRAFT, P. J., FLEISCHER, S., JEYAKUMAR, L. H., NIXON, G. F. & EVANS, A. M. 2008. Lysosomes co-localize with ryanodine receptor subtype 3 to form a trigger zone for calcium signalling by NAADP in rat pulmonary arterial smooth muscle. *Cell Calcium,* 44**,** 190-201.

KINOSHITA, M., SUZUKI, K. G., MATSUMORI, N., TAKADA, M., ANO, H., MORIGAKI, K., ABE, M., MAKINO, A., KOBAYASHI, T., HIROSAWA, K. M., FUJIWARA, T. K., KUSUMI, A. & MURATA, M. 2017. Raft-based sphingomyelin interactions revealed by new fluorescent sphingomyelin analogs. *J Cell Biol,* 216**,** 1183-1204.

KLABUNDE, R. E. 2012. *Cardiovascular physiology concepts,* Philadelphia, PA, Lippincott Williams & Wilkins/Wolters Kluwer.

KLOSE, C., SURMA, M. A., GERL, M. J., MEYENHOFER, F., SHEVCHENKO, A. & SIMONS, K. 2012. Flexibility of a eukaryotic lipidome--insights from yeast lipidomics. *PLoS One,* 7**,** e35063.

KNAUS, H. G., EBERHART, A., GLOSSMANN, H., MUNUJOS, P., KACZOROWSKI, G. J. & GARCIA, M. L. 1994. Pharmacology and Structure of High-Conductance Calcium-Activated Potassium Channels. *Cellular Signalling,* 6**,** 861-&.

KNOT, H. J. & NELSON, M. T. 1998. Regulation of arterial diameter and wall [Ca^{2+}] in cerebral arteries of rat by membrane potential and intravascular pressure. *J Physiol,* 508 (Pt 1)**,** 199-209.

KNOT, H. J., ZIMMERMANN, P. A. & NELSON, M. T. 1996. Extracellular K+-induced hyperpolarizations and dilatations of rat coronary and cerebral arteries involve inward rectifier K+ channels. *Journal of Physiology-London,* 492**,** 419-430.

KOBAYASHI, Y., HIRAWA, N., TABARA, Y., MURAOKA, H., FUJITA, M., MIYAZAKI, N., FUJIWARA, A., ICHIKAWA, Y., YAMAMOTO, Y., ICHIHARA, N., SAKA, S., WAKUI, H., YOSHIDA, S., YATSU, K., TOYA, Y., YASUDA, G., KOHARA, K., KITA, Y., TAKEI, K., GOSHIMA, Y., ISHIKAWA, Y., UESHIMA, H., MIKI, T. & UMEMURA, S. 2012. Mice Lacking Hypertension Candidate Gene ATP2B1 in Vascular Smooth Muscle Cells Show Significant Blood Pressure Elevation. *Hypertension,* 59**,** 854-U213.

KONDO, M., TSUJI, M., HARA, K., ARIMURA, K., YAGI, O., TAGAYA, E., TAKEYAMA, K. & TAMAOKI, J. 2017. Chloride ion transport and overexpression of TMEM16A in a guinea-pig asthma model. *Clin Exp Allergy,* 47**,** 795-804.

KUO, I. Y. & EHRLICH, B. E. 2015. Signaling in muscle contraction. *Cold Spring Harb Perspect Biol,* 7**,** a006023.

KURIKI, K., NAGAYA, T., IMAEDA, N., TOKUDOME, Y., FUJIWARA, N., SATO, J., IKEDA, M., MAKI, S. & TOKUDOME, S. 2002. Discrepancies in dietary intakes and plasma concentrations of fatty acids according to age among Japanese female dietitians. *European Journal of Clinical Nutrition,* 56**,** 524-531.

KURUMA, A. & HARTZELL, H. C. 1999. Dynamics of calcium regulation of chloride currents in Xenopus oocytes. *Am J Physiol,* 276**,** C161-75.

LAMB, F. S. & BARNA, T. J. 1998. Chloride ion currents contribute functionally to norepinephrine-induced vascular contraction. *Am J Physiol,* 275**,** H151-60.

LANDS, W. E. M., MORRIS, A. & LIBELT, B. 1990. Quantitative Effects of Dietary Polyunsaturated Fats on the Composition of Fatty-Acids in Rat-Tissues. *Lipids,* 25**,** 505-516.

LARGE, W. A. 2002. Receptor-operated Ca2(+)-permeable nonselective cation channels in vascular smooth muscle: a physiologic perspective. *J Cardiovasc Electrophysiol,* 13**,** 493-501.

LARGE, W. A. & WANG, Q. 1996. Characteristics and physiological role of the Ca(2+)-activated Cl- conductance in smooth muscle. *Am J Physiol,* 271**,** C435-54.

LEBLANC, N., LEDOUX, J., SALEH, S., SANGUINETTI, A., ANGERMANN, J., O'DRISCOLL, K., BRITTON, F., PERRINO, B. A. & GREENWOOD, I. A. 2005. Regulation of calcium-activated chloride channels in smooth muscle cells: a complex picture is emerging. *Canadian Journal of Physiology and Pharmacology,* 83**,** 541-556.

LEDOUX, J., WERNER, M. E., BRAYDEN, J. E. & NELSON, M. T. 2006. Calcium-activated potassium channels and the regulation of vascular tone. *Physiology (Bethesda),* 21**,** 69-78.

LEE, B. C., KHELASHVILI, G., FALZONE, M., MENON, A. K., WEINSTEIN, H. & ACCARDI, A. 2018. Gating mechanism of the extracellular entry to the lipid pathway in a TMEM16 scramblase. *Nat Commun,* 9**,** 3251.

LEE, J. Y. & DEBERNARDIS, J. F. 1990. Alpha-2-Adrenergic Receptors and Calcium - Alpha-2-Receptor Blockade in Vascular Smooth-Muscle as an Approach to the Treatment of Hypertension. *Methods and Findings in Experimental and Clinical Pharmacology,* 12**,** 213-225.

LEFEVRE, T., LEFEVRE, I. A., COULOMBE, A. & CORABOEUF, E. 1996. Effects of chloride ion substitutes and chloride channel blockers on the transient outward current in rat ventricular myocytes. *Biochim Biophys Acta,* 1273**,** 31-43.

LEHTO, H. R., LEHTO, S., HAVULINNA, A. S., JOUSILAHTI, P. & SALOMAA, V. 2012. Gender differences in the prevalence, causes and treatment of high cardiovascular risk: findings from the FINRISK Survey. *Eur J Prev Cardiol,* 19**,** 1153-60.

LEIFHEIT-LIMSON, E. C., D'ONOFRIO, G., DANESHVAR, M., GEDA, M., BUENO, H., SPERTUS, J. A., KRUMHOLZ, H. M. & LICHTMAN, J. H. 2015. Sex Differences in Cardiac Risk Factors, Perceived Risk, and Health Care Provider Discussion of Risk and Risk Modification Among Young Patients With Acute Myocardial Infarction: The VIRGO Study. *J Am Coll Cardiol,* 66**,** 1949-1957.

LERIAS, J., PINTO, M., BENEDETTO, R., SCHREIBER, R., AMARAL, M., AURELI, M. & KUNZELMANN, K. 2018. Compartmentalized crosstalk of CFTR and TMEM16A (ANO1) through EPAC1 and ADCY1. *Cellular Signalling,* 44**,** 10-19.

LEUNG, F. P., YUNG, L. M., YAO, X., LAHER, I. & HUANG, Y. 2008. Store-operated calcium entry in vascular smooth muscle. *Br J Pharmacol,* 153**,** 846-57.

LEVENTAL, I. & VEATCH, S. 2016. The Continuing Mystery of Lipid Rafts. *J Mol Biol,* 428**,** 4749-4764.

LEVENTAL, K. R., LORENT, J. H., LIN, X. B., SKINKLE, A. D., SURMA, M. A., STOCKENBOJER, E. A., GORFE, A. A. & LEVENTAL, I. 2016. Polyunsaturated Lipids Regulate Membrane Domain Stability by Tuning Membrane Order. *Biophysical Journal,* 110**,** 1800-1810.

LEVITAN, I., FANG, Y., ROSENHOUSE-DANTSKER, A. & ROMANENKO, V. 2010. Cholesterol and Ion Channels. *Cholesterol Binding and Cholesterol Transport Proteins: Structure and Function in Health and Disease,* 51**,** 509-549.

LEVITAN, I., SINGH, D. K. & ROSENHOUSE-DANTSKER, A. 2014. Cholesterol binding to ion channels. *Frontiers in Physiology,* 5.

LEVY, M. N., PAPPANO, A. J. & BERNE, R. M. 2007. *Cardiovascular physiology,* Philadelphia, PA, Mosby Elsevier.

LI, H. Y., SALOMON, J. J., SHEPPARD, D. N., MALL, M. A. & GALIETTA, L. J. V. 2017. Bypassing CFTR dysfunction in cystic fibrosis with alternative pathways for anion transport. *Current Opinion in Pharmacology,* 34**,** 91-97.

LI, Y., ZAYDMAN, M. A., WU, D., SHI, J., GUAN, M., VIRGIN-DOWNEY, B. & CUI, J. 2011. KCNE1 enhances phosphatidylinositol 4,5-bisphosphate (PIP2) sensitivity of IKs to modulate channel activity. *Proc Natl Acad Sci U S A,* 108**,** 9095-100.

LIAO, M., CAO, E., JULIUS, D. & CHENG, Y. 2013. Structure of the TRPV1 ion channel determined by electron cryo-microscopy. *Nature,* 504**,** 107-12.

LIFSHITZ, L. M., CARMICHAEL, J. D., LAI, F. A., SORRENTINO, V., BELLVE, K., FOGARTY, K. E. & ZHUGE, R. 2011. Spatial organization of RYRs and BK channels underlying the activation of STOCs by Ca(2+) sparks in airway myocytes. *J Gen Physiol,* 138**,** 195-209.

LIM, N. K., LAM, A. K. & DUTZLER, R. 2016. Independent activation of ion conduction pores in the double-barreled calcium-activated chloride channel TMEM16A. *J Gen Physiol,* 148**,** 375-392.

LIN, M. J. & YU, B. P. 2018. Colonic Hypermotility in a Rat Model of Irritable Bowel Syndrome Is Associated with Upregulation of TMEM16A in Myenteric Plexus. *Digestive Diseases and Sciences,* 63**,** 3329-3338.

LIN, Y. C., BOONE, M., MEURIS, L., LEMMENS, I., VAN ROY, N., SOETE, A., REUMERS, J., MOISSE, M., PLAISANCE, S., DRMANAC, R., CHEN, J., SPELEMAN, F., LAMBRECHTS, D., VAN DE PEER, Y., TAVERNIER, J. & CALLEWAERT, N. 2014. Genome dynamics of the human embryonic kidney 293 lineage in response to cell biology manipulations. *Nat Commun,* 5**,** 4767.

LISAL, J. & MADUKE, M. 2009. Review. Proton-coupled gating in chloride channels. *Philos Trans R Soc Lond B Biol Sci,* 364**,** 181-7.

LITTLE, R., ZI, M., HAMMAD, S. K., NGUYEN, L., NJEGIC, A., KURUSAMY, S., PREHAR, S., ARMESILLA, A. L., NEYSES, L., AUSTIN, C. & CARTWRIGHT, E. J. 2017. Reduced expression of PMCA1 is associated with increased blood pressure with age which is preceded by remodelling of resistance arteries. *Aging Cell,* 16**,** 1104-1113.

LIU, D., YANG, D., HE, H., CHEN, X., CAO, T., FENG, X., MA, L., LUO, Z., WANG, L., YAN, Z., ZHU, Z. & TEPEL, M. 2009. Increased transient receptor potential canonical type 3 channels in vasculature from hypertensive rats. *Hypertension,* 53**,** 70-6.

LIU, F., CAO, Q. H., LU, D. J., LUO, B., LU, X. F., LUO, R. C. & WANG, X. G. 2015a. TMEM16A overexpression contributes to tumor invasion and poor prognosis of human gastric cancer through TGF-beta signaling. *Oncotarget,* 6**,** 11585-11599.

LIU, F. Y., ZHANG, Z., CSANADY, L., GADSBY, D. C. & CHEN, J. 2017. Molecular Structure of the Human CFTR Ion Channel. *Cell,* 169**,** 85-+.

LIU, J. C., CONKLIN, S. M., MANUCK, S. B., YAO, J. K. & MULDOON, M. F. 2011. Long-chain omega-3 fatty acids and blood pressure. *Am J Hypertens,* 24**,** 1121-6.

LIU, W., LU, M., LIU, B., HUANG, Y. & WANG, K. 2012. Inhibition of Ca(2+)-activated Cl(-) channel ANO1/TMEM16A expression suppresses tumor growth and invasiveness in human prostate carcinoma. *Cancer Lett,* 326**,** 41-51.

LIU, Y., ZHANG, H., HUANG, D., QI, J., XU, J., GAO, H., DU, X., GAMPER, N. & ZHANG, H. 2015b. Characterization of the effects of Cl(-) channel modulators on TMEM16A and bestrophin-1 Ca(2)(+) activated Cl(-) channels. *Pflugers Arch,* 467**,** 1417-1430.

LOEW, L. M. 2007. Where does all the PIP2 come from? *Journal of Physiology-London,* 582**,** 945-951.

LONGDEN, T. A. & NELSON, M. T. 2015. Vascular Inward Rectifier K+ Channels as External K+ Sensors in the Control of Cerebral Blood Flow. *Microcirculation,* 22**,** 183-196.

LOUSSOUARN, G., PARK, K. H., BELLOCQ, C., BARO, I., CHARPENTIER, F. & ESCANDE, D. 2003. Phosphatidylinositol-4,5-bisphosphate, PIP2, controls KCNQ1/KCNE1 voltage-gated potassium channels: a functional homology between voltage-gated and inward rectifier K+ channels. *Embo Journal,* 22**,** 5412-5421.

MA, K., WANG, H., YU, J., WEI, M. & XIAO, Q. 2017. New Insights on the Regulation of Ca(2+) -Activated Chloride Channel TMEM16A. *J Cell Physiol,* 232**,** 707-716.

MAGLEBY, R. L. 2003. Gating mechanism of BK (Slo1) channels: So near, yet so far. *Journal of General Physiology,* 121**,** 81-96.

MALVEZZI, M., CHALAT, M., JANJUSEVIC, R., PICOLLO, A., TERASHIMA, H., MENON, A. K. & ACCARDI, A. 2013. Ca2+-dependent phospholipid scrambling by a reconstituted TMEM16 ion channel. *Nat Commun,* 4**,** 2367.

MALYSZ, J., GIBBONS, S. J., SARAVANAPERUMAL, S. A., DU, P., EISENMAN, S. T., CAO, C. K., OH, U., SAUR, D., KLEIN, S., ORDOG, T. & FARRUGIA, G. 2017. Conditional genetic deletion of Ano1 in interstitial cells of Cajal impairs Ca2+ transients and slow waves in adult mouse small intestine. *American Journal of Physiology-Gastrointestinal and Liver Physiology,* 312**,** G228-G245.

MANOURY, B., ETHERIDGE, S. L., REID, J. & GURNEY, A. M. 2009. Organ culture mimics the effects of hypoxia on membrane potential, K(+) channels and vessel tone in pulmonary artery. *Br J Pharmacol,* 158**,** 848-61.

MANOURY, B., TAMULEVICIUTE, A. & TAMMARO, P. 2010. TMEM16A/anoctamin 1 protein mediates calcium-activated chloride currents in pulmonary arterial smooth muscle cells. *J Physiol,* 588**,** 2305-14.

MARCHAND, A., ABI-GERGES, A., SALIBA, Y., MERLET, E. & LOMPRE, A. M. 2012. Calcium signaling in vascular smooth muscle cells: from physiology to pathology. *Adv Exp Med Biol,* 740**,** 795-810.

MARIN, J. 1993. Mechanisms involved in the increased vascular resistance in hypertension. *J Auton Pharmacol,* 13**,** 127-76.

MARRINK, S. J., RISSELADA, H. J., YEFIMOV, S., TIELEMAN, D. P. & DE VRIES, A. H. 2007. The MARTINI force field: Coarse grained model for biomolecular simulations. *Journal of Physical Chemistry B,* 111**,** 7812-7824.

MARTIN, G. M., YOSHIOKA, C., REX, E. A., FAY, J. F., XIE, Q., WHORTON, M. R., CHEN, J. Z. & SHYNG, S. L. 2017. Cryo-EM structure of the ATP-sensitive potassium channel illuminates mechanisms of assembly and gating. *Elife,* 6.

MATCHKOV, V. V., AALKJAER, C. & NILSSON, H. 2005. Distribution of cGMP-dependent and cGMP-independent Ca2+-activated Cl- conductances in smooth muscle cells from different vascular beds and colon. *Pflugers Archiv-European Journal of Physiology,* 451**,** 371-379.

MATCHKOV, V. V., BOEDTKJER, D. M. & AALKJAER, C. 2015. The role of Ca^{2+} activated Cl^- channels in blood pressure control. *Curr Opin Pharmacol,* 21**,** 127-37.

MATCHKOV, V. V., BROEGGER, T., BOEDTKJER, D. M. B., LARSEN, P., PEDERSEN, F. S. & AALKJAER, C. 2009. BESTROPHIN-3-ASSOCIATED Ca2+-ACTIVATED Cl- CHANNEL

IS IMPORTANT FOR THE RHYTHMIC BUT NOT THE TONIC ACTIVITIES IN THE VASCULAR WALL. *Journal of Physiological Sciences,* 59**,** 412-412.

MATCHKOV, V. V., DAM, V. S., BODTKJER, D. M. B. & AALKJAER, C. 2013. Transport and Function of Chloride in Vascular Smooth Muscles. *Journal of Vascular Research,* 50**,** 69-87.

MATCHKOV, V. V., KUDRYAVTSEVA, O. & AALKJAER, C. 2012. Intracellular Ca(2)(+) signalling and phenotype of vascular smooth muscle cells. *Basic Clin Pharmacol Toxicol,* 110**,** 42-8.

MATHAR, I., VENNEKENS, R., MEISSNER, M., KEES, F., VAN DER MIEREN, G., CAMACHO LONDONO, J. E., UHL, S., VOETS, T., HUMMEL, B., VAN DEN BERGH, A., HERIJGERS, P., NILIUS, B., FLOCKERZI, V., SCHWEDA, F. & FREICHEL, M. 2010. Increased catecholamine secretion contributes to hypertension in TRPM4-deficient mice. *J Clin Invest,* 120**,** 3267-79.

MATSUDA, H. 1991. Magnesium Gating of the Inwardly Rectifying K+ Channel. *Annual Review of Physiology,* 53**,** 289-298.

MATSUDA, T., ARAKAWA, N., TAKUMA, K., KISHIDA, Y., KAWASAKI, Y., SAKAUE, M., TAKAHASHI, K., TAKAHASHI, T., SUZUKI, T., OTA, T., HAMANO-TAKAHASHI, A., ONISHI, M., TANAKA, Y., KAMEO, K. & BABA, A. 2001. SEA0400, a novel and selective inhibitor of the Na+-Ca2+ exchanger, attenuates reperfusion injury in the in vitro and in vivo cerebral ischemic models. *Journal of Pharmacology and Experimental Therapeutics,* 298**,** 249-256.

MATTHEW, A., SHMYGOL, A. & WRAY, S. 2004. Ca2+ entry, efflux and release in smooth muscle. *Biol Res,* 37**,** 617-24.

MCFADZEAN, I. & GIBSON, A. 2002. The developing relationship between receptor-operated and store-operated calcium channels in smooth muscle. *British Journal of Pharmacology,* 135**,** 1-13.

MCGUIGAN, J. A. S. & STUMPFF, F. 2013. Calculated and measured [Ca2+] in buffers used to calibrate Ca2+ macroelectrodes. *Analytical Biochemistry,* 436**,** 29-35.

MCLAUGHLIN, S., WANG, J., GAMBHIR, A. & MURRAY, D. 2002. PIP(2) and proteins: interactions, organization, and information flow. *Annu Rev Biophys Biomol Struct,* 31**,** 151-75.

MEYER, J. W., FLAGELLA, M., SUTLIFF, R. L., LORENZ, J. N., NIEMAN, M. L., WEBER, C. S., PAUL, R. J. & SHULL, G. E. 2002. Decreased blood pressure and vascular smooth muscle tone in mice lacking basolateral Na(+)-K(+)-2Cl(-) cotransporter. *Am J Physiol Heart Circ Physiol,* 283**,** H1846-55.

MILEDI, R. 1982. A calcium-dependent transient outward current in Xenopus laevis oocytes. *Proc R Soc Lond B Biol Sci,* 215**,** 491-7.

MILLER, A. N., VAISEY, G. & LONG, S. B. 2019. Molecular mechanisms of gating in the calcium-activated chloride channel bestrophin. *Elife,* 8.

MILLER, P. E., VAN ELSWYK, M. & ALEXANDER, D. D. 2014. Long-chain omega-3 fatty acids eicosapentaenoic acid and docosahexaenoic acid and blood pressure: a meta-analysis of randomized controlled trials. *Am J Hypertens,* 27**,** 885-96.

MILLMAN, K. J. & AIVAZIS, M. 2011. Python for Scientists and Engineers. *Computing in Science & Engineering,* 13**,** 9-12.

MILNER, R. E., BAKSH, S., SHEMANKO, C., CARPENTER, M. R., SMILLIE, L., VANCE, J. E., OPAS, M. & MICHALAK, M. 1991. Calreticulin, and not calsequestrin, is the major

calcium binding protein of smooth muscle sarcoplasmic reticulum and liver endoplasmic reticulum. *J Biol Chem,* 266**,** 7155-65.

MINER, K., MOHN, D., ELLIOTT, R., POWERS, D., CHEN, J., LIU, B., WANG, P., GAIDA, K., HOCHHEIMER, A., LIU, L., HENCKELS, K., LABITZKE, K. & SULLIVAN, J. K. 2017. The Anthelminthic Niclosamide And Related Compounds Represent Potent Tmem16a Antagonists That Fully Relax Mouse And Human Airway Rings. *American Journal of Respiratory and Critical Care Medicine,* 195.

MINIHANE, A. M., ARMAH, C. K., MILES, E. A., MADDEN, J. M., CLARK, A. B., CASLAKE, M. J., PACKARD, C. J., KOFLER, B. M., LIETZ, G., CURTIS, P. J., MATHERS, J. C., WILLIAMS, C. M. & CALDER, P. C. 2016. Consumption of Fish Oil Providing Amounts of Eicosapentaenoic Acid and Docosahexaenoic Acid That Can Be Obtained from the Diet Reduces Blood Pressure in Adults with Systolic Hypertension: A Retrospective Analysis. *Journal of Nutrition,* 146**,** 516-523.

MINKE, B. 2010. The history of the Drosophila TRP channel: the birth of a new channel superfamily. *J Neurogenet,* 24**,** 216-33.

MISSIAEN, L., DESMEDT, H., DROOGMANS, G., HIMPENS, B. & CASTEELS, R. 1992. Calcium-Ion Homeostasis in Smooth-Muscle. *Pharmacology & Therapeutics,* 56**,** 191-231.

MOHANAKUMAR, S., MAJGAARD, J., TELINIUS, N., KATBALLE, N., PAHLE, E., HJORTDAL, V. & BOEDTKJER, D. 2018. Spontaneous and alpha-adrenoceptor-induced contractility in human collecting lymphatic vessels require chloride. *Am J Physiol Heart Circ Physiol,* 315**,** H389-H401.

MOLLEMAN, A. 2002. *Patch clamping : an introductory guide to patch clamp electrophysiology,* New York, J. Wiley.

MONCADA, S. & VANE, J. R. 1979. The role of prostacyclin in vascular tissue. *Fed Proc,* 38**,** 66-71.

MONTICELLI, L., KANDASAMY, S. K., PERIOLE, X., LARSON, R. G., TIELEMAN, D. P. & MARRINK, S. J. 2008. The MARTINI coarse-grained force field: Extension to proteins. *Journal of Chemical Theory and Computation,* 4**,** 819-834.

MORI, T. A., BAO, D. Q., BURKE, V., PUDDEY, I. B. & BEILIN, L. J. 1999. Docosahexaenoic acid but not eicosapentaenoic acid lowers ambulatory blood pressure and heart rate in humans. *Hypertension,* 34**,** 253-260.

MORI, T. A., WATTS, G. F., BURKE, V., HILME, E., PUDDEY, I. B. & BEILIN, L. J. 2000. Differential effects of eicosapentaenoic acid and docosahexaenoic acid on vascular reactivity of the forearm microcirculation in hyperlipidemic, overweight men. *Circulation,* 102**,** 1264-9.

MORRIS, M. C., SACKS, F. & ROSNER, B. 1993. Does Fish-Oil Lower Blood-Pressure - a Metaanalysis of Controlled Trials. *Circulation,* 88**,** 523-533.

MULIER, M., VRIENS, J. & VOETS, T. 2017. TRP channel pores and local calcium signals. *Cell Calcium,* 66**,** 19-24.

MULVANY, M. J. & HALPERN, W. 1977. Contractile Properties of Small Arterial Resistance Vessels in Spontaneously Hypertensive and Normotensive Rats. *Circulation Research,* 41**,** 19-26.

MURPHY, M. G. 1990. Dietary Fatty-Acids and Membrane-Protein Function. *Journal of Nutritional Biochemistry,* 1**,** 68-79.

NAMKUNG, W., PHUAN, P. W. & VERKMAN, A. S. 2011a. TMEM16A inhibitors reveal TMEM16A as a minor component of calcium-activated chloride channel conductance in airway and intestinal epithelial cells. *J Biol Chem,* 286**,** 2365-74.

NAMKUNG, W., PHUAN, P. W. & VERKMAN, A. S. 2011b. TMEM16A Inhibitors Reveal TMEM16A as a Minor Component of Calcium-activated Chloride Channel Conductance in Airway and Intestinal Epithelial Cells. *Journal of Biological Chemistry,* 286**,** 2365-2374.

NAMKUNG, W., THIAGARAJAH, J. R., PHUAN, P. W. & VERKMAN, A. S. 2010. Inhibition of Ca2+-activated Cl- channels by gallotannins as a possible molecular basis for health benefits of red wine and green tea. *Faseb Journal,* 24**,** 4178-4186.

NAMKUNG, W., YAO, Z., FINKBEINER, W. E. & VERKMAN, A. S. 2011c. Small-molecule activators of TMEM16A, a calcium-activated chloride channel, stimulate epithelial chloride secretion and intestinal contraction. *FASEB J,* 25**,** 4048-62.

NARAGHI, M. 1997. T-jump study of calcium binding kinetics of calcium chelators. *Cell Calcium,* 22**,** 255-268.

NARAYAN, O., PARKER, K. H., DAVIES, J. E., HUGHES, A. D., MEREDITH, I. T. & CAMERON, J. D. 2017. Reservoir pressure analysis of aortic blood pressure: an in-vivo study at five locations in humans. *J Hypertens,* 35**,** 2025-2033.

NEHER, E. 1992. Correction for liquid junction potentials in patch clamp experiments. *Methods Enzymol,* 207**,** 123-31.

NELSON, M. T., CHENG, H., RUBART, M., SANTANA, L. F., BONEV, A. D., KNOT, H. J. & LEDERER, W. J. 1995. Relaxation of arterial smooth muscle by calcium sparks. *Science,* 270**,** 633-7.

NELSON, M. T., CONWAY, M. A., KNOT, H. J. & BRAYDEN, J. E. 1997. Chloride channel blockers inhibit myogenic tone in rat cerebral arteries. *J Physiol,* 502 (Pt 2)**,** 259-64.

NELSON, M. T., HUANG, Y., BRAYDEN, J. E., HESCHELER, J. & STANDEN, N. B. 1990a. Arterial Dilations in Response to Calcitonin Gene-Related Peptide Involve Activation of K+ Channels. *Nature,* 344**,** 770-773.

NELSON, M. T., PATLAK, J. B., WORLEY, J. F. & STANDEN, N. B. 1990b. Calcium channels, potassium channels, and voltage dependence of arterial smooth muscle tone. *Am J Physiol,* 259**,** C3-18.

NELSON, M. T. & QUAYLE, J. M. 1995. Physiological roles and properties of potassium channels in arterial smooth muscle. *Am J Physiol,* 268**,** C799-822.

NESTEL, P., SHIGE, H., POMEROY, S., CEHUN, M., ABBEY, M. & RAEDERSTORFF, D. 2002. The n-3 fatty acids eicosapentaenoic acid and docosahexaenoic acid increase systemic arterial compliance in humans. *American Journal of Clinical Nutrition,* 76**,** 326-330.

NEYLON, C. B., LANG, R. J., FU, Y., BOBIK, A. & REINHART, P. H. 1999. Molecular cloning and characterization of the intermediate-conductance Ca2+-activated K+ channel in vascular smooth muscle - Relationship between K-Ca channel diversity and smooth muscle cell function. *Circulation Research,* 85**,** E33-E43.

NGUYEN, Q. D., PETERS, E., WASSEF, A., DESMARAIS, P., RÉMILLARD-LABROSSE, D. & TREMBLAY-GRAVEL, M. 2018. Evolution of Age and Female Representation in the Most-Cited Randomized Controlled Trials of Cardiology of the Last 20 Years. *Circ Cardiovasc Qual Outcomes,* 11**,** e004713.

NILIUS, B. & DROOGMANS, G. 2001. Ion channels and their functional role in vascular endothelium. *Physiological Reviews,* 81**,** 1415-1459.

NOMA, A. 1983. ATP-regulated K+ channels in cardiac muscle. *Nature,* 305**,** 147-8.

NOORANI, M. M. Z., NOEL, R. C. & MARRELLI, S. P. 2011. Upregulated TRPC3 and downregulated TRPC1 channel expression during hypertension is associated with increased vascular contractility in rat. *Frontiers in Physiology,* 2.

OH, S. J., HWANG, S. J., JUNG, J., YU, K., KIM, J., CHOI, J. Y., HARTZELL, H. C., ROH, E. J. & LEE, C. J. 2013. MONNA, a potent and selective blocker for transmembrane protein with unknown function 16/anoctamin-1. *Mol Pharmacol,* 84**,** 726-35.

OH, U. & JUNG, J. 2016. Cellular functions of TMEM16/anoctamin. *Pflugers Arch,* 468**,** 443-53.

OHTANI, Y., IRIE, T., UEKAMA, K., FUKUNAGA, K. & PITHA, J. 1989. Differential effects of alpha-, beta- and gamma-cyclodextrins on human erythrocytes. *Eur J Biochem,* 186**,** 17-22.

OKAMURA, Y., MURATA, Y. & IWASAKI, H. 2009. Voltage-sensing phosphatase: actions and potentials. *Journal of Physiology-London,* 587**,** 513-520.

ORALLO, F. 1996. Regulation of cytosolic calcium levels in vascular smooth muscle. *Pharmacol Ther,* 69**,** 153-71.

ORKIN, S. 1990. Molecular-Cloning - a Laboratory Manual, 2nd Edition - Sambrook,J, Fritsch,Ef, Maniatis,T. *Nature,* 343**,** 604-605.

ORLOV, S. N., KOLTSOVA, S. V., TREMBLAY, J., BASKAKOV, M. B. & HAMET, P. 2012. NKCC1 and hypertension: role in the regulation of vascular smooth muscle contractions and myogenic tone. *Ann Med,* 44 Suppl 1**,** S111-8.

ORLOV, S. N., TREMBLAY, J. & HAMET, P. 1996. Bumetanide-sensitive ion fluxes in vascular smooth muscle cells: lack of functional Na+, K+, 2 Cl- cotransport. *J Membr Biol,* 153**,** 125-35.

OUSINGSAWAT, J., MARTINS, J. R., SCHREIBER, R., ROCK, J. R., HARFE, B. D. & KUNZELMANN, K. 2009. Loss of TMEM16A causes a defect in epithelial Ca2+-dependent chloride transport. *J Biol Chem,* 284**,** 28698-703.

PACAUD, P., LOIRAND, G., MIRONNEAU, C. & MIRONNEAU, J. 1989. Noradrenaline activates a calcium-activated chloride conductance and increases the voltage-dependent calcium current in cultured single cells of rat portal vein. *Br J Pharmacol,* 97**,** 139-46.

PALMER, R. M., FERRIGE, A. G. & MONCADA, S. 1987. Nitric oxide release accounts for the biological activity of endothelium-derived relaxing factor. *Nature,* 327**,** 524-6.

PANTAZIS, A. & OLCESE, R. 2016. Biophysics of BK Channel Gating. *Int Rev Neurobiol,* 128**,** 1-49.

PAPASSOTIRIOU, J., EGGERMONT, J., DROOGMANS, G. & NILIUS, B. 2001. Ca(2+)-activated Cl- channels in Ehrlich ascites tumor cells are distinct from mCLCA1, 2 and 3. *Pflugers Arch,* 442**,** 273-9.

PAPP, R., NAGARAJ, C., ZABINI, D., NAGY, B. M., LENGYEL, M., MAURER, D. S., SHARMA, N., EGEMNAZAROV, B., KOVACS, G., KWAPISZEWSKA, G., MARSH, L. M., HRZENJAK, A., HOFLER, G., DIDIASOVA, M., WYGRECKA, M., SIEVERS, L. K., SZUCS, P., ENYEDI, P., GHANIM, B., KLEPETKO, W., OLSCHEWSKI, H. & OLSCHEWSKI, A. 2019. Targeting TMEM16A to reverse vasoconstriction and

remodelling in idiopathic pulmonary arterial hypertension. *European Respiratory Journal,* 53.

PARK, W. S., HAN, J. & EARM, Y. E. 2008. Physiological role of inward rectifier K(+) channels in vascular smooth muscle cells. *Pflugers Arch,* 457**,** 137-47.

PARK, W. S., KO, J. H., KIM, N., SON, Y. K., KANG, S. H., WARDA, M., JUNG, I. D., PARK, Y. M. & HAN, J. 2007. Increased inhibition of inward rectifier K+ channels by angiotensin II in small-diameter coronary artery of isoproterenol-induced hypertrophied model. *Arteriosclerosis Thrombosis and Vascular Biology,* 27**,** 1768-1775.

PATEL, S. & KILPATRICK, B. S. 2018. Two-pore channels and disease. *Biochim Biophys Acta Mol Cell Res,* 1865**,** 1678-1686.

PAULINO, C., KALIENKOVA, V., LAM, A. K. M., NELDNER, Y. & DUTZLER, R. 2017. Activation mechanism of the calcium-activated chloride channel TMEM16A revealed by cryo-EM. *Nature,* 552**,** 421-425.

PECHANOVA, O., DOBESOVA, Z., CEJKA, J., KUNES, J. & ZICHA, J. 2004. Vasoactive systems in L-NAME hypertension: the role of inducible nitric oxide synthase. *J Hypertens,* 22**,** 167-73.

PEDEMONTE, N. & GALIETTA, L. J. 2014. Structure and Function of TMEM16 Proteins (Anoctamins). *Physiol Rev. ,* 94**,** 419-59.

PELTOMAA, E., JOHNSON, M. D. & TAIPALE, S. J. 2017. Marine Cryptophytes Are Great Sources of EPA and DHA. *Mar Drugs,* 16.

PENG, H., MATCHKOV, V., IVARSEN, A., AALKJAER, C. & NILSSON, H. 2001. Hypothesis for the initiation of vasomotion. *Circ Res,* 88**,** 810-5.

PEPE, S., BOGDANOV, K., HALLAQ, H., SPURGEON, H., LEAF, A. & LAKATTA, E. 1994. Omega-3 Polyunsaturated Fatty-Acid Modulates Dihydropyridine Effects on L-Type Ca2+ Channels, Cytosolic Ca2+, and Contraction in Adult-Rat Cardiac Myocytes. *Proceedings of the National Academy of Sciences of the United States of America,* 91**,** 8832-8836.

PEREZ, G. J., BONEV, A. D. & NELSON, M. T. 2001. Micromolar Ca(2+) from sparks activates Ca(2+)-sensitive K(+) channels in rat cerebral artery smooth muscle. *Am J Physiol Cell Physiol,* 281**,** C1769-75.

PETERS, C. J., YU, H., TIEN, J., JAN, Y. N., LI, M. & JAN, L. Y. 2015. Four basic residues critical for the ion selectivity and pore blocker sensitivity of TMEM16A calcium-activated chloride channels. *Proc Natl Acad Sci U S A,* 112**,** 3547-52.

PICOLLO, A., MALVEZZI, M. & ACCARDI, A. 2015. TMEM16 proteins: unknown structure and confusing functions. *J Mol Biol,* 427**,** 94-105.

PIPER, A. S. & LARGE, W. A. 2004. Single cGMP-activated Ca2+-dependent Cl- channels in rat mesenteric artery smooth muscle cells. *Journal of Physiology-London,* 555**,** 397-408.

PITMAN, M. C., SUITS, F., MACKERELL, A. D., JR. & FELLER, S. E. 2004. Molecular-level organization of saturated and polyunsaturated fatty acids in a phosphatidylcholine bilayer containing cholesterol. *Biochemistry,* 43**,** 15318-28.

PITT, S. J., REILLY-O'DONNELL, B. & SITSAPESAN, R. 2016. Exploring the biophysical evidence that mammalian two-pore channels are NAADP-activated calcium-permeable channels. *Journal of Physiology-London,* 594**,** 4171-4179.

POMPERMAYER, K., SOUZA, D. G., LARA, G. G., SILVEIRA, K. D., CASSALI, G. D., ANDRADE, A. A., BONJARDIM, C. A., PASSAGLIO, K. T., ASSREUY, J., CUNHA, F. Q., VIEIRA, M.

A. & TEIXEIRA, M. M. 2005. The ATP-sensitive potassium channel blocker glibenclamide prevents renal ischemia/reperfusion injury in rats. *Kidney Int,* 67**,** 1785-96.

POPESCU, L. M., GHERGHICEANU, M., MANDACHE, E. & CRETOIU, D. 2006. Caveolae in smooth muscles: nanocontacts. *J Cell Mol Med,* 10**,** 960-90.

PRADHAN, R. K. & CHAKRAVARTHY, V. S. 2011. Informational dynamics of vasomotion in microvascular networks: a review. *Acta Physiol (Oxf),* 201**,** 193-218.

PRITCHARD, H. A., LEBLANC, N., ALBERT, A. P. & GREENWOOD, I. A. 2014. Inhibitory role of phosphatidylinositol 4,5-bisphosphate on TMEM16A-encoded calcium-activated chloride channels in rat pulmonary artery. *Br J Pharmacol,* 171**,** 4311-21.

PROKS, P., DE WET, H. & ASHCROFT, F. M. 2010. Activation of the K(ATP) channel by Mg-nucleotide interaction with SUR1. *J Gen Physiol,* 136**,** 389-405.

PUTNEY, J. W., STEINCKWICH-BESANCON, N., NUMAGA-TOMITA, T., DAVIS, F. M., DESAI, P. N., D'AGOSTIN, D. M., WU, S. & BIRD, G. S. 2017. The functions of store-operated calcium channels. *Biochim Biophys Acta Mol Cell Res,* 1864**,** 900-906.

QI, H., HUANG, Y., RUDIGER, S. & SHUAI, J. 2014. Frequency and relative prevalence of calcium blips and puffs in a model of small IP(3)R clusters. *Biophys J,* 106**,** 2353-63.

QIAN, L. L., SUN, M. Q., WANG, R. X., LU, T., WU, Y., DANG, S. P., TANG, X., JI, Y., LIU, X. Y., ZHAO, X. X., WANG, W., CHAI, Q., PAN, M., YI, F., ZHANG, D. M. & LEE, H. C. 2018. Mechanisms of BK Channel Activation by Docosahexaenoic Acid in Rat Coronary Arterial Smooth Muscle Cells. *Front Pharmacol,* 9**,** 223.

RAFEEQ, M. M. & MURAD, H. A. S. 2017. Cystic fibrosis: current therapeutic targets and future approaches. *Journal of Translational Medicine,* 15.

RAMEL, A., MARTINEZ, J. A., KIELY, M., BANDARRA, N. M. & THORSDOTTIR, I. 2010. Moderate consumption of fatty fish reduces diastolic blood pressure in overweight and obese European young adults during energy restriction. *Nutrition,* 26**,** 168-74.

RAMSTEDT, B. & SLOTTE, J. P. 2002. Membrane properties of sphingomyelins. *FEBS Lett,* 531**,** 33-7.

RICHIERI, G. V., OGATA, R. T. & KLEINFELD, A. M. 1992. A Fluorescently Labeled Intestinal Fatty-Acid Binding-Protein - Interactions with Fatty-Acids and Its Use in Monitoring Free Fatty-Acids. *Journal of Biological Chemistry,* 267**,** 23495-23501.

ROBERT, R., NOREZ, C. & BECQ, F. 2005. Disruption of CFTR chloride channel alters mechanical properties and cAMP-dependent Cl- transport of mouse aortic smooth muscle cells. *Journal of Physiology-London,* 568**,** 483-495.

ROBERT, R., SAVINEAU, J. P., NOREZ, C., BECQ, F. & GUIBERT, C. 2007. Expression and function of cystic fibrosis transmembrane conductance regulator in rat intrapulmonary arteries. *European Respiratory Journal,* 30**,** 857-864.

ROBERT, R., THOREAU, V., NOREZ, C., CANTEREAU, A., KITZIS, A., METTEY, Y., ROGIER, C. & BECQ, F. 2004. Regulation of the cystic fibrosis transmembrane conductance regulator channel by beta-adrenergic agonists and vasoactive intestinal peptide in rat smooth muscle cells and its role in vasorelaxation. *Journal of Biological Chemistry,* 279**,** 21160-21168.

ROCK, J. R., FUTTNER, C. R. & HARFE, B. D. 2008. The transmembrane protein TMEM16A is required for normal development of the murine trachea. *Developmental Biology,* 321**,** 141-149.

RODRIGUEZ-MENCHACA, A. A., ADNEY, S. K., TANG, Q. Y., MENG, X. Y., ROSENHOUSE-DANTSKER, A., CUI, M. & LOGOTHETIS, D. E. 2012. PIP2 controls voltage-sensor movement and pore opening of Kv channels through the S4-S5 linker. *Proceedings of the National Academy of Sciences of the United States of America,* 109**,** E2399-E2408.

RORSMAN, N. J. G., TA, C. M., GARNETT, H., SWIETACH, P. & TAMMARO, P. 2018. Defining the ionic mechanisms of optogenetic control of vascular tone by channelrhodopsin-2. *Br J Pharmacol,* 175**,** 2028-2045.

ROSASCO, M. G. & GORDON, S. E. 2018. TRP Channels What Do They Look Like? *Neurobiology of Trp Channels***,** 1-9.

ROSEN, D., LEWIS, A. M., MIZOTE, A., THOMAS, J. M., ALEY, P. K., VASUDEVAN, S. R., PARKESH, R., GALIONE, A., IZUMI, M., GANESAN, A. & CHURCHILL, G. C. 2009. Analogues of the Nicotinic Acid Adenine Dinucleotide Phosphate (NAADP) Antagonist Ned-19 Indicate Two Binding Sites on the NAADP Receptor. *Journal of Biological Chemistry,* 284**,** 34930-34934.

ROYAL, A. A., TINKER, A. & HARMER, S. C. 2017. Phosphatidylinositol-4,5-bisphosphate is required for KCNQ1/KCNE1 channel function but not anterograde trafficking. *Plos One,* 12.

SAGHEDDU, C., BOCCACCIO, A., DIBATTISTA, M., MONTANI, G., TIRINDELLI, R. & MENINI, A. 2010. Calcium concentration jumps reveal dynamic ion selectivity of calcium-activated chloride currents in mouse olfactory sensory neurons and TMEM16b-transfected HEK 293T cells. *J Physiol,* 588**,** 4189-204.

SALEH, S. N., ALBERT, A. P. & LARGE, W. A. 2009. Obligatory role for phosphatidylinositol 4,5-bisphosphate in activation of native TRPC1 store-operated channels in vascular myocytes. *Journal of Physiology-London,* 587**,** 531-540.

SAMAHA, F. F., HEINEMAN, F. W., INCE, C., FLEMING, J. & BALABAN, R. S. 1992. Atp-Sensitive Potassium Channel Is Essential to Maintain Basal Coronary Vascular Tone Invivo. *American Journal of Physiology,* 262**,** C1220-C1227.

SANDERS, K. M. 1996. A case for interstitial cells of Cajal as pacemakers and mediators of neurotransmission in the gastrointestinal tract. *Gastroenterology,* 111**,** 492-515.

SARAVANAN, P., DAVIDSON, N. C., SCHMIDT, E. B. & CALDER, P. C. 2010. Cardiovascular effects of marine omega-3 fatty acids. *Lancet,* 376**,** 540-50.

SARKAR, G. & SOMMER, S. S. 1990. The "megaprimer" method of site-directed mutagenesis. *Biotechniques,* 8**,** 404-7.

SAUTER, D., NOVAK, I., PEDERSEN, S., LARSEN, E. & HOFFMANN, E. 2014. TMEM16A (ANO1) in human pancreatic ductal adenocarcinoma (PDAC) cells. *Acta Physiologica,* 210**,** 216-216.

SCHATZMANN, H. J. 1966. ATP-dependent Ca++-extrusion from human red cells. *Experientia,* 22**,** 364-5.

SCHIEBELHUT, L. M., ABBOUD, S. S., GOMEZ DAGLIO, L. E., SWIFT, H. F. & DAWSON, M. N. 2017. A comparison of DNA extraction methods for high-throughput DNA analyses. *Mol Ecol Resour,* 17**,** 721-729.

SCHNITZLER, M. M. Y., DERST, C., DAUT, J. & PREISIG-MULLER, R. 2000. ATP-sensitive potassium channels in capillaries isolated from guinea-pig heart. *Journal of Physiology-London,* 525**,** 307-317.

SCHREIBER, R., ULIYAKINA, I., KONGSUPHOL, P., WARTH, R., MIRZA, M., MARTINS, J. R. & KUNZELMANN, K. 2010. Expression and function of epithelial anoctamins. *J Biol Chem,* 285**,** 7838-45.

SCHROEDER, B. C., CHENG, T., JAN, Y. N. & JAN, L. Y. 2008. Expression cloning of TMEM16A as a calcium-activated chloride channel subunit. *Cell,* 134**,** 1019-29.

SCHUBERT, R., LIDINGTON, D. & BOLZ, S. S. 2008. The emerging role of Ca2+ sensitivity regulation in promoting myogenic vasoconstriction. *Cardiovasc Res,* 77**,** 8-18.

SCUDIERI, P., SONDO, E., FERRERA, L. & GALIETTA, L. J. V. 2012. The anoctamin family: TMEM16A and TMEM16B as calcium-activated chloride channels. *Experimental Physiology,* 97**,** 177-183.

SEINO, S. & MIKI, T. 2003. Physiological and pathophysiological roles of ATP-sensitive K+ channels. *Prog Biophys Mol Biol,* 81**,** 133-76.

SEO, Y., LEE, H. K., PARK, J., JEON, D. K., JO, S., JO, M. & NAMKUNG, W. 2016. Ani9, A Novel Potent Small-Molecule ANO1 Inhibitor with Negligible Effect on ANO2. *PLoS One,* 11**,** e0155771.

SEVERINI, A. & MORGAN, A. R. 1991. An Assay for Proteinases and Their Inhibitors Based on DNA Ethidium-Bromide Fluorescence. *Analytical Biochemistry,* 193**,** 83-89.

SHAIKH, S. R., KINNUN, J. J., LENG, X. L., WILLIAMS, J. A. & WASSALL, S. R. 2015. How polyunsaturated fatty acids modify molecular organization in membranes: Insight from NMR studies of model systems. *Biochimica Et Biophysica Acta-Biomembranes,* 1848**,** 211-219.

SHARMA, A. & JANIS, L. S. 1991. Lipoprotein-cyclodextrin interaction. *Clin Chim Acta,* 199**,** 129-37.

SHERIDAN, J. T., WORTHINGTON, E. N., YU, K., GABRIEL, S. E., HARTZELL, H. C. & TARRAN, R. 2011. Characterization of the oligomeric structure of the Ca(2+)-activated Cl- channel Ano1/TMEM16A. *J Biol Chem,* 286**,** 1381-8.

SHI, Z. Z., SHANG, L., JIANG, Y. Y., HAO, J. J., ZHANG, Y., ZHANG, T. T., LIN, D. C., LIU, S. G., WANG, B. S., GONG, T., ZHAN, Q. M. & WANG, M. R. 2013. Consistent and Differential Genetic Aberrations between Esophageal Dysplasia and Squamous Cell Carcinoma Detected By Array Comparative Genomic Hybridization. *Clinical Cancer Research,* 19**,** 5867-5878.

SIDDIQUI, R. A., HARVEY, K. A. & ZALOGA, G. P. 2008. Modulation of enzymatic activities by n-3 polyunsaturated fatty acids to support cardiovascular health. *Journal of Nutritional Biochemistry,* 19**,** 417-437.

SIMONS, K. & EHEHALT, R. 2002. Cholesterol, lipid rafts, and disease. *Journal of Clinical Investigation,* 110**,** 597-603.

SIMONS, K. & TOOMRE, D. 2000. Lipid rafts and signal transduction. *Nat Rev Mol Cell Biol,* 1**,** 31-9.

SINGER, S. J. & NICOLSON, G. L. 1972. The fluid mosaic model of the structure of cell membranes. *Science,* 175**,** 720-31.

SISCOVICK, D. S., BARRINGER, T. A., FRETTS, A. M., WU, J. H., LICHTENSTEIN, A. H., COSTELLO, R. B., KRIS-ETHERTON, P. M., JACOBSON, T. A., ENGLER, M. B., ALGER, H. M., APPEL, L. J., MOZAFFARIAN, D., AMERICAN HEART ASSOCIATION NUTRITION COMMITTEE OF THE COUNCIL ON, L., CARDIOMETABOLIC, H.,

COUNCIL ON, E., PREVENTION, COUNCIL ON CARDIOVASCULAR DISEASE IN THE, Y., COUNCIL ON, C., STROKE, N. & COUNCIL ON CLINICAL, C. 2017. Omega-3 Polyunsaturated Fatty Acid (Fish Oil) Supplementation and the Prevention of Clinical Cardiovascular Disease: A Science Advisory From the American Heart Association. *Circulation,* 135**,** e867-e884.

SISCOVICK, D. S., RAGHUNATHAN, T. E., KING, I., WEINMANN, S., BOVBJERG, V. E., KUSHI, L., COBB, L. A., COPASS, M. K., PSATY, B. M., LEMAITRE, R., RETZLAFF, B. & KNOPP, R. H. 2000. Dietary intake of long-chain n-3 polyunsaturated fatty acids and the risk of primary cardiac arrest. *American Journal of Clinical Nutrition,* 71**,** 208s-212s.

SMITH, J. M. & JONES, A. W. 1985. Calcium-dependent fluxes of potassium-42 and chloride-36 during norepinephrine activation of rat aorta. *Circ Res,* 56**,** 507-16.

SMITH, K. J., CHADBURN, A. J., ADOMAVICIENE, A., MINORETTI, P., VIGNALI, L., EMANUELE, E. & TAMMARO, P. 2013. Coronary spasm and acute myocardial infarction due to a mutation (V734I) in the nucleotide binding domain 1 of ABCC9. *International Journal of Cardiology,* 168**,** 3506-3513.

SMITH, P. D., BRETT, S. E., LUYKENAAR, K. D., SANDOW, S. L., MARRELLI, S. P., VIGMOND, E. J. & WELSH, D. G. 2008. K-IR channels function as electrical amplifiers in rat vascular smooth muscle. *Journal of Physiology-London,* 586**,** 1147-1160.

SOMLYO, A. P., WU, X., WALKER, L. A. & SOMLYO, A. V. 1999. Pharmacomechanical coupling: the role of calcium, G-proteins, kinases and phosphatases. *Rev Physiol Biochem Pharmacol,* 134**,** 201-34.

SONES, W. R., DAVIS, A. J., LEBLANC, N. & GREENWOOD, I. A. 2010. Cholesterol depletion alters amplitude and pharmacology of vascular calcium-activated chloride channels. *Cardiovascular Research,* 87**,** 476-484.

SONG, Y., GAO, J., GUAN, L., CHEN, X., GAO, J. & WANG, K. 2018. Inhibition of ANO1/TMEM16A induces apoptosis in human prostate carcinoma cells by activating TNF-alpha signaling. *Cell Death Dis,* 9**,** 703.

SONI, S. P., LOCASCIO, D. S., LIU, Y. D., WILLIAMS, J. A., BITTMAN, R., STILLWELL, W. & WASSALL, S. R. 2008. Docosahexaenoic acid enhances segregation of lipids between raft and nonraft domains: H-2-NMR study. *Biophysical Journal,* 95**,** 203-214.

SPRUCE, A. E., STANDEN, N. B. & STANFIELD, P. R. 1987. Studies of the unitary properties of adenosine-5'-triphosphate-regulated potassium channels of frog skeletal muscle. *J Physiol,* 382**,** 213-36.

STAFFORD, N., WILSON, C., OCEANDY, D., NEYSES, L. & CARTWRIGHT, E. J. 2017. The Plasma Membrane Calcium Atpases and Their Role as Major New Players in Human Disease. *Physiological Reviews,* 97**,** 1089-1125.

STANDEN, N. B., QUAYLE, J. M., DAVIES, N. W., BRAYDEN, J. E., HUANG, Y. & NELSON, M. T. 1989. Hyperpolarizing vasodilators activate ATP-sensitive K+ channels in arterial smooth muscle. *Science,* 245**,** 177-80.

STANSFELD, P. J. & SANSOM, M. S. P. 2011. From Coarse Grained to Atomistic: A Serial Multiscale Approach to Membrane Protein Simulations. *Journal of Chemical Theory and Computation,* 7**,** 1157-1166.

STILLWELL, W. & WASSALL, S. R. 2003. Docosahexaenoic acid: membrane properties of a unique fatty acid. *Chem Phys Lipids,* 126**,** 1-27.

STREGE, P. R., GIBBONS, S. J., MAZZONE, A., BERNARD, C. E., BEYDER, A. & FARRUGIA, G. 2017. EAVK segment "c" sequence confers Ca(2+)-dependent changes to the kinetics of full-length human Ano1. *Am J Physiol Gastrointest Liver Physiol,* 312**,** G572-G579.

STRIESSNIG, J., ORTNER, N. J. & PINGGERA, A. 2015. Pharmacology of L-type Calcium Channels: Novel Drugs for Old Targets? *Curr Mol Pharmacol,* 8**,** 110-22.

SUH, B. C. & HILLE, B. 2002. Recovery from muscarinic modulation of M current channels requires phosphatidylinositol 4,5-bisphosphate synthesis. *Neuron,* 35**,** 507-20.

SUH, B. C. & HILLE, B. 2008. PIP2 is a necessary cofactor for ion channel function: How and why? *Annual Review of Biophysics,* 37**,** 175-195.

SUI, Y. J., SUN, M. Y., WU, F., YANG, L. F., DI, W. H., ZHANG, G. Z., ZHONG, L. L., MA, Z. M., ZHENG, J. H., FANG, X. D. & MA, T. H. 2014. Inhibition of TMEM16A Expression Suppresses Growth and Invasion in Human Colorectal Cancer Cells. *Plos One,* 9.

SUI, Y. J., WU, F., LV, J. F., LI, H. X., LI, X., DU, Z. W., SUN, M. Y., ZHENG, Y. H., YANG, L. F., ZHONG, L. L., ZHANG, X. Y. & ZHANG, G. Z. 2015. Identification of the Novel TMEM16A Inhibitor Dehydroandrographolide and Its Anticancer Activity on SW620 Cells. *Plos One,* 10.

SUTTON, K. A., JUNGNICKEL, M. K., JOVINE, L. & FLORMAN, H. M. 2012. Evolution of the Voltage Sensor Domain of the Voltage-Sensitive Phosphoinositide Phosphatase VSP/TPTE Suggests a Role as a Proton Channel in Eutherian Mammals. *Molecular Biology and Evolution,* 29**,** 2147-2155.

SUZUKI, J., FUJII, T., IMAO, T., ISHIHARA, K., KUBA, H. & NAGATA, S. 2013. Calcium-dependent phospholipid scramblase activity of TMEM16 protein family members. *J Biol Chem,* 288**,** 13305-16.

SUZUKI, J., UMEDA, M., SIMS, P. J. & NAGATA, S. 2010. Calcium-dependent phospholipid scrambling by TMEM16F. *Nature,* 468**,** 834-8.

SUZUKI, M. 2006. The Drosophila tweety family: molecular candidates for large-conductance Ca2+-activated Cl- channels. *Exp Physiol,* 91**,** 141-7.

SUZUKI, M. & MIZUNO, A. 2004. A novel human Cl(-) channel family related to Drosophila flightless locus. *J Biol Chem,* 279**,** 22461-8.

SUZUKI, T., SUZUKI, J. & NAGATA, S. 2014. Functional swapping between transmembrane proteins TMEM16A and TMEM16F. *J Biol Chem,* 289**,** 7438-47.

SVEINSDOTTIR, K., MARTINSDOTTIR, E. & RAMEL, A. 2016. Blood pressure-lowering effects of long chain n-3 fatty acids from meals enriched with liquid fish oil and from microencapsulated powder. *Int J Food Sci Nutr,* 67**,** 1017-23.

SWEDENBORG, J., MAYRANPAA, M. I. & KOVANEN, P. T. 2011. Mast cells: important players in the orchestrated pathogenesis of abdominal aortic aneurysms. *Arterioscler Thromb Vasc Biol,* 31**,** 734-40.

TA, C. M., ACHESON, K. E., RORSMAN, N. J. G., JONGKIND, R. C. & TAMMARO, P. 2017. Contrasting effects of phosphatidylinositol 4,5-bisphosphate on cloned TMEM16A and TMEM16B channels. *Br J Pharmacol,* 174**,** 2984-2999.

TA, C. M., ADOMAVICIENE, A., RORSMAN, N. J., GARNETT, H. & TAMMARO, P. 2016. Mechanism of allosteric activation of TMEM16A/ANO1 channels by a commonly used chloride channel blocker. *Br J Pharmacol,* 173**,** 511-28.

TAKAHASHI, M., SEAGAR, M. J., JONES, J. F., REBER, B. F. & CATTERALL, W. A. 1987. Subunit structure of dihydropyridine-sensitive calcium channels from skeletal muscle. *Proc Natl Acad Sci U S A,* 84**,** 5478-82.

TAKEMURA, H., HUGHES, A. R., THASTRUP, O. & PUTNEY, J. W. 1989. Activation of Calcium Entry by the Tumor Promoter Thapsigargin in Parotid Acinar-Cells - Evidence That an Intracellular Calcium Pool, and Not an Inositol Phosphate, Regulates Calcium Fluxes at the Plasma-Membrane. *Journal of Biological Chemistry,* 264**,** 12266-12271.

TAMMARO, P., AARONSON, P. I. & SMIRNOV, S. V. 2001. Modulation of the native Kv2.1 channel by phosphorylation in rat aortic myocytes. *Biophysical Journal,* 80**,** 440a-440a.

TAMMARO, P., SMIRNOV, S. V. & MORAN, O. 2005. Effects of intracellular magnesium on Kv1.5 and Kv2.1 potassium channels. *Eur Biophys J,* 34**,** 42-51.

TAMMARO, P., SMITH, A. L., HUTCHINGS, S. R. & SMIRNOV, S. V. 2004. Pharmacological evidence for a key role of voltage-gated K+ channels in the function of rat aortic smooth muscle cells. *Br J Pharmacol,* 143**,** 303-17.

TANAKA, Y., MEERA, P., SONG, M., KNAUS, H. G. & TORO, L. 1997. Molecular constituents of maxi K-Ca channels in human coronary smooth muscle: predominant alpha+beta subunit complexes. *Journal of Physiology-London,* 502**,** 545-557.

TAPPAREL, C., REYMOND, A., GIRARDET, C., GUILLOU, L., LYLE, R., LAMON, C., HUTTER, P. & ANTONARAKIS, S. E. 2003. The TPTE gene family: cellular expression, subcellular localization and alternative splicing. *Gene,* 323**,** 189-199.

TERASHIMA, H., PICOLLO, A. & ACCARDI, A. 2013. Purified TMEM16A is sufficient to form Ca2+-activated Cl- channels. *Proceedings of the National Academy of Sciences of the United States of America,* 110**,** 19354-19359.

THOMAS-GATEWOOD, C., NEEB, Z. P., BULLEY, S., ADEBIYI, A., BANNISTER, J. P., LEO, M. D. & JAGGAR, J. H. 2011. TMEM16A channels generate Ca(2)(+)-activated Cl(-) currents in cerebral artery smooth muscle cells. *Am J Physiol Heart Circ Physiol,* 301**,** H1819-27.

THUL, R. 2014. Time to blip--stochastic simulation of single channel opening. *Cold Spring Harb Protoc,* 2014.

TIAN, Y. M., SCHREIBER, R. & KUNZELMANN, K. 2012. Anoctamins are a family of Ca2+-activated Cl- channels. *Journal of Cell Science,* 125**,** 4991-4998.

TIEN, J., PETERS, C. J., WONG, X. M., CHENG, T., JAN, Y. N., JAN, L. Y. & YANG, H. 2014. A comprehensive search for calcium binding sites critical for TMEM16A calcium-activated chloride channel activity. *Elife,* 3.

TIEU, B. C., LEE, C., SUN, H., LEJEUNE, W., RECINOS, A., 3RD, JU, X., SPRATT, H., GUO, D. C., MILEWICZ, D., TILTON, R. G. & BRASIER, A. R. 2009. An adventitial IL-6/MCP1 amplification loop accelerates macrophage-mediated vascular inflammation leading to aortic dissection in mice. *J Clin Invest,* 119**,** 3637-51.

TOLAND, H. M., MCCLOSKEY, K. D., THORNBURY, K. D., MCHALE, N. G. & HOLLYWOOD, M. A. 2000. Ca(2+)-activated Cl(-) current in sheep lymphatic smooth muscle. *Am J Physiol Cell Physiol,* 279**,** C1327-35.

TRUONG, E. C., PHUAN, P. W., REGGI, A. L., FERRERA, L., GALIETTA, L. J. V., LEVY, S. E., MOISES, A. C., CIL, O., DIEZ-CECILIA, E., LEE, S. J., VERLANAN, A. S. & ANDERSON, M. O. 2017. Substituted 2-Acylaminocycloalkylthiophene-3-carboxylic Acid

Arylamides as Inhibitors of the Calcium-Activated Chloride Channel Transmembrane Protein 16A (TMEM16A). *Journal of Medicinal Chemistry,* 60**,** 4626-4635.

TSIEN, R. W. 1983. Calcium channels in excitable cell membranes. *Annu Rev Physiol,* 45**,** 341-58.

TYKOCKI, N. R., BOERMAN, E. M. & JACKSON, W. F. 2017. Smooth Muscle Ion Channels and Regulation of Vascular Tone in Resistance Arteries and Arterioles. *Compr Physiol,* 7**,** 485-581.

VAN DER WALT, S., COLBERT, S. C. & VAROQUAUX, G. 2011. The NumPy Array: A Structure for Efficient Numerical Computation. *Computing in Science & Engineering,* 13**,** 22-30.

VAN RENTERGHEM, C. & LAZDUNSKI, M. 1993. Endothelin and vasopressin activate low conductance chloride channels in aortic smooth muscle cells. *Pflugers Arch,* 425**,** 156-63.

WANG, B., LI, C., HUAI, R. & QU, Z. 2015. Overexpression of ANO1/TMEM16A, an arterial Ca2+-activated Cl- channel, contributes to spontaneous hypertension. *J Mol Cell Cardiol,* 82**,** 22-32.

WANG, H., ZOU, L., MA, K., YU, J., WU, H., WEI, M. & XIAO, Q. 2017. Cell-specific mechanisms of TMEM16A Ca(2+)-activated chloride channel in cancer. *Mol Cancer,* 16**,** 152.

WANG, M., YANG, H., ZHENG, L. Y., ZHANG, Z., TANG, Y. B., WANG, G. L., DU, Y. H., LV, X. F., LIU, J., ZHOU, J. G. & GUAN, Y. Y. 2012. Downregulation of TMEM16A calcium-activated chloride channel contributes to cerebrovascular remodeling during hypertension by promoting basilar smooth muscle cell proliferation. *Circulation,* 125**,** 697-707.

WANG, R. X., CHAI, Q., LU, T. & LEE, H. C. 2011. Activation of vascular BK channels by docosahexaenoic acid is dependent on cytochrome P450 epoxygenase activity. *Cardiovascular Research,* 90**,** 344-352.

WARD, A. & HEEL, R. C. 1984. Bumetanide - a Review of Its Pharmacodynamic and Pharmacokinetic Properties and Therapeutic Use. *Drugs,* 28**,** 426-464.

WASSALL, S. R. & STILLWELL, W. 2008. Docosahexaenoic acid domains: the ultimate non-raft membrane domain. *Chemistry and Physics of Lipids,* 153**,** 57-63.

WASSALL, S. R. & STILLWELL, W. 2009. Polyunsaturated fatty acid-cholesterol interactions: domain formation in membranes. *Biochim Biophys Acta,* 1788**,** 24-32.

WEBB, R. C. 2003. Smooth muscle contraction and relaxation. *Adv Physiol Educ,* 27**,** 201-6.

WEISS, G. A., WATANABE, C. K., ZHONG, A., GODDARD, A. & SIDHU, S. S. 2000. Rapid mapping of protein functional epitopes by combinatorial alanine scanning. *Proc Natl Acad Sci U S A,* 97**,** 8950-4.

WELLMAN, G. C., BRAYDEN, J. E. & NELSON, M. T. 1996. A proposed mechanism for the cardioprotective effect of oestrogen in women: enhanced endothelial nitric oxide release decreases coronary artery reactivity. *Clin Exp Pharmacol Physiol,* 23**,** 260-6.

WESTCOTT, E. B., GOODWIN, E. L., SEGAL, S. S. & JACKSON, W. F. 2012. Function and expression of ryanodine receptors and inositol 1,4,5-trisphosphate receptors in

smooth muscle cells of murine feed arteries and arterioles. *J Physiol,* 590**,** 1849-69.

WESTERHOF, N., LANKHAAR, J. W. & WESTERHOF, B. E. 2009. The arterial Windkessel. *Medical & Biological Engineering & Computing,* 47**,** 131-141.

WHITE, C. R., ELTON, T. S., SHOEMAKER, R. L. & BROCK, T. A. 1995. Calcium-Sensitive Chloride Channels in Vascular Smooth-Muscle Cells. *Proceedings of the Society for Experimental Biology and Medicine,* 208**,** 255-262.

WHITLOCK, J. M. & HARTZELL, H. C. 2017. Anoctamins/TMEM16 Proteins: Chloride Channels Flirting with Lipids and Extracellular Vesicles. *Annu Rev Physiol,* 79**,** 119-143.

WILKINSON, C., BEBB, O., DONDO, T. B., MUNYOMBWE, T., CASADEI, B., CLARKE, S., SCHIELE, F., TIMMIS, A., HALL, M. & GALE, C. P. 2019. Sex differences in quality indicator attainment for myocardial infarction: a nationwide cohort study. *Heart,* 105**,** 516-523.

WILLIAMS, J. A., BATTEN, S. E., HARRIS, M., ROCKETT, B. D., SHAIKH, S. R., STILLWELL, W. & WASSALL, S. R. 2012. Docosahexaenoic and Eicosapentaenoic Acids Segregate Differently between Raft and Nonraft Domains. *Biophysical Journal,* 103**,** 228-237.

WYDRO, P. 2011. The interactions between cholesterol and phospholipids located in the inner leaflet of human erythrocytes membrane (DPPE and DPPS) in binary and ternary films--the effect of sodium and calcium ions. *Colloids Surf B Biointerfaces,* 82**,** 209-16.

WYNNE, B. M., CHIAO, C. W. & WEBB, R. C. 2009. Vascular Smooth Muscle Cell Signaling Mechanisms for Contraction to Angiotensin II and Endothelin-1. *J Am Soc Hypertens,* 3**,** 84-95.

XIAO, Q. & CUI, Y. 2014. Acidic amino acids in the first intracellular loop contribute to voltage- and calcium- dependent gating of anoctamin1/TMEM16A. *PLoS One,* 9**,** e99376.

XIAO, Q. H., YU, K., PEREZ-CORNEJO, P., CUI, Y. Y., ARREOLA, J. & HARTZELL, H. C. 2011. Voltage- and calcium-dependent gating of TMEM16A/Ano1 chloride channels are physically coupled by the first intracellular loop. *Proceedings of the National Academy of Sciences of the United States of America,* 108**,** 8891-8896.

XU, X. P., ERICHSEN, D., BORJESSON, S. I., DAHLIN, M., AMARK, P. & ELINDER, F. 2008. Polyunsaturated fatty acids and cerebrospinal fluid from children on the ketogenic diet open a voltage-gated K channel: a putative mechanism of antiseizure action. *Epilepsy Res,* 80**,** 57-66.

YANG, H., KIM, A., DAVID, T., PALMER, D., JIN, T., TIEN, J., HUANG, F., CHENG, T., COUGHLIN, S. R., JAN, Y. N. & JAN, L. Y. 2012. TMEM16F forms a Ca2+-activated cation channel required for lipid scrambling in platelets during blood coagulation. *Cell,* 151**,** 111-22.

YANG, Y. D., CHO, H., KOO, J. Y., TAK, M. H., CHO, Y., SHIM, W. S., PARK, S. P., LEE, J., LEE, B., KIM, B. M., RAOUF, R., SHIN, Y. K. & OH, U. 2008. TMEM16A confers receptor-activated calcium-dependent chloride conductance. *Nature,* 455**,** 1210-5.

YAO, Z., NAMKUNG, W., KO, E. A., PARK, J., TRADTRANTIP, L. & VERKMAN, A. S. 2012. Fractionation of a Herbal Antidiarrheal Medicine Reveals Eugenol as an Inhibitor of Ca2+-Activated Cl- Channel TMEM16A. *Plos One,* 7.

YE, W., HAN, T. W., NASSAR, L. M., ZUBIA, M., JAN, Y. N. & JAN, L. Y. 2018. Phosphatidylinositol-(4, 5)-bisphosphate regulates calcium gating of small-conductance cation channel TMEM16F. *Proc Natl Acad Sci U S A,* 115**,** E1667-E1674.

YE, Z., WU, M. M., WANG, C. Y., LI, Y. C., YU, C. J., GONG, Y. F., ZHANG, J., WANG, Q. S., SONG, B. L., YU, K., HARTZELL, H. C., DUAN, D. D., ZHAO, D. & ZHANG, Z. R. 2015. Characterization of Cardiac Anoctamin1 Ca2+-Activated Chloride Channels and Functional Role in Ischemia-Induced Arrhythmias. *Journal of Cellular Physiology,* 230**,** 337-346.

YIP, K. P., BALASUBRAMANIAN, L., KAN, C., WANG, L., LIU, R., RIBEIRO-SILVA, L. & SHAM, J. S. K. 2018. Intraluminal pressure triggers myogenic response via activation of calcium spark and calcium-activated chloride channel in rat renal afferent arteriole. *Am J Physiol Renal Physiol,* 315**,** F1592-F1600.

YOSHIDA, H., FEIG, J. E., MORRISSEY, A., GHIU, I., ARTMAN, M. & COETZEE, W. A. 2003. Identification and molecular characterization of native K-ATP channels in human coronary artery smooth muscle. *Journal of Molecular and Cellular Cardiology,* 35**,** A23-A23.

YOSHIDA, H., FEIG, J. E., MORRISSEY, A., GHIU, I. A., ARTMAN, M. & COETZEE, W. A. 2004. K-ATP channels of primary human coronary artery endothelial cells consist of a heteromultimeric complex of Kir6.1, Kir6.2, and SUR2B subunits. *Journal of Molecular and Cellular Cardiology,* 37**,** 857-869.

YU, K., WHITLOCK, J. M., LEE, K., ORTLUND, E. A., CUI, Y. Y. & HARTZELL, H. C. 2015. Identification of a lipid scrambling domain in ANO6/TMEM16F. *Elife,* 4**,** e06901.

YU, M., LIU, S. L., SUN, P. B., PAN, H., TIAN, C. L. & ZHANG, L. H. 2016. Peptide toxins and small-molecule blockers of BK channels. *Acta Pharmacol Sin,* 37**,** 56-66.

YURKO-MAURO, K., KRALOVEC, J., BAILEY-HALL, E., SMEBERG, V., STARK, J. G. & SALEM, N. 2015. Similar eicosapentaenoic acid and docosahexaenoic acid plasma levels achieved with fish oil or krill oil in a randomized double-blind four-week bioavailability study. *Lipids in Health and Disease,* 14.

ZAMPONI, G. W., STRIESSNIG, J., KOSCHAK, A. & DOLPHIN, A. C. 2015. The Physiology, Pathology, and Pharmacology of Voltage-Gated Calcium Channels and Their Future Therapeutic Potential. *Pharmacological Reviews,* 67**,** 821-870.

ZARITSKY, J. J., ECKMAN, D. M., WELLMAN, G. C., NELSON, M. T. & SCHWARZ, T. L. 2000. Targeted disruption of Kir2.1 and Kir2.2 genes reveals the essential role of the inwardly rectifying K(+) current in K(+)-mediated vasodilation. *Circ Res,* 87**,** 160-6.

ZAYDMAN, M. A., SILVA, J. R., DELALOYE, K., LI, Y., LIANG, H. W., LARSSON, H. P., SHI, J. Y. & CUI, J. M. 2013. Kv7.1 ion channels require a lipid to couple voltage sensing to pore opening. *Proceedings of the National Academy of Sciences of the United States of America,* 110**,** 13180-13185.

ZENGIN, E., CHALAJOUR, F., GEHLING, U. M., ITO, W. D., TREEDE, H., LAUKE, H., WEIL, J., REICHENSPURNER, H., KILIC, N. & ERGUN, S. 2006. Vascular wall resident progenitor cells: a source for postnatal vasculogenesis. *Development,* 133**,** 1543-51.

ZHANG, F., ZHANG, G., ZHANG, A. Y., KOEBERL, M. J., WALLANDER, E. & LI, P. L. 2006. Production of NAADP and its role in Ca2+ mobilization associated with

lysosomes in coronary arterial myocytes. *Am J Physiol Heart Circ Physiol,* 291**,** H274-82.

ZHANG, H. L., CRACIUN, L. C., MIRSHAHI, T., ROHACS, T., LOPES, C. M. B., JIN, T. H. & LOGOTHETIS, D. E. 2003. PIP2 activates KCNQ channels, and its hydrolysis underlies receptor-mediated inhibition of M currents. *Neuron,* 37**,** 963-975.

ZHANG, J., REN, C. Y., CHEN, L., NAVEDO, M. F., ANTOS, L. K., KINSEY, S. P., IWAMOTO, T., PHILIPSON, K. D., KOTLIKOFF, M. I., SANTANA, L. F., WIER, W. G., MATTESON, D. R. & BLAUSTEIN, M. P. 2010. Knockout of Na+/Ca2+ exchanger in smooth muscle attenuates vasoconstriction and L-type Ca2+ channel current and lowers blood pressure. *American Journal of Physiology-Heart and Circulatory Physiology,* 298**,** H1472-H1483.

ZHANG, S., CHEN, Y., AN, H., LIU, H., LI, J., PANG, C., JI, Q. & ZHAN, Y. 2014. A novel biophysical model on calcium and voltage dual dependent gating of calcium-activated chloride channel. *J Theor Biol,* 355**,** 229-35.

ZHANG, X., LI, H. L., ZHANG, H. R., LIU, Y. N., HUO, L. F., JIA, Z. F., XUE, Y. C., SUN, X. R. & ZHANG, W. 2017. Inhibition of transmembrane member 16A calcium-activated chloride channels by natural flavonoids contributes to flavonoid anticancer effects. *British Journal of Pharmacology,* 174**,** 2334-2345.

ZHOU, Y. & LINGLE, C. J. 2014. Paxilline inhibits BK channels by an almost exclusively closed-channel block mechanism. *Journal of General Physiology,* 144**,** 415-440.